EXCITED STATE REACTIONS OF SOME AROMATIC CARBONYL COMPOUNDS

John Frame Ireland

A Thesis Submitted for the Degree of PhD
at the
University of St Andrews

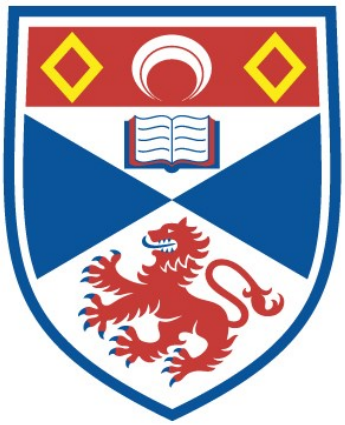

1972

EXCITED STATE REACTIONS OF SOME AROMATIC CARBONYL COMPOUNDS.

A Thesis

presented for the degree of

DOCTOR OF PHILOSOPHY

in the Faculty of Science of the

University of St. Andrews

by

John Frame Ireland, B.Sc.

August 1972.

United College of
St. Salvator and St. Leonard
St. Andrews.

DECLARATION

I declare that this thesis is my own composition, that the work of which it is a record has been carried out by me, and that it has not been submitted in any previous application for a Higher Degree.

This thesis describes results of research carried out at the Department of Chemistry, United College of St. Salvator and St. Leonard, University of St. Andrews, under the supervision of Professor P.A.H. Wyatt since the 1st of October 1969.

John F. Ireland

CERTIFICATE

I hereby certify that John F. Ireland has spent eleven terms of research work under my supervision, has fulfilled the conditions of ordinance No. 16 (St. Andrews), and is qualified to submit the accompanying thesis in application for the degree of Doctor of Philosopy.

P.A.H. Wyatt

Director of Research

ACKNOWLEDGEMENTS

I would like to express my gratitude to Professor P.A.H. Wyatt for his help and encouragement during the course of this research.

My thanks are also due to Dr. T.M. Shepherd for his help with many experimental and computational problems, to Mr. I. Ritchie for his help and advice with the CNINDO calculations and to my friends and colleagues Dougie Brown, John Curran, Rob Henson, Dave Powell, Dave Rayner and John Ride without whom my time in the laboratory would have been, to say the least, less enjoyable.

I am indebted to the Carnegie Trust for their scholarship which has kept me above subsistence level from 1969-1972 and to Professor Lord Tedder and Professor P.A.H. Wyatt for research facilities during this period.

Finally I wish to thank the technical staff of the Chemistry Department for their assistance and Mrs. Pat Cooper for her skilful typing.

CONTENTS

SUMMARY

The pK values for xanthone protonation in the S_o, S_1 and T_1 states have been determined by direct measurement and by Förster Cycle calculation. Both methods for determining pK give the order for xanthone of $pK(T_1) > pK(S_1) > pK(S_o)$. A study of benzophenones and acetophenones showed this pK order to be a common one for aromatic carbonyl compounds. The pK order for these compounds has been explained in terms of the type of transitions involved and the S_1-T_1 splitting of these transitions. In the case of substituted aromatic carbonyl compounds the pK order reflects the effect of substitution on the lowest S_o-S_1 and S_o-T_1 transitions. Results are also presented on the effect of inorganic anions, solvent, and temperature on xanthone fluorescence. Spectral details are reported for several xanthones, benzophenones, acetophenones, and anthraquinones.

CHAPTER 1

INTRODUCTION

1. General Photochemistry

(a) Excitation and Deactivation of Excited States

In order to understand fully the reactions of a molecule in an excited state, one must have detailed knowledge of all the primary photochemical processes of the molecule under consideration. A very good definition of a primary photochemical process was given by Noyes, Porter and Jolley[1]: "the primary photochemical process comprises the series of events beginning with the absorption of a photon by a molecule and ending either with the disappearance of that molecule or with its conversion to a state such that its reactivity is statistically no greater than that of similar molecules in thermal equilibrium. There may exist several different paths for loss of absorbed energy and not all of these may result in either dissociation or in conversion of the absorbing molecule to a new molecular species. The complete elucidation of a primary photochemical process must include an understanding of all that transpires, whether or not a chemical reaction occurs". The primary photochemical process includes all radiative and non-radiative photophysical processes which do not lead to a net chemical change but lead to loss of energy by the excited molecule, as well as chemical paths which can lead to the degradation of the electronic energy of excitation by, for example, intramolecular rearrangements or the formation of free radicals and excited molecules which may react in secondary processes.

The excited states of organic molecules are normally depicted by means of a Jablonski diagram[2] (See Fig. 1.1). Most organic molecules at room temperature or below, and in the absence of external

FIG. 1.1 Jablonski Diagram

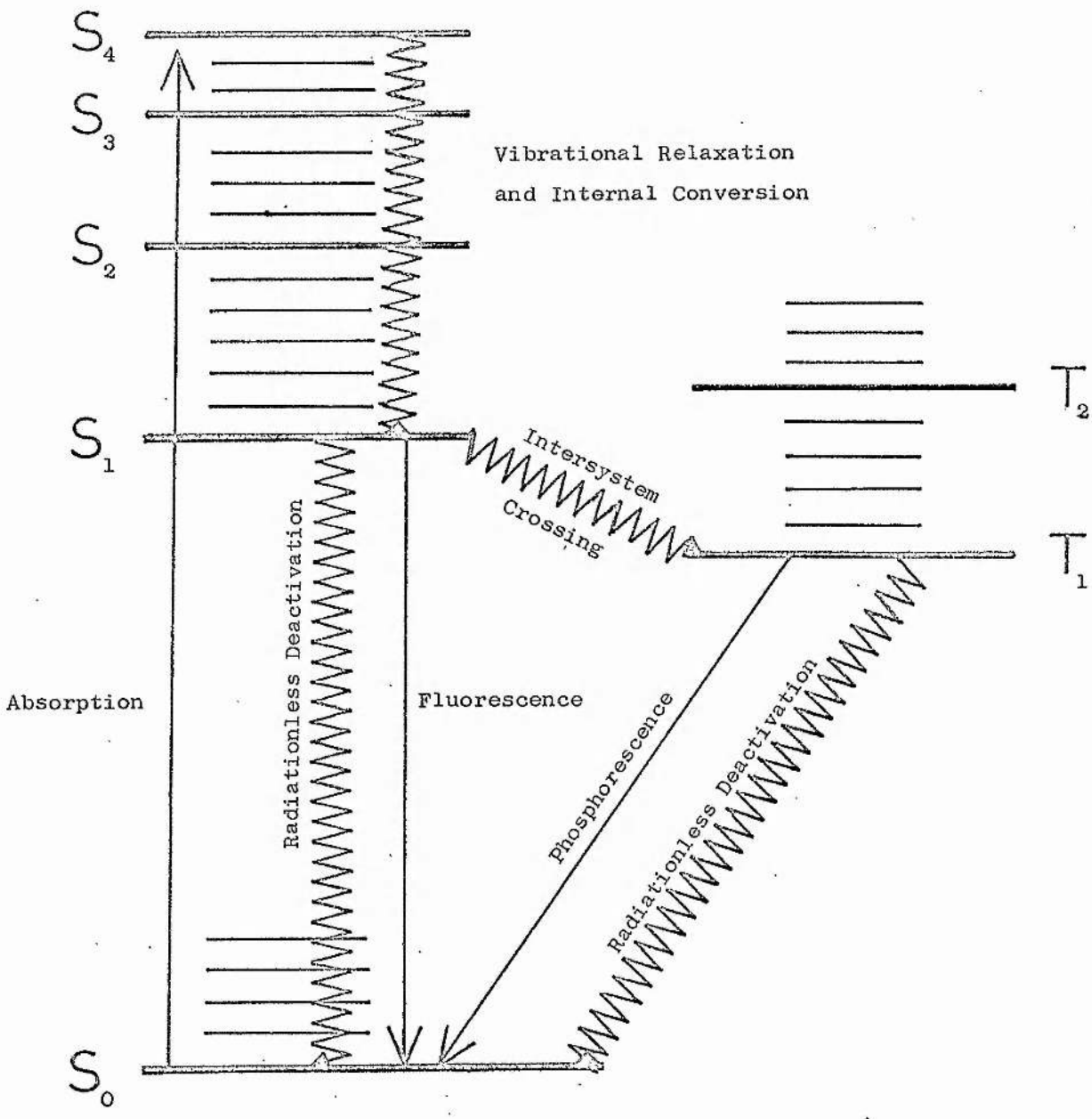

electromagnetic influence, can be described in the following manner. With few exceptions all filled molecular orbitals contain two spin-paired electrons which results in each molecular orbital contributing no net spin to the entire molecular system. When the above condition is fulfilled, the molecule is said to exist in its electronic ground state. Since the resultant spin, S, equals zero the multiplicity, M = 2S + 1, of this state will be one. States with multiplicities of one are traditionally referred to as singlet states and the above-mentioned ground state is the singlet ground state (S_o), while excited electronic states whose multiplicity remains one although an electron is promoted to a higher electronic level are referred to as excited singlet states (S_1, S_2, S_3 etc.). For every excited singlet state it is easily seen that there will be a state in which the spin of the promoted electron has been reversed. These states with S = 1 and M = 3 are termed triplet states (T_1, T_2, T_3 etc.).

When a photon with the appropriate energy is absorbed by a molecule, an electron is raised from the zero vibrational level of the singlet ground state to one of the several vibrational levels of an excited singlet state. According to the Frank-Condon principle[3] this process occurs in 10^{-15} seconds which is short relative to the time required for all other electronic processes. In a condensed medium, a liquid or a solid, an electron in a high vibrational level rapidly (10^{-12}s) loses its excess vibrational energy in collision with neighbouring molecules, a process called vibrational relaxation. Since the energy separation between excited singlet states in an aromatic molecule is smaller than the energy separation between the lowest excited singlet state and the ground state the vibrational levels of the excited singlet states overlap and a molecule excited to a singlet state of greater energy than S_1 can be considered by a process called <u>internal conversion</u>

to be converted from S_n to S_1 in about the same time that it requires to convert from an excited vibrational level of S_1 to its zeroth vibrational level. This situation leads to the formulation of the general rule that a molecule can be considered to undergo internal conversion to the lowest vibrational level of its lowest excited singlet state regardless of the singlet state to which it was excited initially. If the molecule can remain in its lowest excited singlet state, S_1, for 10^{-9} s or longer then the situation is favourable for this molecule to emit <u>fluorescence</u> radiation and thus return to the S_o state. This radiational deactivation from S_o to S_1 results in a band spectrum; any number of vibrational levels in S_o may be populated by the S_1 to S_o transition. Thus we have an interesting comparison to make between the two phenomena, absorption and fluorescence: whereas an absorption spectrum depicts the vibrational spacing of the first excited state, a fluorescence spectrum displays the vibrational spacing of the ground state and in many cases both bands show similar structured intensity patterns.

Other modes of deactivation of S_1 are available. If the excited S_1 molecule interacts with its solvent environment or with a particular quenching molecule, then there may be a radiationless deactivation of S_1 resulting in the production of S_o; the nature of some of these quenching processes is considered later. It is also possible that high-lying vibrational levels of S_o will overlap the S_1 state; internal conversion can then occur from the S_1 to the S_o state with no net loss in energy. All of the above radiational and radiationless deactivation steps may produce an S_o molecule in excited vibrational levels which through vibrational relaxation give the unexcited ground state molecules.

In addition to the above sequences of events a molecule in the S_1 state can cross from the singlet manifold to the triplet manifold.

This process, intersystem crossing, does in many cases compete effectively with the fluorescence emission process to deactivate the S_1 state. Vibrational relaxation of any vibrationally excited triplet molecules yields molecules in the lowest vibrational level of the T_1 state. A molecule with its excitation energy in the triplet level can remain in this condition for a relatively long time and therefore, the level is sometimes called a metastable level. There are several deactivation routes open to these T_1 molecules; they are in most respects identical in qualitative nature to the deactivation routes described for the S_1 to S_o transition. Radiational deactivation of T_1 to S_o is the phenomenon known as phosphorescence.

The lifetime of a triplet state is much longer than that of an excited singlet state[4] (the radiative transition $T_1 \longrightarrow S_o$ is spin forbidden) and therefore loss of excitation energy by collisional transfer in solution is greatly enhanced. In fact, this process is so important that in solution at room temperature it is often the predominant pathway for loss of triplet state excitation energy. It is only relatively recently that the development of very sensitive detectors has allowed the detection of weak phosphorescence emission from solutes at room temperature, phosphorescence being mainly observed from solid solutions at liquid nitrogen temperature.

There are further modes of radiational deactivation open to the excited molecule. For example, consider the consequences of a T_1 to S_1 transition. Once the S_1 state is produced, all of the S_1 deactivation routes described above are available. In particular the radiational deactivation of S_1 to S_o (after a T_1 to S_1 transition) is called delayed fluorescence. The circumstances under which this type of luminescence occurs are rare and a relatively small number of examples are known.

Just as conventional absorption spectra are obtained by exciting molecules in the ground state (S_o) to higher levels of the singlet manifold so singlet (S_1) - singlet (S_n) and triplet (T_1) - triplet (T_n) absorption spectra can be obtained. Because of the very short lifetime of the molecule in the S_1 state, absorption spectra originating from that state have only recently been observed using nanosecond flash photolysis techniques with a pulsed laser flash as source[5]. Triplet-triplet absorption is more easily observable because the lifetime of the lowest triplet is sufficiently long to allow study of the molecule by more conventional flash sources. This technique has been used extensively in the study of primary photochemical processes and in the elucidation of excited state reaction mechanisms and other secondary processes.

It is possible to populate the triplet manifold by direct absorption from the S_o state rather than by intersystem crossing from S_1. The low intensity of most singlet to triplet (S_o-T_1) absorption spectra demands long path lengths of concentrated solutions or pure liquid for their observation. The intensity of the S_o-T_1 absorption is governed by, among other factors, the spin-orbit interaction, and in a series of like molecules this absorption will increase with the atomic number of substituent atoms. It is also possible to enhance the spin-orbit coupling by external perturbation with molecules containing heavy atoms and thus increase the probability of the S_o-T_1 transition.

(b) Type and Nature of Electronic Transitions

Only these transitions of primary importance in the photochemistry of aromatic molecules will be discussed here. It is convenient for

photochemical purposes to discuss electronic transitions in terms of the initial and final orbitals of the electron involved in the transition. This form of description is less precise than the symmetry notation but adequate for most purposes. The classification of transitions given is that first used by Kasha[6].

π-π^* transitions

π^* orbitals are delocalised like the ground state π orbitals but have a nodal plane perpendicular to the bond axis and are therefore antibonding. The π-π^* transitions are generally of relatively low energy and have high intensities ($\varepsilon_{max} \approx 10^4$-$10^5$) unless forbidden by spin or symmetry selection rules. Although in ethylene the lowest energy π-π^* singlet state is observed below 200 nm, the energy falls off rapidly as the π system is extended, reaching the region of visible absorption for the pentaenes or linear four ring aromatics. Fluorescence is nearly always associated with the π^* level of an unsaturated molecule when that is the lowest excited singlet state of the molecule. The corresponding lowest triplet π-π^* states have been characterised by their phosphorescence or in certain systems their singlet-triplet absorption. The singlet-triplet splitting of π-π^* is in general large, and the emission process from S_1 usually competes favourably with the rate of intersystem crossing so that the quantum yield of fluorescence (ϕ_f) is greater than that of phosphorescence (ϕ_p). Also, from consideration of the large extinction coefficient of π-π^* transition, it is easily understood that the probability of the emission process must be high and that the excited singlet π^* state will be short lived (about 10^{-9} to 10^{-7} seconds) and therefore intersystem crossing is unlikely to have a high quantum yield.

$n-\pi^*$ transitions

Unsaturated systems containing an atom having a lone pair of electrons often give rise to a transition of lower energy than the $\pi-\pi^*$ transition. For example the carbonyl group is made up of one pair of electrons occupying a σ orbital, one pair of electrons in a π-orbital, and two pairs of electrons on the oxygen, one pair of which occupy a non-bonding or n-orbital. The spatial overlap between the n and π orbitals is small and therefore the transition from the n orbital which has highest energy to an upper π^* orbital i.e. an $n-\pi^*$ transition, which is generally the singlet-singlet transition of lowest energy, has low probability ($\varepsilon_{max} < 2000$). The $n-\pi^*$ excited singlet states have comparatively long lifetimes and are thus much more subject to radiationless deactivation processes than $\pi-\pi^*$ states and the fluorescence from them is weak. The lack of overlap between the n and π^* orbitals also results in a small singlet-triplet splitting and this factor, together with the longer life of the S_1 state, contributes to the fact that intersystem crossing to the triplet from singlet $n-\pi^*$ states is an efficient process. In most cases in which the $n-\pi^*$ state is the lowest excited singlet state, the emission that occurs is phosphorescence. This is by far the most common situation among molecules containing a carbonyl group and among aza aromatic compounds.

Charge transfer transitions

When several active substituent groups are attached to a π-electron system it is no longer possible to describe the electronic transitions or the excited states in terms of one-electron transitions. This is particularly the case when both electron donor substituents, D (e.g. O^- and NH_2), and electron-acceptor substituents, A (e.g. C=O and NO_2), are present, but this type of

transition is considered with substituted aromatic (Ar) molecules of general formulas A-Ar, D-Ar and A-Ar-D. Several kinds of one-electron transition have to be regarded as contributing to the transition that actually occurs and Porter and Suppan[7] have classified the excited states of lowest energy that result from such transitions as charge transfer (CT) states. They argue that since, in most cases, the symmetry is not exactly preserved, even in the ground state, it would be incorrect to class these transitions as of π-π^* type. The transitions are of high intensity, and if the charge transfer state is the excited state of lowest energy, it can give rise to fluorescence. This is the case with some substituted benzophenones in polar solvents where both fluorescence and phosphorescence are observed at 77 K in rigid solution (See Chapter 4). The most characteristic property of these transitions is the large solvent shift of the band on passing from non-polar to polar solvents. The singlet-triplet splitting is smaller than that for π-π^* transitions and comparable with that observed in n-π^* transitions. Essential evidence on the concept of CT states rests in the measurement of excited state dipole moments which have led to values as high as 14 D (p-aminobenzophene) for the first excited singlet state, corresponding to a charge transfer of 0.7 e from the ring to the acceptor group[8].

(c) Spectroscopic Properties of Aromatic Molecules

Absorption can occur to any of the excited singlet states S_1, S_2, S_3 etc., with an efficiency dependent upon the type of transition involved. This is high for π-π^* and CT transitions and much lower for n-π^* transitions. In many cases the n-π^* transition occurs at lower energy than the π-π^* transition observed in the hydrocarbon analogue of the compound concerned while CT absorption occurs at much longer wavelengths than in related molecules having no donor or acceptor substituents. In aromatic

systems containing an atom with a lone pair of electrons these criteria are often insufficient to distinguish between transitions of different types.

The change in wavelength of a transition with solvent change is one of the most useful methods for characterisation of transitions. π-π^* transitions show a relatively small red shift in changing from a hydrocarbon solvent to a polar one while CT transitions undergo a much larger red shift and n-π^* transitions, by contrast, exhibit a blue shift[8]. The excited state in a π-π^* transition is more polarisable than the ground state and on changing to polar solvent the solvent interaction with both states increases, but the corresponding decrease in energy of the excited state is slightly greater than that of the ground state, and hence the absorption band shifts towards the red. If the transition is of CT type, the excited state is much more polar than the ground state so that change to a polar solvent has a more striking effect and may shift the spectrum to longer wavelengths by several thousand wavenumbers. For n-π^* transitions in polar solvents the ground state is hydrogen bonded at the n-electron site and promotion of the non-bonding electron into the π-electron system reduces the hydrogen bonding forces in the excited state. Thus change to polar solvents reduces the energy of the ground state to a greater degree than that of the excited state and the absorption band shifts to higher wavenumbers.

The relative position of the different types of transition governs the type of lowest excited singlet and triplet state and thus determines the luminescence properties observed for a particular molecule. An important factor in the relative positioning of singlet and triplet states is the singlet-triplet splitting of states of different character. It is thus possible to have a molecule with a lowest singlet state of n-π^* type but, due to the magnitude of the singlet-

triplet splitting of a higher π-π^* state, to have a lowest triplet state of π-π^* character. McGlynn et al[9,10] have discussed the origins of singlet-triplet splitting. The singlet-triplet separation depends on the magnitude of the two-electron exchange integral between donor and acceptor orbitals. In the case of n-π^* transition because the n and π^* orbitals occupy, in the main, different regions of space the overlap is small and a small singlet-triplet splitting is a characterstic of an n-π^* transition[11]. For example the S-T intervals in formaldehyde, acetophenone, benzophenone and anthraquinone are respectively 2996[12], 1820[13], 2135[13] and 1400 cm^{-1}.[14] n_N-π^* transitions of aza-aromatics exhibit an S-T split which is approximately twice that of the lowest energy n-π^* transition of carbonyls. This difference has been attributed[15] to the lesser charge transfer characteristic in n_N-π^* transitions and is to be expected since nitrogen is less electronegative than oxygen.

The singlet-triplet splitting of π-π^* states is usually large; in anthracene for example the energy of the lowest triplet is little more than half that of the corresponding singlet[10], and in ethylene the triplet π-π^* energy is about 28,000 cm^{-1} compared with an energy of the lowest singlet state of 50,000 cm^{-1}.[11] Unlike n-π^* transitions the orbitals involved in the above π-π^* transitions show strong spatial overlap between the π and π^* orbitals, thus explaining the large S_1-T_1 separation of these molecules. In general the size of the singlet-triplet split decreases as the size of the π system grows[10] and in large dye molecules where extensive delocalisation of these oribtals is possible the separation can become very small. In dyes of the fluorescein group, splits of less than 5000 cm^{-1} are common.[16]

The singlet-triplet splitting of charge -transfer states is smaller than that for π-π^* states and of the same order as that

observed for $n-\pi^*$ states.

Considering the relative singlet-triplet splittings of the $n-\pi^*$ and $\pi-\pi^*$ states, molecules containing both these transitions can be classified into five groups with respect to the relative positions of the singlet and triplet states of different character[17,18].

Group I $S_{\pi\pi^*} > T_{\pi\pi^*} > S_{n\pi^*} > T_{n\pi^*}$

Group II $S_{\pi\pi^*} > S_{n\pi^*} > T_{\pi\pi^*} > T_{n\pi^*}$

Group III $S_{\pi\pi^*} > S_{n\pi^*} > T_{n\pi^*} > T_{\pi\pi^*}$

Group IV $S_{n\pi^*} > S_{\pi\pi^*} > T_{n\pi^*} > T_{\pi\pi^*}$

Group V $S_{n\pi^*} > T_{n\pi^*} > S_{\pi\pi^*} > T_{\pi\pi^*}$

The possible ordering $S_{n\pi^*} > S_{\pi\pi^*} > T_{\pi\pi^*} > T_{n\pi^*}$ is highly improbable due to the expected S-T splitting of the $n-\pi^*$ and $\pi-\pi^*$ states, FIG. 1.3 and FIG. 1.4 show energy level diagrams of molecules belonging to two of these groups.

Since it has been shown[19,20,21] that the probability of singlet-triplet conversion between states of different configuration ($S_{n\pi^*}$-$T_{\pi\pi^*}$ or $S_{\pi\pi^*}$-$T_{n\pi^*}$) is larger by a factor of 10^2-10^3 than the probability of S-T conversion between states of identical configuration ($S_{n\pi^*}$-$T_{n\pi^*}$ or $S_{\pi\pi^*}$-$T_{\pi\pi^*}$), and is at the same time somewhat higher than the probability of the S_1-S_o radiative transition (fluorescence), we can make generalisations about the luminescence properties of the above five groups. Molecules of group I may undergo fluorescence or phosphorescence from an $n-\pi^*$ state while for group II intersystem crossing is more efficient and only phosphorescence from the $n-\pi^*$ state is expected. Molecules of groups III and IV are mainly phosphorescent while group V molecules show luminescence properties which differ in no way from that of molecules without n electrons and both fluorescence and phosphorescence from the $\pi-\pi^*$ state is observed.

Thus aromatic hydrocarbons all have lowest excited $\pi-\pi^*$ states and they always show some fluorescence[22], often very intense and generally

they also show phosphorescence in rigid media. Molecules with both $n-\pi^*$ and $\pi-\pi^*$ states can, as mentioned above, show differing luminescence properties and these properties can also, unlike molecules with only $\pi-\pi^*$ states, be substantially changed by change of solvent. Thus quinoline in non-polar solvents has an $n-\pi^*$ lowest state and is substantially non-fluorescent[20]. In polar solvents the positions of the $\pi-\pi^*$ and $n-\pi^*$ levels are reversed and quinoline gives fluorescence emission under these conditions. Substitution of certain groups can also change the nature of the energy levels and give rise to fluorescence e.g. pyridine and 3-hydroxypyridine[22]. The effects of chemical substitution on fluorescence emission have been extensively studied by Williams et al[23-25] and McGlynn et al[10] have recently discussed the effects of substitution on the T_1 state.

(d) Photochemistry of Aromatic Carbonyl Compounds

The general properties of the carbonyl group, its absorption, singlet-triplet splitting and general luminescence properties, have been mentioned in the consideration of the $n-\pi^*$ state. In unsubstituted aromatic aldehydes and ketones the carbonyl group plays a dominant role in their photochemistry and while this is also generally true for substituted derivatives, substitution can have marked effects on the spectroscopic and photochemical properties of aromatic carbonyl compounds.

Formaldehyde provides the model compound for this type of system since it is the only case for which there is a satisfactory theoretical treatment[26]. The behaviour of more complex molecules is described by analogy with theories developed for explaining the structure of this molecule and its excited states. FIG. 1.2 shows a molecular orbital diagram for the excitation of formaldehyde.

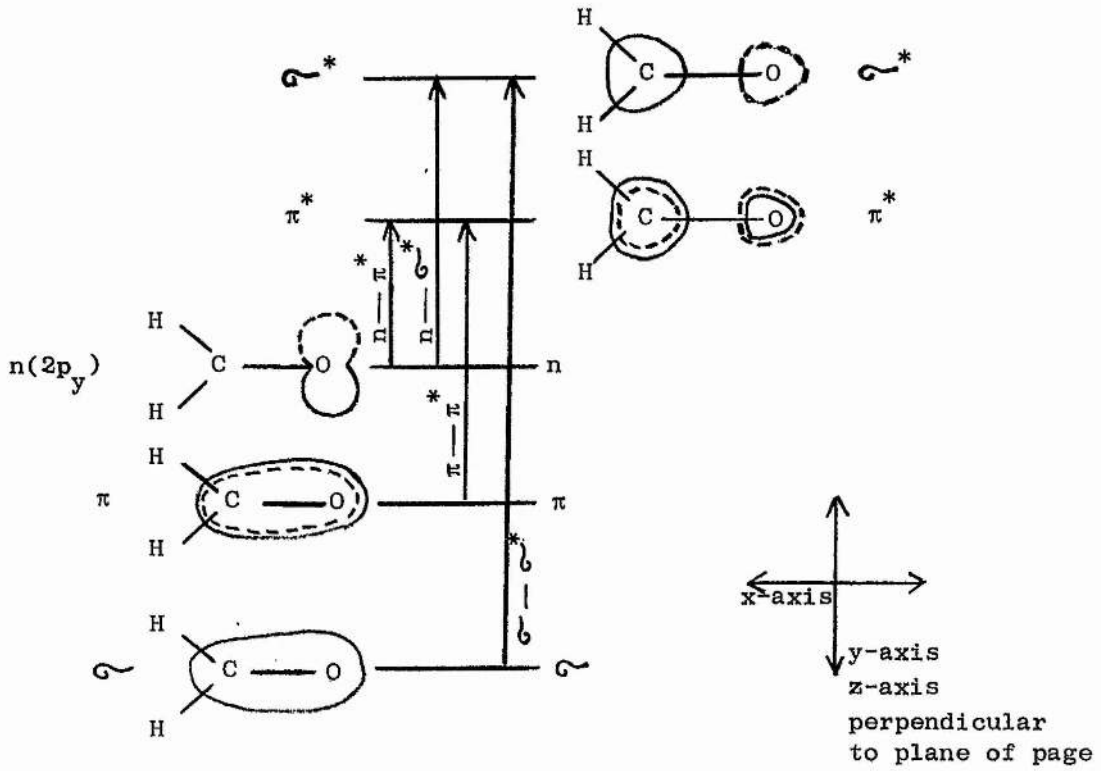

FIG. 1.2 Diagrammatic representation of the molecular orbitals of formaldehyde, due to Kasha.

The lowest energy transition is of the n-π^* type which involves removal of a non-bonded electron from an in-plane atomic orbital of oxygen and its placement in a π^* orbital which is C-O antibonding and antisymmetric with respect to the molecular plane. There is considerable charge transfer in the n-π^* transition of the carbonyl group. Electronic charge is transferred from the vicinity of the oxygen to the vicinity of the carbon. This means in effect that both singlet and triplet n-π^* states have a highly localised unpaired electron which accounts for the radical-like behaviour of some carbonyls in the excited state. There is a vast volume of literature concerning the photochemistry of carbonyl compounds. They undergo a wide variety of reactions in the excited state but we will only consider here the hydrogen atom abstraction reaction and, with benzophenone and some substituted benzophenones as examples,

consider the relationship between the spectroscopic and photochemical properties of benzophenones in particular, but thereby in effect also of aromatic carbonyl compounds in general. The discussion of the properties of benzophenones is based on the work of Porter and Suppan[29,30]. They studied, in some detail, the relationship between the spectral properties and reactivities of substituted benzophenones and interpreted these properties in terms of the electron distribution in the lowest triplet level. A review of the photochemistry of carbonyl compounds has been given by Pitts and Wan[27] and the varied reactions (the hydrogen-transfer reaction in particular) have been discussed by Yang[28].

Benzophenone itself has lowest singlet and triplet states of $n-\pi^*$ character under all conditions. In all solvents only phosphorescence is observed and the emission is characterised as originating from an $n-\pi^*$ state by the short lifetime of the emission, the 1600-1700 cm^{-1} carbonyl vibration shown in the phosphorescence intensity pattern and by the high yield of photoreduction. It has been proposed[31] that the energy levels of benzophenone are as represented in FIG. 1.3 i.e. this molecule belongs to group II.

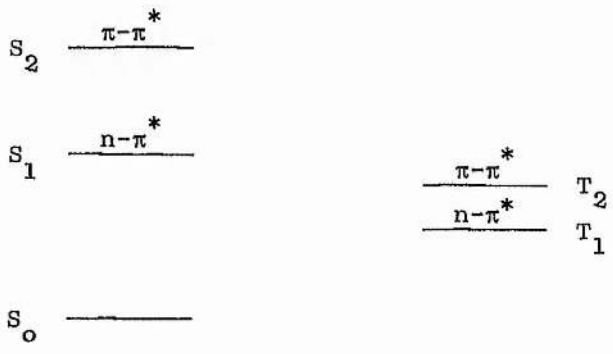

FIG. 1.3 Schematic representation of the energy levels of the singlet and triplet states of benzophenone.

The pathway for population of T_1 is therefore postulated as $S_{n\pi^*} \rightsquigarrow T_{\pi\pi^*} \rightsquigarrow T_{n\pi^*}$ which is expected to be efficient and therefore the large phosphorescence and intersystem crossing quantum yields found for benzophenone are expected.

Substitution altering the character of the triplet level from $n\text{-}\pi^*$ to $\pi\text{-}\pi^*$ alters the luminescence characteristics. $\pi\text{-}\pi^*$ phosphorescence as expected shows a relatively large singlet-triplet split, the phosphorescence lifetime is relatively long (10-1000 times longer than that from a $T_{n\pi^*}$ state[32,33]), the $S_o\text{-}T_{\pi\pi^*}$ absorption will be 10-100 times weaker than that for $S_o\text{-}T_{n\pi^*}$[34], and the vibrational progression is not expected to show a dominant C=O frequency spacing.

4-phenylbenzophenone still has an $n\text{-}\pi^*$ lowest singlet level but the lowest triplet is $\pi\text{-}\pi^*$ owing to the large singlet-triplet splitting of the $\pi\text{-}\pi^*$ state[29]. The spectral properties of this molecule are consistent with a $\pi\text{-}\pi^*$ triplet and also the reactivity in hydrogen abstraction reactions is 10% of that expected of an $n\text{-}\pi^*$ triplet thus showing the change in electron distribution of the lowest triplet state. FIG. 1.4 shows an energy level diagram for 4-phenylbenzophenone.

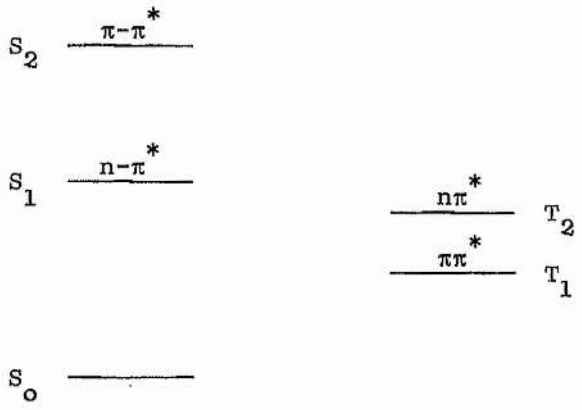

FIG. 1.4 Schematic representation of the singlet and triplet energy levels of 4-phenylbenzophenone.

This molecule would be classified as belonging to group III and as expected only phosphorescence is observed.

Substitution of strongly electron-donating groups such as amino in the benzene rings of benzophenone produces strong new absorption bands at long wavelengths. These have been ascribed to charge transfer transitions. The phosphorescence emission of CT triplet states shows similar properties to these mentioned for π-π^* triplets and can easily be distinguished from an n-π^* emission. Molecules with CT lowest triplet states are almost completely unreactive with quantum yields of photoreduction less than 1%. This is in accordance with the measurement of dipole moments[7] which indicates a transfer of 0.7 e to the carbonyl group (in the CT state) in complete contrast to the transfer in the opposite sense which occurs in the n-π^* state. Molecules with lowest singlet states of CT character also show fluorescence which, although no CT states were mentioned in the group classification, put the properties of these molecules with lowest singlet and triplets of CT character in group V.

Extensive studies[10,35] of other ketones, aldehydes and quinones have shown that this type of classification given to benzophenone derivatives can be extended.

2. Reactions of the Excited State

(a) General

The production of several different types of excited states by absorption of radiation has been described. The resultant state differs from the ground state in two important respects: the excited state molecule possesses more energy than the ground state molecule; and the molecular orbitals of the excited state molecule are filled in a manner appreciably different from the manner in which the orbitals of the ground state molecule were filled. The excited molecule can therefore be considered to be a new molecular species which will undergo reactions not observed for, or under different conditions from, similar reactions of the unexcited molecule. The magnitude of the difference in properties of the ground state and excited state molecules will depend on the extent to which the electronic charge has been redistributed in the excited state and hence on the type of excited state involved. Here the reactions of the excited state which we will consider will be of the type in which there is no net chemical change i.e. the molecule excited is again obtained on deactivation. The reactions looked at experimentally are the reversible protonation of the excited state, and the deactivation of the excited state through a quenching reaction with a foreign molecule or ion.

Excited state reactions in which there is a net chemical change have been increasingly studied in recent years[36,37]. The advent of gas-chromatography and the development of new spectroscopic tools made it feasible for organic chemists to study the often small quantities of compounds which are formed by chemical transformation of electronically excited molecules. Several reviews of this 'organic' photochemistry have appeared[37,39] and recently the same type of techniques have been used by inorganic and organometallic chemists[36]. A large amount of

the work has dealt with compounds containing a carbonyl group[36,40]. The Woodward-Hoffmann orbital symmetry rules[41] have been used in rationalising many varieties of photochemical behaviour in the field of organic photochemistry.

(b) Acid-Base Properties

The definition of an acid and a base used here will be the Brönsted definition[42,43]; an acid is a proton donor, and a base is a proton acceptor. The carbonyl group in its ground state is generally a weak base and accepts a proton in strongly acid solutions. A review of the acid-base properties of carbonyl compounds in their ground state has been given by Palm, Haldna and Talvik[44]. Here equilibria are discussed in aqueous solutions and the general reaction for the protonation of a base in any electronic state can be considered as:

$$B + H_3O^+ \rightleftharpoons BH^+ + H_2O$$

The equilibrium constant is given in terms of concentrations (neglecting activity coefficients) for dilute solutions by the approximation:

$$K = \frac{[BH^+]}{[B]\ [H_3O^+]}$$

The following notations will be used for pK values, obtained by the above approximation, of different electronic states.

$pK(S_o)$	pK of the ground state,
$pK(S_1)$	pK of the lowest excited singlet state,
$pK(T_1)$	pK of the lowest excited triplet state,
pK^*	pK of an unspecified excited state.

If we consider the processes involved in the production and deactivation of excited molecules (See FIG. 1.1) then it is easily

understood that a thermodynamic equilibrium can never be established in singlet states higher than S_1 and triplet states higher than T_1 because of the rate of internal conversion and vibrational relaxation. Nevertheless, some pK^* values in S_2 and S_3 states have been determined approximately, by calculations using the spectroscopically determined energy levels. Also a value of $pK(T_2)$ has been determined for xanthone (See Chapter 3) applying the same method to energies obtained from triplet-triplet absorption spectra. The results obtained for these higher states are only of theoretical interest since no chemical process takes place.

Determination of pK^* Values

Both $pK(S_1)$ and $pK(T_1)$ values can often be obtained by direct measurement of the $[BH^+]/[B]$ ratios involved. A discussion of these methods is followed by a consideration of the simpler and less time-consuming technique known as the Förster Cycle which permits the excited state pK values to be estimated from spectral data obtained for the base and its protonated form.

$pK(S_1)$: Fluorescence Spectroscopy

Weber[45] made the first observation of a fluorescence change due to a protolytic reaction in the excited state. He found that the fluorescence of solutions of 1-naphthylamine-4-sulphonate changed in strongly alkaline solutions although there was no change in the absorption spectrum. This effect was interpreted by Förster[46,47,48] who obtained results using other naphthalene derivatives and with hydroxy- and amino-pyrene sulphonates.

For 2-naphthylamine $pK(S_o) = 4.07$ and at pH values greater than 6 it is present in solution almost entirely as the free base (BNH_2).

$$BNH_2 + H_3O^+ \rightleftharpoons BNH_3^+ + H_2O$$

Förster observed that this species showed a fluorescence maximum at 420 nm and that this fluorescence persisted although the pH of the solution was changed to values less than 2 where the solution contains substantially only protonated molecules. The BNH_3^+ must dissociate after excitation and hence the pK value in the excited state must be considerably lower than 2. The naphthylammonium ion fluoresces at shorter wavelengths and, to obtain the fluorescence spectrum of this species alone, Förster had to use strongly acidic solutions. From the fluorescence changes Förster[49] obtained an approximate value of $pK(S_1)$ of -1.5. A more negative value for this $pK(S_1)$ has recently been suggested[50]. The $pK(S_1)$ is at least 6 units less than $pK(S_o)$ showing that the BNH_2 form is a much weaker base in the excited state.

In solutions of pH = 14 a further change in the fluorescence spectrum was detected, although again there was no change in the absorption spectrum. The same fluorescence had been observed from 2-naphthylamide anions produced by ionisation of 2-naphthylamine in liquid ammonia containing sodamide. In aqueous solution these ions do not exist at all in the ground state, but due to the increased acidity of 2-naphthylamine in the S_1 state the characteristic fluorescence of the 2-naphthylamide can be observed in aqueous solutions because of the following reaction:

$$BNH_2^* + OH^- \rightleftharpoons BNH^{*-} + H_2O$$

N-methyl-2-naphthylamine shows a similar change but N,N-dimethylnaphthylamine does not, showing that a proton must be available for the reaction and thus confirming the proposed mechanism.

For fluorescence intensity measurements to give a direct value of $pK(S_1)$ the acid-base equilibrium must be established within the lifetime of the excited molecule. In the case of 2-naphthol, also studied by Förster, equilibrium is not established before fluorescence occurs.

For the equilibrium

$$BOH + H_2O \rightleftharpoons BO^- + H_3O^+$$

$pK(S_o) = 9.6$. The fluorescence emissions of both forms are present over a wide range of pH values from above 9 to below 3. This is due to the fact that some excited BOH molecules ionise but, before the change is complete and equilibrium is reached, the remaining BOH^* molecules return to the ground state with the emission of their characteristic fluorescence. The $pK(S_1)$ value of the excited state dissociation has been shown to be 2.81[51] showing that 2-naphthol becomes a stronger acid in the excited state.

Weller[51,52,53,54] has developed, on the grounds of the steady state method, a theory in which are correlated the ratios of the fluorescence intensities of the two forms involved in an excited state protolytic reaction at a given pH value and the various rate constants of the several processes open to the two forms. Independent measurement of the natural lifetimes of both species and determination of fluorescence intensity versus pH curves permits the determination of the rate constants of the protolytic reaction. From these values the equilibrium constant can be obtained. This method enables the $pK(S_1)$ to be obtained in cases where the equilibrium is not established in the lifetime of the excited molecule. Since the reaction takes place in a time comparable with the period needed to obtain steady state conditions the steady state theory must be modified to take into account the fraction of molecules which, immediately after excitation, are involved in a protolytic reaction[55]. For example, in the case of an excited state protonation, it is these molecules that have an H_3O^+ within the reaction distance and therefore protonation can be considered to occur as soon as excitation occurs. The full algebraic treatment of the above reaction kinetics is not given here but can be found in a

review[56] and in the original papers of Weller. In the cases studied experimentally in this work the $pK(S_1)$ values obtained from fluorescence intensity measurements have been calculated directly from $[\overset{*}{B}H^+]/[\overset{*}{B}]$ ratios, the validity of the values obtained are discussed in the appropriate section.

$pK(T_1)$: Flash Spectroscopy

Phosphorescence is mainly observed in rigid media and since under these conditions the ground state thermodynamic equilibrium cannot quickly be modified after excitation, it is not, in general, possible to use emission intensity measurements to obtain $pK(T_1)$ in the way that fluorescence intensity is used to give $pK(S_1)$. Recently phosphorescence has been observed from molecules in aqueous solution and quenching reactions have been followed by observation of the emission intensity. The quenching reactions may in fact be due to protonation reactions of the excited state and are discussed in Chapter 4. It is entirely feasible that cases will be found where the protolytic reaction can be studied by phosphorescence intensity measurements of solutions.

Direct determination of $pK(T_1)$ is normally achieved by the method developed by Jackson and Porter[57]. The triplet states of the two species involved in a protolytic reaction are monitored by measurement of their T-T absorption spectra as a function of pH.

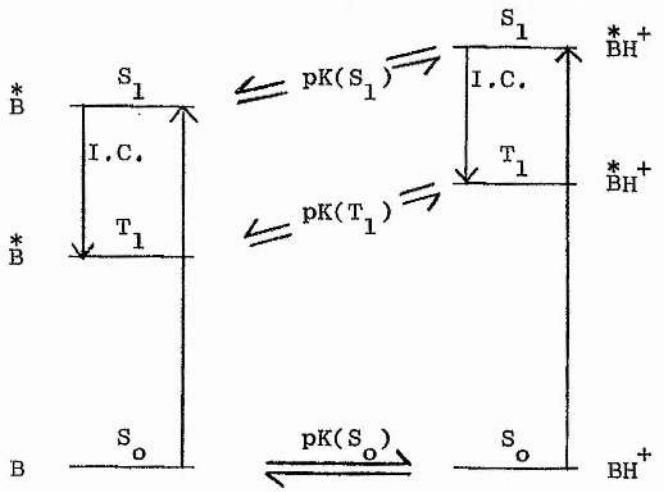

FIG. 1.5 Schematic representation of the processes involved in the flash photolysis determination of $pK(T_1)$.

Consider the possible acid-base equilibria between a base (B) and its protonated form (BH^+). The high intensity photoflash (500 J in our case) excites molecules of both forms to the various singlet states. We need only consider the S_1 state as this is populated after 10^{-13} s by internal conversion from higher levels. The system can now move towards protolytic equilibrium of the S_1 state but at the same time, according to the ratio of intersystem crossing (I.C.) and fluorescence quantum yields of the two species, a fraction of B and BH^+ will cross over from their respective S_1 to T_1 states. Since the lifetime of the triplet states is relatively long, in most cases, the protolytic equilibrium will be established in a time smaller than the natural lifetime of the triplet state[58]. The excitation route of the triplet state is therefore not important nor is the excited singlet state equilibrium, since the T_1 equilibrium is always likely to be established. Since the flash duration (10^{-5} s) is much longer than the S_1 state lifetime, the molecules deactivated by fluorescence will be re-excited and after a few "pumping cycles" a high acid and base triplet state concentration in equilibrium is obtained[59]. The quantity of triplet molecules produced by direct excitation is negligible in comparison.

A spectroflash fired microseconds after the photoflash allows photographic recording of the T-T absorption spectra of both species. Since the lifetime of the S_1 states is comparatively short and the T-T absorption bands for most aromatic compounds are located at longer wavelengths than the S_o-S_1 transitions, the detection of the T-T bands is not hindered by either S_1-S_n or S_o-S_n absorptions. The interpretation of results is similar to that used in the determination of $pK(S_o)$ by absorption spectroscopy[60]. For many cases it is not easy to obtain values for the extinction coefficient of the triplet absorptions but Jackson and Porter[57] have shown that calculations, assuming equal extinction coefficients for the absorptions of the two species, give $pK(T_1)$ values which depend little on this assumption.

For certain acid-base pairs either the acid or basic form shows no detectable T-T absorption in the spectral range and the time resolution available and the $pK(T_1)$ is then taken as the pH value for which the T-T absorption of one of the species is decreased to half its maximum value[61].

This technique is very time-consuming and consequently most $pK(T_1)$ values reported have been obtained by the indirect method which will now be described. The $pK(T_1)$ values obtained by the flash photolysis technique, unlike those from the indirect method, are absolute values of the acidity constants obtained directly at room temperature in aqueous solutions without making any fundamental theoretical assumption. Thus the $pK(T_1)$ values obtained correspond to the $pK(S_1)$ values obtained by the kinetic method developed by Weller.

The Förster Cycle[47,53,56]

The technique known as the Förster Cycle provides a method for determining the difference of pK (ΔpK) between the ground and an excited state. It is primarily used to obtain values of $pK(S_1)$ and $pK(T_1)$ but since the method does not consider whether or not equilibrium is established in the excited state before deactivation, the method can, in principle, be applied to higher energy states than S_1 and T_1. To obtain pK^* values from the Δ pK's obtained, the $pK(S_o)$ value for the reaction under consideration must be known.

This thermodynamic calculation uses the spectroscopically determined energy differences between the ground and excited state of the species involved in a protolytic reaction. The transition from the lowest vibrational level of the ground state to the lowest vibrational level of an excited state (i.e. the 0-0 band) for both the base (B) and the conjugate acid (BH^+) are shown in FIG. 1.6.

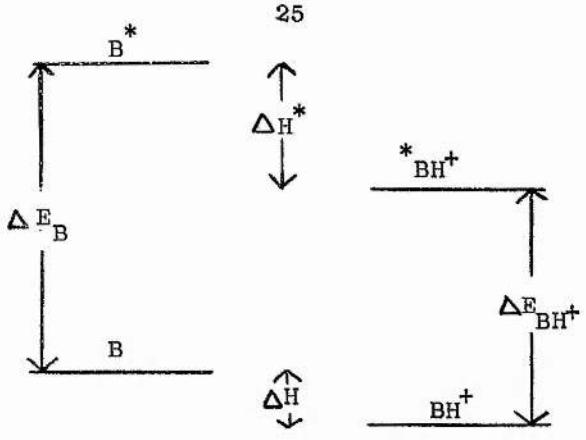

FIG. 1.6 Schematic diagram of the ground state and an excited state of a base and its conjugate acid.

ΔH and ΔH^* are the heats of protonation in the ground and excited state respectively. ΔE_B and ΔE_{BH^+} are the 0-0 energy differences of the two states for the base and its conjugate acid respectively. From FIG. 1.6:

$$\Delta H^* + \Delta E_{BH^+} = \Delta H + \Delta E_B$$

$$\text{or} \quad \Delta H - \Delta H^* = \Delta E_{BH^+} - \Delta E_B \qquad (1.1)$$

But $\Delta H = \Delta G - T\Delta S$ and therefore

$$\Delta H - \Delta H^* = (\Delta G - T\Delta S) - (\Delta G^* - T\Delta S^*)$$

If the entropies of reaction are equivalent in the two states i.e. $\Delta S = \Delta S^*$, then

$$\Delta H - \Delta H^* = \Delta G - \Delta G^*$$

and equation 1.1 becomes

$$\Delta G - \Delta G^* = \Delta E_{BH^+} - \Delta E_B \qquad (1.2)$$

Since $\Delta G^o = -RT \ln K$ equation 1.2 becomes

$$\Delta E_{BH^+} - \Delta E_B = -RT(\ln K - \ln K^*)$$

$$\text{or} \quad pK - pK^* = \frac{\Delta E_{BH^+} - \Delta E_B}{2.303\ RT} \qquad (1.3)$$

The ΔE values are obtained from the spectra of the species involved since $\Delta E = h\nu$, where ν is the 0-0 frequency of the transition. For the excited singlet states the 0-0 energy can be obtained directly from

the absorption or fluorescence spectra if these bands show vibrational structure. In many cases no vibrational structure is observed in either of these bands but an estimate of the position of the O-O transition can be obtained by averaging the absorption and fluorescence maxima[62]. $pK(S_1)$ values can be obtained by application of the Förster Cycle to absorption maxima alone, fluorescence maxima alone, or to O-O frequencies obtained by averaging the two but the values derived may differ significantly.

In the case of the determination of $pK(T_1)$ by application of the Förster Cycle, since the probability of the $S_o \longrightarrow T_1$ transition is extremely small in aqueous solutions absorption measurements are not normally used. The O-O transitions of the base and its conjugate acid are usually estimated directly from the phosphorescence spectra recorded at liquid nitrogen temperature. The usual optical glasses used to record the phosphorescence of different prototropic forms at 77 K are:

Basic Media; ethanol + KOH

Neutral Media; E.P.A. (ether, isopentane, ethanol, 5:5:2 in volume)

Acid Media; H_2SO_4: n-propanol: ethanol (1:10:2 in volume).

In many cases the phosphorescence spectra show no fine structure and estimation of the O-O transition is uncertain. In some cases the above glasses cannot be used, being either too weakly acidic or basic to produce the required prototropic species in the ground state. In these cases other solvents must be used which may not form good optical glasses at 77 K and hence give phosphorescence spectra with poorer resolution making the O-O energy more difficult to determine.

If we substitute $\Delta E = h\nu$ into equation 1.3 we obtain the form of the Förster Cycle most often used.

$$pK - pK^* = \frac{(\nu_{BH^+} - \nu_B)\, h}{2.303\, RT} \qquad (1.4)$$

or

$$\Delta pK = \frac{6.25 \times 10^3}{T} \quad (\bar{\nu})$$

where $\bar{\nu}$ is the frequency difference in cm^{-1}. The inherent assumptions in the Förster Cycle and the difficulties in, and limitations of, its use have been widely discussed and will be considered in Chapter 5.

Experimentally Determined pK^* Values

Table 1.1 shows some well-known values of $pK(S_1)$ for compounds of various types plus some more recently published results. More comprehensive tables of $pK(S_1)$ values can be obtained in the literature[22,31,59,63,64]. Schulman et al[72-76] have investigated the excited state acid-base properties of several heterocyclic and substituted heterocyclic compounds. Similar studies have been reported on phenazine by Grabowska and Pakula[77] and on α,α'-Dipyridyl and 1,10-phenanthroline by Lahiri and Aditya[78]. Leonhardt et al[79] have followed up the work of Lindqvist[58] on fluorescein by an investigation of the acid-base equilibria of fluorescein and 2'-7'-Dichloro-fluorescein in the S_o and S_1 states.

It is evident from Table 1.1 that, in general, $\Delta pK(S_o-S_1)$ is several units large. Weller[56] divides organic compounds into two groups. Acids belonging to Group A: ArOH, Ar $N\langle^{R}_{H}$; Ar $\overset{R}{\underset{H}{N}}H^+$; ArSH

have $pK^* < pK$

whereas those of Group B: Ar COOH; Ar $\overset{R}{\underset{+}{C}}=OH$; Ar $\overset{R}{C}=\overset{R'}{\underset{+}{N}}H$

have $pK^* > pK$.

If, on the other hand, we consider the relative strength of the conjugate bases, a base of the type A (Ar NH_2) becomes a weaker base in the excited state ($pK^* < pK$) whereas bases of the type B (Ar $\overset{R}{C}=O$) become stronger bases in the excited state ($pK^* > pK$). This means that bases of type A we would expect to show a first absorption band at longer wavelengths than their conjugate acid, while the opposite is true for type B.

Less experimental results are available for $pK(T_1)$ and of those the

TABLE 1.1 $pK(S_1)$ values obtained by (1) the Förster Cycle (2) fluorescence intensity measurements.

MOLECULE	REACTION	$pK(S_o)$	$pK(S_1)$	Method	Reference
1-Naphthol	deprotonation	9.23	2.0	1	51
2-Naphthylamine	protonation	4.07	-1.5	2	48
2 Aminoanthracene	protonation	3.4	-4.4	1	61
Acridine	protonation	5.45	10.3	1	65
			10.65	2	65
Acridone	protonation	-0.6	0.92	1	66,67
			2.0	2	66,67
Acetophenone	protonation	-6.0	-1.0	2	68
1-Naphthoic acid	deprotonation	3.7	7.7	1	70
1-Naphthoic acid	protonation	-7.7	2	2	69
2-Naphthoic acid	deprotonation	4.2	6.6	1	70
2-Naphthoic acid	protonation	-7.7	0.7	2	69
9-Anthroic	deprotonation	3.0	6.5	1	61
1-Naphthaldehyde	protonation	-6.6	3.8	1	63
			1.0	2	63
Methyl-1-naphthylketone	protonation	-6.2	5.8	1	63
			1.5	2	63
Phthalide	protonation	-8.0	1.3	1	63
			0	2	63
Anthrone	protonation	-5.0	6.15	1	63
2 Naphthamide	protonation	-2.35	2.47	1	63
			2.5	2	63
			2.79	2	71
2-Aminopyridine	protonation	6.9	9.4	1	72
2-Aminopyridine	Second protonation	-7.6	-19.8	1	72

majority are obtained by the Förster Cycle method. Table 1.2 shows some values of $pK(T_1)$ with $pK(S_o)$ and $pK(S_1)$ values given for comparison. It is evident that in most cases the $pK(T_1)$ value lies much closer to the $pK(S_o)$ value than the $pK(S_1)$ value does. For some time after Jackson and Porter's initial results it was thought that all $pK(T_1)$ values would lie very close to the value of $pK(S_o)$ but several results since have shown $pK(T_1)$ values spread over the $pK(S_o\text{-}S_1)$ range.

Vander Donckt and Porter[61] showed this to be true for anthracence carboxylic acids. For dyes of the thiazine (Thionine, Methylene Blue, Methylene Green, Novomethylene Blue, Azur A, B and C) and azine (safranine and phenosafranine) classes, $pK(T_1)$ differes from $pK(S_o)$ by more than 6 units[83-85]. A major problem when considering dye molecules which have several different sites where protolytic reactions can occur is whether the same equilibrium is being considered in each excited state. It has been suggested[59] that in the case of thionine the site of protonation does not remain the same in the different states and therefore the $pK(S_o)$, $pK(S_1)$, and $pK(T_1)$ values cannot be compared. Grabowska and Pakula[82] report pK values for the second protonation of phenazine which indicate a large $\Delta\ pK(S_o\text{-}T_1)$. No phosphorescence or $S_o\text{-}T_1$ absorption could be detected for the di-protonated species and an estimate of its O-O transition had to be made. The uncertainty in the $pK(T_1)$ obtained was considered to be less than $\pm$ 1.5 pK units, which means that the increase in the $pK(T_1)$ value on excitation was of the same order as that observed in the S_1 state.

The generalisation has been made for $\pi\text{-}\pi^*$ states that

$$pK(S_o) > pK(T_1) > pK(S_1)$$

or

$$pK(S_o) < pK(T_1) < pK(S_1)$$

and that this system of inequalities is independent of the type of $\pi\text{-}\pi^*$ state considered[61]. Several approaches have been used to obtain an understanding of these pK differences. Murrell[11] put forward an explanation based on the charge transfer theory. The hydroxyl group, for example, is

TABLE 1.2 pK values for aromatic compounds in the S_o, S_1, and T_1 states.

$pK(T_1)$. 1. Values obtained by Förster Cycle

$pK(T_1)$. 2. Values obtained by flash photolysis

Molecule	Reaction*	$pK(S_o)$	$pK(S_1)$	$pK(T_1)$ 1	$pK(T_1)$ 2	Reference
2-Naphthol	D	9.5	3.0	7.7	8.1	57
1-Naphthoic acid	D	3.7	7.7	4.6	3.8	57
2-Naphthoic acid	D	4.2	6.6	4.2	4.0	57
1-Anthroic	D	3.7	6.9		5.6	61
2-Anthroic	D	4.2	6.6		6.0	61
9-Anthroic	D	3.0	6.5		4.2	61
Quinoline	P	4.9		5.6	6.0	57,82
Acridine	P	5.5	10.6	5.4	5.6	57,82
2-Naphthylamine	P	4.1	-2	3.1	3.3	57
N,N-dimethylaniline	P	4.9		2.9	2.7	57
2-Aminoanthracene	P	3.4	-4.4		3.3	61
o-Phenanthroline	P	4.85	11.4	6.7		75,80
o-Phenanthroline-H^+	P	-1.4	-0.1	3.8		75,80
Phenol	D	10	4.0	8.5		31
4-bromophenol	D	9.3	3.1	7.7		31
4-methoxyphenol	D	10.2	5.6	8.6		31
4-nitrophenol	D	10.46	-4.0	9.2		81
6-nitroquinoline	P	2.10	4.4	2.1		81
Phenazine	P	1.2	6.0	4.0		82
Phenazine-H^+	P	-4.3	4.1	5.7		82
Thionine-H^+	P	0	9	6.3		83,84

* In this column D $\equiv$ deprotonation reaction
P $\equiv$ protonation reaction
but pK still always refers to the acid strength of BH^+.

an electron donor, so that any contributions of the charge transfer structure

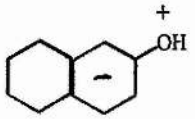

in the excited state will increase their acidity. The charge transfer state would lie at higher energy than the singlet or triplet, but since the amount of mixing is dependent on the energy gap between the two states it will always be greater for the singlet state which lies at higher energy. This theory explains the direction of the inequalities but fails to explain why the $pK(T_1)$ is often very similar to that of the ground state although detailed calculations for aniline have indicated that the contribution of charge transfer to the first singlet state is 17% whereas it is only 4% to the first triplet[8]. Jackson and Porter suggested, on the basis of spin correlation considerations that the relative contribution of the CT structures compared with the diradical structures would be greater in the S_1 than in the T_1 state.

The resonance theory has also been applied to explain ΔpK values. $\Delta pK(S_o-S_1)$ for phenols and aromatic amines have been found to be greater than 6 units while the values for dissociation of aromatic carboxylic acids have been only 2-3 units (See Table 1.2). The former compounds all have a resonance formula in which there is a net charge on the actual site of the protolytic reaction.

For carboxylic acids the resonance structure has a negative charge on the oxygen of the carbonyl group and thus only effects the OH acidity indirectly. From these structures it is easy to see why the amino group will be a weaker base in the excited state and that the carbonyl group (including that of carboxylic acid) will be affected in the opposite direction.

3. Introduction to the Experimental Investigation

In an attempt to characterise the proton-donating ability of strongly acidic solutions Hammett and Deyrup[86] introduced a logarithmic term, similar to pH, and called it the acidity function H_o. Referring to the protonation of a base B

$$B + H^+ \rightleftharpoons BH^+$$

H_o is defined as

$$H_o = - \log \frac{a_{H^+} \quad f_B}{f_{BH^+}}$$

$$= pK_{BH^+} - \log \frac{C_{BH^+}}{C_B} \qquad (1.5)$$

where a_i, f_i and c_i are the activity, activity coefficient, and concentration of species i and $pK_{BH^+} = -\log K_{BH^+}$ where

$$K_{BH^+} = \frac{a_B \quad a_{H^+}}{a_{BH^+}} \qquad (1.6)$$

Hammett used a series of weak organic bases, mainly nitro anilines, and measured the variation of the indicator ratio $[BH^+]/[B]$ with increasing acidity. By using indicators which protonate at different acidities and defining the slope of the graph of $\log_{10} \frac{[BH^+]}{[B]}$ against H_o as unity, a complete acidity scale was evaluated up to 100% sulphuric acid. The scale was anchored in the pH range by the most basic compound 4-nitroaniline.

The Hammett treatment assumes that the ratio of activity coefficients for the conjugate acid and its neutral base, f_{BH^+}/f_B is only a function of the solvent; i.e. at an acidity in which two of the indicators overlap

$$\frac{f_{BH_1^+}}{f_{B_1}} = \frac{f_{BH_2^+}}{f_{B_2}}$$

and

$$pK_a^1 - pK_a^2 = \log_{10} I_1 - \log_{10} I_2 \qquad (1.7)$$

where I is the indicator ratio $[BH^+]/[B]$.

Primary anilines were used up to 65% sulphuric acid and then a tertiary amine followed by ketones. Hammett observed that the indicators used above 65% H_2SO_4 did not obey equation 1.7 and suggested it was due to

the medium effect on the spectra. Paul and Long[87] questioned the activity coefficient postulate, suggesting that it was not valid for different classes of compounds but satisfactory for compounds of similar structure. Jorgenson and Hartter[88] have established an acidity function H_o', using only primary anilines, which deviates at high acidities to more negative values than the original H_o scale.

Other acidity scales for sulphuric acid have been obtained using similar methods but different classes of compound.

1. Tertiary Amines (H_o''')[89]
2. Amides (H_A)[90]
3. Indoles (H_I)[91]
4. Benzophenones (H_B)[92]
5. Triphenylcarbinols (J_o)[93]
6. Carbon Bases (azulenes, diarylethylenes and aromatic polyethers) (H_c)[94,95]

All the acidity functions for different classes of compounds are different (See FIG. 1.7). Similar behaviour to that in sulphuric acid has been observed in other strong acids[96].

Hopkinson and Wyatt[63] tested the applicability of acidity scales to the excited state protonation of weak bases by determining the ground state pK_{BH^+} values of several fluorescent bases and also obtaining $pK_{BH^+}^*$ values of the S_1 state by Förster Cycle calculations and by fluorescence intensity measurements. The fluorescence intensity measurements were not precise enough to determine $pK_{BH^+}^*$ directly to better than half a unit, but for some compounds a comparison could be made between this value and that calculated (Förster Cycle) from the ground state pK_{BH^+}, which depends upon the chosen scale of acidity. If the assumption is made that both methods for $pK_{BH^+}^*$ determination should give the same value then the deviations observed, if any, can be attributed to failure of the acidity scale. The ground state pK_{BH^+} value depends upon a chain of indicators, while the Förster Cycle $pK_{BH^+}^*$ goes straight to the energy difference and may span

FIG. 1.7 Acidity Functions

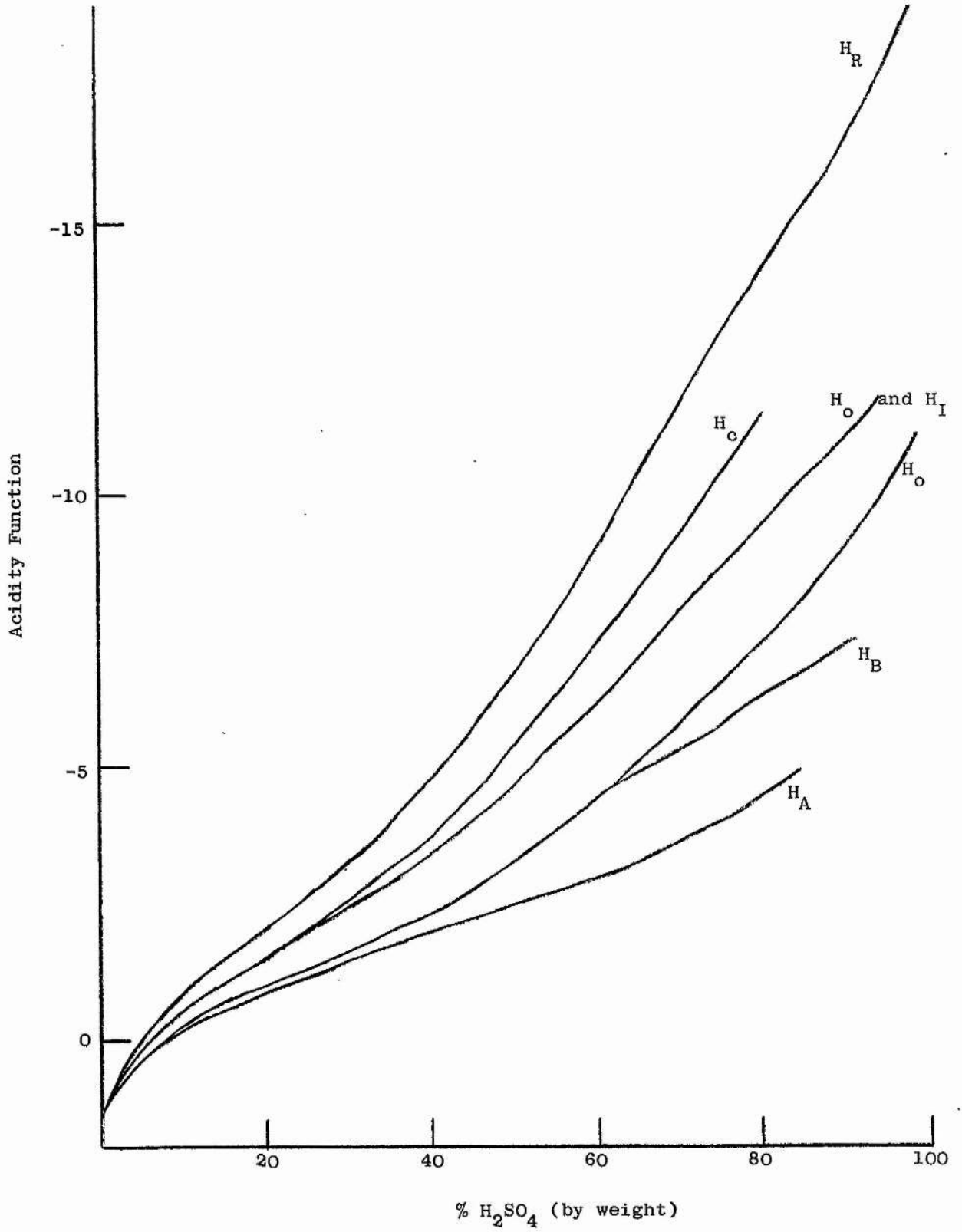

several log a_{H^+} units in one step. Hopkinson and Wyatt concluded that for some compounds the existing acidity scales gave reasonable agreement for the two pK_{BH^+} values but that for others a different acidity scale was appropriate to the excited molecule.

The kinetics of excited state protolytic equilibria in aqueous solution in the pH range have been well established by Weller. In order to follow up the work of Hopkinson[97] and to examine the kinetics of excited state reactions in concentrated acid media, an investigation of some triarylmethanes and fluorescein dyes was initiated. Qualitative investigation of fluorescein and several of its substituted derivatives indicated that the excited state processes were complicated by the many possible sites of protonation and by the equilibrium between the lactone (L) and quinoid (Q) forms of the dyes.

Xanthone was therefore chosen as a model compound for this system.

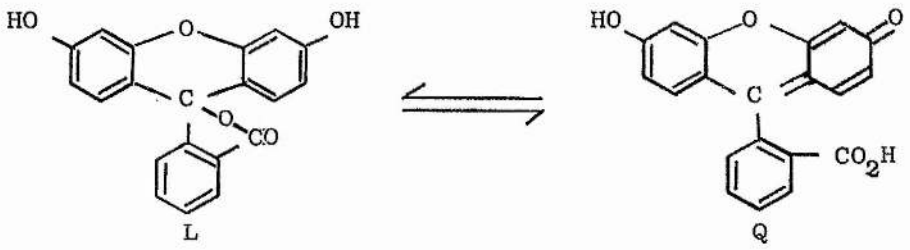

Fluorescein

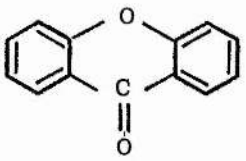

Xanthone

The possible protonation sites are reduced to two with xanthone: the carbonyl oxygen; and the bridging ether oxygen. Experimental results showed xanthone to have interesting photochemical properties which led to a study of other aromatic carbonyl compounds.

CHAPTER 2

EXPERIMENTAL TECHNIQUES

1. General Techniques

The sources of the compounds studied and any special purification procedures used on them are listed in Appendix I. The acids and inorganic chemicals used in the spectral work were of Analytical reagent grade. Water was purified by distillation from alkaline permanganate using a 4ft fractionating column and for ethanol Parker's[22] method of purification was used. Other solvents were either of analar or spectroscopic grade.

Fluorescence and phosphorescence measurements are used as analytical methods because of the low concentrations that can be detected. The degree of purity, therefore, of the specimens and the cleanliness of the general glass apparatus used must be high. The hazards encountered and the precautions to be taken have been recorded[22,98] and found to be useful guides in this work.

The pH values of solutions $> 10^{-2}$ M in acid were calculated from the acid concentration by titration with standard alkali: for solutions of pH > 2 a Radiometer PHM 26 pH meter was used. The main buffer mixtures used were as follows: $HClO_4$ + CH_3CO_2Na for pH 2 to 4; CH_3CO_2H + CH_3CO_2Na for pH 4 to 7; KH_2PO_4 + NaOH for pH 7 to 10.

In a particular case a check was always made to ensure that any of the buffering molecules or ions were not themselves affecting the system being studied.

Strongly acidic solutions were prepared by diluting weighed amounts of 98% H_2SO_4 or 60-70% $HClO_4$ which had been previously standardised by dilution and titration with standard alkali.

2. Ground-State Absorption Spectroscopy

Absorption spectra were recorded on either a Unicam SP 500 or a Unicam

SP 800 Spectrophotometer. The SP 800 was used, in general, to obtain continuous absoption curves vs. wavelength while with the more precise SP 500 optical densities at a set wavelength were measured. Thus the SP 500, which had temperature control facilities, was used to measure the pK's of protonation reactions in the ground state and the optical densities of solutions used in quantum yield determinations. Quartz cells were used in all measurements. The blank solutions to which the sample absorbance was compared were, as far as possible, an exact sample of the solution without the particular solute of interest.

Continuous spectra are reported as optical density against wavelength at a given absorber concentration. In cases where the wavelength of maximum absorbtion is reported the molar extinction coefficient at that wavelength is also given. The extinction coefficients are quoted without units. The units are cm^{-1} mol^{-1} l which can be converted into SI units, m^2 mol^{-1} by multiplying by 10 .

3. Emission Spectroscopy

The measurement and correction of fluorescence and phosphorescence emission and excitation spectra.

(a) General Description of Spectrophotometer

The emission spectra were obtained using a Perkin Elmer Hitachi MPF-2A Spectrophotometer[99]. The spectrometer includes two grating monochromators: one for irradiating a sample with monochromatic light in the 200 to 700 nm range (excitation monochromator); the other for permitting selective measurement of the intensity of light emitted by the sample in the 200 to 800 nm range (emission monochromator). The source is a 150 watt Xenon lamp. Before dispersion at the excitation monochromator the light beam is split and a portion deflected on to a reference photomultiplier where a reference signal is produced. This reference signal is used in the ratio recording mode to correct for

source intensity fluctuation. The portion of the beam which is not deflected by the splitter is dispersed and the light focused on the sample. Light emitted by the sample is directed into the emission monochromator and after dispersion focused on to the sample photomultiplier, producing a signal proportional to the emission intensity which is amplified and passed to the recorder.

(b) Sampling Techniques

Emission from fluid solutions

Dilute solution emission was normally measured in the controlled temperature cell holder accessory of the MPF-2A. The fluorescence cell was allowed to equilibrate and the emission detected at right angles to the incident light. The temperature was controlled using a Grants water bath and could be varied between 0° and $80^{\circ}C$. The temperature was stable (inside the fluorescence cell) to $\pm$ $0.1^{\circ}C$ at or near room temperature but the error range increased as the required temperature deviated from room temperature. Continuous spectra were run using the reference mode of the MPF-2A although in cases where a series of measurements was being taken a reference solution was also used. This reference was either a solution of the compound being studied (if stable) or a sample of quinine sulphate in 0.5 M H_2SO_4. The intensity of emission from the reference was measured immediately before that of the sample and all sample measurements could then be corrected to the same light intensity. Solutions were normally dilute enough to avoid inner filter effects but if this were not so corrections were made using the method of Parker[100].

Two methods were employed to remove dissolved oxygen from the solutions being studied (a) replacing oxygen with nitrogen by nitrogen bubbling or by a freeze/thaw technique over a nitrogen atmosphere; (b) degassing by a freeze/thaw process and keeping the solution under vacuum during measurement. Method (b) was the method used to look at phosphorescence emission from fluid solution, e.g. that of benzophenone in water. The

apparatus used is shown in FIG. 2.1. The solution is degassed in the Pyrex bulb and then transferred to the quartz tube which fits into an adapted cell compartment of the variable temperature unit and the emission intensity is then measured.

For rapid measurement of fluorescence quenching reactions the apparatus shown in FIG. 2.2 was designed. This has the correct dimensions to fit into the phosphorescence attachment of the MPF-2A. A solution of the fluorescent solute was placed in the cell and the initial intensity measured. The cell was removed and a portion of a solution of quencher, which contained the same concentration of solute, thus keeping the overall solute concentration constant, was added from a micro-burette. The mixture was shaken, the cell replaced and the intensity measured. This was repeated until the required concentration of quencher had been added. The results using this method were in agreement with those obtained using separate solutions for each quencher concentration, but using this method no temperature control could be obtained. Temperature controlled studies of quenching reactions had to be carried out by the more tedious single solution method. This method and apparatus were also used to study the effects of acid concentration on the emission intensity of a solute. Weighed amounts of acid were added instead of quencher. Again there was no temperature control and a further difficulty was the heat of mixing the acid, which had to be minimised. The original design of the above apparatus had three Quickfit cones in the top, two of which were fitted with pH electrodes while the other was used for addition of acid or base to alter the pH in qualitative studies of the effect of pH change on emission intensity.

Emission from very concentrated solutions cannot be measured using the normal cell arrangement of the MPF-2A. Frontal illumination is the best method for observing the fluorescence emission spectra of concentrated solutions[22]. This was achieved on the MPF-2A using the solid sampler accessory which had been adapted to hold a 1 mm pathlength quartz cell.

FIG. 2.2 Equilibrium cell for studying quenching reactions

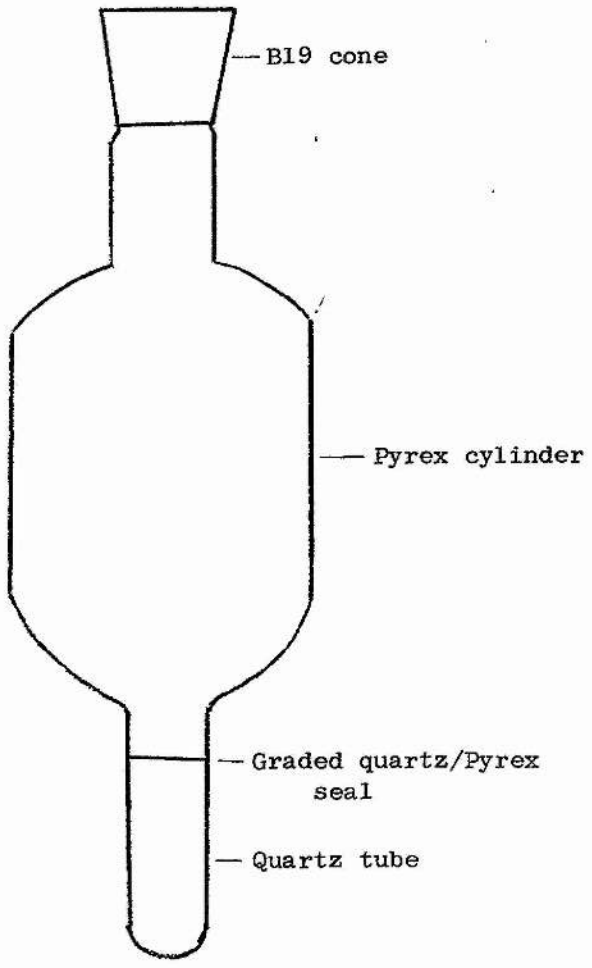

FIG. 2.1 Degassing cell

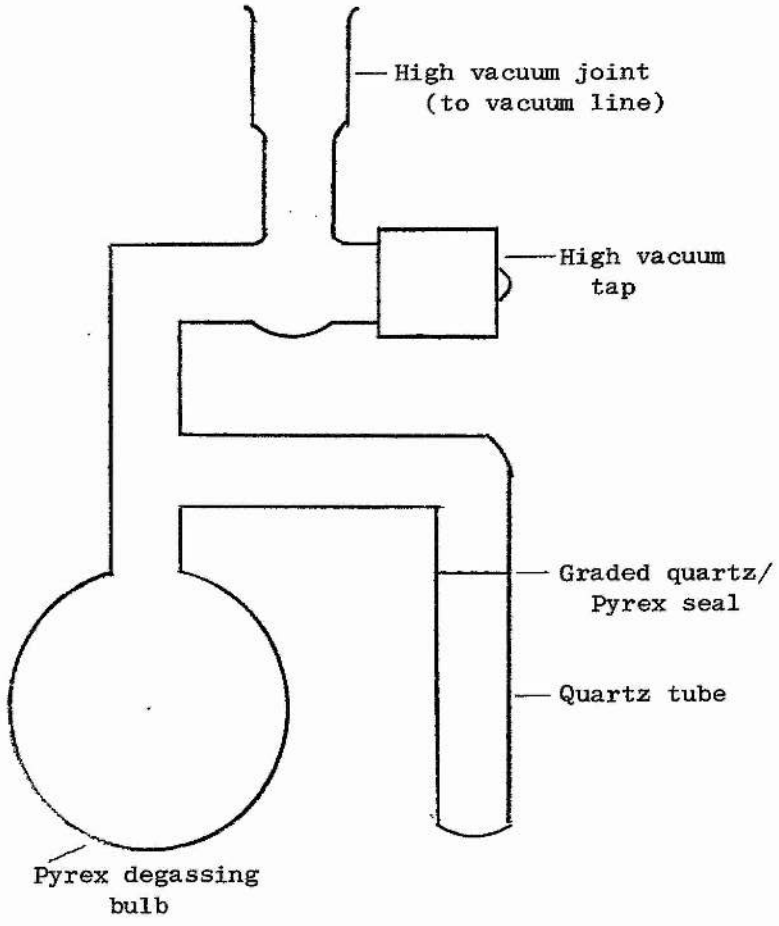

The cell is held at an angle of 30° to the incident beam and the emission from the front surface of the cell is detected.

Emission from solid solutions at low temperature

Phosphorescence and total emission spectra at 77 K were obtained using the phosphorescence accessory of the MPF-2A. Total emission spectra (fluorescence and phosphorescence) were obtained by right-angled optics, the sample being contained in a quartz tube which fitted into the Dewar flask containing lqiuid nitrogen, with the chopper removed from the unit. Using the chopper the fluorescence was cut off because of its short lifetime and the phosphorescence spectrum alone was obtained. The most suitable solvents for this type of measurement are those which form perfect clear glasses at low temperature but, unfortunately, only a few solvents and solvent mixtures do this[101]. Many of the acidic solutions used in this work form on freezing cracked glasses or opaque solids which make quantitative measurements impossible. The amount of incident light reflected from the sample is dependent on the extent of cracking and thus the emission intensity is very sensitive to the position of the sample tube relative to the incident beam. It is possible to obtain the emission spectrum, although in many cases the resolution is not good, but it is not possible to make quantitiative measurements of the intensity. This makes quantum yield determinations in these cases impossible. The amount of light scattered from these solid solutions is sometimes very high and can interfere with the measurement of the total luminescence spectrum, although this does not affect the measurement of phoshporescence spectra as the scattered light is cut off by the chopper

(c) Correction of Excitation Spectra

Experimentally the excitation spectrum of a solution is obtained by setting the emission monochromator at, or near, the wavelength of maximum emission intensity and then scanning lower wavelengths with the excitation

monochromator. The intensity of fluorescence is plotted against the wavelength of exciting radiation. This uncorrected excitation spectrum depends on the characteristics of the instrument and may be a grossly distorted version of the absolute spectrum. It can easily be shown[22] that the experimentally obtained excitation spectrum is a function of the molar extinction coefficient, $\varepsilon(\lambda)$, the quantum efficiency of the solution emission, ϕ_f, and the radiative output, $I(\lambda)$, of the excitation source, i.e. the photomultiplier output, $P(\lambda)$, may be expressed as:

$$P(\lambda) \propto I(\lambda).\ \varepsilon(\lambda).\ \phi_f \qquad (2,1)$$

$I(\lambda)$ is dependent on the nature of the source and the characteristics of the monochromator. The quantitiy $\varepsilon(\lambda)\ \phi_f$ is a fundamental characteristic of the solution and a plot of $\varepsilon(\lambda)\ \phi_f$ against wavelength gives the absolute excitation spectrum. Since for many compounds ϕ_f is independent of the excitation wavelength the true excitation spectrum is, in these cases, identical in profile to the absorption spectrum. To obtain the true excitation spectrum from the recorded curve, the variation of $I(\lambda)$ with wavelength must be determined i.e. it is necessary to determine the relative energy distribution of the source. Several methods have been used to obtain this function and can be classified as follows:

(a) use of the ferrioxalate actinometer[102];

(b) photographic methods[103];

(c) calibrated phototubes[104];

(d) thermophiles[22];

(e) fluorescent screen quantum counters[105].

The method used in this work was that described by Argauer and White[106], a variation of method (e) using a dilute fluorescent solution.

This method utilises the fact that the absorption spectrum and the true excitation spectrum of a compound, which has a constant quantum yield over the wavelengths scanned, are identical and thus a comparison of the uncorrected excitation spectrum with the absorption spectrum should give a measure of the relative spectral intensity of the excitation source. The

compound used must have a constant quantum yield with change in excitation wavelength and to be useful for this method must have a broad absorption band and an appreciable absorbance at all wavelengths. Also the fluorescence of the compound should be at least 25 nm longer than the longest wavelength calibration desired. After studying a number of compounds Argauer and White found that the Aluminium chelate of 2,2'-dihydroxy-1,1'-azo-naphthalene-4-sulphonic acid (PBBR) sodium salt was satisfactory.

Experimental

PBBR was obtained from B.D.H. (Solochrome Dark Blue C.I. 15705) and used without further purification. The ethanol used was purified by distillation from KOH. The chelate was prepared as follows: 40 ml of 0.01% PBBR in ethanol was added to 16.5 ml of 0.05 M $AlCl_3.6H_2O$ in ethanol. The mixture was diluted to 250 ml and allowed to stand for 30 mins before use. The absorbance was determined from 235 nm to 600 nm on a Unicam SP800 spectrophotometer. To avoid distortion of the recorded excitation spectrum, due to the inner filter effect the above solution had to be diluted before the excitation spectrum was measured: 2 ml was diluted to 25 ml and the excitation spectrum recorded from 235 nm to 600 nm. FIG. 2.3 shows the absorption and uncorrected excitation spectra of the Al-PBBR chelate. Table 2.1 records the absorbance (B) and excitation values (A) at 5 nm intervals. A divided by B gives the relative quantum distribution of the excitation source which is shown in FIG. 2.5 converted into energy units and normalised.

For compounds with absorption in the range 235 nm to 600 nm the true excitation spectrum is obtained by dividing the uncorrected excitation spectrum by the correction factors shown in TABLE 2.1, i.e. excitation correction factor = A/B = $C_{ex}(\lambda)$ $\therefore$ Corrected excitation spectrum = Apparent excitation spectrum/$C_{ex}(\lambda)$. FIG. 2.4 shows the absorption spectrum and uncorrected and corrected excitation spectra of quinine sulphate in 0.5 M H_2SO_4. The absorption curve of quinine sulphate shows

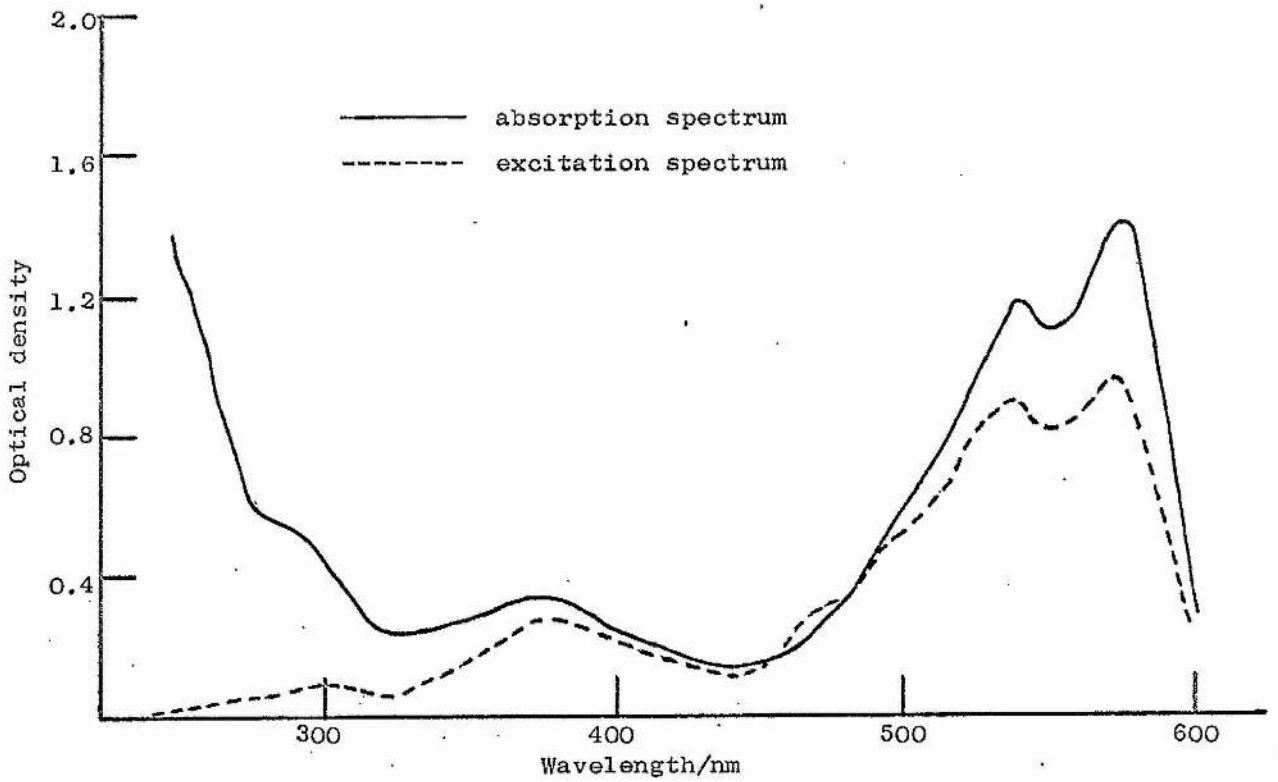

FIG. 2.3 Absorption and uncorrected excitation spectra of Al-PBBR chelate.

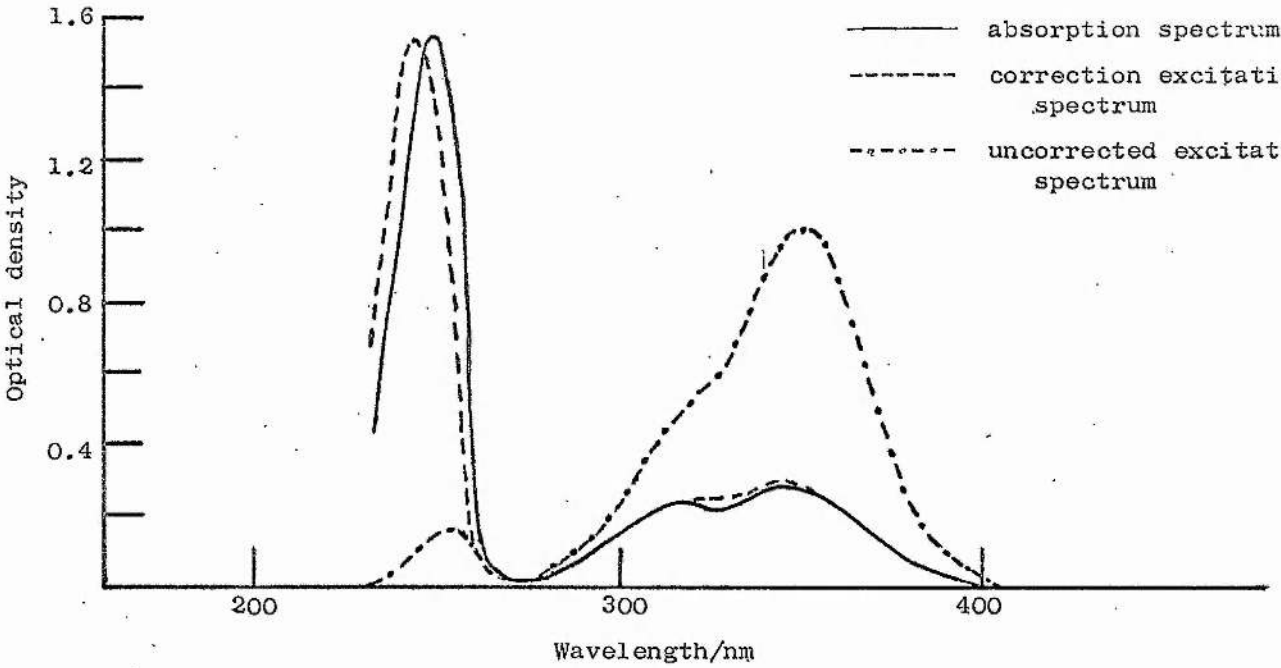

FIG. 2.4 Absorption and excitation spectra of quinine sulphate in 0.5 M H_2SO_4

FIG. 2.5 Relative energy distribution of the xenon lamp of the MPF-2A spectrophotometer.

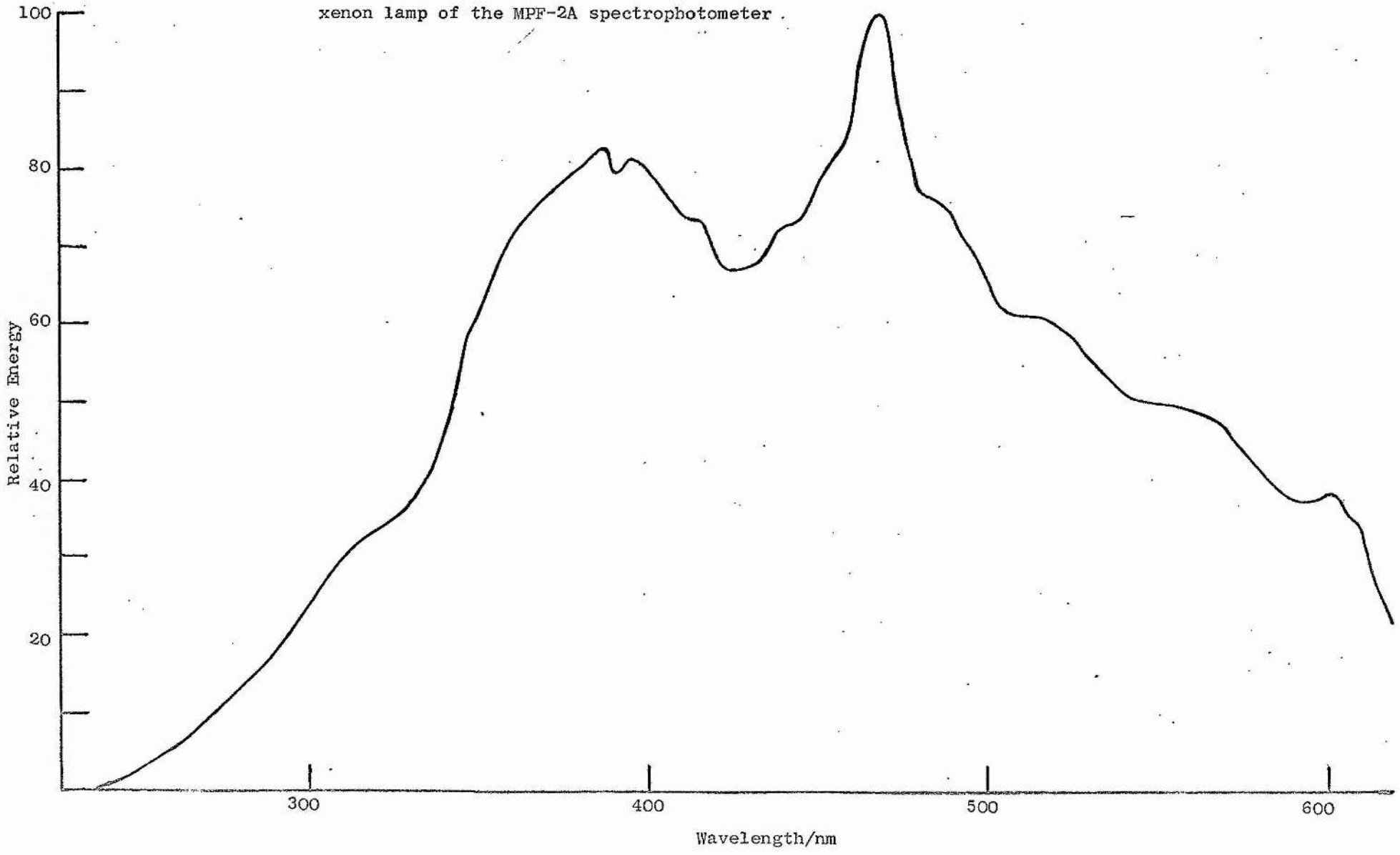

TABLE 2.1 Excitation Correction Factors

A: Excitation values for PBBR - aluminium chelate as recorded on MPF-2A

B: Absorbance of PBBR – aluminium chelate

C_{ex}:A/B, excitation correction factors.

WAVELENGTH (nm)	B	A	C_{ex}	Wave-length (nm)	B	A	C_{ex}	Wave-length (nm)	B	A	C_{ex}
235	1.86	0.12	0.07	380	0.33	5.35	16.26	525	0.94	15.50	16.49
240	1.58	0.20	0.13	385	0.31	5.27	17.06	530	1.06	16.95	15.99
245	1.44	0.25	0.17	390	0.30	5.00	16.67	535	1.15	17.65	15.38
250	1.34	0.45	0.34	395	0.29	4.95	17.37	540	1.17	17.65	15.09
255	1.24	0.65	0.52	400	0.26	4.45	17.12	545	1.13	16.90	14.96
260	1.07	0.83	0.78	405	0.23	3.85	16.60	550	1.09	16.15	14.89
265	0.91	0.90	0.99	410	0.22	3.57	16.30	555	1.09	16.10	14.77
270	0.74	0.97	1.31	415	0.21	3.45	16.51	560	1.13	16.80	14.87
275	0.60	1.00	1.67	420	0.20	3.10	15.50	565	1.21	17.70	14.63
280	0.56	1.05	1.89	425	0.18	2.75	15.28	570	1.32	18.80	14.30
285	0.56	1.30	2.34	430	0.16	2.50	15.63	575	1.39	19.10	13.74
290	0.55	1.50	2.75	435	0.15	2.40	16.00	580	1.34	17.50	13.06
295	0.50	1.60	3.32	440	0.15	2.49	17.17	585	1.18	14.65	12.42
300	0.43	1.62	3.77	445	0.15	2.53	17.45	590	0.92	10.85	11.79
305	0.39	1.70	4.42	450	0.15	2.75	18.97	595	0.62	7.45	12.62
310	0.33	1.65	5.00	455	0.16	3.15	19.94	600	0.37	4.60	12.43
315	0.26	1.40	5.39	460	0.18	3.75	20.95				
320	0.24	1.39	5.79	465	0.21	5.00	24.39				
325	0.24	1.45	6.04	470	0.25	6.20	25.31				
330	0.24	1.60	6.58	475	0.29	6.15	21.58				
335	0.26	1.90	7.36	480	0.33	6.45	19.85				
340	0.26	2.25	8.59	485	0.39	7.70	20.00				
345	0.27	2.70	10.00	490	0.46	8.65	18.80				
350	0.28	3.20	11.41	495	0.53	9.90	18.68				
355	0.29	3.70	12.63	500	0.58	10.20	17.59				
360	0.31	4.15	13.61	505	0.63	10.65	16.99				
365	0.32	4.65	14.53	510	0.67	11.30	16.82				
370	0.33	5.00	15.06	515	0.73	12.35	16.92				
375	0.33	5.25	15.81	520	0.83	14.00	16.97				

strong absorption of 249 nm and much less at 349 nm. The experimentally obtained excitation curve has a maximum near 349 nm because of the low intensity of exciting light at the shorter wavelengths, but correction of this curve gives a good representation of the absorption spectrum.

The above correction factors have now been incorporated in a computer programme which is described later.

(d) Correction of Emission Spectra

Absolute emission spectra relate the quantum intensity (in quanta per unit wavenumber interval) to wavenumber (in cm^{-1}). If Q represents the total number of quanta (of all wavenumbers) emitted by the solution per unit time, then $dQ/d\bar{\nu}$ represents the intensity at a wavenumber $\bar{\nu}$ and the plot of $dQ/d\bar{\nu}$ against $\bar{\nu}$ is the true luminescence emission spectrum. Few spectrofluorimeters measure this directly; most provide an apparent emission curve which is obtained by setting the excitation monochromator at a wavelength at which the sample absorbs and scanning longer wavelengths with the emission monochrmator. The observed photomultiplier output ($A_{\bar{\nu}}$) must therefore be corrected for variation in the photomultiplier sensitivity, the dispersions of the emission monochromator, and light losses. Thus $A_{\bar{\nu}}$ is given by:

$$A_{\bar{\nu}} = (dQ/d\bar{\nu})(S_{\bar{\nu}}) \qquad (2.2)$$

where $S_{\bar{\nu}}$ is the spectral sensitivity factor of the monochromator-photomultiplier combination. This spectral sensitivity curve may be obtained in various ways[106-109] by taking measurements:

(a) using a calibrated tungsten lamp source (for the visible region);

(b) using a fluorescent screen monitor for the u/v region;

(c) using a thermopile;

(d) using fluorescent solutions which function as quantum counters;

(e) using reference fluorescent solutions, the absolute fluorescence spectra of which have been previously determined.

Method (e) was used in this work. If the absolute fluorescence emission spectrum has been determined precisely for a series of compounds that emit over the range for which a spectral sensitivity factor is required, then measurement of the uncorrected emission spectrum of these compounds with the instrument to be calibrated permits direct calculation of $S_{\bar{\nu}}$ by application of equation 2.2. $dQ/d\bar{\nu}$ now represents the known spectral distribution of one of the standard compounds and $A_{\bar{\nu}}$ the observed readings. The compounds must be free from fluorescent impurities and their fluorescence spectrum must be obtained under the conditions stipulated for the standard fluorescence curve. Quinine sulphate in dilute sulphuric acid and anthracene in ethanol have been widely used but have only a limited usable wavelength range. Lippert et al[107] have measured the corrected emission spectra of five compounds that together cover almost the entire visible region of the spectrum. Lippert used a prism instrument and front surface illumination of relatively concentrated solutions. Argauer and White[104], using dilute solutions and right angle illumination, found that β-naphthol showed a changed in spectral shape on dilution and is therefore not a satisfactory standard under these conditions. They found the other compounds (quinine sulphate, 3-aminophthalimide, m-nitro-dimethylaniline, and 4-dimethylamino-4'-nitro-stilbene) satisfactory for right-angle measurement in dilute solutions.

With the use of the emission spectrum of the aluminium chelate of 2,2'-dihydroxy-1,1'-azonaphthalene-4-sulphonic acid (PBBR), which Argauer and White also recommend, this gives standard compounds which cover in all the range 400-750 nm. In addition Eisenbrand and Hauprich[110] have reported the fluorescence emission curve of p-(dimethylaminobenzylidene) hippuric acid which covers the region of 488 to 614 nm in dioxane and 527 to 800 nm in N,N-dimethylformamide and Rusakowicz and Testa[111] have reported 2-aminopyridine as a standard for the range 300 to 400 nm. Therefore using this general method it is possible to obtain a spectral sensitivity curve for the range 300 to 800 nm.

The uncorrected spectrum recorded using a grating monochromator, to analyse the emission, is linear in wavelength and it is simpler to calculate the corrected spectrum on a wavelength basis. In this case the spectral sensitivity curve, S_λ , is obtained by comparing the apparent and absolute spectra of the standards on a wavelength basis.

Experimental

The six compounds listed in TABLE 2.2 were used to obtain a spectral sensitivity curve for the Perkin Elmer (Hitachi) Spectrophotometer over the range 300-750 nm.

TABLE 2.2

Compounds used to obtain spectral sensitivity curve

	COMPOUND	SOLVENT	CONC. (M)	EXCITATION w/l (nm)	RANGE (nm)	ABSOLUTE SPECTRUM REF.
A	2-Aminopyridine	0.05 M H_2SO_4	1.3×10^{-5}	285	300-450	111
B	Quinine Sulphate	0.05 M H_2SO_4	1.1×10^{-5}	366	400-550	106
C	3-Aminophthalimide	0.05 M H_2SO_4	6×10^{-6}	390	450-630	106
D	N,N-Dimethyl-m-nitroaniline	30/70 benzene/hexane	1.4×10^{-4}	390	470-650	106
E	Aluminium PBBR chelate	95% Ethanol	3×10^{-6} PBBR 2.5×10^{-4} $AlCl_3 6H_2O$	390	580-700	106
F	4-Dimethylamino-4'-nitrostilbene	o-dichloro-benzene	8×10^{-6}	470	600-750	106

These compounds were obtained commercially. All except E were recrystallised not less than five times from recommended solvents[112], and their purities checked by melting point determinations and carbon and hydrogen analysis. PBBR (2,2'-dihydroxy-1,1'-azonaphthalene-4-sulphonic acid) was used as obtained; (a T.L.C. showed only one component). The absorption spectrum of the aluminium chelate was identical to that reported[106].

Unfortunately Argauer and White[106] give no details of the excitation wavelengths used with their standard compounds. Theoretically the excitation wavelength should not affect the shape of the emission band but deviations were found to be marked in the case of quinine sulphate. The excitation

wavelength finally used (i.e. 366 nm) was that used by Lippert et al[107]. The concentrations of solutes used were checked to show that dilution did not affect the band shape.

In order to determine the effect of different excitation and emission slit widths on the spectral sensitivity curve, the apparent fluorescence curves for the six standard compounds were determined at various slit width settings. The procedure followed was to prepare a fresh solution of the standard as described in Table 2.2 and then allow a sample of this solution to equilibrate in the constant temperature accessory of the spectrophotometer (all spectra were recorded at 25 ± 0.1°C). The slit widths were set to the required values, the instrument was set to zero using the reference mode and the emission intensity measured every 10 nm within the required range. A blank reading was then obtained by placing a cell containing only the solvent in the same cell position and measuring the intensity at the same intervals. The intensity of the blank was subtracted from the intensity of the sample to give the apparent emission curve of the compound. The apparent and corrected emission curves of the six standard compounds are shown in FIG. 2.6

Apparent emission curves of the six standard compounds were obtained at eleven slit width settings. The excitation and emission slits used were respectively 2:2, 4:2, 10:2, 16:2, 32:2, 4:4, 10:4, 32:4, 8:8, 10:8, and 16:8 (nm). The data for the apparent and the absolute spectra were then transferred onto punched cards and used as the input in a computer program (CALIB See Appendix II) which calculated the relative spectral sensitivity curve. The program obtains relative sensitivity factors at 10 nm intervals for each compound by dividing the apparent curve by the absolute curve. Since the emission curves of the compounds overlap, the sensitivity factors overlap. The sensitivity factors for each compound were normalised at an arbitrary wavelength within the regions of overlap. A and B were normalised at 410 nm, C to A and B at 480 nm, D

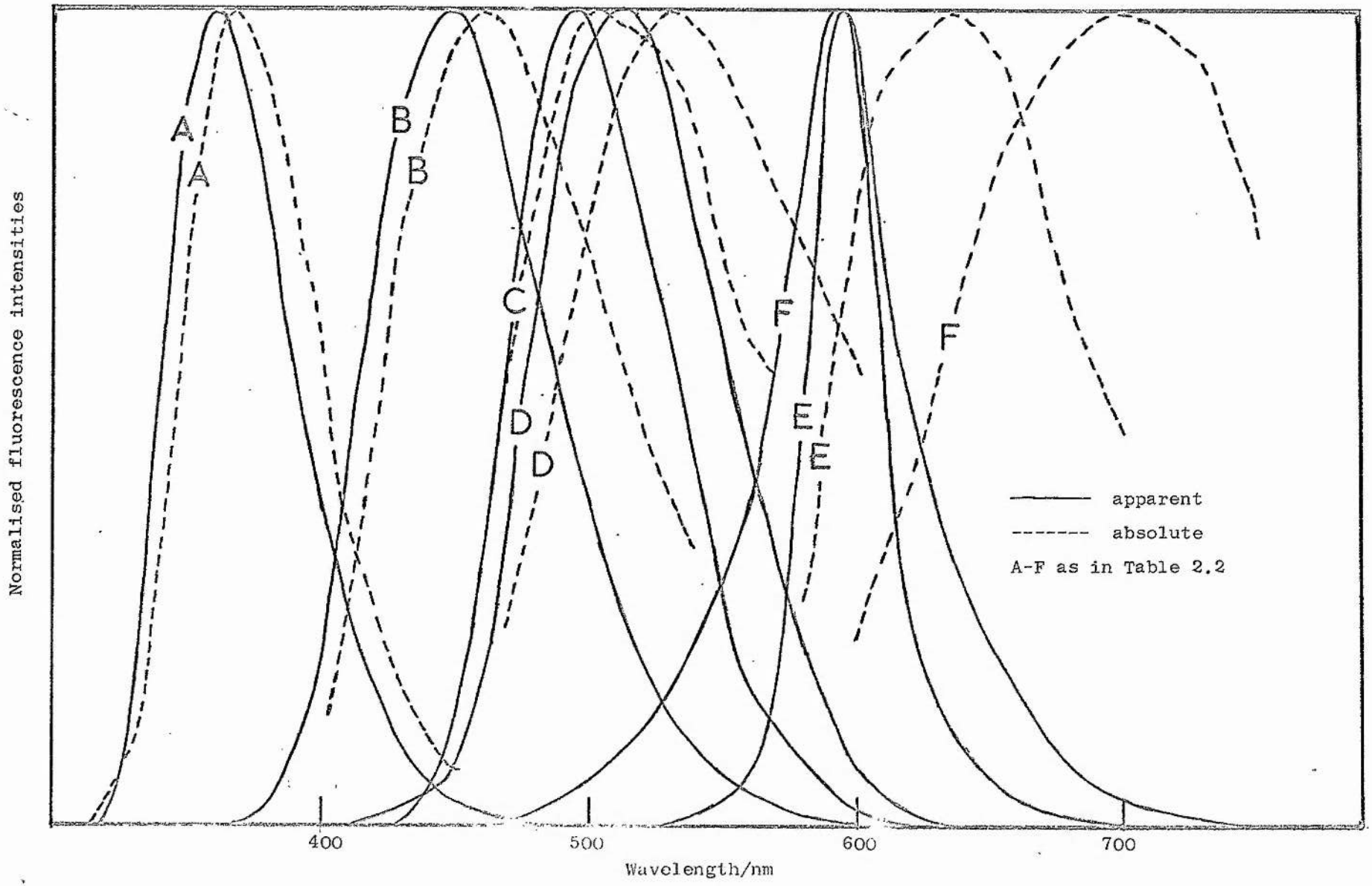

FIG. 2.6 Apparent and absolute fluorescence emission curves for the six standard compounds.

to A, B and C at 530 nm, E to A, B, C and D at 580 nm and F to A, B, C, D and E at 620 nm. The sensitivity factors obtained in the overlap regions showed good agreement and the final sensitivity factor for a particular slit width setting was obtained by taking the mean of the normalised values. These factors and their reciprocals were obtained in the computer printout. (A specimen computer printout is shown in Appendix II with the program CALIB.) The standard deviations of the sensitivity factors obtained at different slit widths were small up to 600 nm and so the overall sensitivity curve was obtained by averaging the values obtained at each slit width setting. TABLE 2.4 shows a list of the reciprocal of the sensitivity curve against wavelength. This shows that the sensitivity of this instrument falls off sharply above 600 nm, mainly due to the response characteristics of the R106 photomultiplier[113]. These reciprocal values of the sensitivity curve were used in a program to correct emission spectra obtained on this instrument.

$$\text{Emission correction factors, } C_{em}(\lambda) = \frac{1}{S_\lambda}$$

$$S_\lambda = \text{spectral sensitivity curve} = \frac{\text{Apparent Emission Spectrum}}{\text{Absolute Emission Spectrum}}$$

$\therefore$ Absolute emission spectrum of sample

$$= \text{Apparent emission spectrum} \times C_{em}(\lambda).$$

An experimental check on the sensitivity curve obtained was accomplished by comparing the relative peak heights of the corrected anthracene emission spectrum with those reported by Meluish[108]. TABLE 2.3 shows a comparison of the data.

TABLE 2.3 Relative peak heights of anthracene fluorescence.

Maximum wavelength (nm)	I/I_{max} (This Work)	I/I_{max} (Meluish)
379	0.82	0.87
400	1.00	1.00
424	0.54	0.55
450	0.18	0.17

TABLE 2.4 Emission Correction Factors. C_{em} = reciprocal of spectral sensitivity values.

WAVELENGTH (nm)	C_{em}	WAVELENGTH (nm)	C_{em}
300	0.71	610	46.68
310	2.46	620	93.59
320	0.96	630	164.38
330	0.26	640	272.04
340	0.32	650	409.68
350	0.41	660	593.30
360	0.52	670	906.04
370	0.59	680	1512.20
380	0.71	690	2283.85
390	0.88	700	4518.67
400	1.00	710	8342.22
410	1.11	720	13409.03
420	1.24	730	24609.44
430	1.44	740	42605.15
440	1.57	750	45112.66
450	1.78		
460	2.00		
470	2.24		
480	2.54		
490	2.80		
500	3.15		
510	3.59		
520	4.08		
530	4.92		
540	5.76		
550	7.10		
560	8.99		
570	12.11		
580	13.56		
590	16.59		
600	24.12		

(e) Automatic Digitilisation and Correction of Excitation and Emission Spectra

Correction of emission spectra using the described correction factors can be a tedious process. Several directly correcting spectrofluorimeters have been described where the correction function is stored internally e.g. on a mechanical cam or its electronic analogue[114-117]. Indirect correction of emission spectra using computers has also been used[118,119] but the full potential of these compouter-based methods can only be realised if the spectral data can be conveniently and rapidly transferred into a computer-readable form. The apparatus described below achieves this requirement using automatically punched paper tape.

A schematic diagram of the apparatus is shown in FIG. 2.7

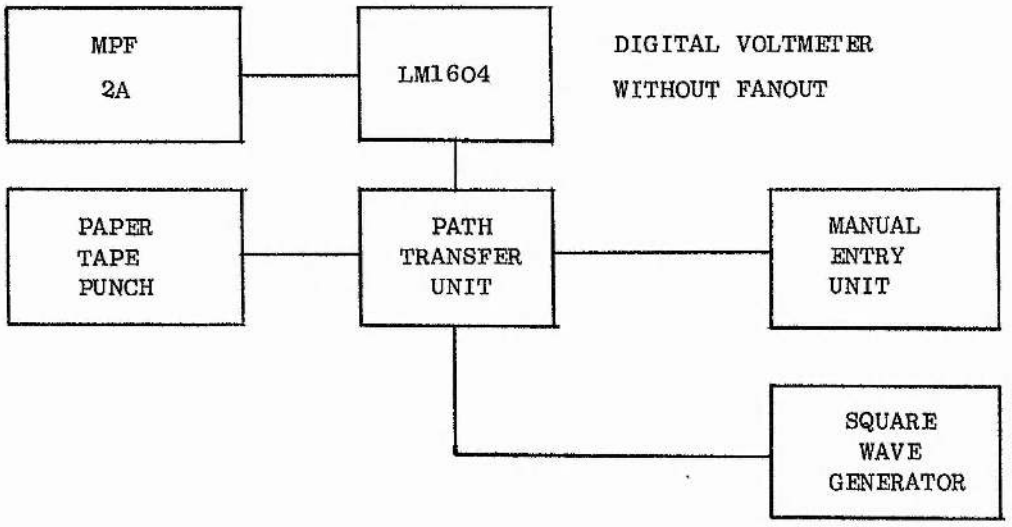

FIG. 2.7 Schematic diagram of automatic digitalisation apparatus.

The output signal from the spectrophotometer (MPF-2A) is connected to a Solartron LM1604 digital voltmeter with an EX3054 positive logic fan-out unit. The voltmeter is interlinked with a Solarton 3230 data transfer unit with a Facit 4070 paper tape punch acting as an output device. This arrangement allows the uncorrected detector voltage of the MPF-2A to be sampled and recorded at rates up to a maximum of about four samples for second. This corresponds to a reading approximately every 0.1 nm when the spectrofluorimeter is scanning at its slowest rate of 25 nm per minute. Slower sampling rates are obtained by initiating the sampling cycle from a variable square wave signal generator.

Operation: To record a spectrum over the wavelength region λ_1 to λ_2, the tape punched is activated only when the spectrophotometer is scanning between these limits. A symbol (s) indicating the end of the data set is then punched on the tape via a Solartron 3209 manual entry unit. Since the wavelength scan is linear with time the wavelength corresponding to the nth record on the tape can be computed from

$\lambda_n = \lambda_1 + (n-1)(\lambda_2 - \lambda_1)/(N-1)$, where N is the total number of records. N is counted during the subsequent processing of the tape.

This method has been found more convenient and more accurate than attempting to obtain readings at predetermined wavelength intervals. λ_1, λ_2 and a spectrum identification code, which includes the information as to whether it is an excitation or emission spectrum, are manually punched before each spectrum is recorded. The paper tape is now a digital record of the uncorrected spectrum and can be processed in conjunction with the predetermined correction factors to give a corrected spectrum.

Computer Processing

The computer used is an IBM 360/44 with a Honeywell 3691 paper tape reader. The programs are written in Fortran IV with the exception of a short translation program in PL360. The paper tape is read, translated and the data transferred to magnetic tape before use in the programs. Two programs are used, SPEKA and SPEKBA. A brief description of these is given below.

Program SPEKA:- This provides a line printer output of wavelength, wavenumber, and experimental and corrected spectral intensities in terms of detector voltages and also normalised to 100 units maximum intensity. In addition an incremental integration of the corrected unnormalised spectral intensities, with respect to wavenumber using a Simpson's approximation method, is printed. A punched card output of the corrected spectrum is also produced which, apart from being the input data for SPEKBA, gives a computer readable record of the spectrum in more convenient form than the original paper tape.

The correction factors ($C_{em}(\lambda)$) for emission spectra are included in SPEKA and the corrected intensities are obtained from

$$I_{corr}(\lambda) = C_{em}(\lambda). \quad I_{expt}(\lambda) \qquad (2.3)$$

Values of $C_{em}(\lambda)$ are computed for all wavelengths by interpolation. To correct excitation spectra a similar procedure was followed but using the appropriate excitation correction factors which were also incorporated in SPEKA. (A listing of program SPEKA is given in Appendix III.)

Program SPEKB:- This plotting program uses the punched card output from SPEKA as input data. The decision to keep the plotting routine separate from the correction program was based on the experience that not all spectra required to be plotted. Corrected emission or excitation spectra may be plotted with linear wavelength or wavenumber scales. In addition several spectra may be presented on the same plot with correct relative intensities. In both single and composite plots the maximum intensity is plotted as full scale. (A listing of program SPEKBA is given in Appendix IV.)

In operation this system has considerably simplified the handling and presentation of emission and excitation spectral data. The accuracy of the emission correction routine has been checked by relative quantum efficiency measurements on materials with well documented quantum efficiencies (described in the following section) and has been estimated to be better than $\pm$ 5%. The excitation correction, although basically inferior to quantum counter techniques, has been found satisfactory since a high degree of accuracy is seldom required.

The automatic digitalisation system was set up and the programs SPEKA and SPEKBA were written by Dr. T.M. Shepherd in conjunction with T.D. Brown and J.F. Ireland.

(f) Determination of Quantum Yields of Fluorescence

The various methods of obtaining luminescence quantum yields have recently been received by Parker[22] and Demas and Crosby[120]. In this work only the quantum yields of emission from fluid solution were determined because of inherent difficulties in the other sampling procedures. (This is discussed in Chapter 2.3(a).)

The determination of the relative fluorescence efficiencies of two substances, both in solution, is a relatively simple matter. Under conditions where the inner filter effects are negligible, the total rate of emission of fluorescence is proportional to the product $I_o \varepsilon c l \phi_f$:

(I_o is the incident light intensity, ε the molar extinction coefficient, c the concentration, and ϕ_f the quantum yield of the fluorescer). The total rate of emission of fluorescence is also proportional to the integrated area under the corrected fluorescence spectrum and thus, if the fluorescence emission spectra of two solutions are measured with the same instrumental geometry and at the same intensity of exciting light, the ratio of the two observed fluorescence intensities is given by:

$$\frac{F_2}{F_1} = \frac{\text{area 2}}{\text{area 1}} = \frac{I_o \varepsilon_2 c_2 1 \phi_2}{I_o \varepsilon_1 c_1 1 \phi_1}$$

$$= \frac{\phi_2}{\phi_1} \frac{\text{optical density of 2}}{\text{optical density of 1}} \qquad (2.4)$$

If the absolute fluorescence efficiency (ϕ_1) of one of the substances is known, that of the other is then simply calculated. A convenient method is to obtain for both solutions separately the factor (area of corrected spectrum)/(uncorrected peak height) and then accurately compare the fluorescence intensities at their respective peak heights. The ratio of observed peak intensities multiplied by the ratio of the factors gives the value F_2/F_1 for insertion in equation 2.4.

A change in refractive index of solvent is in effect a change in the geometrical arrangement and thus a correction factor must be inserted when the two substances to be compared are dissolved in different solvents. The observed intensities are corrected by multiplying by n^2 where n is the refractive index of the solution.

As dilute solutions must be used the optical density must be measured either by the use of a long path-length cuvette or by measuring the optical density on more concentrated solutions and diluting, (assuming Beer's Law is obeyed). The latter method was found to be the more convenient and in practice the solutions to be compared were diluted so as to give equal optical densities at the excitation wavelength.

Parker gives a detailed account of the likely errors and precautions

needed in this type of quantum yield determination[22].

Experimental

With the automatic digitalisation procedure already described it is a quick, easy process to obtain the area under the corrected emission curves. Before measuring any unknown quantum yields the method was tested by comparing the quantum yields of well-known standards. Comparison of the fluorescence quantum yields of quinine sulphate and anthracene;-

A weighed amount of quinine sulphate was dissolved in 0.5 M H_2SO_4 and the solution's optical density at 366 nm measured. Anthracene was dissolved in redistilled ethanol and its optical density, also at 366 nm, measured. Both solutions were then diluted to give equal optical densities at 366 nm of less than 0.02 (to avoid the inner filter effect). The anthracene solution was degassed. The emissions of both these solutions excited by 366 nm radiation were then recorded and the corrected spectra and area under the curves obtained from the computer printout. Blank solutions were treated in an identical fashion and the area of scattered light etc. subtracted from the emission area.

Taking a value of 0.55[22] for the quantum yield of quinine sulphate in 0.5 M H_2SO_4 a value of 0.28 (lit. 0.29[22]) was obtained for anthracene in ethanol using equation 2.4. This was repeated several times using in some cases solutions of anthracene and quinine sulphate of different optical densities and making the appropriate correction. The quantum yields obtained were found to be reproducible within $\pm$ 5%.

4. Triplet-State Absorption Spectroscopy

(a) Introduction

Triplet-triplet absorption occurs when the lowest triplet is excited to higher triplet levels by radiation. This is observable in many cases because the lifetime of the lowest triplet is sufficiently long for an appreciable concentration of molecules to exist in the triplet state.

The observation of triplet-triplet absorptions is commonly accomplished by flashing a sample in fluid solution, whence either the absorption or the spectral decay processes can be monitored. The term flash photolysis is used to describe this method of irradiating a sample by high intensity light flashes of short duration and studying the effects at various wavelengths and times.

The experimental method of flash photolysis has been described in detail and only a brief description is given here. Basically two methods are used[121-125]:

(a) The flash photographic technique: This is used for the detection of short-lived species using a spectrograph and photographic plate. Information covering a large range of wavelengths at one specific time is obtained by this technique.

(b) The flash photo-electric technique: This is used for the measurement of light absorption changes in the sample by means of a photomultiplier and gives information over a limited range of wavelengths during a specific time interval.

In method (a) a second discharge (spectroscopic flash) is used to produce a photograph via the spectrograph with the absorption of the sample shown at the time when the second flash is initiated. Hence by varying the delay between the photolytic flash and the spectroscopic flash one can study the absorption at a series of wavelengths at specific times after excitation of the sample.

In method (b) a continuous source is used to monitor the absorbance at an appropriate wavelength. Ideally the only light reaching the photomultiplier should be from the monitoring source, but due to the physical arrangement some of the light from the photo-flash is scattered back into the photomultiplier, thus producing a pulse of equal duration to the flash and this will mask any transient produced which has a shorter lifetime; therefore the shorter the flash duration the wider is the range of transients which may be studied. This difficulty

was particularly marked in some of the cases studied here and all the flash photolysis results reported were in fact obtained using the spectrographic arrangement (a) for which the apparatus used is described below.

(b) General Description of Instrument

All flash photolysis experiments were performed on a Northern Precision FP-I-pH apparatus. Although the apparatus permitted the sample cell to be held in either a vertical or a horizontal position, the former was always used and the instrumental lay-out for this is shown in FIG. 2.8. The spectrograph (1) is positioned on the main (photolytic) capacitor case (2) which also supports the sample holder assembly (3). The spectroscopic flash lamp is housed in (4) and the spectroscopic capacitor case must be placed nearby (5). The power supplies (6), control units (7), (8) and delay unit (9) are placed on a table (10) beside the main capacitor banks. With this arrangement several mirrors (contained in a flexible light guide) are used to drive the beam onto the spectrograph slit. This (WITH GLASS LENSES) is useful only in the visible regions of the spectrum and for shorter wavelengths the beam must be focussed on the slit by means of a quartz lens.

The main capacitor consists of two banks of five microfarad capacitors which can be operated singly or together. Normally both capacitors were charged to 10 kV before triggering, thus on firing giving a flash energy of 500 J. The type of switch used for the photoflash is the simplest type, of just two contacts and a connecting bar operated by a solenoid, which operates when the trigger button on the control unit is pressed. This method of triggering is used because of its simplicity, direct action and lack of electrical interference but was found in practice to cause several problems. When firing the photolytic flash large fields are produced and therefore the spectrographic unit must have a high interference immunity. This is achieved by using a device known as an ignitron which gives reliable triggering of the spectrographic flash.

FIG. 2.8 Flash photolysis apparatus

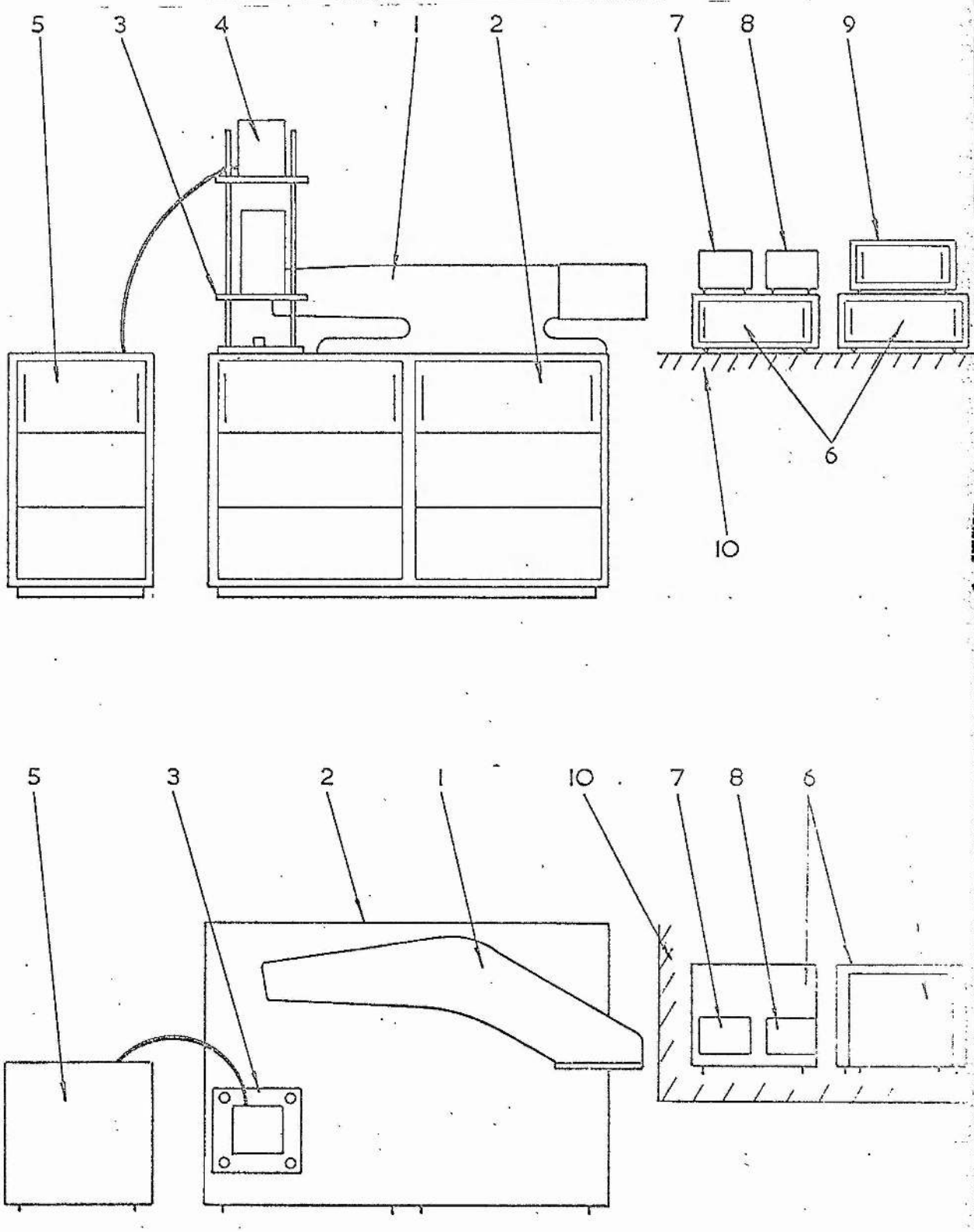

(c) Preparation of Samples

The longer lifetime of the triplet state, which puts triplet-triplet absorption in a much more accessable time scale than (S_1-S_n) singlet-singlet absorptions, also means that quenching processes tend to affect the triplet molecules to a greater extent than excited singlet species. In many cases oxygen has no effect on the quantum yield of fluorescence emission but on the other hand oxygen quenching has been used as a diagnostic test for the presence of triplet molecules. To eliminate the effect of oxygen on a sample being flashed the solution must be thoroughly degassed.

The vacuum line used to degas solutions has a mercury diffusion pump backed by a rotary oil pump with which pressures $> 10^{-5}$ torr were easily obtained. A schematic diagram of the vacuum line is shown in FIG. 2.9, all the taps being Young's greaseless high vacuum taps and the gauge on Edwards Pirani Penning Model 4. In this diagram (FIG. 2.9):-

X, Y and Z are liquid nitrogen traps and 1, 2, 3 and 4 are the connection points for the degassing vessels. The degassing vessel is shown in FIG. 2.10 and is connected to the vacuum line by means of a Young's high vacuum joint (i.e. position 5 of FIG. 2.10 is connected to either position 1, 2, 3 or 4 of FIG. 2.9). This method was also used to connect the sample cell FIG. 2.11 to the degassing bulb (i.e. position 7 of FIG. 2.11 is connected to position 6 of FIG. 2.10). The vacuum taps on the degassing cell were originally Young's greaseless taps but they proved to be less robust than the Rotoflow greaseless taps now used, although they gave a more reliable vacuum. The sample cell used to measure transient absorption is shown in FIG. 2.11, the main body of the cell being a quartz cylinder 18.5 cm in length and 17 mm in internal diameter.

The general degassing procedure was as follows: the degassing bulb (FIG. 2.10) containing the sample was attached to the vacuum line and the vacuum line outlet tap and tap A were opened. The solution in the bulb was then frozen to liquid nitrogen temperature and then

FIG. 2.9 Schematic diagram of vacuum line.

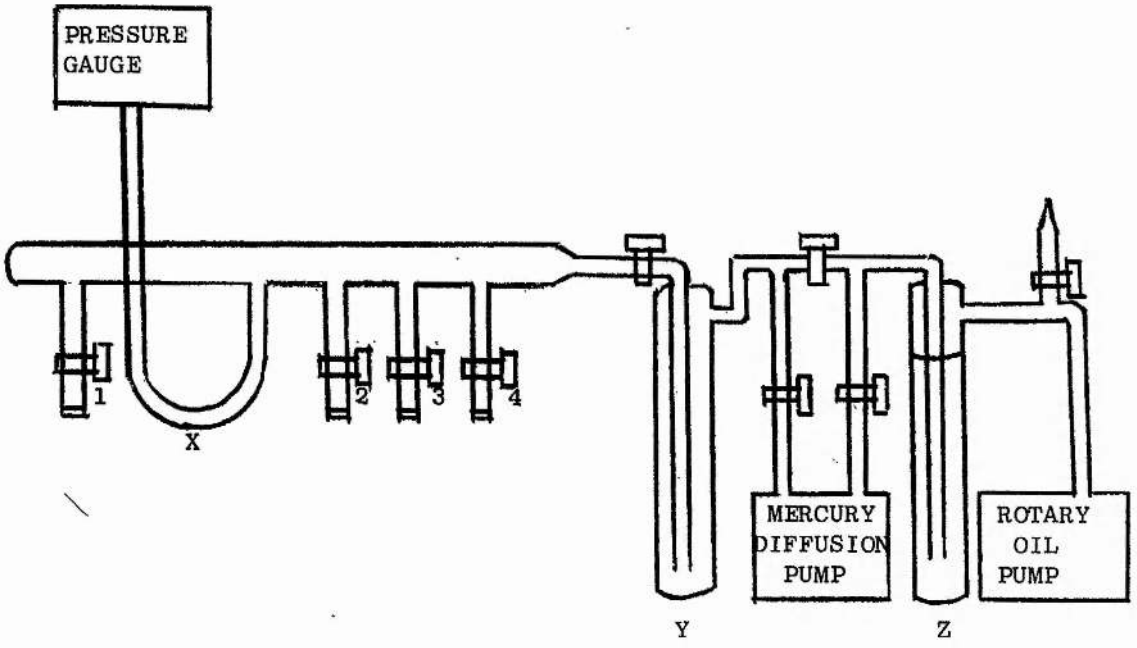

FIG. 2.10
Degassing Cell

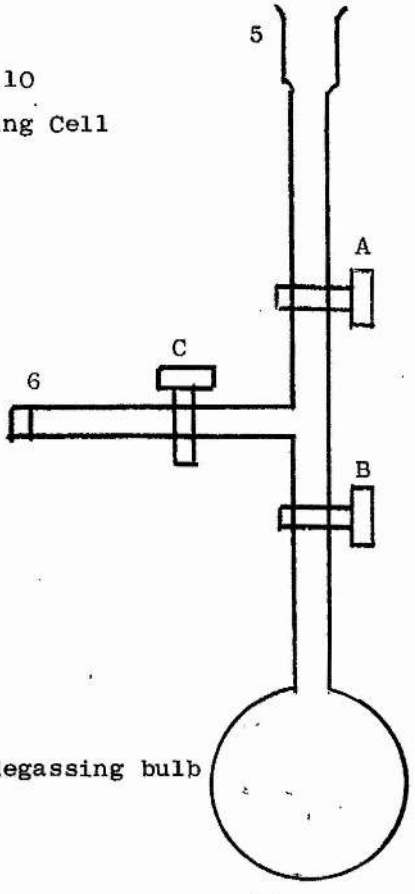

FIG. 2.11
Flash Photolysis Cell

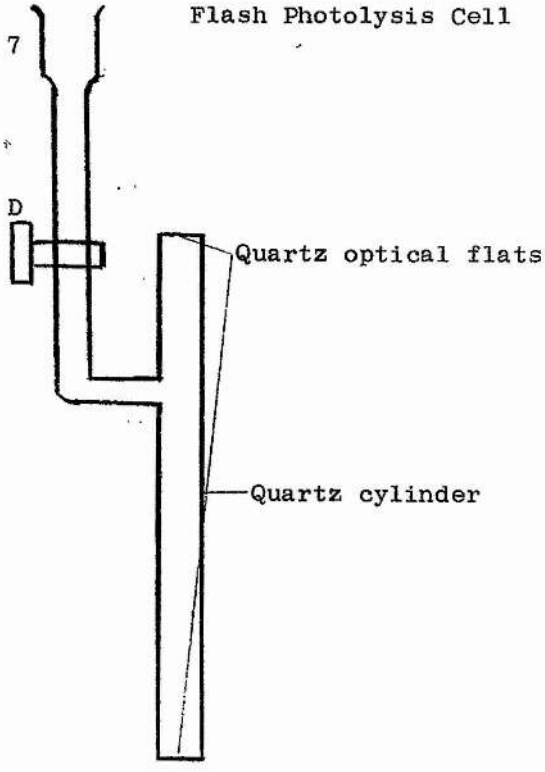

tap B opened. When the vacuum had recovered tap B was closed and the liquid nitrogen removed. A great deal of trouble was experienced during the thawing procedure. Many solutions, particularly strong acid/water mixtures, expanded and cracked the degassing cell. A round-bottomed sample holder was found to be the best shape and the best procedure proved to be that of surrounding the frozen cell with hot water immediately after the liquid nitrogen was removed. This procedure appeared to loosen the solid from the glass and thus to make any sudden expansion harmless. It also speeded up the thawing process considerably. This freeze-pump-thaw procedure was repeated until the sample was degassed, as indicated by no change in the line pressure on opening tap B after freezing. During thawing on one of the last cycles the reaction vessel FIG. 2.11 was attached to the degassing cell and evacuated by opening taps A, C and D, B being closed. After the final cycle tap A was closed and the combined cells were removed from the vacuum line, the solution was poured over into the quartz vessel and tap D closed. This procedure was found to be effective. The classical experiment described by Porter[126], in which the transient spectra on flashing a solution of anthracene in hexane are recorded at a series of times after the flash, was repeated successfully using the above degassing procedure and our flash photolysis apparatus.

(d) Operation and Analysis of Data

The sealed sample cell containing the degassed solution (or the untreated solution) is placed in the flash photolysis apparatus between the photolytic flash lamps and the cell holder casing closed. All units are switched on and allowed to warm up while a photographic plate (Ilford HP3) is placed, in a dark room, in the spectrograph plate holder. The following sequence of experiments was then usually performed: (1) spectroflash only to give the starting spectrum; (2) photoflash alone to obtain a measure of the scattered light and any emission from the sample; (3) a double flash with a set delay between the flashes: this was

repeated for the required number of delay settings; (4) the spectroflash alone was again recorded to give the final spectrum of the sample. A wavelength scale was taken on the photographic plate at the start of the run and the plate was, of course, moved for each flash. This general procedure was used for preliminary investigations of samples but in cases where measurements were to be made on a particular transient the spectrographic plate had to be calibrated . This was achieved by keeping the sample in position, introducing a (Barr and Stroud) neutral density filter in front of the spectrograph and firing the spectroflash. This was repeated for a series of filters, the spectroflash energy being exactly the same (i.e. the capacitor was charged to the same tension) each time and a measure of the optical density of the transient was thus obtained.

The photographic record of the experiments described above is (after developing, fixing and drying) interpreted using a Vickers M41 microdensitometer. The microdensitometer measures the extent of the exposure of a particular spot on the plate and a record of this against wavelength is traced on chart paper. Microdensitometer traces of all the calibration spectra are first obtained without changing the microdensitometer's settings. Traces of the sample spectra are taken on the same recorder sheet; from the intersection points the actual absorption spectra of the transients can be constructed.

CHAPTER 3

XANTHONE

1. Acid-Base Properties

(a) Introduction

The photochemical properties of xanthone have not been as extensively investigated as those of many related aromatic ketones. The triplet state energy has been measured and xanthone suggested as a triplet state sensitizer[127]. Shigorin et al have studied the effect of the nature of the solvent on the relative location of the $n-\pi^*$ and $\pi-\pi^*$ levels[128,129]. Recently a similar but more detailed study of this molecule, with particular emphasis on the polarisation of emission spectra and solvent effects, has been reported[130].

Xanthone is an example of a compound with its lowest $n-\pi^*$ and $\pi-\pi^*$ triplet states of very similar energy. It has been suggested that compounds of this type have a lowest triplet state of a substantially mixed character and that this is due to vibrational coupling between the two closely spaced electronic states[131]. Due to the very small energy gap between the states it is possible to alter the photochemical behaviour of the molecule by changing the solvent, since $n-\pi^*$ and $\pi-\pi^*$ states are solvent shifted in different directions. Thus in non-polar solvents xanthone has an $n-\pi^*$ triplet level while in polar solvents the emission is characteristic of a lowest triplet level of $\pi-\pi^*$ type[128,130].

The non-exponential decay of xanthone phosphorescence observed by Pownall and Huber[130] is similar to an effect observed with other carbonyl compounds[132,133]. In some cases the decay has been analysed in terms of two first order processes due to simultaneous emission from both $n-\pi^*$ and $\pi-\pi^*$ triplet levels. This conclusion is inconsistent with internal conversion to the T_1 level especially in these compounds as the two triplet states concerned lie close together. Kanda, Stanislaus, and Lim[134] suggest that the anomalous emission in 1-indanone is due to the

production of new species such as an enol or enolate ion in the excited state. Chu and Kearns[135] indicate that this is incorrect and that this phenomenon in a number of cases is due to photoproducts which are formed at room temperature and then observed in phosphorescence at 77 K. In the case of xanthone the mixed emission has been attributed to xanthone molecules in different solvent cage systems at 77 K. Thus in a mixed solvent the short lived emission is due to xanthone $n-\pi^*$ triplet state in a predominantly hydrocarbon system while the long lived emission is attributed to the $\pi-\pi^*$ state in a polar environment. Experiments by Wang[136] indicating that mixed solvents, when frozen to 77 K, tend to aggregate as do solute molecules agree with the explanation of Pownall and Huber. The results now presented for xanthone have in the main been obtained in fluid solution where the above effect, if observed at all will not be marked.

(b) Absorption Spectroscopy: Determination of pK (S_o)

The absorption spectra of xanthone in hexane and in ethanol are shown in FIG. 3.1 The weak long-wavelength band which is partially hidden by the more intense second band in hexane is completely hidden in ethanol. The intense band which has been attributed to a $\pi-\pi^*$ transition[130] shows, as expected, a shift to longer wavelength on changing from non-polar to polar solvents while the weak transition, $n-\pi^*$, although hidden in alcohol solution probably shifts to shorter wavelengths. Because of the complete change in the shape of the long-wavelength bands on changing the solvent it is difficult to determine an exact value for the shift of the absorption maximum. If we take the mid-point of the slope of the long-wavelength side of the first intense band as the reference point this shifts by 1100 cm^{-1} to the red on changing from hexane to alcohol. This shift is somewhat longer than that expected for a $\pi-\pi^*$ band but less than that for a CT transition. The bands at 337 nm (I) and 283 nm (II) in hydrocarbon solvents (cf. xanthone in hexane, FIG. 3.1) have been attributed[130] to $\pi-\pi^*$ transitions while that at 257 nm (III) was assigned to a CT state. Band III undergoes a 400 cm^{-1}

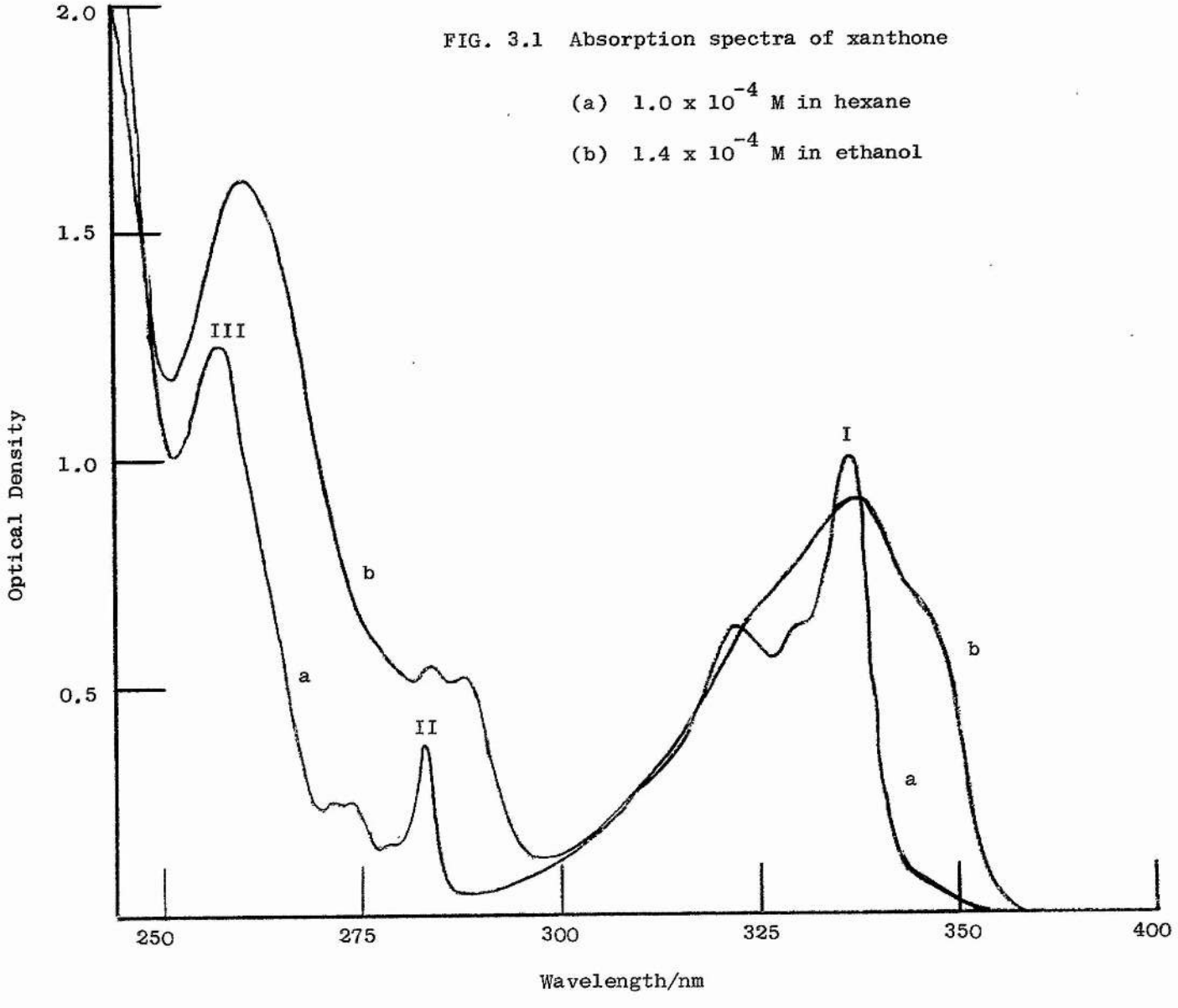

FIG. 3.1 Absorption spectra of xanthone

(a) 1.0×10^{-4} M in hexane

(b) 1.4×10^{-4} M in ethanol

shift to the red from hexane to ethanol and a further 1000 cm^{-1} in changing from ethanol to water. Band I exhibits an overall shift of 1900 cm^{-1} on going from hexane to water while band II shifts to the red by 800 cm^{-1}. The solvent shift results therefore agree with the π-π^* assignment of band II but if this criterion is used as evidence of the CT character of band III[130] then band I must also have charge transfer character.

In aqueous solutions the xanthone absorption bands show considerable medium effects as the acidity of the solution is increased. Xanthone is a weak base and protonates in strongly acidic solutions. The protonated form (BH^+) has its first absorption band at longer wavelengths than that of the unprotonated (B) form. The absorption spectra of the B and BH^+ forms are shown in FIG. 3.2 at several different acidities near the $pK(S_o)$ value. The absence of an isobestic point indicates the large medium effects occurring. The $pK(S_o)$ of xanthone has been reported as -4.08[137], -4.12[138] and -4.83[139]. All these values were obtained from changes in optical density with acidity but the last of the values was obtained by measurements at 333 nm where appreciable medium effects occur (see FIG. 3.2). Here it was found that the calculated $pK(S_o)$ varied with the analytical wavelength chosen. As well as repeating the determination of $pK(S_o)$ by optical density measurements a fluorescence technique was used. Since only the BH^+ form absorbs at 400 nm and $pK(S_1) > pK(S_o)$ (see following sections), the intensity of fluorescence emitted by xanthone solutions excited at 400 nm is directly proportional to the BH^+ concentration. The $pK(S_o)$ is determined by the same method used for optical densities[140] i.e. from the equation

$$pK = H_o + \log \frac{I - I_B}{I_{BH^+} - I} \qquad (3.1)$$

where H_o gives the acidity of the sample being considered and I is its fluorescence intensity. I_B and I_{BH^+} are respectively the fluorescence intensities of the base form alone and the protonated form alone. Several solutions with constant xanthone concentration, but differing H_o values were prepared and the relative fluorescence intensities measured. The pK

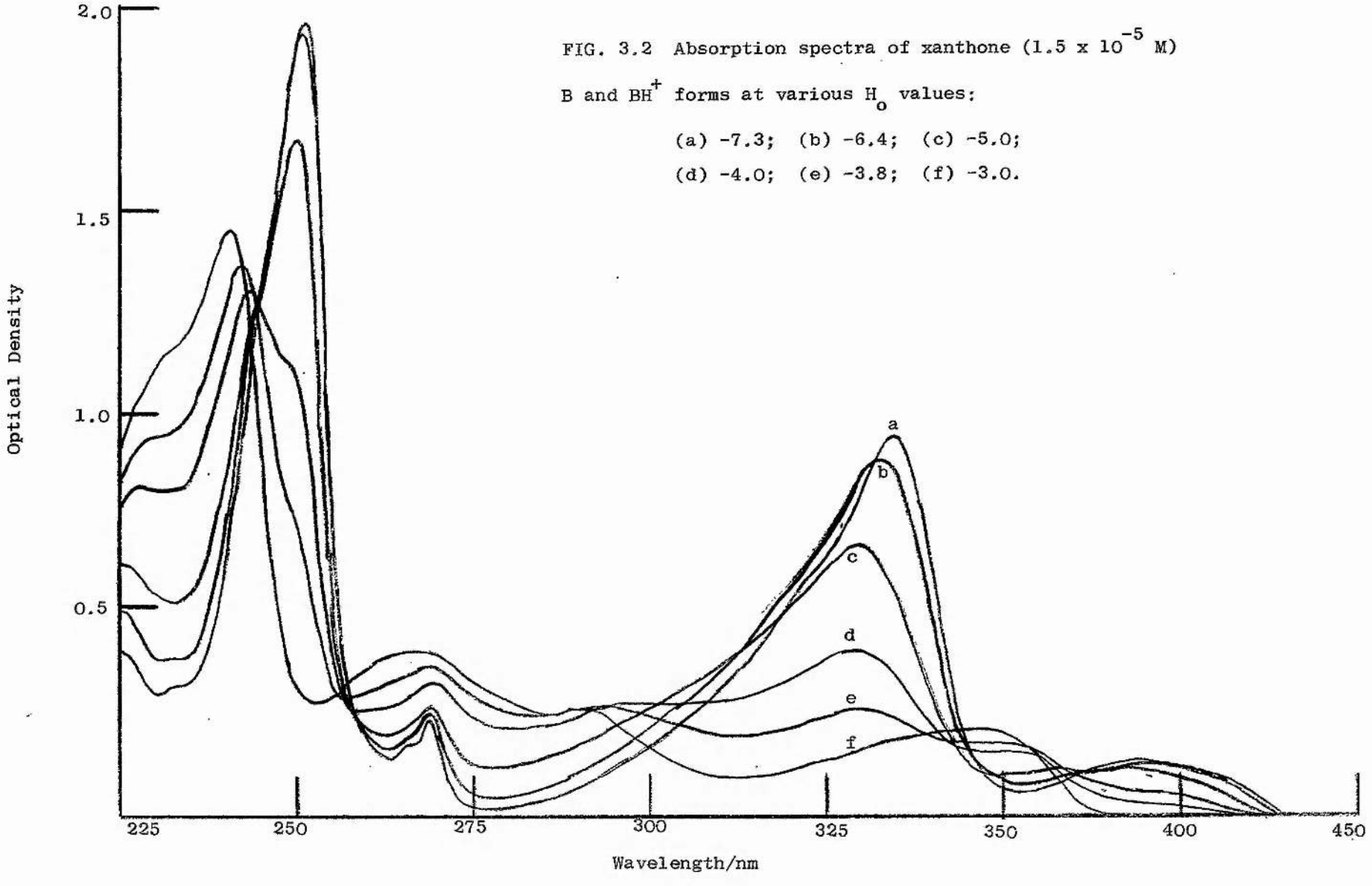

FIG. 3.2 Absorption spectra of xanthone (1.5×10^{-5} M)

B and BH^+ forms at various H_o values:

(a) -7.3; (b) -6.4; (c) -5.0;

(d) -4.0; (e) -3.8; (f) -3.0.

values shown in Table 3.1 were calculated with I_B = 0 and I_{BH^+} = 80.0. Fluorescence intensity measurements were taken at three temperatures and although the deviation of the pK values is greater at higher temperatures the results indicate that the temperature has very little effect on the pK. The results agree with the more positive $pK(S_o)$ values quoted above for xanthone. In any following calculations a value of -4.1 is used for the $pK(S_o)$ of xanthone.

TABLE 3.1 Calculation of $pK(S_o)$ values from fluorescence intensity measurements.

TEMPER-ATURE	20.0°C		40.0 °C		60.0 °C	
$-H_o$	$\log\frac{I-I_B}{I_{BH^+}-I}$	-pK	$\log\frac{I-I_B}{I_{BH^+}-I}$	-pK	$\log\frac{I-I_B}{I_{BH^+}-I}$	-pK
3.29	-0.79	4.08	-0.80	4.09	-0.80	4.09
3.54	-0.50	4.04	-0.51	4.05	-0.52	4.06
3.79	-0.23	4.02	-0.24	4.03	-0.27	4.06
4.01	0.00	4.01	-0.04	4.05	-0.07	4.08
4.25	0.22	4.03	0.17	4.08	0.14	4.11
4.49	0.46	4.03	0.40	4.09	0.34	4.15
4.65	0.59	4.06	0.49	4.16	0.45	4.20
4.85	0.77	4.08	0.67	4.18	0.59	4.26

(c) Fluorescence Spectroscopy: Determination of $pK(S_1)$

In aqueous solutions xanthone fluoresces weakly as the neutral molecule, B, and more strongly as the protonated form, BH^+ (see FIG. 3.3). The quantum yields of these emissions were determined with respect to a quinine sulphate, in 0.5 M H_2SO_4, reference (ϕ_f = 0.55) and values of 0.02 and 0.46 obtained for B in aqueous solutions, pH = 3, and BH^+ in 3 M $HClO_4$ respectively. No fluorescence emission could be detected from xanthone in the polar solvents methanol, ethanol, acetonitrile, and formamide nor in the non-polar solvents hexane, cyclohexane and isopentane.

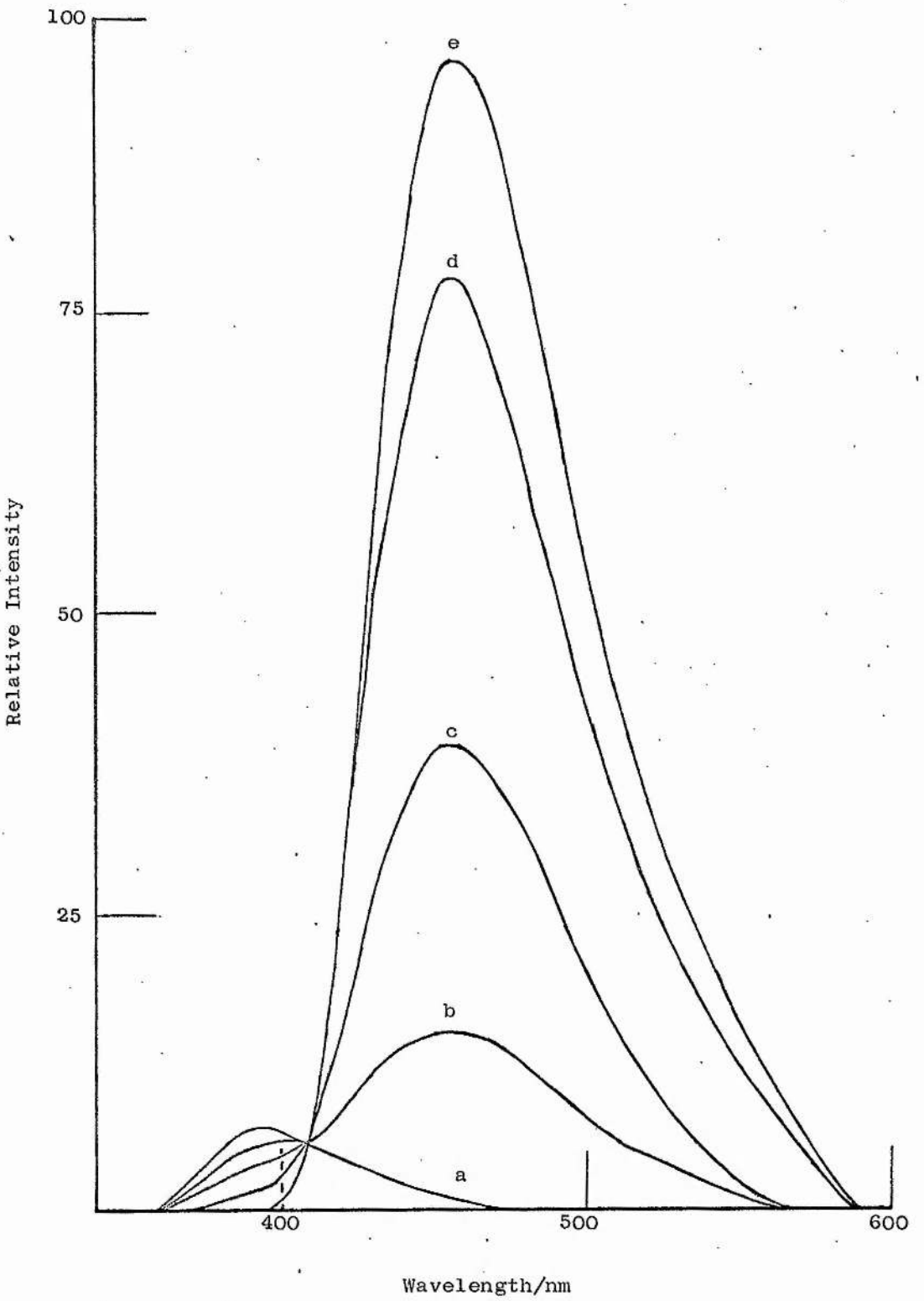

FIG. 3.3 Fluorescence intensity curves of xanthone (excited at λ = 350 nm) at various pH values: (a) pH = 3, (b) pH = 1.7, (c) pH = 1.1, (d) pH = 0.3; curve (e) 4M $HClO_4$.

The relative position of the energy levels of xanthone in various solvents is discussed in section (e).

The change in fluorescence emission, due to a protolytic reaction in the excited state, occurs in solutions of much lower acid concentration than those in which ground state protonation occurs, showing that xanthone is a stronger base in the excited state. FIG. 3.3 shows the fluorescence intensity curves of xanthone, in aqueous solutions, at various pH values. The neutral and protonated forms have fluorescence maxima at 395 nm and 456 nm respectively and there is an isoemissive point at 409 nm. That both these emissions originate from the xanthone neutral molecule follows from the identity of both their corrected excitation spectra and the absorption spectrum of B. To determine $pK(S_1)$ fluorescence intensity measurements were made on aqueous $HClO_4$ solutions containing xanthone at $< 10^{-5}$ M (to avoid the inner filter effect). Although $pK(S_1)$ is not expected to be sensitive to ionic strength when the protonation of a neutral molecule is involved, all solutions up to 1 M in $HClO_4$ were made up to I = 1.0 M with $NaClO_4$: above this concentration a few measurements were made with $HClO_4$ alone to complete the curves. $HClO_4$ and $NaClO_4$ were used because strong quenching of the excited forms, $\overset{*}{B}$ and $\overset{*}{BH}^+$, by certain anions was observed, but not by ClO_4^-, H^+ or OH^- (see section 2(a) for details of the quenching reactions). TABLE 3.2 gives the fluorescence intensity measurements of the B and BH^+ forms of xanthone as a function of pH at room temperature (ca. 20^oC). The intensities of the B and BH^+ forms were measured at their uncorrected maxima; 388 nm and 448 nm respectively.

I = measured fluorescence intensity at 388 nm ($\overset{*}{B}$)

I' = measured fluorescence intensity at 448 nm ($\overset{*}{BH}^+$).

TABLE 3.2. Fluorescence intensities of the protonated and unprotonated forms of xanthone as a function of pH.

Excitation Wavelength = 350 nm

pH or H_o	$^*B$ measured at 388 nm				$^*BH^+$ measured at 448 nm			
	I	kI	$\frac{I-k'I'}{I-kk'}$	ϕ/ϕ_o	I'	k'I'	$\frac{I'-kI}{I-kk'}$	ϕ'/ϕ'_o
-1	0.2	0.0	0.0	0.00	92.9	0.2	92.9	1.00
-0.8	1.0	0.04	0.8	0.02	92.0	0.2	92.0	0.99
-0.6	1.0	0.04	0.8	0.02	92.0	0.2	92.0	0.99
-0.4	1.4	0.06	1.2	0.03	90.0	0.2	89.9	0.98
0.0	4.1	0.14	3.9	0.10	85.6	0.2	85.5	0.92
0.02	4.2	0.15	4.0	0.10	84.0	0.2	82.8	0.90
0.05	4.7	0.16	4.5	0.11	82.8	0.2	82.6	0.89
0.10	5.1	0.18	4.9	0.12	80.5	0.2	80.7	0.87
0.19	5.7	0.20	5.5	0.14	78.5	0.2	78.3	0.84
0.32	7.6	0.26	7.4	0.18	76.8	0.2	76.5	0.82
0.40	8.3	0.29	8.1	0.20	72.3	0.2	72.0	0.78
0.50	9.7	0.34	9.3	0.23	68.0	0.1	67.7	0.73
0.62	11.6	0.40	11.1	0.27	62.6	0.1	62.2	0.67
0.70	11.8	0.41	11.1	0.27	51.6	0.1	51.2	0.55
0.80	14.7	0.51	13.8	0.34	51.1	0.1	50.6	0.54
0.92	17.7	0.61	16.7	0.41	46.6	0.1	46.0	0.50
1.10	23.7	0.82	23.6	0.58	38.7	0.1	37.9	0.41
1.40	28.1	0.98	28.0	0.69	23.9	0.1	22.9	0.25
1.70	33.0	1.15	33.0	0.82	15.2	0.0	14.0	0.15
2.00	35.3	1.20	35.3	0.87	10.1	0.0	8.9	0.10
2.40	38.0	1.30	38.0	0.94	4.8	0.0	3.5	0.04
2.70	39.5	1.40	39.5	0.98	4.2	0.0	2.8	0.03
3.00	39.8	1.40	39.8	0.99	3.0	0.0	1.6	0.02
3.40	39.8	1.40	39.8	0.99	1.6	0.0	0.3	0.00
6.00	40.4	1.40	40.4	1.00	1.4	0.0	0.0	0.00

$$k = \frac{1.4}{40.4} = \underline{0.035} \qquad k' = \frac{0.2}{92.9} = \underline{0.002}$$

$$\phi_o = \underline{40.4} \qquad \phi'_o = \underline{92.9}$$

To obtain the true fluorescence intensities of the B and BH^+ forms (ϕ and ϕ' respectively) the measured intensities must be corrected for overlap between the emission spectra of the two species. In the case of xanthone the overlap is small and consequently the corrections are also small. The measured and true fluorescence intensities are related as follows:

$$I = \phi + k'\phi' \qquad (3.2)$$

and

$$I' = \phi' + k\phi \qquad (3.3)$$

where k and k' are the overlap ratios of the B and BH^+ forms respectively. To obtain the overlap ratios measurements are made on solutions, 2 to 3 pH units either side of the $pK(S_1)$ value, which contain only one species in the excited state. Thus k is obtained in the more alkaline solutions showing only the characteristic fluorescence of the unprotonated form and is the ratio of the fluorescence intensity of B measured at the wavelength where BH^+ emission (I') is observed to the intensity at the wavelength where B emission (I) is measured, i.e.

$$k = \frac{\text{Fluorescence intensity at } BH^+ \text{ emission wavelength (448 nm)}}{\text{Fluorescence intensity at B emission wavelength (388 nm)}}$$

$$\text{or} \quad k = \frac{I'}{I}$$

Similarly for k', taking measurements in a solution having $\overset{*}{B}H^+$ as the only excited state species,

$$k' = \frac{\text{Fluorescence intensity at 388 nm}}{\text{Fluorescence intensity at 448 nm}}$$

$$\text{or} \quad k = \frac{I}{I'}$$

Rearranging equations 3.2 and 3.3 we can obtain the true fluorescence intensities (ϕ and ϕ') in terms of I, I', k and k':

$$\phi = \frac{I - k'I'}{1 - kk'} \qquad (3.4)$$

and

$$\phi' = \frac{I' - kI}{1 - kk'} \qquad (3.5)$$

The true fluorescence intensities at various pH values are given in Table 3.2 as well as the relative fluorescence intensities ϕ/ϕ_o and ϕ'/ϕ'_o of B and BH^+ respectively where ϕ_o and ϕ'_o are the maximum true fluorescence intensities of the respective forms. A plot of the relative fluorescence intensity as a function of pH is shown in FIG. 3.4, from which a value of 0.96 for $pK(S_1)$ is obtained. This assumes that the protolytic equilibrium is established in the lifetime of the excited state. In these solutions xanthone is excited as its base form (the absorption spectra of the solutions show no change in this acid region). The protonation reaction must therefore be complete within the fluorescence lifetime of B. No measurement of this lifetime has been obtained although a preliminary investigation of the lifetime of the protonated form indicated a value of approximately 26 ns. Since the fluorescence of the B form is weaker than that of BH^+ and the first singlet level of B might have some $n-\pi^*$ character we would expect the fluorescence lifetime of B to be somewhat longer than that of BH^+. In any case, at acid concentrations near $pK(S_1)$, protonation should be rapid enough for equilibrium to be established sufficiently before emission. Kinetic corrections will therefore be small and any allowance for non-stationary state effects will reduce them still further[56].

The above procedure was repeated, this time using the constant temperature cell holder of the MPF-2A spectrophotometer. Fluorescence intensity as a function of pH was measured at several temperatures and the results, processed as described above, are given in TABLE 3.3. For the results at each temperature curves similar to FIG. 3.4 were drawn and from them the $pK(S_1)$ values shown in TABLE 3.4 obtained.

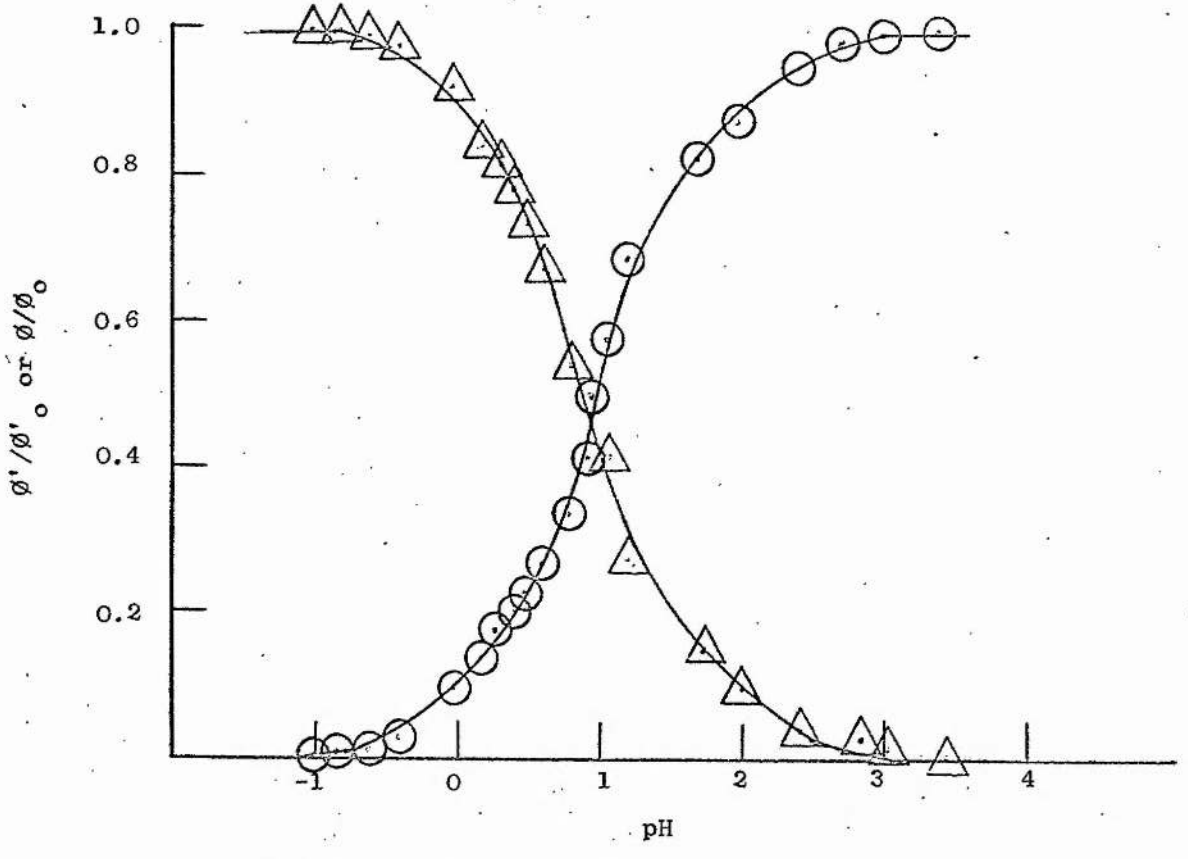

FIG. 3.4 Relative fluorescence intensities of protonated and unprotonated xanthone as a function of pH: △, $Ø/Ø'_o$ at 448 nm (protonated form); ⊙, $Ø/Ø_o$ at 388 nm (unprotonated form).

TABLE 3.3 Fluorescence intensities of the protonated and unprotonated forms of xanthone as a function of pH at several temperatures.

TEMPERATURE	20°C				30°C				40°C	
	$^*B$		$^*BH^+$		$^*B$		$^*BH^+$		$^*B$	
Ph or H_o	I	ϕ/ϕ_o	I'	ϕ'/ϕ'_o	I	ϕ/ϕ_o	I'	ϕ'/ϕ'_o	I	ϕ/ϕ_o
-2.2	1.2	0	85.0	0.99	1.5	0.00	84.5	0.99	0.4	0.00
-2.0	1.2	0	85.5	1.00	1.4	0.00	84.7	1.00	1.4	0.00
-1.1	1.9	0	85.8	1.00	1.9	0.02	84.5	0.99	2.0	0.03
0.01	4.9	0.07	81.0	0.94	5.0	0.12	77.8	0.92	4.7	0.15
0.11	5.7	0.09	79.5	0.92	5.6	0.13	75.9	0.90	5.1	0.17
0.24	7.1	0.12	85.7	0.88	6.9	0.18	72.1	0.85	6.5	0.23
0.34	8.4	0.15	73.9	0.86	7.9	0.21	69.4	0.82	7.1	0.26
0.42	9.5	0.18	71.9	0.83	8.8	0.24	66.5	0.78	8.1	0.30
0.50	10.8	0.21	67.8	0.79	10.0	0.28	62.7	0.74	9.1	0.35
0.62	13.9	0.28	62.7	0.72	12.3	0.36	57.0	0.67	11.0	0.43
0.70	15.7	0.33	59.4	0.68	13.8	0.40	53.4	0.62	12.0	0.48
0.80	18.2	0.39	54.7	0.63	15.7	0.47	48.1	0.56	13.3	0.54
0.85	19.9	0.43	51.6	0.59	16.2	0.48	44.6	0.52	14.0	0.58
0.92	21.5	0.46	47.7	0.55	17.7	0.53	40.7	0.47	15.0	0.62
1.00	23.6	0.51	43.3	0.49	19.1	0.58	36.3	0.42	16.0	0.67
1.10	26.1	0.57	38.4	0.44	21.2	0.65	32.1	0.37	17.0	0.71
1.22	28.9	0.64	31.8	0.36	23.6	0.72	26.6	0.30	18.1	0.76
1.30	31.1	0.70	28.1	0.31	24.6	0.76	23.2	0.26	18.9	0.80
1.40	33.1	0.74	24.0	0.26	25.9	0.80	19.6	0.22	19.7	0.83
1.55	35.6	0.80	17.9	0.19	27.0	0.84	14.5	0.16	20.9	0.89
1.62	36.6	0.82	16.3	0.17	27.4	0.85	12.8	0.14	21.0	0.89
1.70	38.2	0.86	13.7	0.14	28.1	0.87	10.5	0.11	21.1	0.90
1.80	39.4	0.89	11.9	0.12	29.9	0.93	9.1	0.09	21.6	0.92
2.10	41.7	0.95	5.9	0.05	30.6	0.95	4.6	0.04	22.7	0.97
7.0	43.9	1.00	1.9	0.00	32.0	1.00	1.4	0.00	23.3	1.00
12.3	43.7	1.00	1.8	0.00	31.1	0.97	1.2	0.00	22.1	0.95
13.0	41.9	0.95	1.9	0.00	30.1	0.94	1.2	0.00	21.0	0.90

TABLE 3.3 continued

TEMPERATURE	40°C				50°C				60°C			
	$\overset{*}{B}H^+$		$\overset{*}{B}$		$\overset{*}{B}H^+$		$\overset{*}{B}$		$\overset{*}{B}H^+$			
pH or H_o	I'	$\emptyset'/\emptyset'_o$	I	$\emptyset/\emptyset_o$	I'	$\emptyset'/\emptyset'_o$	I	$\emptyset/\emptyset_o$	I'	$\emptyset'/\emptyset'_o$		
-2.2	84.9	1.00	5.7	0.01	82.6	0.97	6.2	0.02	84.6	0.98		
-2.0	85.2	1.00	5.2	0.00	85.0	1.00	5.5	0.00	86.0	1.00		
-1.1	84.2	0.99	7.4	0.04	83.1	0.98	7.7	0.06	82.7	0.96		
0.01	75.3	0.88	15.9	0.21	71.7	0.84	15.4	0.27	67.8	0.79		
0.11	73.3	0.86	17.4	0.24	69.7	0.82	17.0	0.31	64.4	0.75		
0.24	68.2	0.80	19.8	0.29	62.4	0.73	19.3	0.37	59.0	0.69		
0.34	65.0	0.76	21.9	0.33	58.2	0.68	20.7	0.42	53.4	0.62		
0.42	62.4	0.73	24.0	0.37	55.3	0.65	22.0	0.45	50.1	0.58		
0.50	57.9	0.68	26.2	0.42	49.9	0.58	23.7	0.50	44.9	0.52		
0.62	51.5	0.60	30.6	0.51	43.4	0.51	26.4	0.58	37.7	0.44		
0.70	47.0	0.55	33.2	0.56	39.4	0.46	28.0	0.62	32.6	0.38		
0.80	41.7	0.48	36.3	0.62	34.1	0.40	30.1	0.68	28.1	0.32		
0.85	38.2	0.44	37.9	0.65	31.4	0.37	31.4	0.72	25.8	0.30		
0.92	34.8	0.40	39.5	0.69	27.5	0.32	32.4	0.74	22.8	0.26		
1.00	30.8	0.35	42.2	0.74	24.8	0.29	33.5	0.78	19.7	0.22		
1.10	26.1	0.30	44.1	0.78	20.9	0.25	34.7	0.81	16.0	0.18		
1.22	21.0	0.24	46.3	0.84	16.5	0.19	36.3	0.86	12.8	0.14		
1.30	18.2	0.20	48.2	0.86	14.1	0.16	37.7	0.89	11.0	0.12		
1.40	15.1	0.17	48.9	0.87	11.2	0.13	37.8	0.90	8.9	0.10		
1.55	11.4	0.12	51.1	0.92	8.5	0.09	38.1	0.91	6.3	0.07		
1.62	9.8	0.11	51.7	0.93	7.4	0.08	38.6	0.92	5.5	0.06		
1.70	7.9	0.08	51.8	0.94	5.9	0.06	38.6	0.92	4.5	0.05		
1.80	6.8	0.07	52.6	0.95	5.0	0.05	39.0	0.94	3.7	0.04		
2.10	3.6	0.03	53.6	0.97	2.4	0.02	39.9	0.96	1.8	0.02		
7.0	1.0	0.00	55.0	1.00	0.6	0.00	40.8	0.98	0.5	0.00		
12.3	1.0	0.00	54.0	0.98	0.7	0.00	41.5	1.00	0.5	0.00		
13.0	0.9	0.00	53.3	0.97	0.8	0.00	39.1	0.94	0.5	0.00		

TABLE 3.4 $pK(S_1)$ values of xanthone at several temperatures

TEMPERATURE (^{o}C)	$pK(S_1)$
20	0.98
30	0.87
40	0.75
50	0.63
60	0.53

Since $\Delta G^{o} = 2.303\ RT\ pK$

and $pK = \frac{\Delta H^{o}}{2.303\ RT} - \frac{\Delta S^{o}}{2.303\ R}$

a plot of $pK(S_1)$ vs. I/T should give a straight line if ΔH^{o} is constant over the temperature range. FIG. 3.5 shows a plot of $pK(S_1)$ against I/T for xanthone in aqueous solutions. The data give a reasonably good straight-line plot and from the slope a value of ΔH^{o} of 21 ± 2 kJ mol^{-1} is obtained. From the results in the previous section, since $pK(S_o)$ was not affected to any great extent by temperature, the ΔH^{o} value for the protonation in the ground state must be near zero. The greater ΔH^{o} value in the excited state is as expected from Förster Cycle calculations (see section (f)). Using the values $\Delta H^{o} = 0 \pm 2$ and $\Delta H^{o*} = 21 \pm 2$ kJ mol^{-1} in a Förster Cycle type calculation i.e. using the equation

$$pK(S_o) - pK(S_1) = \frac{\Delta H^{o} - \Delta H^{o*}}{2.303\ RT}$$

a value of -0.2 ± 0.5 is obtained for $pK(S_1)$. Using the slightly negative ΔH^{o} value previously determined[139] a $pK(S_1)$ value nearer that experimentally determined can be calculated. In any case the calculated value does indicate that non-equilibrium effects can be neglected.

(d) Flash Spectroscopy: Determination of $pK(T_1)$

Flash photolysis of xanthone in degassed ethanol and hexane solutions at room temperature showed a transient absorption immediately to the

FIG. 3.5 $pK(S_1)$ against the reciprocal of the temperature (K) for xanthone in aqueous solutions.

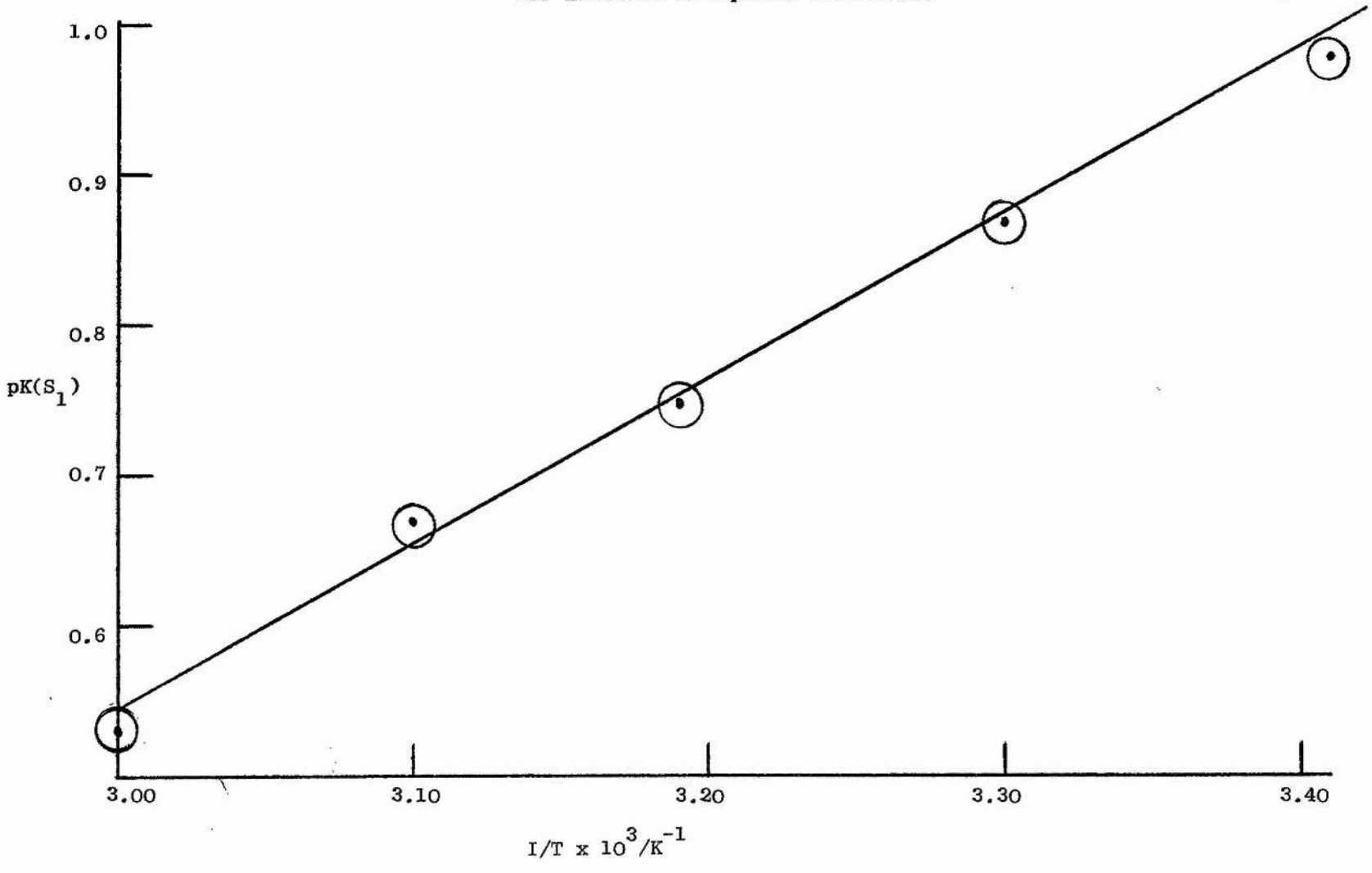

long-wavelength side of the S_o-S_1 absorption band i.e. in the region 360-400 nm. Due to the cut off of the glass optics and the overlapping bands an absorption spectrum of this weak transient was difficult to construct. No transient was observed in degassed benzene solution. Using a flash energy of 150 J (cf. 500 J in our case), Pownall and Huber[130] did not observe any transients on flashing xanthone in ethanol or benzene but did observe a weak transient with a maximum at 390 nm using a laser flash apparatus.

In ethanol and hexane solutions the xanthone was considerably decomposed on flashing. FIG. 3.6 shows the spectral changes resulting from flash irradiation of xanthone in ethanol. This is similar to the changes observed by Zanker and Ehrhardt who showed that on continuous irradiation with ultraviolet light xanthones in ethanol solution were reduced to xanthenes[141].

In aqueous solutions both the neutral, B, and protonated, BH^+, form of xanthone show a transient absorption on flashing. The shape of the T-T absorption band found in 98% H_2SO_4 changes little on decreasing the acidity to pH = 0. This absorption was assumed to be that of the BH^+ form of xanthone. On increasing the pH from 0 to 7 a stronger absorption appeared which was ascribed to the unprotonated xanthone molecule. The extent of decomposition, as measured by changes in the S_o absorption spectrum (the fluorescence emission intensity showed a corresponding change), was less in aqueous solutions than in ethanol or hexane. Assuming that the reaction causing the changes is hydrogen abstraction by the carbonyl group in the triplet state this decreased activity is expected and has been observed in an analogous reaction with benzophenone[142]. Aqueous solutions in which the excited triplet species was the protonated form showed much less decomposition than those in which the B triplet was observed. In the following $pK(T_1)$ determination the photolysis light was filtered through a 0.25 cm thick Pyrex glass

FIG. 3.6 Absorption spectrum of xanthone in ethanol
(a) before and (b) after flashing.

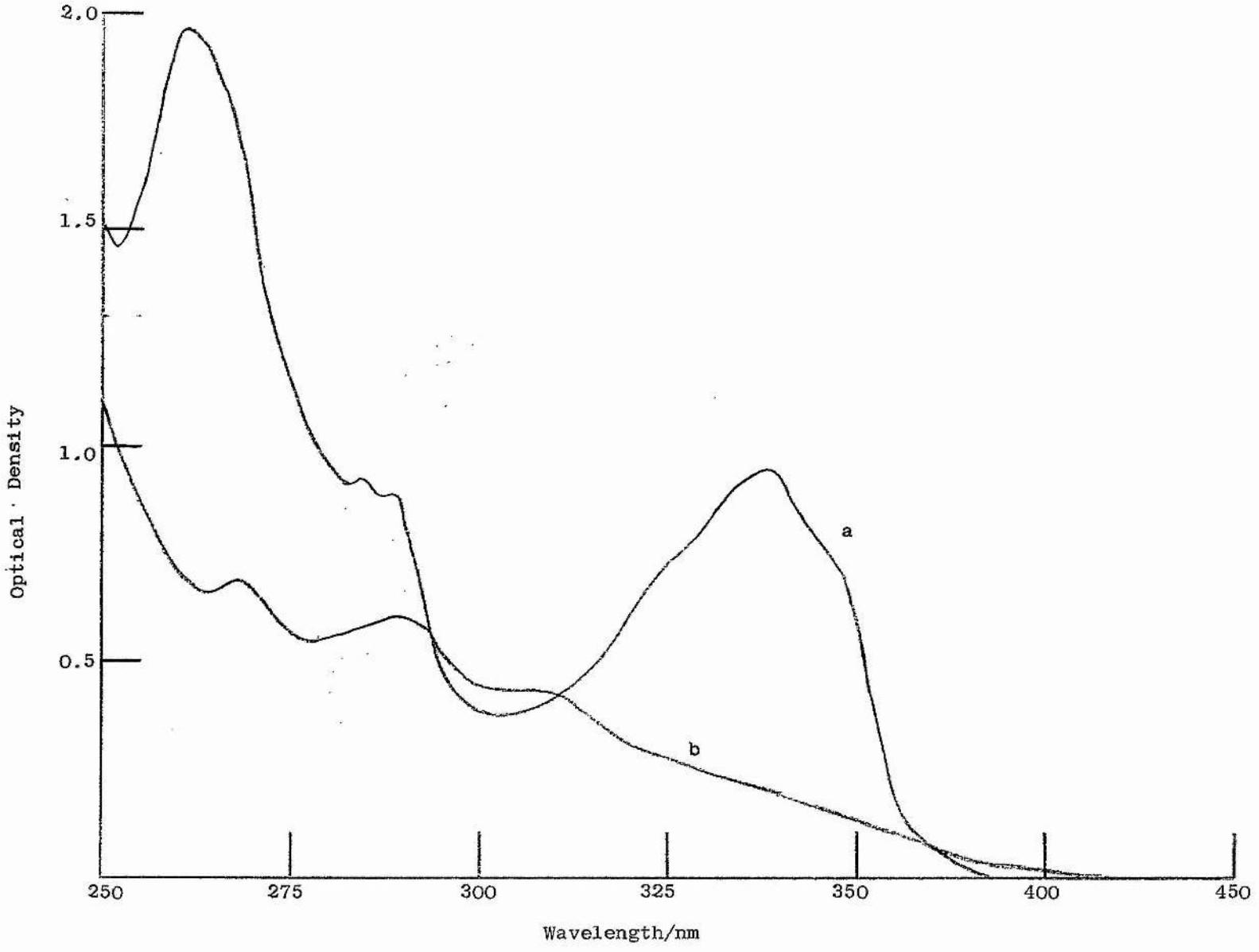

cylinder, thus exciting xanthone mainly to the S_1 state and reducing the extent of decomposition to < 10% after 6 flashes in all cases.

A series of xanthone solutions of differing acidity was flashed and the optical density changes with pH, for both the B and BH^+ T-T absorptions, observed. The concentration of xanthone was 2×10^{-5} M in 10% ethanol/water mixtures. The addition of alcohol to the solutions was necessary to prevent xanthone precipitating during the freezing involved in the degassing procedure. For pH values of 2-12 buffer solutions (10^{-2} M) were employed; for pH > 12 aqueous sodium hydroxide and for pH < 2 aqueous perchloric acid were used.

The preliminary study over a wide acidity range showed that the change in form of the T-T absorption took place in the 2-4 pH region. A detailed study of the pH range was therefore performed. FIG. 3.7 shows the T-T absorption at three pH values. The B and BH^+ triplet show absorption maxima at 585 nm and 530 nm respectively. Within experimental errors there is an isobestic point at 556 nm which indicates that the species are in equilibrium. FIG. 3.7 shows that there is considerable overlap of the absorption bands of the two species. To obtain the true optical densities of B and BH^+ (i.e ϕ and ϕ' respectively) the measured optical densities (I and I') were corrected for overlap by the same method as that used for fluorescence. Table 3.5 shows the measured and the corrected optical densities as well as the relative optical densities, ϕ/ϕ_o and ϕ'/ϕ'_o. At pH values above 9 marked quenching of the T-T absorption (probably by OH^-) is observed but a value of ϕ_o can be obtained from the plateau region (pH 5-8) before quenching commences. A value for the maximum optical density of BH^+, inaccessible experimentally due to the S_1 equilibrium, was obtained from the relationship,

$$\phi/\phi_o + \phi'/\phi'_o = 1 \qquad (3.6)$$

since ϕ_o was known and values of ϕ and ϕ' could be used in the region

FIG. 3.7 T-T absorption of xanthone at three pH values: (a) pH = 7.0, (b) pH = 2.8, (c) pH = 2.1.

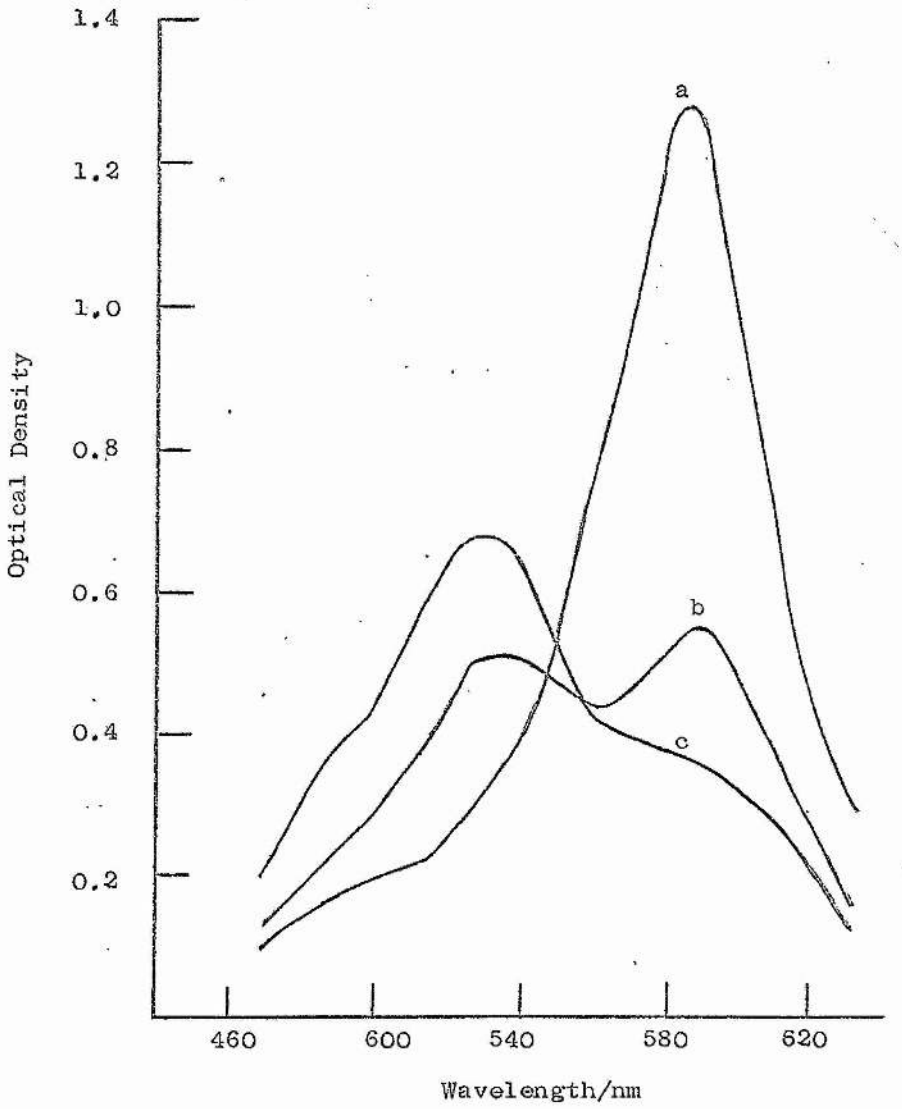

TABLE 3.5. Optical densities of the T-T absorption of protonated and unprotonated xanthone as a function of pH.

pH or H_o	B^* at 585 nm. $\phi_o = 1.31$, $k = 0.28$				BH^{+*} at 530 nm. $\phi_o' = 0.84$, $k = 0.37$			
	I	kI	$\frac{I-k'I'}{I-kk'}$	ϕ/ϕ_o	I'	k'I'	$\frac{I'-kI}{I-kk'}$	ϕ'/ϕ_o'
-8.6	0.15	0.04	0.00	0.00	0.48	0.17	0.47	0.56
-3.0	0.12	0.03	0.00	0.00	0.37	0.13	0.36	0.43
-1.0	0.11	0.03	0.01	0.01	0.28	0.10	0.28	0.33
-0.5	0.16	0.04	0.04	0.03	0.31	0.11	0.29	0.35
0.04	0.15	0.04	0.04	0.03	0.31	0.11	0.30	0.36
0.53	0.10	0.03	0.00	0.00	0.37	0.13	0.36	0.43
0.89	0.27	0.07	0.08	0.06	0.54	0.19	0.49	0.58
1.23	0.17	0.05	0.00	0.00	0.55	0.20	0.56	0.67
1.40	0.25	0.07	0.03	0.02	0.61	0.21	0.57	0.68
2.11	0.40	0.10	0.14	0.11	0.70	0.25	0.63	0.75
2.76	0.55	0.15	0.40	0.31	0.52	0.19	0.41	0.49
3.29	1.00	0.28	0.90	0.69	0.52	0.19	0.26	0.31
3.77	1.18	0.32	1.14	0.87	0.41	0.15	0.10	0.12
4.31	1.29	0.36	1.28	0.98	0.39	0.14	0.03	0.04
6.26	1.32	0.36	1.31	1.00	0.39	0.14	0.03	0.04
6.98	1.31	0.36	1.32	1.01	0.32	0.12	0.03	0.04
8.36	1.35	0.35	1.30	0.99	0.33	0.11	0.00	0.00
9.30	1.20	0.33	1.20	0.92	0.32	0.12	0.00	0.00
11.04	1.06	0.28	1.00	0.76	0.33	0.11	0.00	0.00
11.43	0.72	0.19	0.67	0.51	0.22	0.08	0.06	0.07
12.06	0.27	0.07	0.24	0.18	0.14	0.05	0.04	0.05
12.30	0.08	0.02	0.07	0.05	0.05	0.02	0.08	0.10
14.00	0.00	0.00	0.00	0.00	0.00	0.00	0.03	0.04

above pH 3 unaffected by the S_1 equilibrium. FIG. 3.8 shows the relative optical densities as a function of pH from which a value of 3.0 is obtained for $pK(T_1)$. The relative optical density of B(⊙) gives a straightforward sigmoid curve when plotted against pH. For BH^+ (Δ) the optical density increases as the pH value is decreased below 5 due to the formation of BH^+ triplets by protonation of $\overset{*}{B}$ (the B form is the only species present in the ground state). As the pH is further decreased the optical density of BH^+ triplets reaches a maximum value and then decreases (see FIG. 3.8). This is due to the effect of the S_1 equilibrium on the quantum yield of triplet formation. In solutions of pH $\approx$ 1 the protonation reaction of the S_1 state can compete with intersystem crossing from $S_1 \longrightarrow T_1$. Molecules protonated in the S_1 state can still undergo intersystem crossing and contribute to the optical density of BH^+ triplets but since $\overset{*}{BH}^+$ is a much more efficient fluorescer than $\overset{*}{B}$ we can reasonably assume that the quantum yield of triplet formation is less for BH^+ than for B. Hence S_1 protonation produces the observed decrease in $\overset{*}{BH}^+$ optical density. A confirmatory indication of $pK(S_1)$ at 0.9 is obtained from the relative optical density plot at acidities greater than $pK(T_1)$. On increasing the acidity beyond $pK(S_o)$, an increase in the optical density of the BH^+ T-T absorption was observed, as expected from the different absorption characteristics of the ground state forms. The implied possibility of determining $pK(S_o)$, $pK(S_1)$, and $pK(T_1)$ all from T-T absorption measurements may have applications (e.g. for obtaining $pK(S_1)$ of non-fluorescent compounds.)

With triplet life-times in the μs region (the BH^+ triplet was longer lived than that of B, an indication of the $n\text{-}\pi^*$ character of the B triplet[31]), the simple determination of $pK(T_1)$ from the pH of half protonation is presumably not vitiated by non-equilibrium effects. Confirmation that protonation rates were indeed fast enough was obtained

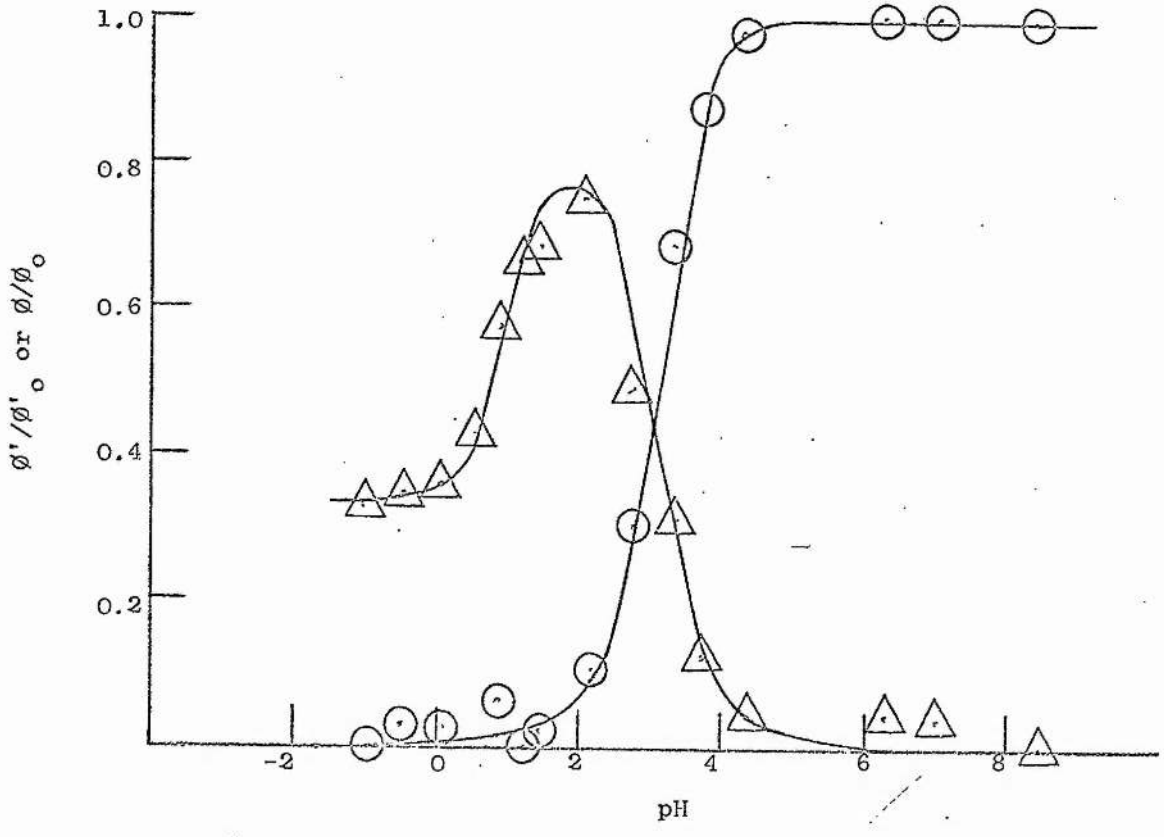

FIG. 3.8 Relative optical densities of T-T absorption of protonated and unprotonated xanthone as a function of pH: △, ϕ'/ϕ'_o at 350 nm (protonated form); ○, ϕ/ϕ_o at 585 nm (unprotonated form).

from a few measurements at different delay settings: the proportions of triplet B and BH^+ were found to be independent of the time of delay.

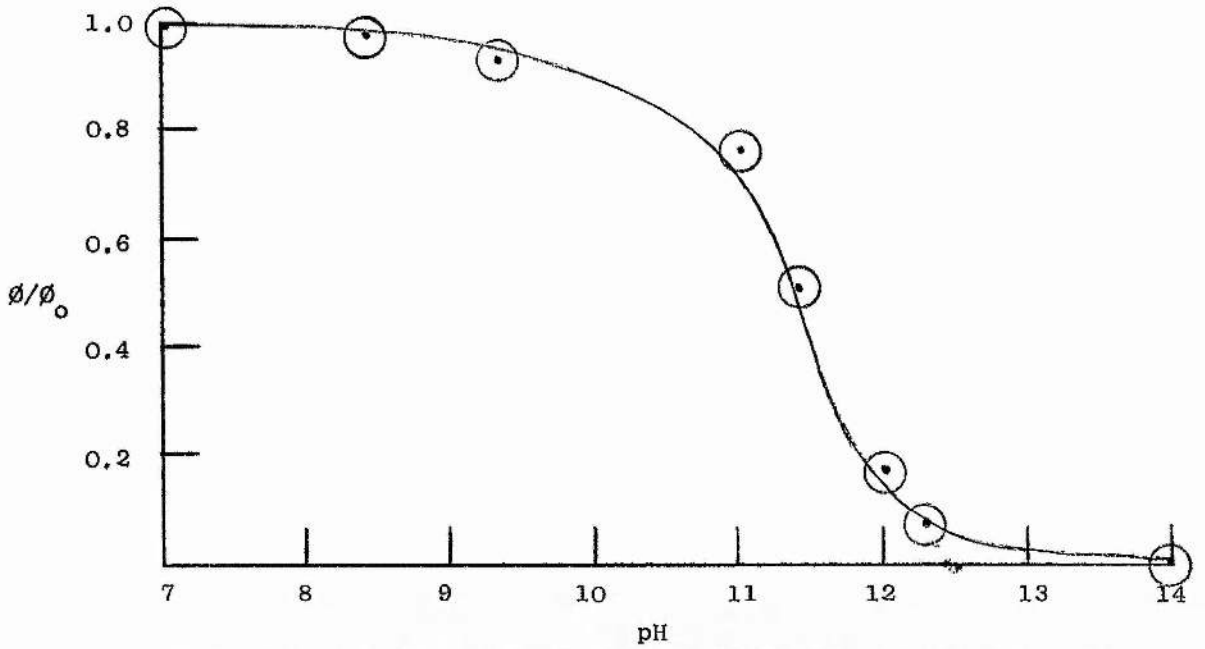

FIG. 3.9 Relative optical density ($\emptyset/\emptyset_o$) of the T-T absorption of xanthone (B form) as a function of pH.

FIG. 3.9 shows the relative optical density of $\overset{*}{B}$ against pH in alkaline solutions. The sigmoid curve obtained would be consistent with either a protolytic reaction or with a collision quenching reaction of the neutral xanthone triplet. The extent of decomposition on flashing appeared to increase in this region where the T-T absorption disappears. This may be due to the quenching reaction being irreversible. The fact that no new transient species is observed may indicate that the process is collisional quenching, probably by OH^- ions but in any case the products formed by the reaction would seem to be in their ground states. The reaction involves the triplet state since the fluorescence intensity is not affected by the OH^- concentration.

The flash photolysis experiments in aqueous solutions appeared to indicate that the extent of decomposition of xanthone was very dependent on the acidity of the solution. If this was due to protonation

of the carbonyl triplet competing with hydrogen abstraction then a possible method of $pK(T_1)$ determination will be to plot the extent of decomposition against pH. A series of experiments was performed, in conjunction with J. Arnott during the course of her Senior Honours project, in which the optical density of xanthone solutions was monitored while under continuous irradiation from a 150 watt xenon lamp. The solutions and buffers were as in the flash photolysis experiments and the optical density was monitored at 350 nm. Although the spread of the results is large (see FIG. 3.10) they indicate a change in the rate of decomposition at approximately pH 3 ($pK(T_1)$ = 3.0) and a further change at higher pH values where the quenching of $\overset{*}{B}$ triplet-triplet absorption was observed. The extent of decomposition was reduced when oxygen was present in solution probably due to oxygen quenching of the triplet and very little decomposition of xanthone in benzene or carbon tetrachloride was noted.

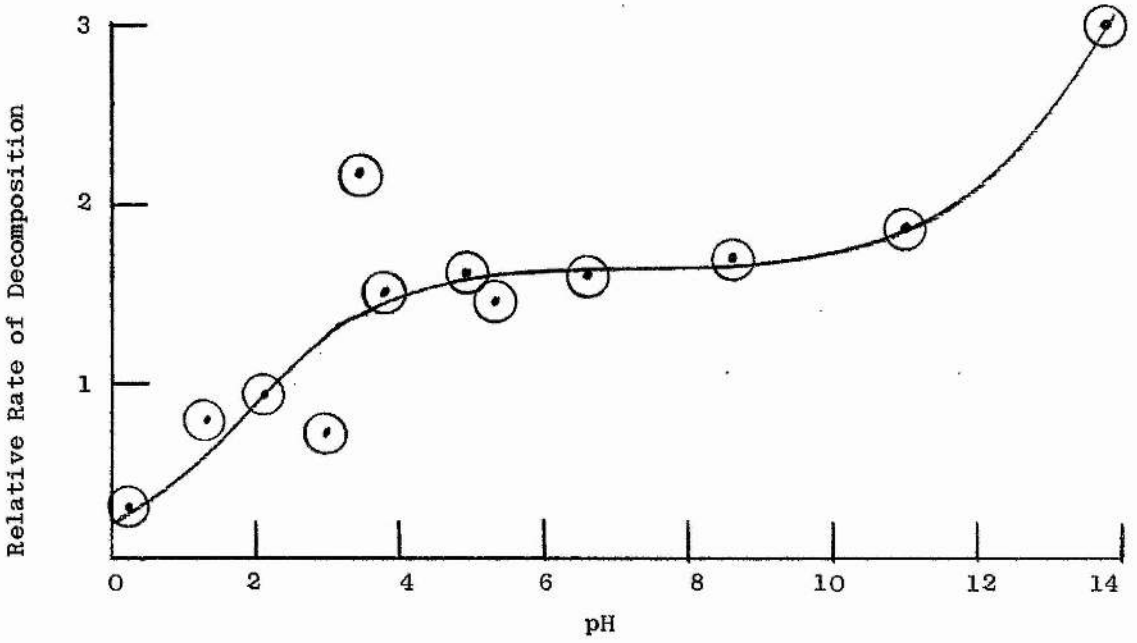

FIG. 3.10 Relative rate of decomposition of xanthone on irradiation as a function of pH.

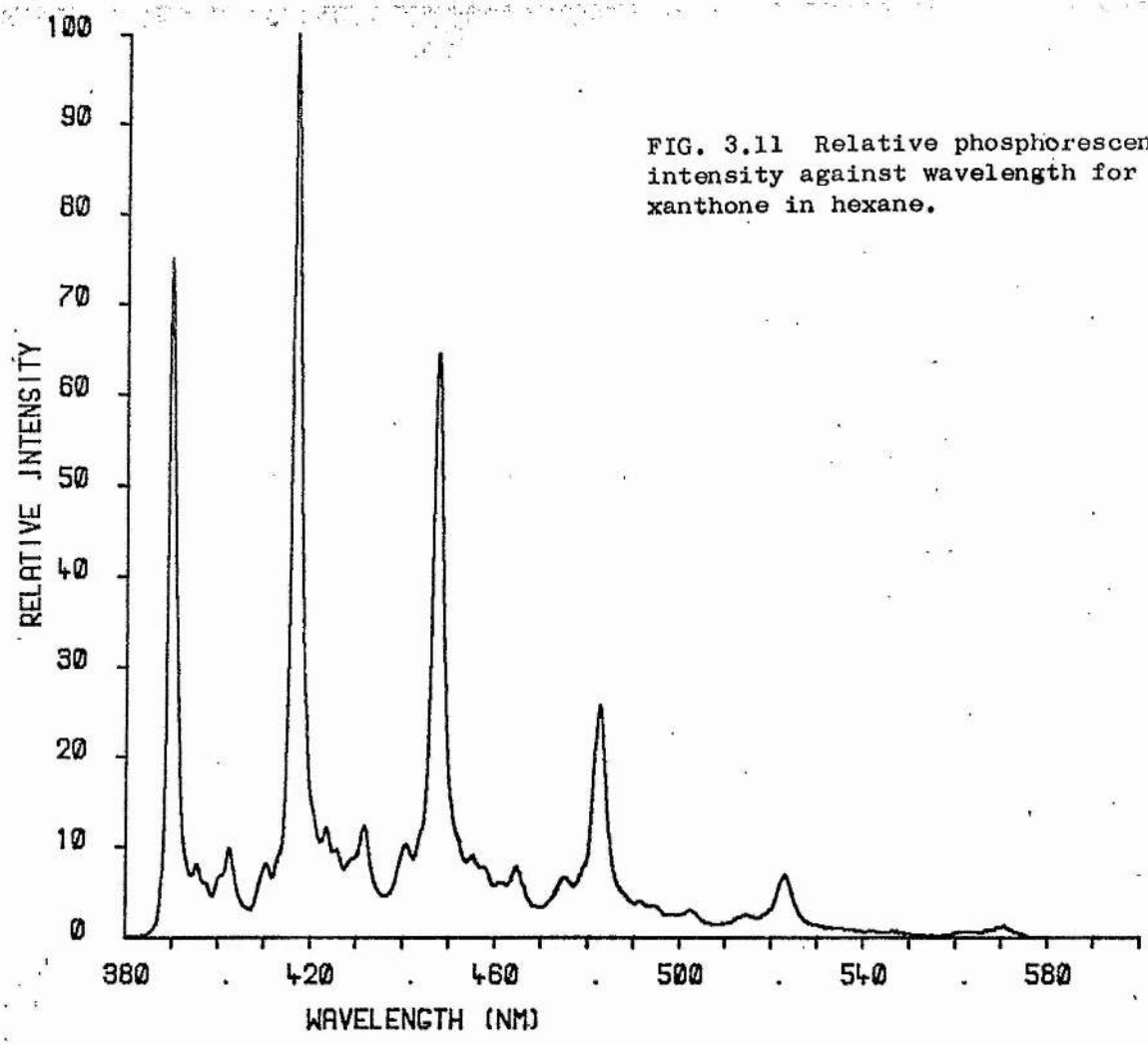

FIG. 3.11 Relative phosphorescence intensity against wavelength for xanthone in hexane.

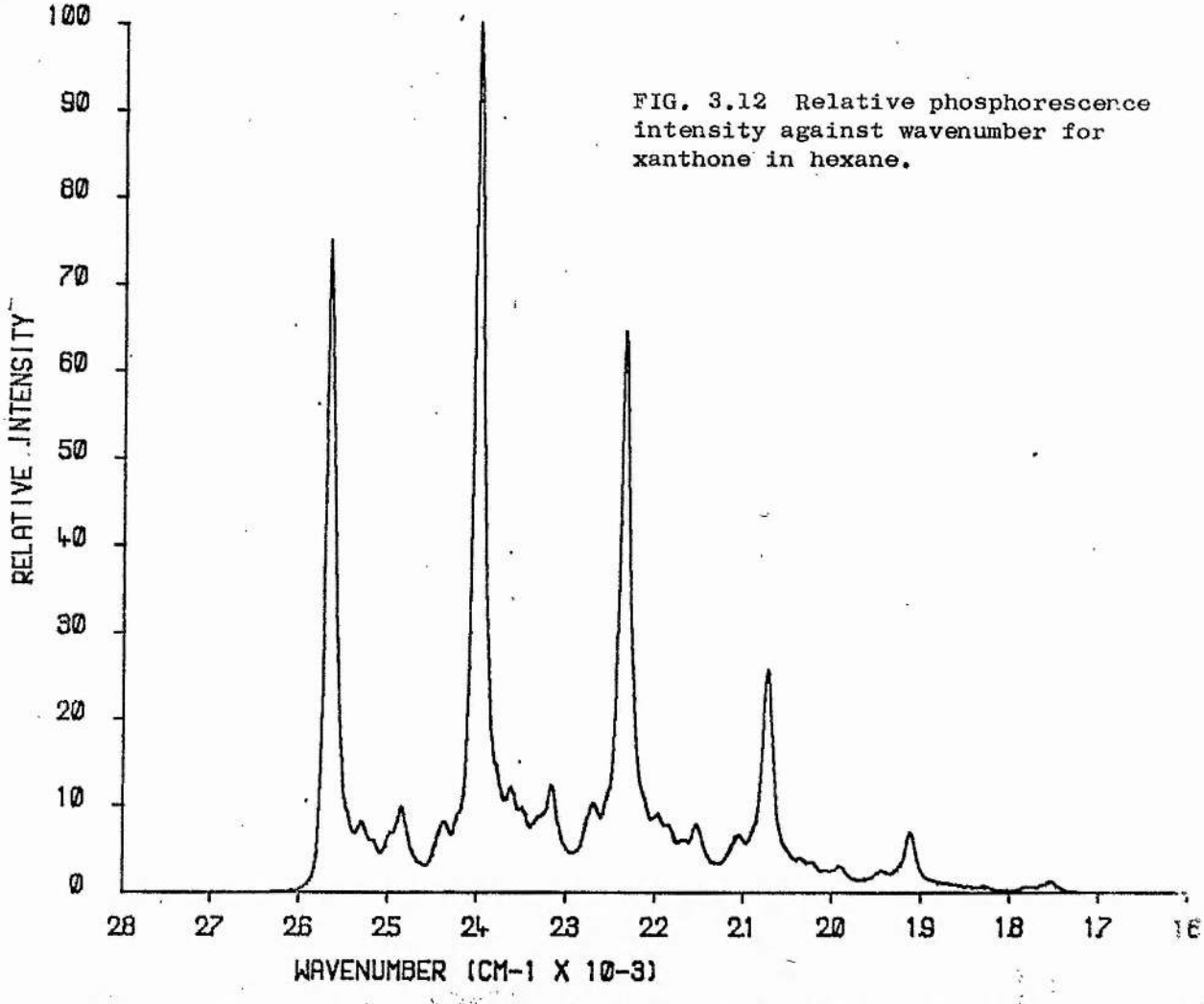

FIG. 3.12 Relative phosphorescence intensity against wavenumber for xanthone in hexane.

(e) Phosphorescence Spectroscopy

In hexane solution at liquid nitrogen temperature xanthone shows a short-lived structured phosphorescence. The corrected phosphorescence intensity is shown in FIG. 3.11 plotted against wavelength and in FIG. 3.12 plotted against wavenumber. This highlights the advantages of the semiautomatic computer correction procedure described in Chapter 2.3(e). The process of manually correcting spectra with this extent of fine structure would be extremely tedious. The ability to obtain plots of intensity vs. wavenumber is also advantageous. In this case (FIG. 3.12) the C=O vibration frequency (1670 cm^{-1}) is clearly indicated in the equal spacing of the main intensity peaks. A similar emission was observed at 77 K with xanthone in isopentane solution. No fluorescence emission was observed at low temperature with these solutions. An energy level diagram for xanthone in non-polar solvents is shown schematically in FIG. 3.13.

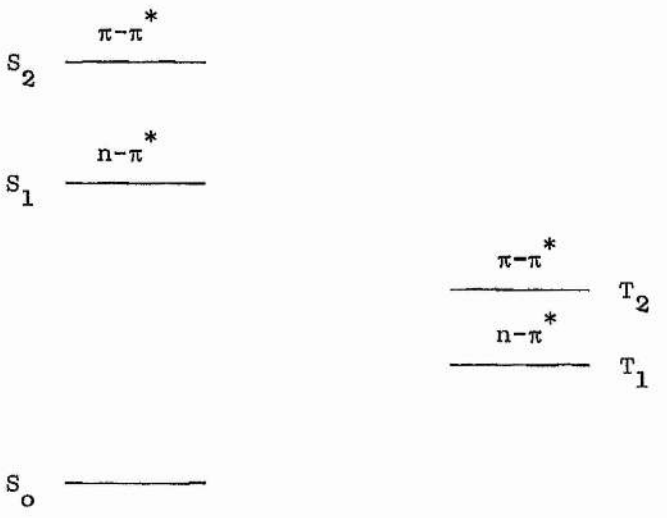

FIG. 3.13 Schematic energy level diagram for xanthone in non-polar solvents.

In these solvents xanthone is a group II molecule and shows only phosphorescence, the pathway to T_1 population, $S_{n\pi^*} \rightsquigarrow T_{\pi\pi^*} \rightsquigarrow T_{n\pi^*}$, being an efficient process.

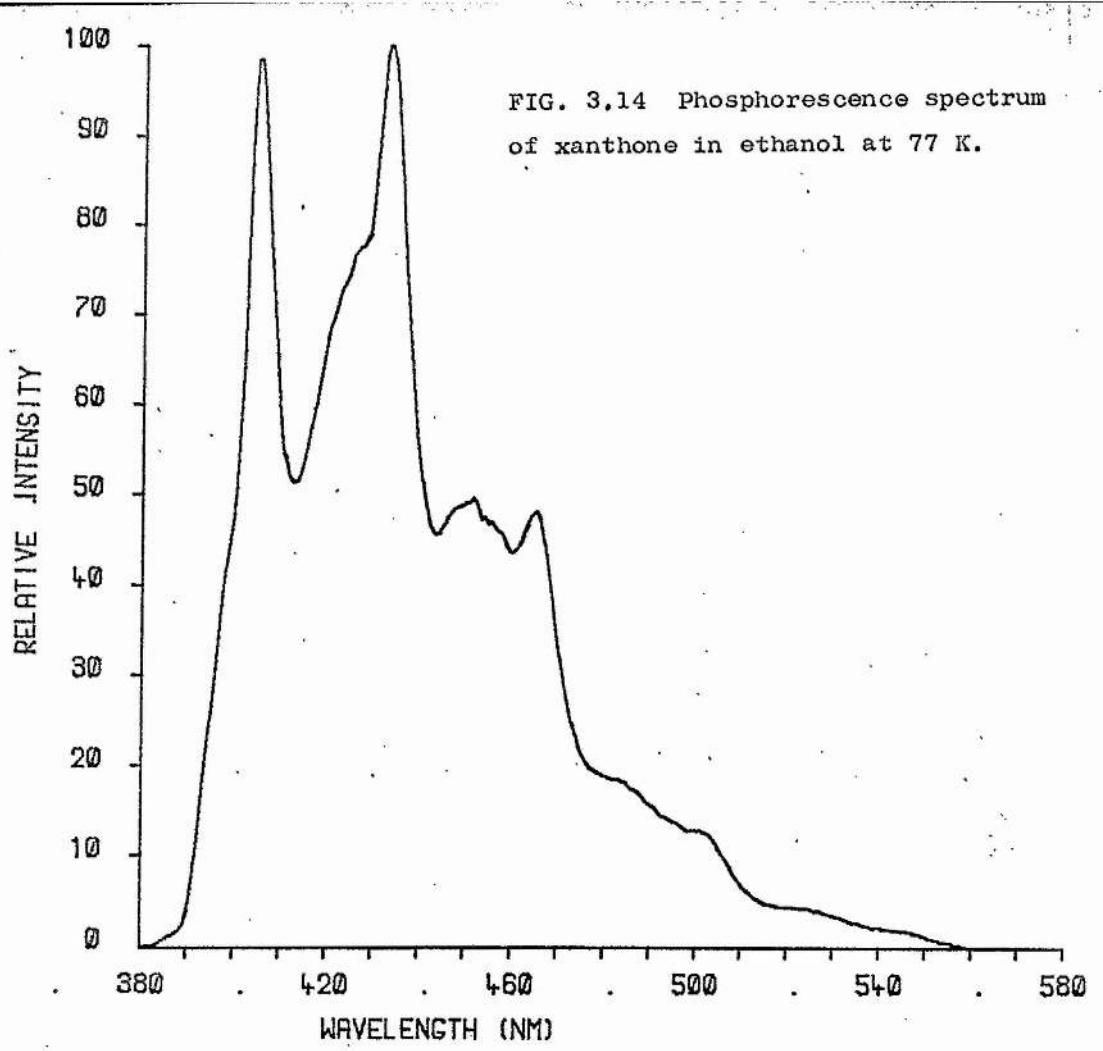

FIG. 3.14 Phosphorescence spectrum of xanthone in ethanol at 77 K.

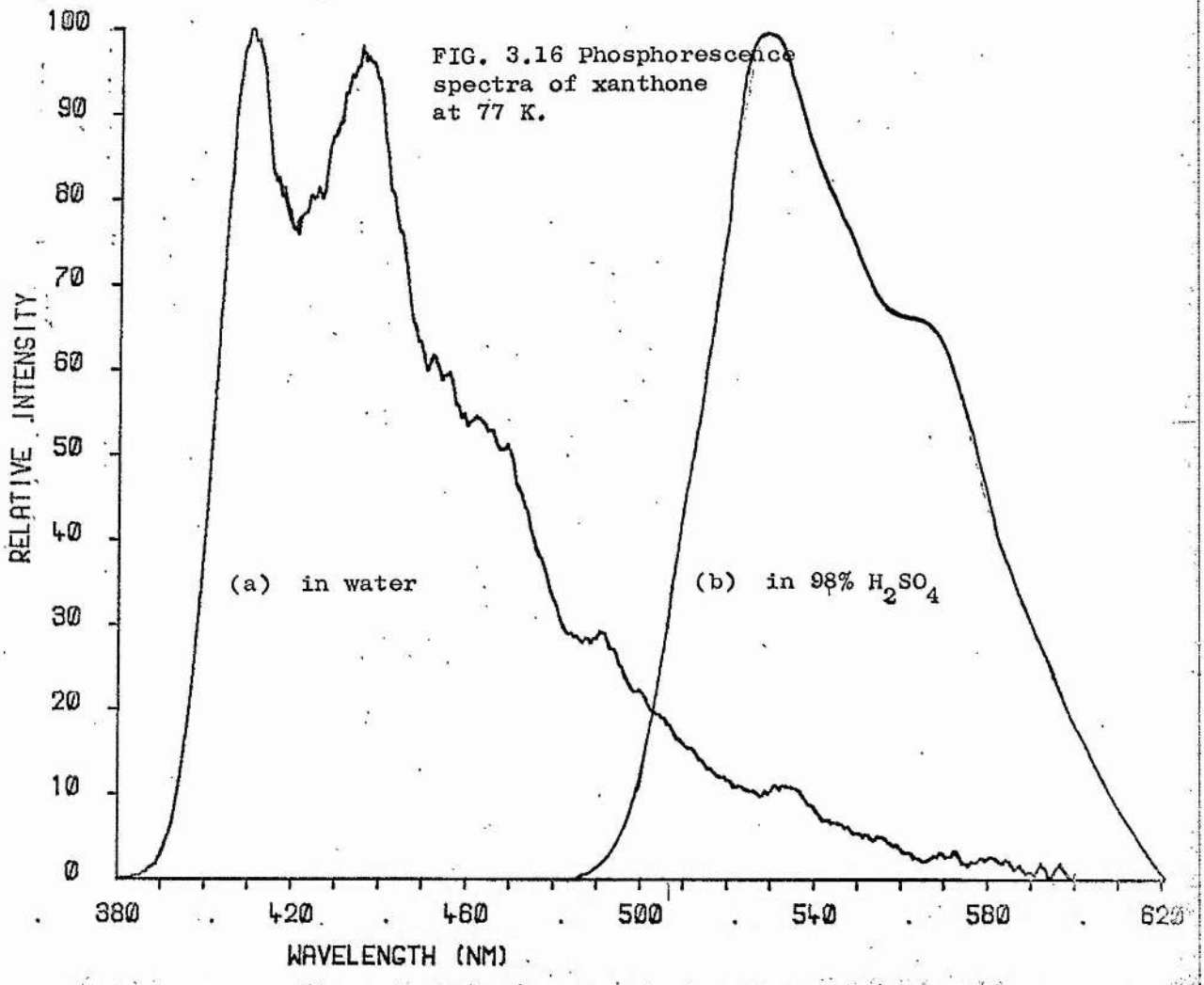

FIG. 3.16 Phosphorescence spectra of xanthone at 77 K.

In ethanol the phosphorescence emission spectrum is completely changed and is much longer lived indicating that the triplet is now of the π-π^* type[31]. The phosphorescence spectrum of xanthone in ethanol is shown in FIG. 3.14. Similarly structured phosphorescence spectra were obtained in E.P.A. and CH_3CN. No low temperature fluorescence was observed from these solutions. The nature of the S_1 state of xanthone in ethanol cannot be unequivocally established from the absorption spectrum but the molecule in polar solvents belongs to group III or IV and only phosphorescence emission is expected.

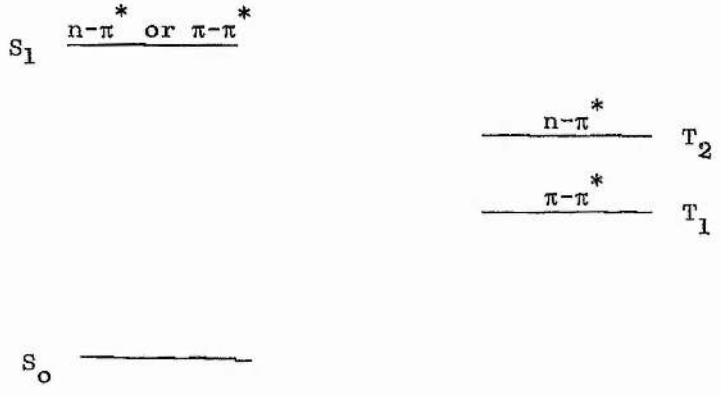

FIG. 3.15 Schematic energy level diagram for xanthone in polar solvents.

The fluorescence observed from $\overset{*}{B}$ in aqueous solutions could be due to a hydrogen-bonded complex in the excited state (see this Chapter section 2(b)) but it is also possible that the n-π^*, π-π^* character of the S_1 state changes and results in the emission.

The phosphorescence spectrum of xanthone in water is similar to that in ethanol but not as well resolved. Addition of very small amounts of ethanol to the aqueous solutions appeared to increase the intensity of the phosphorescence substantially but it was not possible to determine whether this was a real effect on the phosphorescence quantum yield or due to the better 'glass' formed with ethanol present. The BH^+ form of xanthone in a 98% H_2SO_4 or 60% $HClO_4$ glass showed a

phosphorescence weaker than that of the B form and at longer wavelengths. The phosphorescence spectra of B and BH^+ are shown in FIG. 3.16. Both these emissions were long lived, compared with the phosphorescence of xanthone in hexane, indicating that π-π^* triplet levels were involved.

Due to the poor qualities of the solid formed by water at 77 K a total emission spectrum at 77 K could not be obtained because of the scattered light. The phosphorescence was observed but fluorescence, if any, was hidden by this scattered light. In the total emission spectrum of the BH^+ form at 77 K (see FIG. 3.17) the phosphorescence is completely masked by the strong fluorescence. The fluorescence band shows some fine structure not observed in the corresponding emission from fluid solution. Phosphorescence was observed from alkaline solutions of xanthone. The quenching of the triplet, observed in fluid media by the flash experiments, probably does not operate in solid solutions due to the limited possibility of encounter between the molecule in its triplet state and the quenching ion.

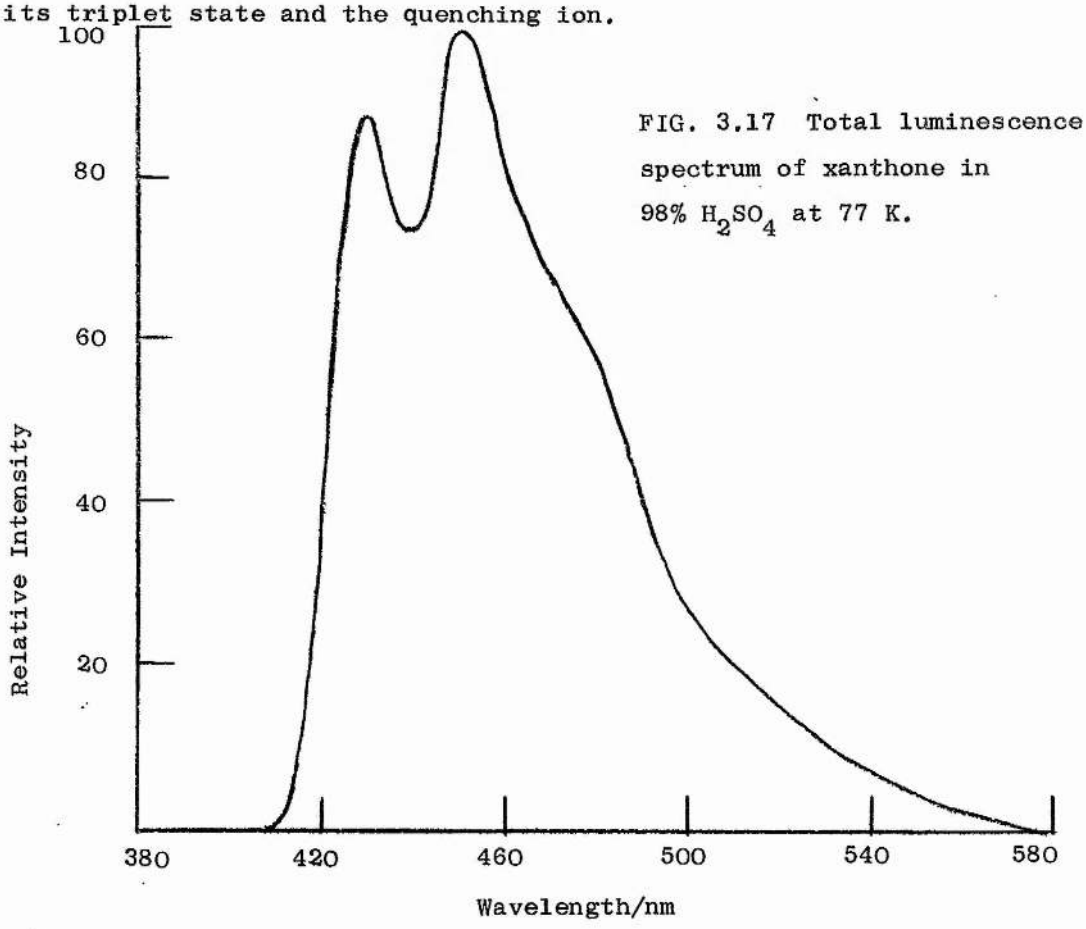

FIG. 3.17 Total luminescence spectrum of xanthone in 98% H_2SO_4 at 77 K.

(f) Förster Cycle calculations; the ordering of xanthone pK values.

Table 3.6 gives the spectral data used in the Förster cycle calculations on xanthone and the pK values calculated.

TABLE 3.6 pK^* values of xanthone based on Förster cycle calculations

	λ_{max}/nm for B	λ_{max}/nm for BH^+	$\Delta\bar{\nu}$/cm^{-1}	Δ pK	pK^* (Förster)	pK^* (expt)
absorption	345	398	3860	8.1	4.0(S_1)	
fluorescence	395	456	3390	7.2	3.1(S_1)	0.96(S_1)
average of absorption and fluorescence	370	427	3610	7.6	3.5(S_1)	
phosphorescence	410	512	4860	10.3	6.2(T_1)	3.0(T_1)
T-T absorption	585	530	-1770	-3.7	-0.7(T_2)	

For the calculation of $pK(S_1)$ and $pK(T_1)$ a value of -4.1 is used for $pK(S_o)$ and in the calculation of $pK(T_2)$ a $pK(T_1)$ value of 3.0 is used. When $pK(S_o)$ is based on an acidity function scale the Förster Cycle may not give a very good quantitative estimate of $pK(S_1)$ or $pK(T_1)$ (see Chapter 5), but nevertheless the values of $pK(S_1)$ and $pK(T_1)$ for xanthone so calculated are in the same order relative to $pK(S_o)$ as the values obtained experimentally from the $[B]/[BH^+]$ ratios. The experimental values given in Table 3.6 are those obtained at room temperature. Thus with the experimentally obtained values of $pK(S_o) = -4.1$, $pK(S_1) = 0.96$ and $pK(T_1) = 3.0$ we obtain the pK order $pK(T_1) > pK(S_1) > pK(S_o)$ for xanthone. This order is reproduced in the Förster Cycle calculated values whether the differences are calculated from absorption maxima or fluorescence maxima alone or from averaging the two. This pK order is unusual since it has been postulated that all $pK(T_1)$ values will lie within the $pK(S_o)$-$pK(S_1)$ range and former experimental determinations

have apparently confirmed this (see Table 1.2). The three pK values for xanthone can only be compared if they refer to the same reaction in each case. Xanthone (I) has two possible protonation sites,

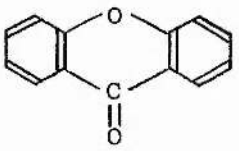

I

the carbonyl oxygen and the bridging ether oxygen. In the ground state the carbonyl group is the most basic and protonnates at high acid concentrations. In the excited state it is possible that in either the S_1 or T_1 state or both the bridging oxygen becomes a stronger base than the carbonyl group although several factors suggest that this is not the case. The spectral data used for the Förster Cycle calculation of $pK(T_1)$ were obtained from solid solutions of xanthone at 77 K and we might expect the emitting species to be the same as the ground state species. Also the constant illumination study of the decomposition of xanthone indicates that there is a change in the reaction rate in the region of $pK(T_1)$ which can be explained by competing reactions at the carbonyl group. To obtain further information on the position of protonation calculations of the ground and excited state charge densities were performed.

The Förster Cycle, applied to the triplet-triplet absorption spectra of the protonated and unprotonated species, indicates a $pK(T_2)$ of -0.7, so that in basic strength the second triplet state lies between S_o and S_1. In this calculation we have assumed that the absorptions correspond in each case to the T_1-T_2 transition. Since internal conversion from $T_2 \rightarrow T_1$ will be very fast compared to the rate of protonation, equilibrium cannot possibly be established in the T_2 state and therefore the $pK(T_2)$ value obtained above is only of theoretical interest.

(g) Theoretical Calculations on Xanthone

Calculations were carried out using a modified CNINDO program (distributed by the QCPE organisation[143]) working on single precision. Xanthone was assumed to be planar and the molecular geometry used was based on that reported for anthraquinone and benzophenone derivatives[144]. The numbering system used in the tables is

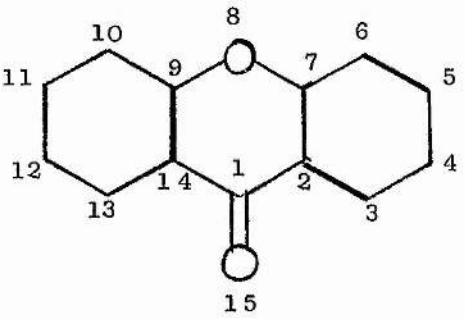

The calculated orbital populations and the atomic charges for xanthone in the ground and triplet states are shown in Tables 3.7 and 3.8 respectively. The calculations indicate that there is a movement of electrons away from the carbonyl oxygen on going from the ground to the triplet state although the π electron density on this oxygen is increased. Calculations on the benzophenone molecule have indicated a similar redistribution of charge in the excited state[145,146,147]. It has been suggested that there is a linear relationship between the charge on the basic atom of a given molecule in various electronic states and the pK in that state[148]. This has not been found for all cases and arguments have been developed which suggest that identical charges do not have an equivalent effect on the pK if they do not correspond to the same distribution of spin density[149]. If this linear relationship existed for xanthone the calculated charge densities indicate that xanthone would be a weaker base in the triplet state, and that the position of protonation would change from the carbonyl oxygen in the ground state to the ether oxygen in the triplet state. Calculations showed

TABLE 3.7 Orbital populations and atomic charges for xanthone in the ground state.

Position	σ	π	Total	Atomic Charge
C_1	2.9010	0.8144	3.7154	+0.2846
C_2, C_{14}	3.0262	1.0694	4.0956	-0.0956
C_3, C_{13}	2.9747	0.9520	3.9267	+0.0733
C_4, C_{12}	2.9795	1.0275	4.0070	-0.0070
C_5, C_{11}	2.9693	0.9611	3.9304	+0.0696
C_6, C_{10}	2.9801	1.0622	4.0423	-0.0423
C_7, C_9	2.8207	0.9420	3.7627	+0.2373
O_8	4.4304	1.8464	6.2768	-0.2768
O_{15}	5.0373	1.3089	6.3462	-0.3462

TABLE 3.8 Orbital populations and atomic charges for xanthone in the triplet state.

Position	σ	π	Total	Atomic Charge
C_1	2.7850	1.1297	3.9147	+0.0853
C_2, C_{14}	2.9813	1.0416	4.0229	-0.0229
C_3, C_{13}	2.9634	1.0006	3.9640	+0.0360
C_4, C_{12}	2.9781	1.0129	3.9910	+0.0090
C_5, C_{11}	2.9588	0.9945	3.9533	+0.0467
C_6, C_{10}	2.9794	1.0509	4.0303	-0.0303
C_7, C_9	2.8133	0.9808	3.7941	+0.2059
O_8	4.4204	1.8584	6.2788	-0.2788
O_{15}	4.2836	1.8466	6.1302	-0.1302

that in the triplet state the two oxygen atoms of xanthone do not have similar spin densities. In any case, the charge densities cannot be a principal factor in determining the pK values since the basicity of xanthone in both the singlet and triplet states is greater than in the ground state, irrespective of the position of protonation. From a simple consideration of the $n-\pi^*$ transition of a carbonyl group, since the transition involves charge transfer from the oxygen to the carbon, the basicity of the oxygen might be expected to decrease in both the singlet and triplet states but for many aromatic carbonyl compounds this has not been found to be the case (see Table 1.1).

In a further attempt to determine the position of protonation calculations of the total energy of the base form and possible protonated forms of xanthone were made. Table 3.9 shows the total energies of the three forms in their ground and triplet states. The electron densities and atomic charges for the protonated forms are given in Table 3.10

Table 3.9 Calculated total energies for xanthone B and BH^+ forms.

Molecular Form	Total Energy A.U.	
	Ground State	Triplet State
B	-130.12788	-130.05879
BH^+ (protonated carbonyl)	-130.66962	-130.53851
BH^+ (protonated ether)	-130.60119	-130.48892

The calculated energies indicate that in both the ground and triplet states protonation of the carbonyl oxygen produces the more stable molecule. Very limited geometry optimisation was performed in calculating these energies. For the unprotonated form the optimum length of the carbonyl carbon-oxygen bond was determined to be 1.23 and 1.24 Å in the ground and triplet states respectively. The increased bond length in the triplet state is expected since the promoted electron occupies an antibonding π^* orbital. In the case of the carbonyl

TABLE 3.10 Total electron densities and atomic charges calculated for protonated xanthone in the ground and triplet states.

	BH^+ (protonated carbonyl)				BH^+ (protonated ether)			
	Ground State		Triplet State		Ground State		Triplet State	
Position	Total Electron Density	Atomic Charge	Total Electron Density	Atomic Charge	Total Electron Density	Atomic Charge	Total Electron Density	Atomic Charge
C_1	3.6287	+0.3713	3.8951	+0.1049	3.6947	+0.3053	3.8998	+0.1002
C_2, C_{14}	4.0873	-0.0873	3.9873	+0.0127	4.0529	-0.0529	3.9565	+0.0435
C_3, C_{13}	3.9081	+0.0919	3.9541	+0.0459	3.9224	+0.0776	3.9688	+0.0312
C_4, C_{12}	3.9903	+0.0097	3.9189	+0.0811	3.9689	+0.0311	3.9706	+0.0294
C_5, C_{11}	3.8878	+0.1122	3.9634	+0.0366	3.9250	+0.0750	3.9630	+0.0370
C_6, C_{10}	4.0363	-0.0363	3.9444	+0.0556	4.0098	-0.0098	3.9972	+0.0028
C_7, C_9	3.7178	+0.2822	3.8474	+0.1526	3.8113	+0.1887	3.8218	+0.1782
O_8	6.2259	-0.2259	5.9674	+0.0326	6.0449	-0.0449	6.0231	-0.0232
O_{15}	6.2230	-0.2230	6.2305	-0.2305	6.2657	-0.2657	6.0727	-0.0727

protonated form the optimum energy corresponded to a structure with the added proton in the plane of the molecule. Further geometry optimisation would probably lead to better calculated energy values of the molecule.

(h) Xanthone Derivatives

4-hydroxyxanthone (II)

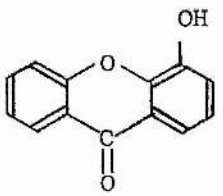

II

The absorption spectrum of this compound in ethanol or water is very similar to that of xanthone in these solvents but with the bands shifted slightly to longer wavelengths. In hexane it is not possible to detect a weak $n-\pi^*$ band as the first absorption band presumably because this band is, in this compound, overlapped by the more intense $\pi-\pi^*$ band which is red shifted compared to the corresponding band in xanthone. In 98% H_2SO_4 the absorption spectrum is identical in profile to the BH^+ absorption of xanthone but with maxima red shifted. With the identity of spectra in solutions of lower acidity this suggests that the compound is monoprotonated in 98% H_2SO_4.

Only a very weak low temperature emission could be detected from hexane solutions but solutions in alcohol and water showed both fluorescence and phosphorescence. This compound fluoresced in alcohol thus differing from xanthone. The emission properties of the BH^+ form were different from those of xanthone. No strong emission was observed from fluid solutions but at low temperature a short lived yellow emission and a very long lived phosphorescence were observed. Spectral data for 4-hydroxy-xanthone are given in Table 3.11 as well as ΔpK values calculated using the Förster Cycle.

TABLE 3.11 Spectral data and Δ pK values for 4-hydroxyxanthone.

	λ_{max}/nm for B	λ_{max}/nm for BH^+	$\Delta\bar{\nu}$/cm^{-1}	Δ pK
absorption	356	415	4000	8.4 (S_1-S_o)
fluorescence	425	480	2700	5.7 "
average of absorption and fluorescence	390	447	3300	7.0 "
phosphorescence	465	533	2700	5.7 (T_1-S_o)

The calculations indicate that 4-hydroxyxanthone becomes a stronger base in the S_1 and T_1 states but that, unlike xanthone itself, it has Δ pK(S_1-S_o) slightly larger than Δ pK(T_1-S_o).

In alkaline solutions a different absorption spectrum is observed, presumably due to deprotonation of the OH group, which has a first absorption maximum at longer wavelengths (λ_{max} = 400 nm) than the neutral molecule. Only very weak emission was observed from this form of the molecule but the absorption spectra indicate that in the S_1 state the hydroxyl group is a stronger acid (as expected from the behaviour of, e.g., the naphthols).

3,6-dihydroxyxanthone (III)

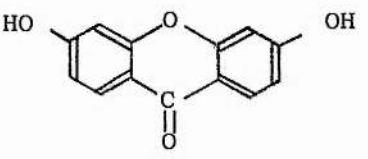

III

The absorption spectrum of the B and BH^+ forms of this compound showed several differences from the spectra of xanthone. In ethanol solution at low temperature a phosphorescent emission very similar to that of xanthone was observed as was the fluorescence and phosphorescence

of the BH^+ form. In fluid solution the strong blue fluorescence (430 nm) observed from BH^+ was replaced in less acidic solutions by a strong green (470 nm) fluorescence. Since there are several sites for protolytic reaction on this molecule a quantitative study of the fluid solution emissions would be needed to interprete the excited state reactions. The luminescence spectral data given in Table 3.12 refer to emission from solid solutions and the ΔpK values obtained should refer to the protonation of the carbonyl group. In aqueous solutions less acidic than $pK(S_o)$ the blue and the green fluorescence disappeared on freezing the solutions indicating that the emitting species were formed by excited state reactions.

TABLE 3.12 Spectral data and Δ pK values for 3,6-dihydroxyxanthone.

	λ_{max}/nm for B	λ_{max}/nm for BH^+	$\Delta\bar{\nu}/cm^{-1}$	Δ pK
absorption	325	374	4100	$8.6(S_1-S_o)$
fluorescence		430		
phsophorescence	405	475	3600	$7.6(T_1-S_o)$

The calculations indicate a similar pK ordering to the 4-hydroxy-xanthone although calculation of $\Delta pK(S_1-S_o)$ from the absorption spectra alone probably gives too large a ΔpK value[59]. It is interesting to note the difference in luminescence properties of xanthone produced by substitution at different positions on the benzene rings.

2. Quenching of Xanthone Fluorescence

(a) Quenching by foreign ions

Introduction

The detailed mechanism of intermolecular quenching of fluorescence has been extensively studied for various systems and details can be

found in recent reviews[150,151,152]. Different mechanisms have been found to fit the experimental results for different systems. The following general classification of quenching mechanisms has been made: (a) quenching by heavy atom or paramagnetic molecules due to catalysis of intersystem crossing[153]; (b) quenching involving electronic energy transfer[154]; (c) quenching processes proceeding via charge transfer interactions[155,156]; (d) quenching due to enhanced radiationless decay through an excited complex[157,158].

In 1852 Stokes reported that the fluorescence intensity of a solution of quinine sulphate was reduced by the addition of halide ions and since then a great many papers have appeared on fluorescence quenching by inorganic salts[159,160]. This quenching is characterised by the following properties: (1) the decrease in fluorescence intensity is related to the quencher concentration; (2) the absorption spectrum of the fluorescent solute remains unchanged even at high quencher concentrations, showing that quenching is not due to the formation of a complex in the ground state; (3) the lifetime of the molecule in the excited state decreases as quenching increases; (4) the rate constant of the quenching process decreases with increasing viscosity of the solvent and it has been observed to vary with ionic strength in the same way that the rate constant of a second order ionic reaction does[161].

The first three properties point to quenching being the result of interaction between the excited molecule and the quencher. The quenching process can therefore be represented for the molecule X as follows:

Excitation: $X + h\nu \longrightarrow X^*$ (3.7)

Fluorescence: $X^* \xrightarrow{k_f} X + h\nu'$ (3.8)

Solvent and Internal Quenching: $X^* \xrightarrow{k_i} X$ (3.9)

External Quenching: $X^* + Q \xrightarrow{k_Q} X + Q$ (3.10)

In equation 3.10 the only quenching process that has been considered is that which leads to the deactivation of X without change in X or in the quenching ion. If the intensity of exciting light is kept constant then the rate of production of excited molecules is constant. When no external quencher is present and since process 3.9 includes deactivation of X^* by radiationless decay, intersystem crossing etc. the overall rate of disappearance of X^* by the competing processes 3.8 and 3.9 is:

$$-d(X^*)/dt = (X^*)(k_f + k_i) \qquad (3.11)$$

The corresponding relaxation time τ_i, usually called the mean lifetime of the excited state in the given solvent in absence of quencher, is the reciprocal of the overall first-order rate constant, so that:

$$1/\tau_i = k_f + k_i \qquad (3.12)$$

The quantum yield of fluorescence, ϕ_o, is given by:

$$\phi_o = \frac{k_f}{k_f + k_i} \qquad (3.13)$$

In the presence of quenching reagent, Q, the overall rate of disappearance of X^* is:

$$-d(X^*)/dt = (X^*)(k_f + k_i + k_Q[Q]) \qquad (3.14)$$

and the mean lifetime, τ_Q, in presence of quencher is thus related to the concentration [Q] by:

$$1/\tau_Q = k_f + k_i + k_Q[Q] \qquad (3.15)$$

The quantum yield of fluorescence becomes:

$$\phi = \frac{k_f}{k_f + k_i + k_Q[Q]} \qquad (3.16)$$

and since the fluorescence intensity, I, is proportional to the quantum yield

$$\frac{I_o}{I} = \frac{\phi_o}{\phi} = \frac{k_f + k_i + k_Q[Q]}{k_f + k_i}$$

$$= 1 + \frac{k_Q[Q]}{k_f + k_i} \qquad (3.17)$$

In terms of τ_i this may be written:

$$I_o/I = 1 + k_Q \tau_i [Q] \qquad (3.18)$$

With $k_Q \tau_i = k$, this becomes

$$I_o/I - 1 = k[Q] \qquad (3.19)$$

where $k = k_Q \tau_i = k_Q/(k_f + k_i)$

Equation 3.19 is known as the Stern-Volmer equation and is usually valid for low quencher concentrations. A plot of $I_o/I - 1$ against quencher concentration should give a straight line, the slope of which gives k, the 'quenching constant'. The above processes have only considered dynamic fluorescence quenching where the excitation energy of the excited molecule is removed on diffusional encounter with the quenching molecule. Non-stationary state effects have not been considered as this simple treatment of the quenching process has been found adequate for the quenching results presented. A more detailed treatment of the kinetics of the quenching process can be found in the review by Weller[56].

The mechanism of quenching by inorganic anions has not definitely been established. The deactivation in most cases cannot occur by way of a straightforward energy transfer because the absorption spectrum of the ion does not overlap with the emission spectrum of the excited molecule. Theories of the charge transfer type in which an electron is exchanged between the molecules in the act of quenching have been put forward[162]. It has also been suggested that fluorescence quenching by inorganic anions is due to enchanced inter-system crossing in the excited molecule[163]. Leonhardt and Weller[164] in a flash photolysis investigation of the quenching of perylene fluorescence observed the perylene-monoanion with amines as quenchers. This anion was formed by electron transfer through a charge transfer intermediate. In the case of quenching by iodide ions no such

intermediate was observed but an increased yield of triplet molecules was noted. Weller suggested that in the case of iodide quenching occurs by the "heavy atom" mechanism i.e. by enhanced intersystem crossing. Watkins has recenty studied the quenching of aromatic hydrocarbons by inorganic anions in acetonitrile[165]. He suggests that quenching is due to enhanced intersystem crossing through an encounter complex with some charge transfer character. A different approach was taken by Karyakin and Babicheva[166] who suggested that inorganic salts affect the radiative and non-radiative transitions of dye molecules in aqueous solution by their effect on the structure of water.

Experimental

Quenching of xanthone by ions was initially detected, by the decreased fluorescence intensity of the compound in HCl compared to $HClO_4$ or H_2SO_4, during the course of experimental work on the acid-base properties of the molecule. The xanthone system proved to be a good example of this type of quenching. This subject was not exhaustively studied, the results shown being an initial survey of the system.

The quenching of the BH^+ form of xanthone was studied in 3M $HClO_4$. The xanthone molecule is excited as its B form but protonation in solutions of this acidity will occur immediately. FIG. 3.18 shows the relative fluorescence intensity of BH^+ fluorescence against the concentration of chloride ion at room temperature and FIG. 3.19 the Stern-Volmer plot for several anions at room temperature. This shows that the quenching efficiency of the ions follows the order $I^- > SCN^- > Br^- > Cl^- > NO_3^- \approx F^- \approx SO_4^{2-} \approx ClO_4^-$. The last four ions produced very little quenching effect and very high concentrations had to be used to produce an observable effect on the emission intensity. It was therefore not possible to determine accurately quenching constants for these ions. Solutions containing iodide were unstable and turned yellow on standing. Thus measurements on the iodide system had to be taken immediately after mixing. Table 3.13 shows

FIG. 3.18 Relative fluorescence intensity of xanthone in 3M $HClO_4$ against added chloride ion concentration.

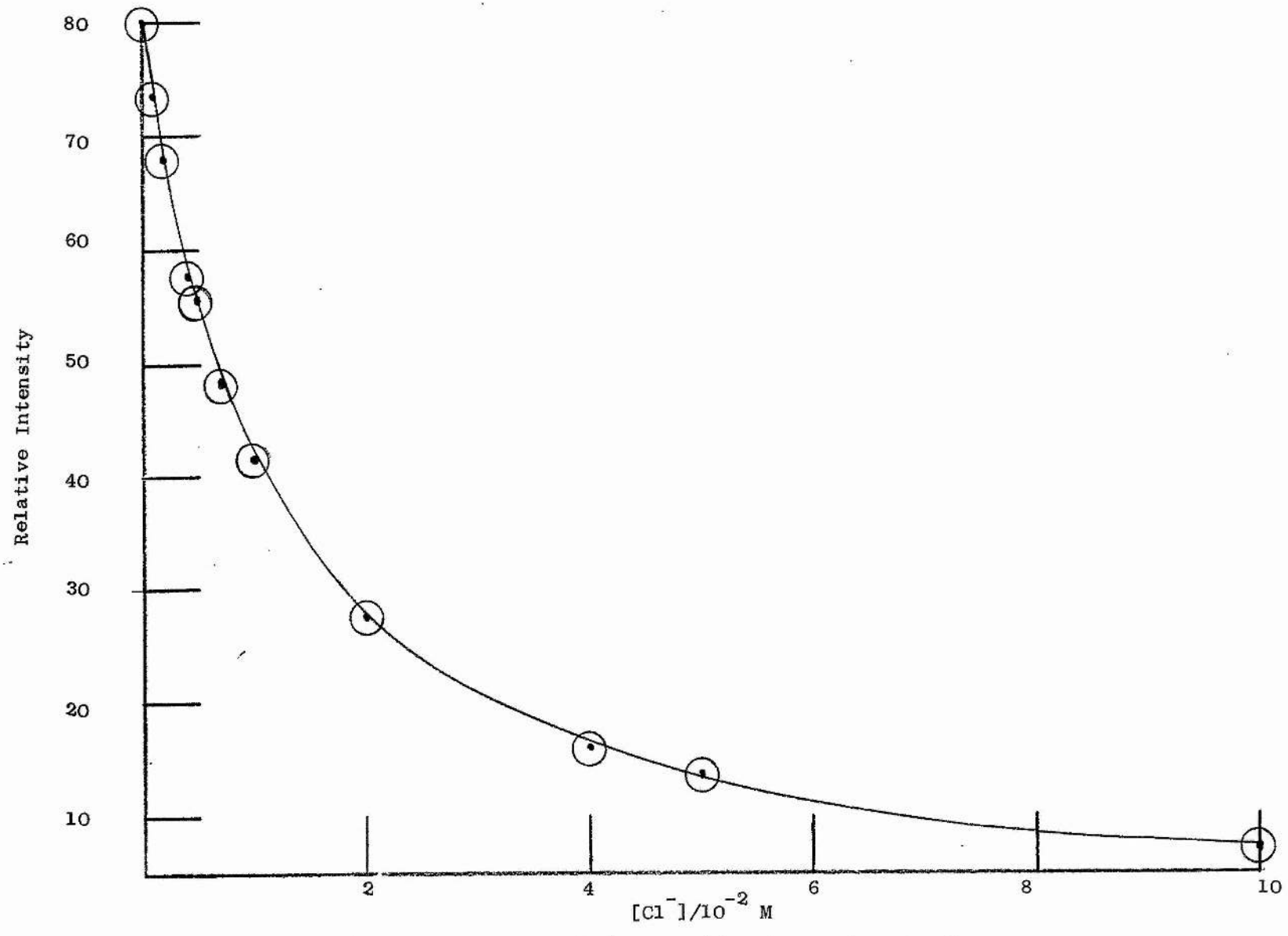

FIG. 3.19 Stern-Volmer plot for the quenching of the fluorescence of xanthone in 3M $HClO_4$ by added anions.

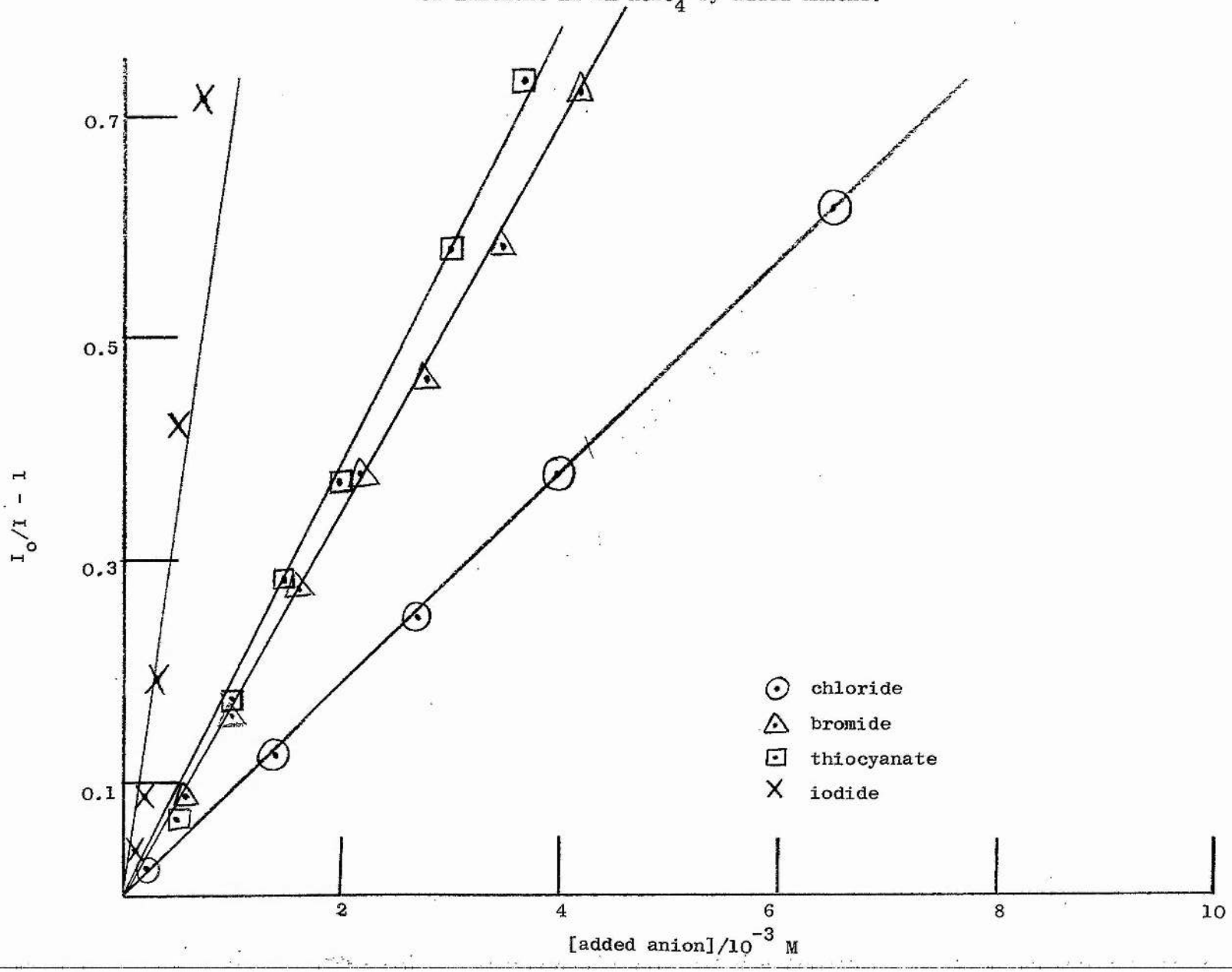

TABLE 3.13 Quenching of xanthone BH^+ form fluorescence in 3 M $HClO_4$ by inorganic anions.

$I_o/I - 1$ values at various temperatures.

	CHLORIDE Temperature °C						BROMIDE Temperature °C						THIOCYANATE Temperature °C					
$[Cl^-]$ x10^3	20	30	40	50	60	$[Br^-]$ x10^3	20	30	40	50	60	$[SCN^-]$ x10^3	20	30	40	50	60
0.0	0.0	0.0	0.0	0.0	0.0	0.0	0.0	0.0	0.0	0.0	0.0	0	0.0	0.0	0.0	0.0	0.0
0.79	0.09	0.10	0.12	0.14	0.15	0.46	0.07	0.08	0.09	0.09	0.13	0.22	0.05	0.05	0.06	0.07	0.07
1.58	0.18	0.20	0.23	0.29	0.30	0.92	0.16	0.18	0.21	0.24	0.28	0.52	0.09	0.11	0.13	0.14	0.16
2.38	0.25	0.29	0.35	0.42	0.45	1.39	0.24	0.27	0.31	0.37	0.41	0.87	0.17	0.21	0.23	0.28	0.33
3.17	0.34	0.39	0.47	0.56	0.61	1.85	0.33	0.38	0.43	0.57	0.59	1.31	0.26	0.30	0.35	0.43	0.49
3.96	0.43	0.51	0.59	0.69	0.78	2.32	0.40	0.46	0.54	0.65	0.72	1.74	0.35	0.41	0.49	0.55	0.67
4.75	0.51	0.59	0.70	0.84	0.94	2.78	0.50	0.56	0.68	0.79	0.87	2.18	0.44	0.48	0.62	0.71	0.81
5.94	0.63	0.74	0.87	1.03	1.15	3.24	0.56	0.65	0.78	0.92	1.02	2.62	0.53	0.59	0.71	0.85	0.97
19.8	2.14	2.51	2.93	3.39	3.92	3.71	0.65	0.73	0.90	1.04	1.19	3.05	0.60	0.68	0.81	1.00	1.12

TABLE 3.13 (continued)

	CHLORIDE						BROMIDE						THIOCYANATE					
	Temperature °C						Temperature °C						Temperature °C					
$[Cl^-]$ $x10^3$	20	30	40	50	60	$[Br^-]$ $x10^3$	20	30	40	50	60	$[SCN^-]$ $x10^3$	20	30	40	50	60
39.6	4.28	5.20	6.01	6.90	7.79	4.17	0.73	0.82	1.00	1.15	1.32	3.49	0.70	0.79	0.94	1.15	1.32
59.4	6.43	7.61	8.94	10.45	12.25	4.64	0.82	0.92	1.08	1.30	1.40	3.92	0.79	0.91	1.00	1.30	1.48
0.39	0.04	0.04	0.05	0.07	0.09	5.10	0.89	1.03	1.17	1.41	1.62	4.36	0.92	1.07	1.26	1.48	1.63
7.8	0.85	1.01	1.18	1.39	1.59	5.50	0.97	1.11	1.40	1.60	1.82						
11.7	1.29	1.51	1.77	2.11	2.25	6.03	1.07	1.17	1.49	1.69	1.97						
15.6	1.72	2.03	2.41	2.76	3.12	6.90	1.23	1.46	1.72	2.0	2.23						
79.0	8.72	10.07	12.08	13.63	16.38	0.23	0.02	0.04	0.05	0.05	0.07						

the relative intensity measurements for the addition of quenchers, Cl^-, Br^-, and SCN^- to solutions of xanthone in 3M $HClO_4$ at various temperatures. For each quencher at each temperature a plot of $I_o/I - 1$ against quencher concentration was constructed and from the slopes values of the quenching constants were obtained. In every case a straight line plot was obtained for low quencher concentrations. At comparatively high quencher concentrations positive deviations from the Stern-Volmer equation were observed possibly due to non-stationary state effects, since at the highest quencher concentrations xanthone molecules will have quenching ions within their reaction sphere and will be deactivated immediately on excitation.

A change of temperature may affect the quenching constant in the following ways: (1) it may change the viscosity of the solution; (2) it may change the number of collisions between the excited molecular species and the quencher ions; (3) if the quenching process requires activation energy an increase in temperature will increase the number of molecules with the necessary energy.

Table 3.14 Quenching constants for the fluorescence quenching of BH^+ by inorganic anions at various temperatures.

	Quenching Constants ($m^3\ mol^{-1}$)			
Temperature (^oC)	Chloride	Bromide	Thiocyanate	Perchlorate
20	105.8	176.0	200.0	≈0.1
30	125.0	200.6	225.1	
40	144.5	228.0	268.8	
50	172.8	268.6	325.7	
60	193.8	302.3	375.3	

The quenching constants obtained from the data in Table 3.13 are shown in Table 3.14. The change in the quenching constants in this case can be accounted for qualitatively by the viscosity changes. Plots of the quenching constants against the reciprocal of the viscocity (viscosities of water at the various temperatures were used) gave straight lines (see FIG. 3.20). This means that there can be no appreciable energy of activation for the quenching process. Stroughton and Rollefson[167] obtained similar results with other systems. The quenching constant obtained for ClO_4^- at room temperature is included in Table 3.14 for comparison. In the case of quenching by chloride ions the quenching constant was determined at several excitation wavelengths and found to be independent of this. This is as expected if the reaction is diffusion controlled, the molecule always reaching the S_1 state before quenching.

A preliminary investigation of this system was made using flash photolysis techniques. The transients observed by flashing a 10^{-5} M solution of xanthone in 3 M $HClO_4$ were compared with those observed in a similar solution containing chloride ion as quencher. The quencher concentration was such that the fluorescence intensity of the solution was reduced to 10% of its original value. Only the transient absorption which has been attributed to the BH^+ form of xanthone in its triplet state was observed on flashing both solutions. There appeared to be a decrease in the optical density of the triplet-triplet absorption in the solution containing chloride ion compared to that without the quencher. This would indicate that the quenching mechanism is not one in which intersystem crossing is enchanced but that radiationless deactivation from S_1 was increased. The solutions described above were flashed with and without filtering the photolytic flash. In the cases where the flash was filtered (i.e. xanthone was only being excited to the S_1 state) the decrease in the optical density appeared to be greater

FIG. 3.20 Quenching constant for the chloride quenching of xanthone in 3M $HClO_4$ against the reciprocal of the viscosity of the solution.

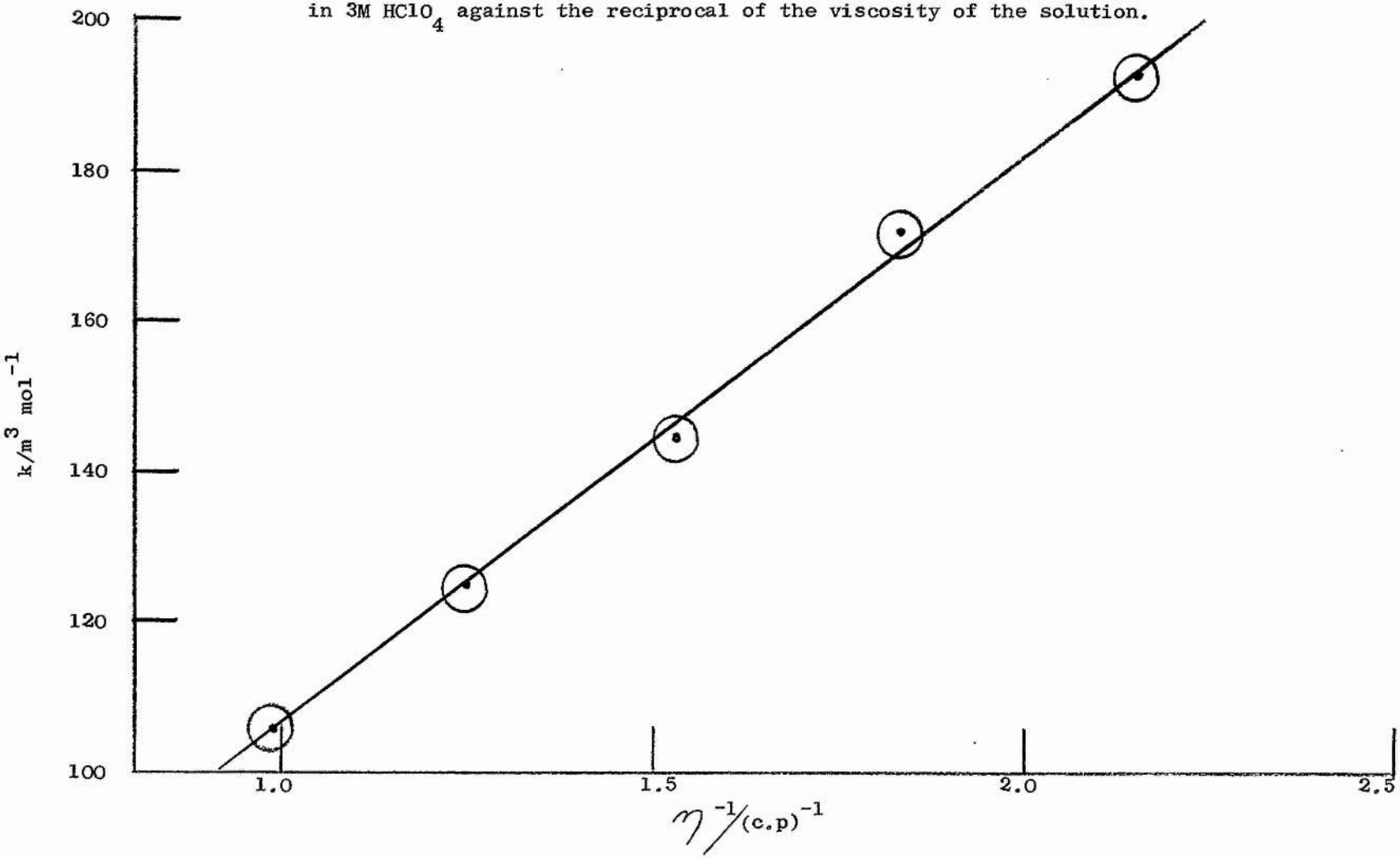

than in the non-filtered case. This might suggest that intersystem crossing was occuring above the S_1 state although the experiments indicating this were only qualitative. It is of course possible that the decreased triplet yield was due to quenching of the triplet molecules by Cl^-. Both the above solutions were flashed the same number of times but the extent of decomposition was less in the solution containing quencher. This again could either be due to less triplet molecules being formed or to quenching of triplet molecules.

Only a qualitative investigation of the fluorescence quenching of the B form of xanthone was made. The same order of quenching efficiency of the B form by inorganic anions as for BH^+ was observed but in this case the Stern-Volmer plots did not give as good straight lines as in the case of BH^+. The only measurements made on the B form were by the equilibrium cell method (see Chapter 2.3(b)) and hence no temperature control was obtained. The fluorescence intensity of the B form was subsequently found to have a marked temperature dependence which could explain the scatter of points on the Stern-Volmer plots. The approximate values of the quenching constants obtained i.e. $k \approx 70\ m^3\ mol^{-1}$ for Cl^-, $k \approx 83\ m^3\ mol^{-1}$ for SCN^- and $k \approx 175\ m^3\ mol^{-1}$ for I^- are considerably smaller than the corresponding values obtained for the quenching of the BH^+ form. This is to be expected as in the case of the BH^+ form, unlike the B, there is electrostatic attraction between the species involved in the quenching reaction.

The quenching of xanthone fluorescence in solutions of greater acid strength than $pK(S_o)$ cannot in many cases be compared with the quenching observed in solutions of lower acidity due to the protonation of the quenching species. In 98% H_2SO_4 a quenching constant, $k = 17.3\ m^3\ mol^{-1}$, was obtained for quenching presumably by the HCl molecule.

(b) Effect of Solvent and Temperature on Xanthone Fluorescence

The xanthone neutral molecule was found to be non-fluorescent in most solvents studied (see section 1.(c)). Weak fluorescence emissions were detected from solutions in water and in glacial acetic acid. Both these solvents have the ability to form strong hydrogen bonds with the carbonyl group and this may be a prerequisite for fluorescent emission to be observed. Since ethanol was being added to the solutions used in the $pK(T_1)$ determination, to increase the solubility of xanthone in the aqueous solutions, an investigation was made of the effect of additions of ethanol and other solvents on the emission intensity of xanthone in aqueous solution. Plots of $I_o/I - 1$ against molarity of added solvent are shown in FIG. 3.21. In each case a curved plot is obtained and the effect of the solvent on the fluorescence intensity increases as the dielectric constant of the solvent decreases.

A similar effect has been observed with the base form of acridine[168]. The quantum yield of acridine fluorescence was measured in a series of mixtures of water with ethanol, formamide, dioxane and dimethylformamide and found to decrease to zero in pure dioxane or dimethylformamide, but not in pure ethanol or formamide. It was suggested that fluorescence occurs only from excited acridine molecules that are hydrogen-bonded to solvent molecules, and that the decrease in fluorescence intensity is due to decreasing ability of the solvent to form hydrogen bonds. This explanation may also hold for the xanthone case but it is also possible that the effect is due to changes in the relative energies of the π-π^* and n-π^* transitions with change of solvent. As the polarity of the solvent is increased we expect the π-π^* S_1 level to be stabilised in comparison to the n-π^* level and this may lead to a situation favourable for fluorescence emission in water but not in alcohol. In other words, we could explain the effect by saying that the π-π^* character of the first excited singlet state increases with increasing polarity

FIG. 3.21 Stern-Volmer plot for the quenching of the fluorescence of xanthone in aqueous solution, pH = 11, by added solvents.

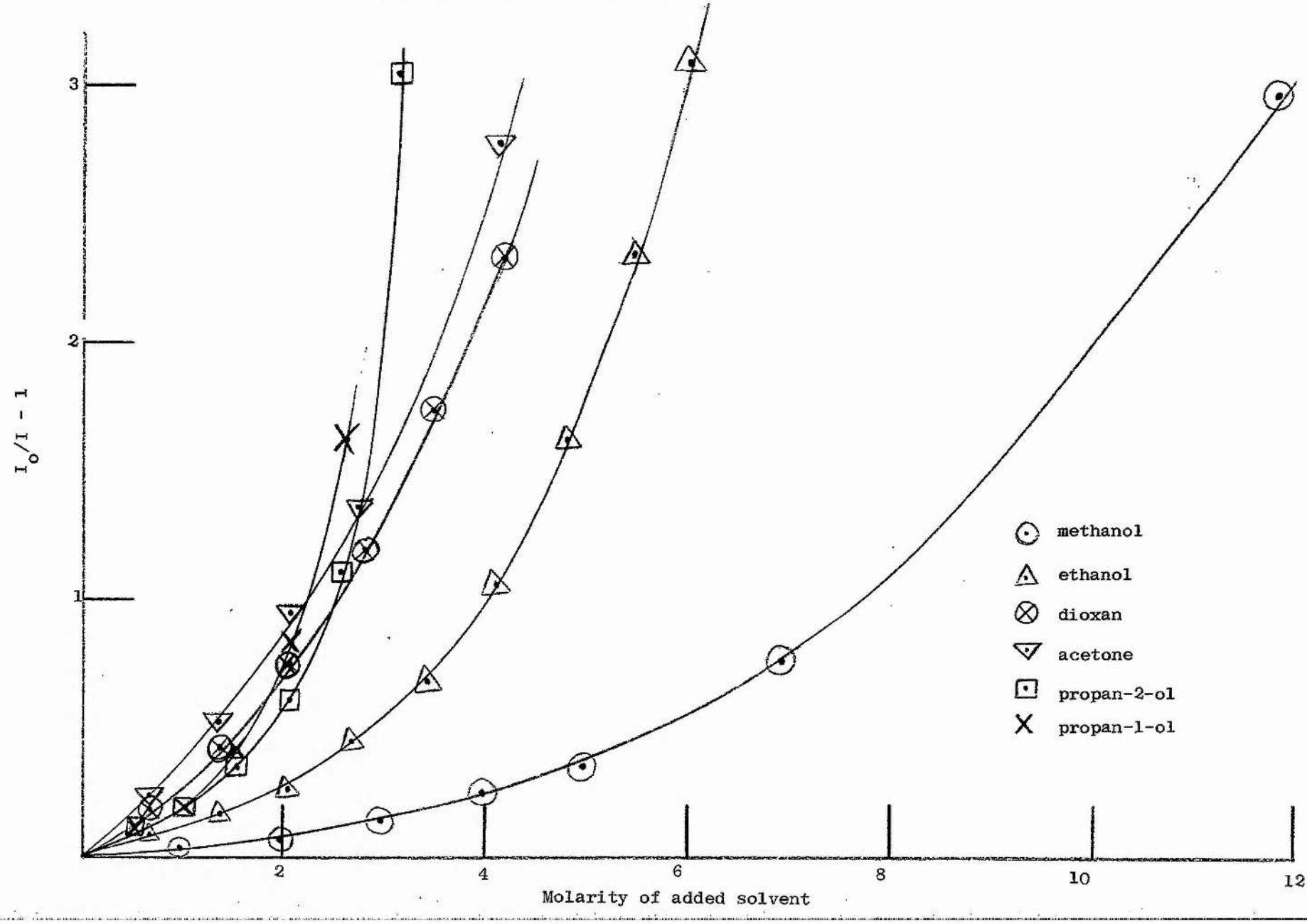

of solvent and leads to increased fluorescent yields.

Additions of the same solvents were made to solutions of xanthone in 3 M $HClO_4$ and the effect on the BH^+ fluorescence intensity is shown in FIG. 3.22. Both acetone and dioxane were unstable in this medium. The curves obtained are similar to those for the B form although the decrease in fluorescence intensity is less for a given addition of solvent. In more concentrated acid solutions, of greater acidity than $pK(S_o)$, replacing H_2O by EtOH or MeOH had no effect on the fluorescence intensity of BH^+. In the 3 M $HClO_4$ solutions, where xanthone is excited as the base form and protonates in the excited state before fluorescing, it is possible that the solvent effect observed is due to solvent interaction with the B form leading to radiationless deactivation before protonation can occur.

FIG. 3.23 shows the relative fluorescence intensity of xanthone B and BH^+ forms and quinine sulphate as a function of temperature. The striking effect of temperature is that on the emission intensity of the unprotonated form of xanthone. Again a similar effect was observed for acridine[168]. The decrease in fluorescence intensity with rise in temperature was suggested to be due to breaking of the hydrogen bonds to the excited molecule to give a non-fluorescent molecule. It is also possible that the effect of the solvent on the transitions involved will decrease as the temperature rises. The BH^+ form in 3 M $HClO_4$ shows a relatively small decrease in fluorescence intensity with temperature which again could be mainly due to an effect on B^* before protonation, while the BH^+ form shows a slight increase in intensity as temperature rises. In the above results no correction was made for the effect of solvent addition or temperature on the ground state absorption spectra but this was noted to be relatively small compared to the effects observed on the emissions.

FIG. 3.22 Stern-Volmer plot for quenching of the fluorescence of xanthone in 3M $HClO_4$ by added solvents

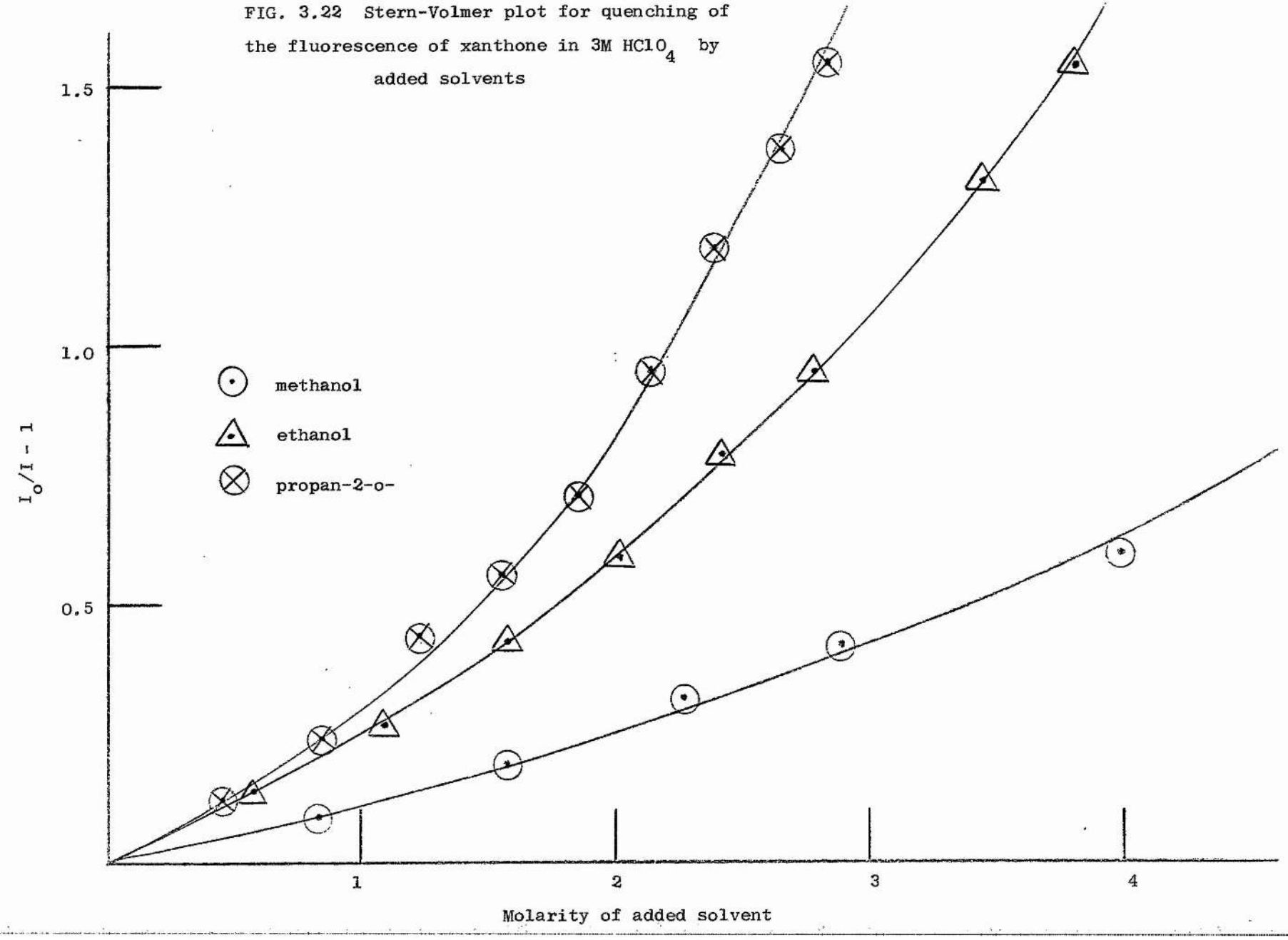

FIG. 3.23 Relative fluorescence intensity as a function of temperature

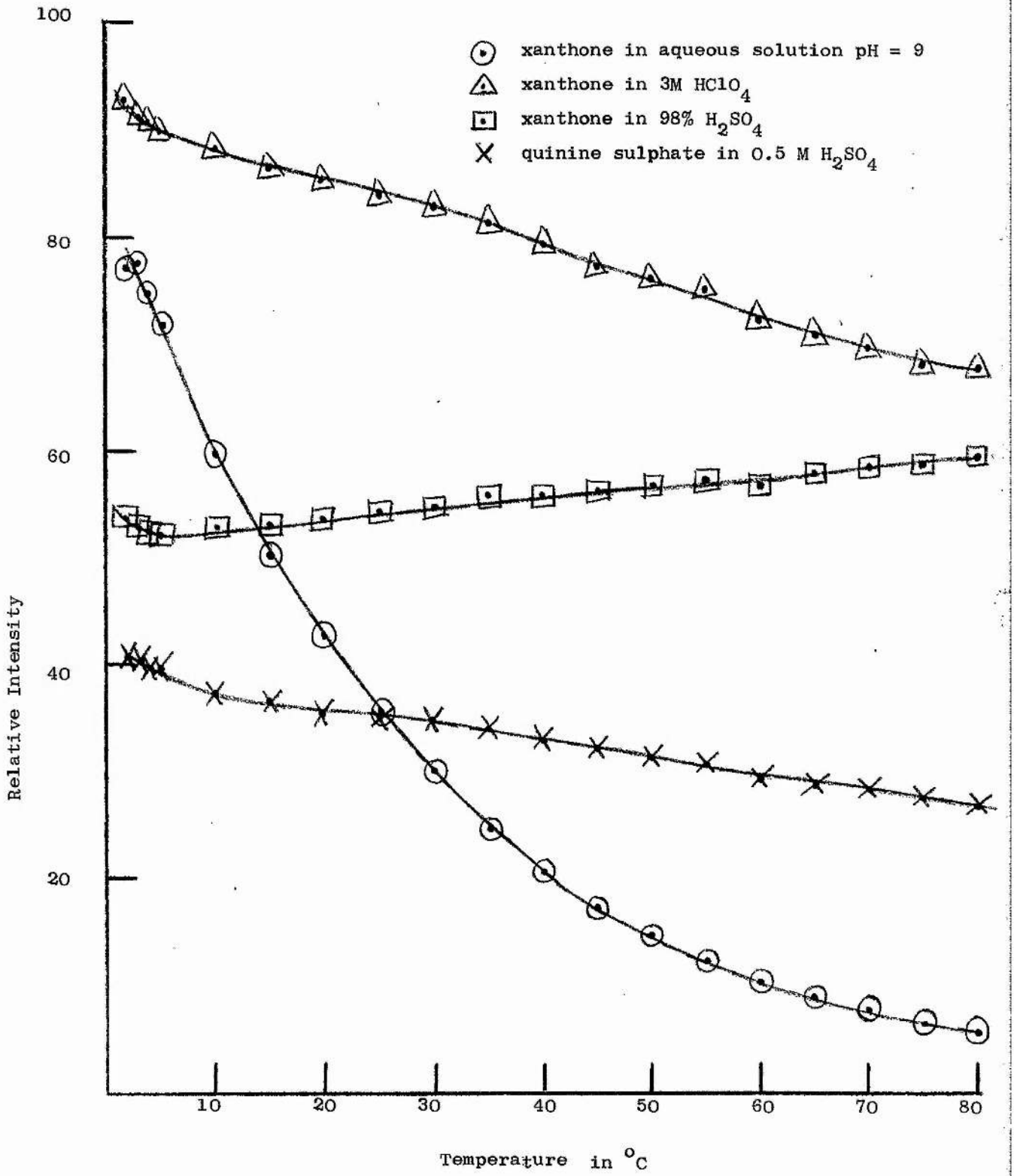

CHAPTER 4

BENZOPHENONE AND RELATED AROMATIC CARBONYL COMPOUNDS

1. Benzophenone

(a) Introduction

Since protonation at the ether oxygen might have affected the pK order ($T_1 > S_1 > S_o$) found for xanthone, a similar study was initiated on benzophenone (I)

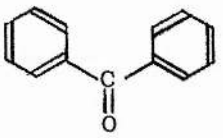

(I)

Benzophenone and xanthone differ considerably in their photochemical properties but in the benzophenone case we can be reasonably sure that the carbonyl group will be the position of protonation in all states[145,146].

The photochemistry of benzophenone has been extensively studied and the primary processes involved are now largely understood. A great deal is now known of many aromatic carbonyl compounds and the excited state properties have been rationalised in terms of the type of excited states involved and the effect of substituents and solvents on these states. Benzophenone itself has been studied, using flash photolytic[169] and continuous irradiation techniques[170] in a variety of solvents[142]. Porter and Ledger[171] have recently reported benzophenone's photochemical properties in aqueous solution and some of their work overlaps with that reported here. Apart from the use of the absorption spectrum of the protonated form in a determination of $pK(S_o)$[172], the protonated molecule has not been studied and nothing appears to have been published about the acid-base properties of benzophenone in the excited state. Leisten and Walton[173] showed by cryoscopy that near 100% H_2SO_4 benzophenone undergoes simple protonation and that even in dilute oleums sulphonation is imperceptible. Hence, we can be sure that the observed photochemical

properties of benzophenone in concentrated sulphuric acid are due to the protonated molecule itself and not to other species formed by reaction between the benzophenone and the sulphuric acid.

(b) Absorption Spectra

Benzophenone shows in polar and non-polar solvents an absorption spectrum which has a weak long wavelength band of the $n-\pi^*$ type and at shorter wavelengths a more intense band of $\pi-\pi^*$ type. The absorption spectrum of benzophenone in water and for comparison the uncorrected phosphorescence excitation spectrum are shown in FIG. 4.1. (The uncorrected excitation spectrum is shown as the correction factor cuts down the intensity of the $n-\pi^*$ band relative to the $\pi-\pi^*$ band and although the fine structure is still there it is not as easily demonstrated.) The excitation spectrum is helpful in showing the fine structure of the $n-\pi^*$ band which is not observed in the absorption spectrum of the solution. The first transition in the absorption spectrum of the BH^+ form has an intense, broad band of the $\pi-\pi^*$ type without fine structure (see FIG. 4.1). On decreasing the acidity of the solution the BH^+ absorption disappears and is replaced by that of B but no isobestic point is observed due to large medium effects on the spectra.

(c) Low Temperature Emission Spectra

At 77 K in solid solution in water or alcohol benzophenone shows a short-lived structured phosphorescence but no fluorescence. (see FIG. 4.3). This is characteristic of a molecule with S_1 and T_1 states of $n-\pi^*$ type. Intersystem crossing is very efficient in this compound and the quantum yield of triplet formation has been shown to be near unity[127].

The BH^+ form in 98% H_2SO_4 glass at 77 K exhibits both fluorescence and phosphorescence (see FIG. 4.2). The phosphorescence is much longer lived than that of the B form, as would be expected for a triplet of $\pi-\pi^*$ type[31]. The fluorescence is weak and shows no structure although

FIG. 4.1 Benzophenone absorption spectra: (a) B form (1.1×10^{-4} mol dm^{-3}) in water; (b) BH^+ form (8×10^{5} mol dm^{-3}) in 98% H_2SO_4 and (c) phosphorescence excitation spectrum of the B form in water at 77 K.

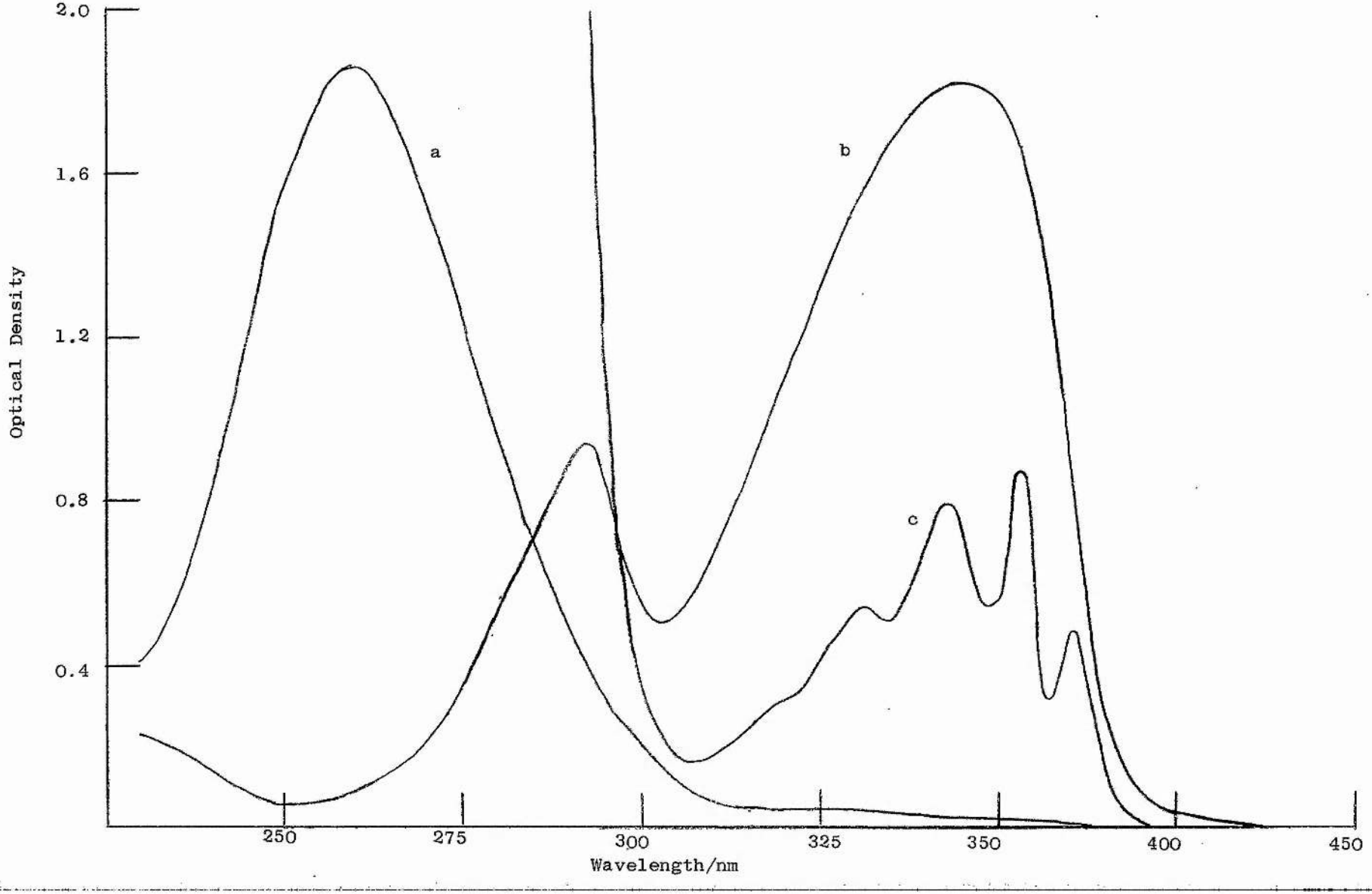

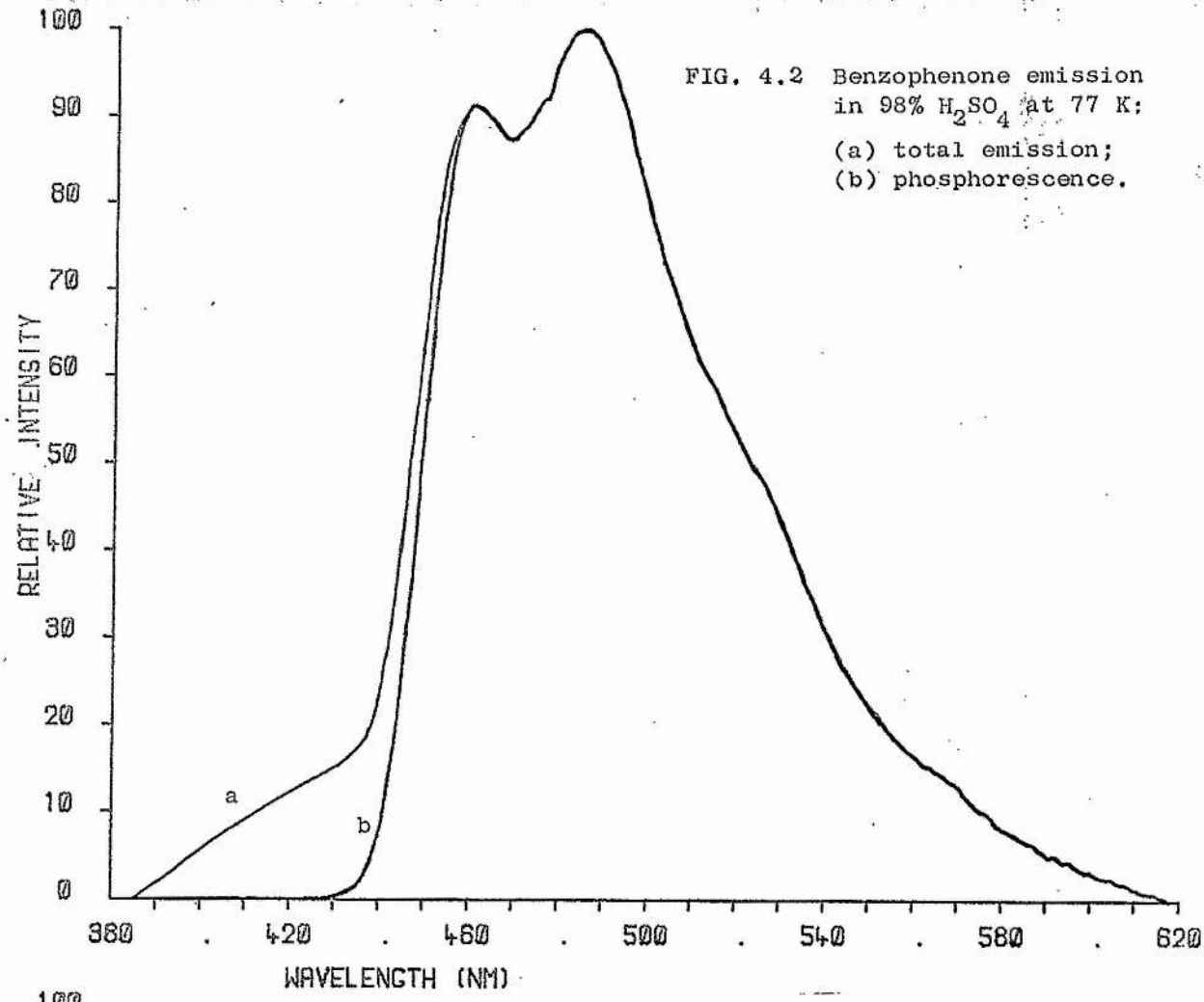

FIG. 4.2 Benzophenone emission in 98% H_2SO_4 at 77 K:
(a) total emission;
(b) phosphorescence.

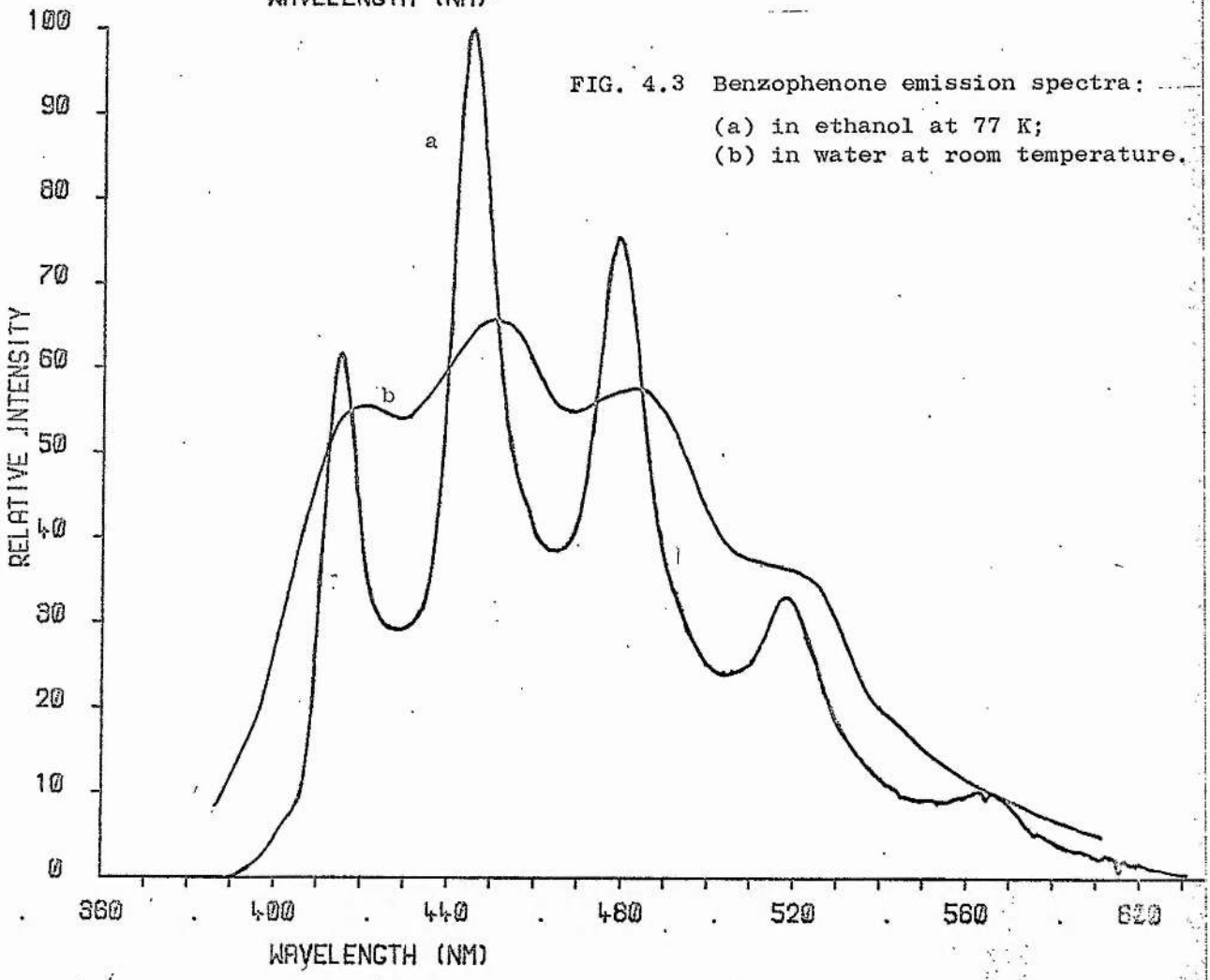

FIG. 4.3 Benzophenone emission spectra:
(a) in ethanol at 77 K;
(b) in water at room temperature.

some structure is observed in the phosphorescence band. If we assume that the quantum yield of fluorescence (ϕ_f) plus the quantum yield of phosphorescence is unity, then a comparison of the emission areas involved gives protonated benzophenone a ϕ_f = 0.1 and ϕ_p = 0.9 at 77 K.

(d) Emission from Fluid Solution

Parker and Joyce[174] have reported the phosphorescence of the B form in solvents in which benzophenone was not photoreduced. Beckett and Porter[142] in a study of photoreduction in various solvents found that the quantum yield of photoreduction in water was very low. It therefore seemed possible that phosphorescence might be observed in aqueous solutions at room temperature. This emission has been observed and, although quenched by oxygen, can be detected in undegassed aqueous solutions with its intensity reduced by an amount consistent with Ledger and Porter's[171] quenching constant for dissolved oxygen. The emission in aqueous solution (see FIG. 4.3) is similar to the phosphorescence at 77 K but has less well-defined structure. The emission from B is acid-quenched and falls to about half its full intensity at pH 5, as also shown by Ledger and Porter.

At room temperature BH^+ (i.e. benzophenone in 98% H_2SO_4) gave a broad emission band (maximum 470 nm) which was not resolvable into fluorescence and phosphorescence on our apparatus but which, by comparison with the low temperature emission, appeared to be mainly phosphorescence. The excitation spectrum was identical with that for fluorescence and phosphorescence at 77 K, whence (unless some form of energy transfer from $\overset{*}{BH}^+$ to another species is occuring) all these emissions are attributable to $\overset{*}{BH}^+$. (Other possible interpretations of this emission, e.g. excimer formation, are discounted by the fact that the emission spectrum is unchanged by dilution to very low concentrations.)

FIG. 4.4 shows the effect of H_2SO_4 concentration upon the relative intensity of the BH^+ emission at room temperature. The quantum yield of the emission is so low (< 0.01) that relatively concentrated solutions

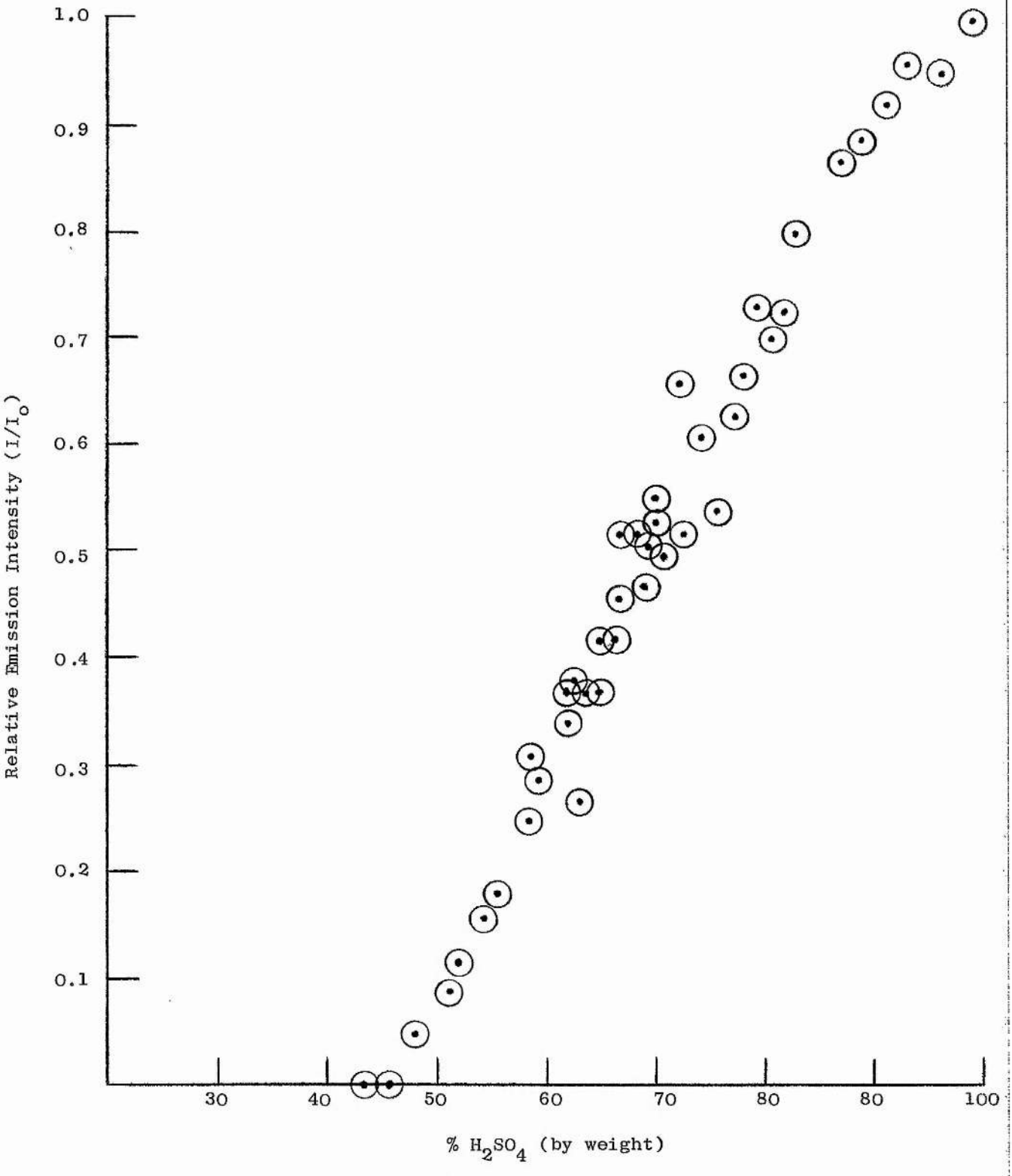

FIG. 4.4. Acid dependence of the relative emission intensity of protonated benzophenone (BH^+)

had to be used and correction for the inner filter effect was necessary. Corrections were also made for the different absorption coefficients of B and BH^+ and for medium effects upon the optical density as the H_2SO_4 concentration was varied. The emission intensity decreases steadily with acid concentration. If the emission was phosphorescence, we might expect it to be quenched by dissolved oxygen and part of the slope of the curve to be due to the increasing effectiveness of the quenching reaction because of the decreasing viscosity of the H_2SO_4; but this cannot be the case as degassing solutions at 98%, 80%, 74% and 60% H_2SO_4 had no effect on their emission intensity. According to the Förster Cycle calculation (Table 4.1) the BH^+ excited singlet and triplet forms might be expected to occur at lower acidities than $pK(S_o)$ (i.e. lower than 74% H_2SO_4)[92] but FIG. 4.4 seems to indicate, to a first approximation, that the emission from BH^+ is only observed when BH^+ is present in sufficient concentrations for excitation from the ground state. Attempts to obtain an excitation spectrum of the emitting species in solutions of relatively low acid concentration failed because the emission was very weak and therefore concentrated solutions had to be used and the excitation spectrum obtained was distorted due to the inner filter effect.

(e) Transients observed in Flash Photolysis

Comparison of the transient absorption spectra observed on flashing benzophenone solutions in benzene and water (FIG. 4.5) confirms that the spectrum is attributable to the B triplet, as explained by Ledger and Porter[171]. As expected from the phosphorescence quenching results, the T-T absorption of the B form disappears in dilute acid solutions.

In 98% H_2SO_4 a different transient is observed which has been attributed to the BH^+ triplet (see FIG. 4.6). At a fixed delay setting after the photoflash, the optical density of the transient is greater when the solution is degassed, just as expected from an oxygen quenching effect, which is surprising as the emission intensity (apparently

FIG. 4.5 Triplet-triplet absorption spectrum of benzophenone (a) in benzene and (b) in water.

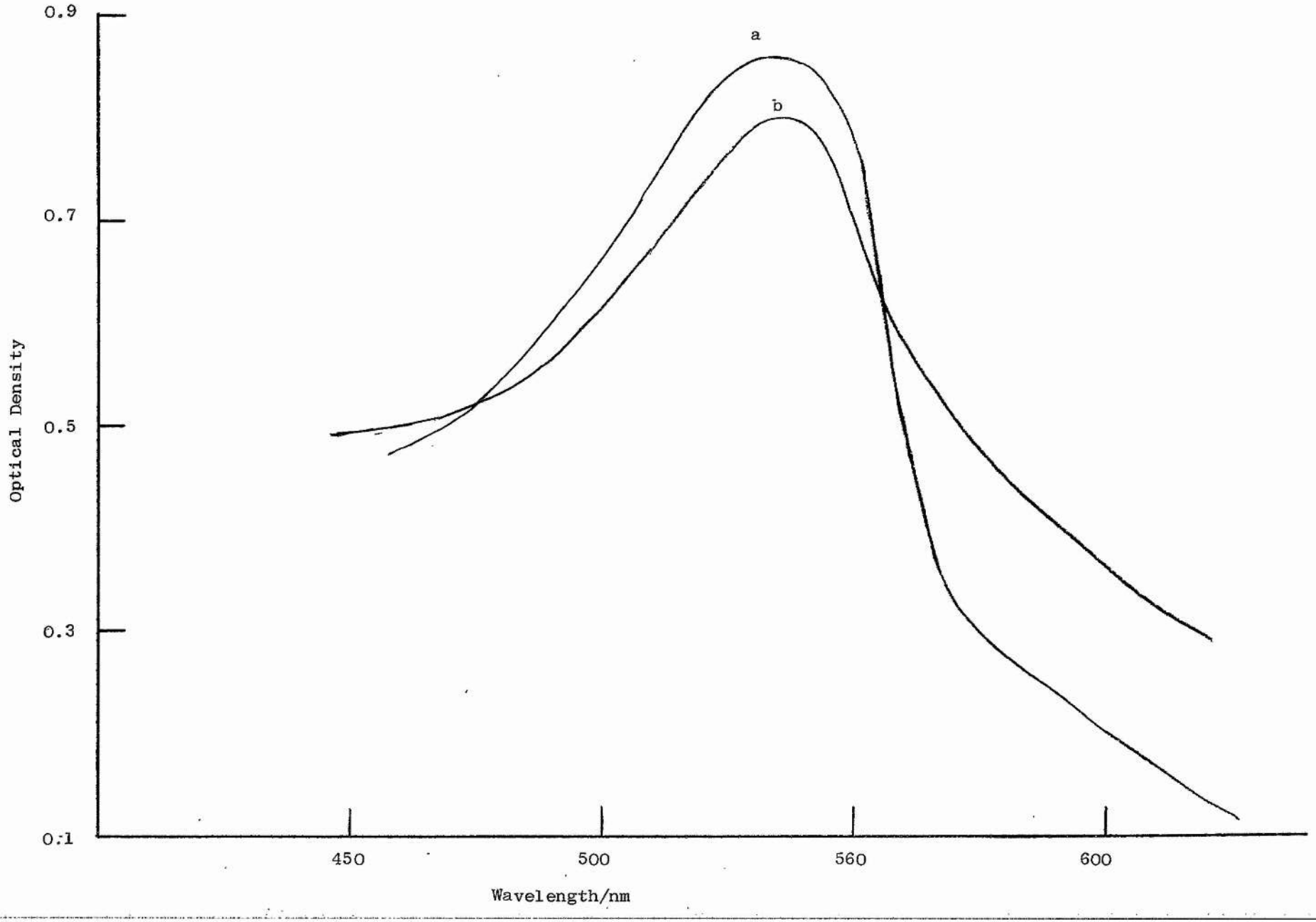

FIG. 4.6 Effects of degassing upon the triplet-triplet absorption spectrum of protonated benzophenone (BH^+): (a) before and (b) after degassing.

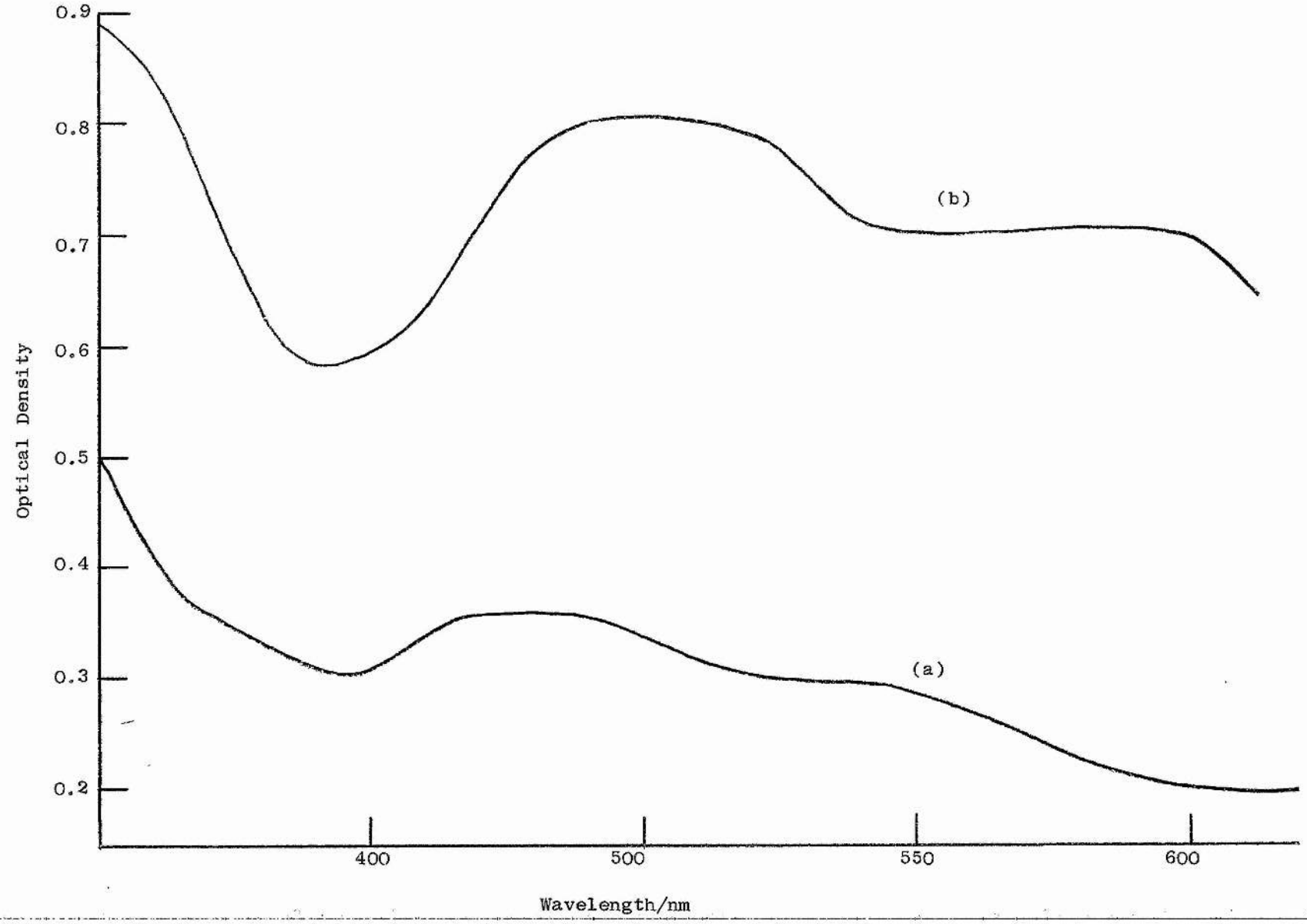

phosphorescence) from BH^+ in 98% H_2SO_4 seems insensitive to the presence of oxygen. While the apparent discrepancy could possibly be due to a fortuitous compensation between the effect of oxygen upon the triplet quantum yield and the triplet lifetime, further work is needed for clarification. In particular a lifetime study of the emission and the transient would indicate whether or not both effects were due to the same species. Attempts were made to determine the lifetime of the emission on the apparatus available at present, but the lifetime was too short to be measured on the millisecond apparatus[175] and the emission intensity was too weak for the repeating spark technique[176].

The spectral changes resulting from flash irradiation of benzophenone in 98% H_2SO_4 are shown in FIG. 4.7. The absorption bands appearing at 410 nm and 268 nm are similar to bands observed in the protonated xanthone absorption spectrum but other bands of xanthone BH^+ are absent. Attempts to isolate the product of this decomposition using constant irradiation techniques were unsuccessful. The extent of decomposition was less when the solution was not degassed. This could indicate more triplet molecules available for reaction in the absence of oxygen either because of a quantum yield or a lifetime effect.

(f) Discussion and Förster Cycle Calculations

These results indicate that there is a gap in the acidity scale between the regions where B and BH^+ are detectable in the excited state, whence direct determination of excited state pK values from measured $[BH^+]/[B]$ ratios is not possible. Förster Cycle calculations must therefore be employed to estimate the pK's. The absence of transients or emission from B and BH^+ in the region mentioned would appear to be due to H^+ quenching. Ledger and Porter[171] attribute the disappearance of B phosphorescence to this and suggest that the positive protonic field inverts the relative positions of the $n-\pi^*$ and $\pi-\pi^*$ triplet states, then protonation of the $\pi-\pi^*$ triplet, which would be expected to be more

FIG. 4.7 Spectral changes accompanying flash irradiation of benzophenone in 98% H_2SO_4: (a) before and (b) after flashing.

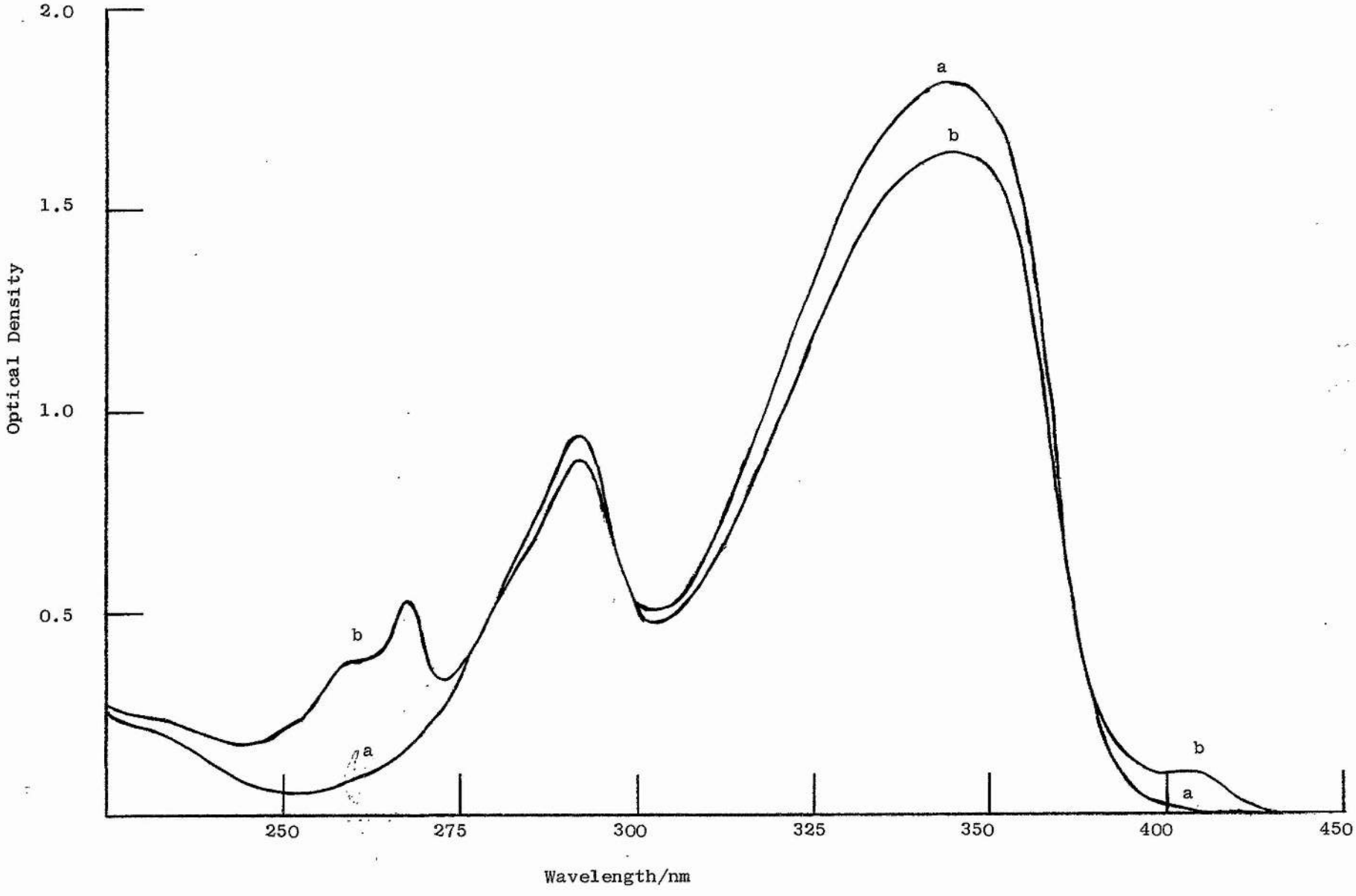

basic than the ground state, occurs. This is in fact equivalent to saying that this reaction is the protonation reaction in the triplet state i.e. the reaction to which $pK(T_1)$ refers. On the other hand, there are several factors which indicate that simple protonation is not involved. The Förster Cycle calculations indicate that $pK(T_1)$ would lie in a considerably more acid region ($H_o \approx -0.5$) and if it were a simple protonation reaction we would expect to be able to detect BH^+ triplet in more acid regions than $pK(T_1)$. Acid quenching must also be postulated as the reason for the emission intensity of BH^+ disappearing as BH^+ is removed from the ground state. Presumably acid quenching of excited B is so efficient in this composition range that excited BH^+ is not formed in the encounter: this could amount to a case of non-adiabatic proton transfer[177].

Förster Cycle Calculations for Benzophenone

The absence of fluorescence from the unprotonated benzophenone molecule (B) precludes the location of the 0-0 transition of the $n-\pi^*$ band by averaging the absorption and fluorescence maxima[62], but fortunately the structured phosphorescence excitation spectrum (see FIG. 4.1) allows a direct determination of the 0-0 frequency for Förster Cycle calculation. The BH^+ form shows no structure in either the absorption or excitation spectrum of the long-wavelength $\pi-\pi^*$ band but, since fluorescence was detected from BH^+ at 77 K, we can resort to averaging the absorption and fluorescence maxima to obtain the 0-0 frequency. The phosphorescence spectra of both the B and BH^+ forms exhibit some fine structure and estimates of the 0-0 frequency of the S_o-T_1 transition were obtained directly from the spectra.

Table 4.1 gives spectral details of the B and BH^+ forms of benzophenone while Table 4.2 gives the energy differences between the B and BH^+ forms in the S_1 and T_1 states and the calculated pK values

TABLE 4.1 Spectral Data for Benzophenone (B and BH^+ forms; carbonyl protonation)

Absorption Maxima λ/nm				Long Wave-length Excitation Maximum λ/nm		Fluore-scence Maximum λ/nm		Phosphore-scence Maxima λ/nm	
B	ε	BH^+	ε	B	BH^+	B	BH^+	B	BH^+
335	1.45×10^2	346	2.36×10^4	372	350		426	415	462
253	1.71×10^4	293	1.18×10^4					445	485
								480	
								519	
								563	

of benzophenone in those states. (Note:- the actual spectral values used in the Förster Cycle calculations on benzophenone are given in Table 4.3 together with similar data for substituted benzophenones.) The results in Table 4.2 indicate that the ordering of the pK's of benzophenone is the same as that found for xanthone. Benzophenone

TABLE 4.2 Benzophenone pK^* values based on Förster Cycle calculations.

$\Delta\bar{\nu}\ (S_1-S_o)/cm^{-1}$	$\Delta\bar{\nu}\ (T_1-S_o)/cm^{-1}$	$\Delta pK(S_1-S_o)$	$\Delta pK(T_1-S_o)$	$pK(S_o)$	$pK(S_1)$	$pK(T_1)$
1000	2500	2.1	5.2	-5.7	-3.6	-0.5

becomes a stronger base upon excitiation to both the first excited singlet and triplet states, the increase in basicity being greater for the triplet state. The Förster Cycle pK's of xanthone showed a similar difference between $pK(S_1)$ and $pK(T_1)$ i.e. ≈ 3 units, but in the xanthone case the increase in basicity was larger for both states. These calculated pK's of benzophenone confirm that the pK values obtained for xanthone were in fact the pK's associated with the protonation of the carbonyl group and that, in agreement with the energy calculations on the B and BH^+ forms of xanthone, the oxygen bridge of xanthone was not acting as the reactive site.

2. Benzophenones

(a) Introduction

The order $pK(T_1) > pK(S_1) > pK(S_o)$ would appear to be a fairly general property of aromatic carbonyl compounds. Just as the relative positioning of $n-\pi^*$ and $\pi-\pi^*$ states is different in xanthone and benzophenone, the energies of these transitions are altered in benzophenones by substituents on the benzene rings. To determine the effect of these changes on the ordering of pK values the spectral data necessary to perform Förster Cycle calculations on a series of benzophenones were obtained. The spectral properties of each derivative are discussed in terms of the classification of benzophenone excited states made by Porter and Suppan[7] (see Chapter 1.1(d)).

(b) Spectral properties of and Förster Cycle calculations for substituted benzophenones

Table 4.3 shows the spectral data, used in Förster Cycle calculations, of benzophenone and several of its substituted derivatives. All the data for the B forms were obtained in ethanol solutions as all the derivatives were soluble in this solvent which is a polar solvent resembling water but which conveniently forms a clear glass at low temperatures. The phosphorescence maximum of benzophenone in ethanol and in water was the same although better resolution was obtained using the ethanol glass. Data for the BH^+ forms were obtained in 98% H_2SO_4. The $pK(S_o)$ values of the benzophenones differ by several H_o units and as the weakest bases were not protonated in 60% $HClO_4$ a solvent, 98% H_2SO_4, in which all the derivatives were fully protonated was used. Sulphuric acid has disadvantages as a solvent due to its ability to react with or facilitate reactions of organic compounds. Already mentioned is the fact that benzophenone is stable in 98% H_2SO_4[173] but the presence of activating groups such as hydroxy and amino would

TABLE 4.3 Spectral data used in Förster Cycle calculations on substituted benzophenones.

SUBSTITUENTS		λ_{max}/nm for B	λ_{max}/nm for BH^+			$\Delta\bar{\nu}$/cm^{-1} for S_1-S_o	Phosphorescence λ_{max}/nm		$\Delta\bar{\nu}$/cm^{-1} for T_1-S_o
Pos.4	Pos.4'		Absorption	Fluorescence	Mean		B	BH^+	
H	H	372	346	426	386	1000	415	462	2500
Cl	Cl	373	378	417	398	1700	419	506	4100
CH_3O	CH_3O	364	404	451	430	4100	412	510	4700
OH	H	366	372	430	401	2400	422	485	3100
C_6H_5	H	374	386	480	433	3600	471	535	2500
NH_3^+	H	369	334	427	380	800	415	470	2700
NO_2	H	345	338			-600	410	515	5000
Pos.2									
OH		337	390			4000	417	481	3200
CH_3O		372	398	440	419	3000	417	482	3300
Pos.2	Pos.5								
OH	NO_2	400	382	470	426	1600	531	505	-1100
Pos.2,2'	Pos.4,4'								
OH	OH	350	403	440	421	4800	410	480	3600

TABLE 4.4 Spectral data used in Förster Cycle calculations of substituent group pK's

SUBSTITUENTS POSITION 4	λ_{max}/nm for B			λ_{max}/nm for BH^+	$\Delta\bar{\nu}$/cm^{-1} for S_1-S_o	Phosphorescence λ_{max}/nm		$\Delta\bar{\nu}$/cm^{-1} for T_1-S_o
	Absorption	Fluorescence	Mean			B	BH^+	
O^-	350	425	388	366	-1500	469	422	-2400
NH_2	335	439	387	369	-1300	481	415	-3300

TABLE 4.5 pK^* values, for carbonyl protonation of substituted benzophenones, based on Förster Cycle calculations.

SUBSTITUENTS Pos.4	SUBSTITUENTS Pos.4'	Δ pK(S_1-S_o)	Δ pK(T_1-S_o)	pK(S_o)	pK(S_1)	pK(T_1)
H	H	2.1	5.3	-5.7[11]	-3.6	-0.4
Cl	Cl	3.6	8.6	-6.5[11]	-2.9	2.1
CH_3O	CH_3O	8.6	9.9	-4.4[11]	4.2	5.5
OH	H	5.0	6.5	-5.0[11]	0	1.5
C_6H_5	H	7.6	5.3			
NH_3^+	H	1.7	5.7			
NO_2	H	-1.2	10.5			
Pos.2						
OH		8.4	6.7	-6.3[21]	2.1	0.4
CH_3O		6.3	7.0			
Pos.2	Pos.5					
OH	NO_2	3.3	-2.3	-7.4[21]	-4.1	-9.7
Pos.2,2'	Pos.4,4'					
OH	OH	10.0	7.5			

TABLE 4.6 pK^* values, for substituent group protonation of substitued benzophenones, based on Förster Cycle calculations.

Pos.4 Substituent undergoing protonation	ΔpK(S_1-S_o)	ΔpK(T_1-S_o)	pK(S_o)	pK(S_1)	pK(T_1)
O^-	-3.1	-5.0	6.5[17]	3.4	1.5
NH_2	-2.7	-7.0	$\approx$0.5[16]	-2.2	-6.5

be expected to make these derivatives more reactive. All of the compounds listed in Table 4.3 were found to be relatively stable in 98% H_2SO_4 over a period of days. The absorption spectra showed slight changes on standing as would be consistent with slow sulphonation. The phosphorescence spectra also changed slightly on standing but the values in Table 4.3 were obtained using freshly prepared solutions which were immediately cooled to liquid nitrogen temperature.

Tables 4.3, 4.4, 4.5 and 4.6 give the values used in the Förster Cycle calculations, the pK shifts calculated and the estimated $pK(S_1)$ and $pK(T_1)$ in those cases where a value of $pK(S_o)$ was available. The values of the O-O transitions of the B and BH^+ forms were, in general, obtained as described for benzophenone itself but details of the individual cases are given below. The spectral values in Table 4.3 and the calculated pK's in Table 4.5 refer to the protonation of the carbonyl group while Tables 4.4 and 4.6 concern protonation at particular substituent groups.

4,4'-dichlorobenzophenone

The absorption spectra of the B and BH^+ forms are shown in FIG. 4.8. The spectra are similar to those of benzophenone, the greatest difference being the red shift of the first absorption band of BH^+. The phosphorescence excitation spectrum of the B form shows the structured $n-\pi^*$ band as the lowest singlet level while the structure and short lifetime of the phosphorescence emission indicate that the lowest triplet is also of $n-\pi^*$ type. Porter and Suppan[7] found that 4-fluoro and 4-bromobenzophenone had lowest $n-\pi^*$ levels. At 77 K in 98% H_2SO_4 both fluorescence and phosphorescence were detected from the protonated form (see FIG. 4.9). The separation of these emission bands has increased on substitution and the relative quantum yield

FIG. 4.8 Absorption Spectra of 4,4'-dichlorobenzophenone: (a) B form (5×10^{-5} mol dm^{-3}) in ethanol; (b) BH^+ form (4×10^{-4} mol dm^{-3}) in 98% H_2SO_4.

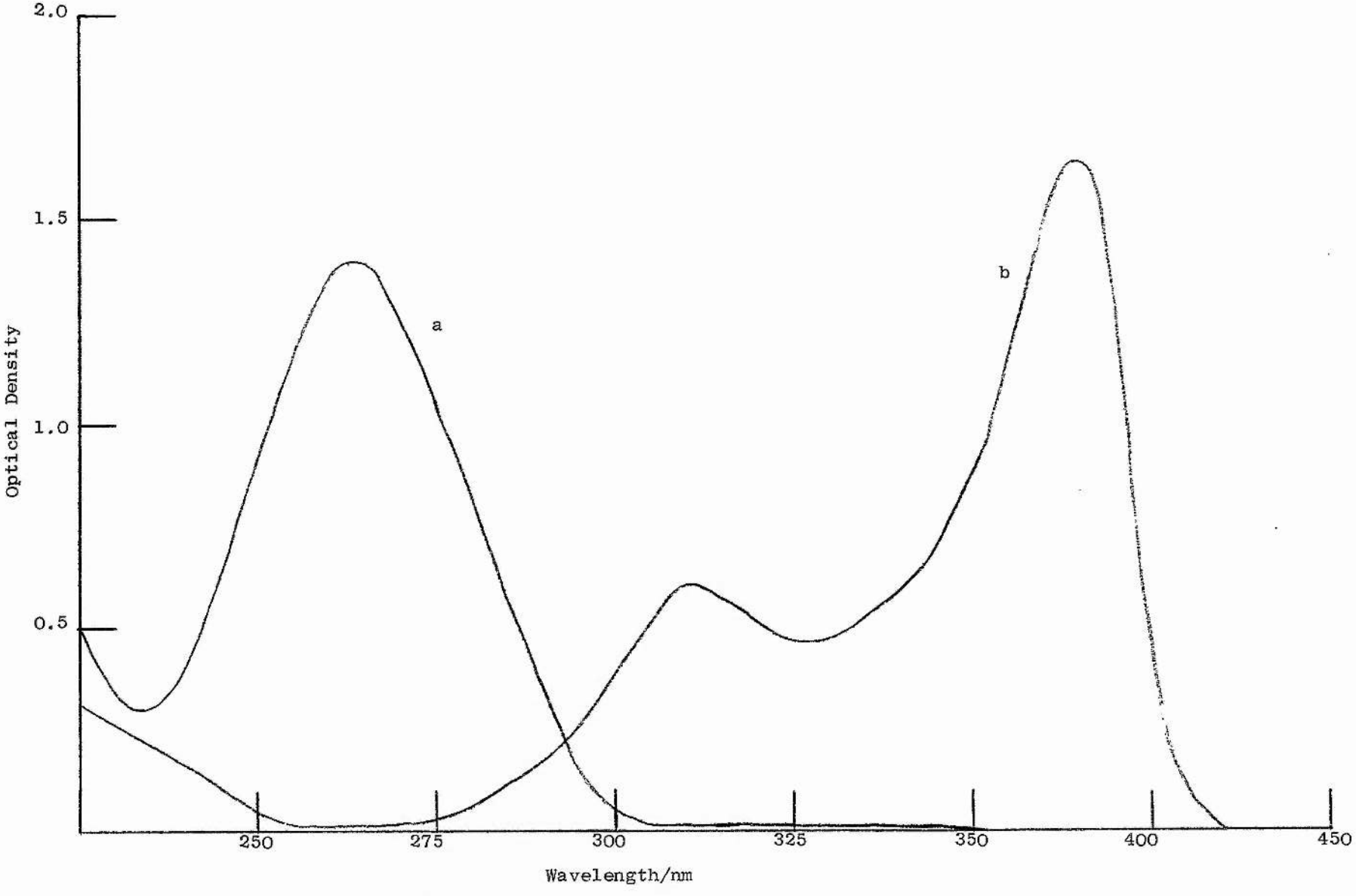

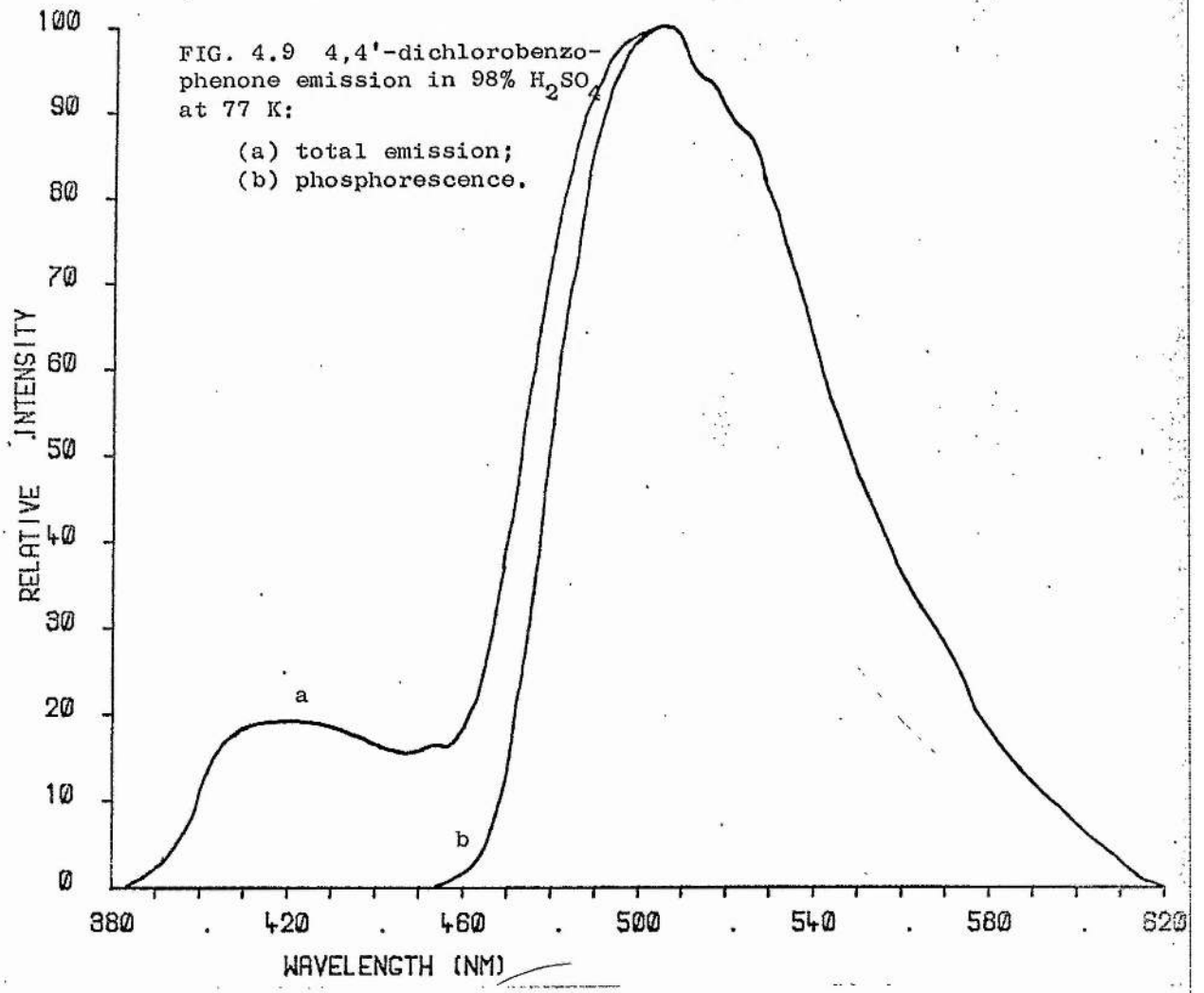

FIG. 4.9 4,4'-dichlorobenzophenone emission in 98% H_2SO_4 at 77 K:

(a) total emission;
(b) phosphorescence.

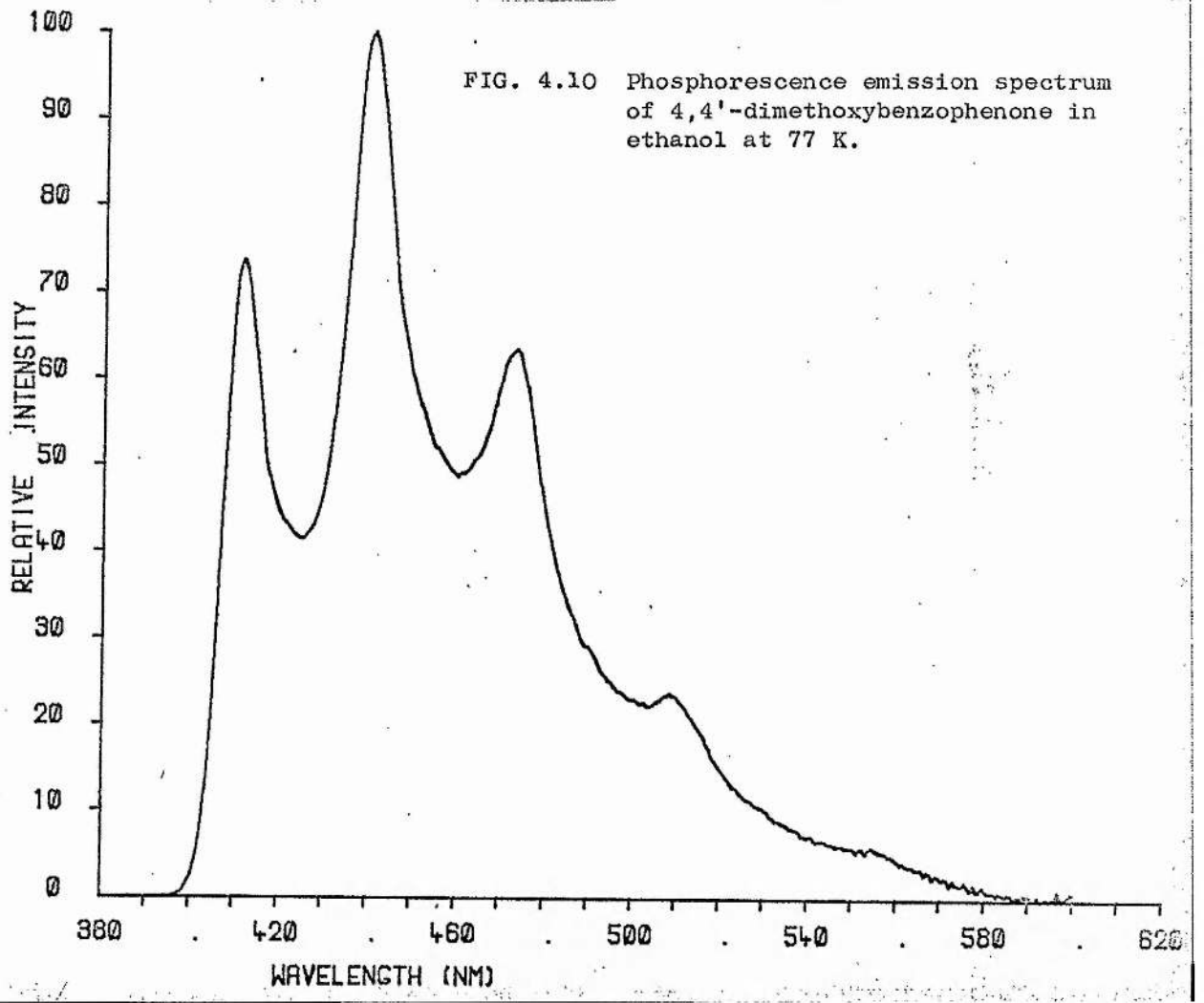

FIG. 4.10 Phosphorescence emission spectrum of 4,4'-dimethoxybenzophenone in ethanol at 77 K.

of fluorescence is larger than in the case of benzophenone itself (ϕ_f = 0.2, ϕ_p = 0.8). It is not surprising that the use of the spectroscopically determined energy levels of this compound in the Förster Cycle gives the same pK order as that obtained for benzophenone (see Table 4.5).

TABLE 4.7 Spectral Data for 4,4'dichlorobenzophenone (B and BH^+ forms: carbonyl protonation).

Absorption Maxima λ/nm				Long Wavelength Excitation Maximum λ/nm		Fluorescence Maximum λ/nm		Phosphorescence Maxima λ/nm	
B	ε	BH^+	ε	B	BH^+	B	BH^+	B	BH^+
335	2.4×10^2	378	4.1×10^3	373	385		417	419	506
267	2.6×10^4		1.5×10^3					450	
								485	
								525	
								571	

4,4'-dimethoxybenzophenone

The well defined short-lived phosphorescence (see FIG. 4.10) of the B form, similar to that of the parent compound is again indicative of the lowest n-π^* triplet level. The π-π^* absorption bands of both the B and BH^+ forms are red-shifted by the substitution thus bringing the n-π^* and π-π^* bands close together in the B form. The absorption spectra show these overlapping bands; in the phosphorescence excitation spectrum of B some of the fine structure of the n-π^* band is shown superimposed on the more intense π-π^* band but the n-π^* band is the transition of lowest energy (see FIG. 4.13 for the similar case of 4-hydroxybenzophenone). Therefore as in the case of 4-methoxybenzophenone[7], the lowest states of B are n-π^* in character. The BH^+ form exhibits fluorescence and the long-lived phosphorescence typical of the protonated forms of these molecules. In the total emission

spectrum at 77 K (see FIG. 4.11) the phosphorescence band is completely obscured by the fluorescence indicating a large increase in ϕ_f on substitution. The calculated pK^* values have the expected order but the $pK(S_1)$-$pK(T_1)$ separation is decreased by the substitution.

TABLE 4.8 Spectral Data for 4',4-dimethoxybenzophenone (B and BH^+ forms: carbonyl protonation).

Absorption Maxima λ/nm				Long Wavelength Excitation Maximum λ/nm		Fluorescence Maximum λ/nm		Phosphorescence Maxima λ /nm	
B	ε	BH^+	ε	B	BH^+	B	BH^+	B	BH^+
340	9.5×10^2	404	3.7×10^4	364	395		451	412	510
294	2.3×10^4	318	8.1×10^3					440	
								473	
								508	

4-hydroxybenzophenone

The types of lowest excited states found for this molecule in propan-2-ol by Porter and Suppan[7] are found to be unchanged in ethanol.

TABLE 4.9 Spectral Data for 4-hydroxybenzophenone (B and BH^+ forms: carbonyl protonation).

Absorption Maxima λ/nm				Long Wavelength Excitation Maximum λ/nm		Fluorescence Maximum λ/nm		Phosphorescence Maxima λ /nm	
B	ε	BH^+	ε	B	BH^+	B	BH^+	B	BH^+
340	8.6×10^2	372	2.6×10^4	366	365		430	422	485
295	5.9×10^3	295	7.9×10^3					450	
								483	
								521	
								570	

The spectral properties of the B and BH^+ forms are found to be very similar to those of the dimethoxy derivative. The $n-\pi^*$ and $\pi-\pi^*$ S_1 levels of the B form lie close together although the $n-\pi^*$ level is the

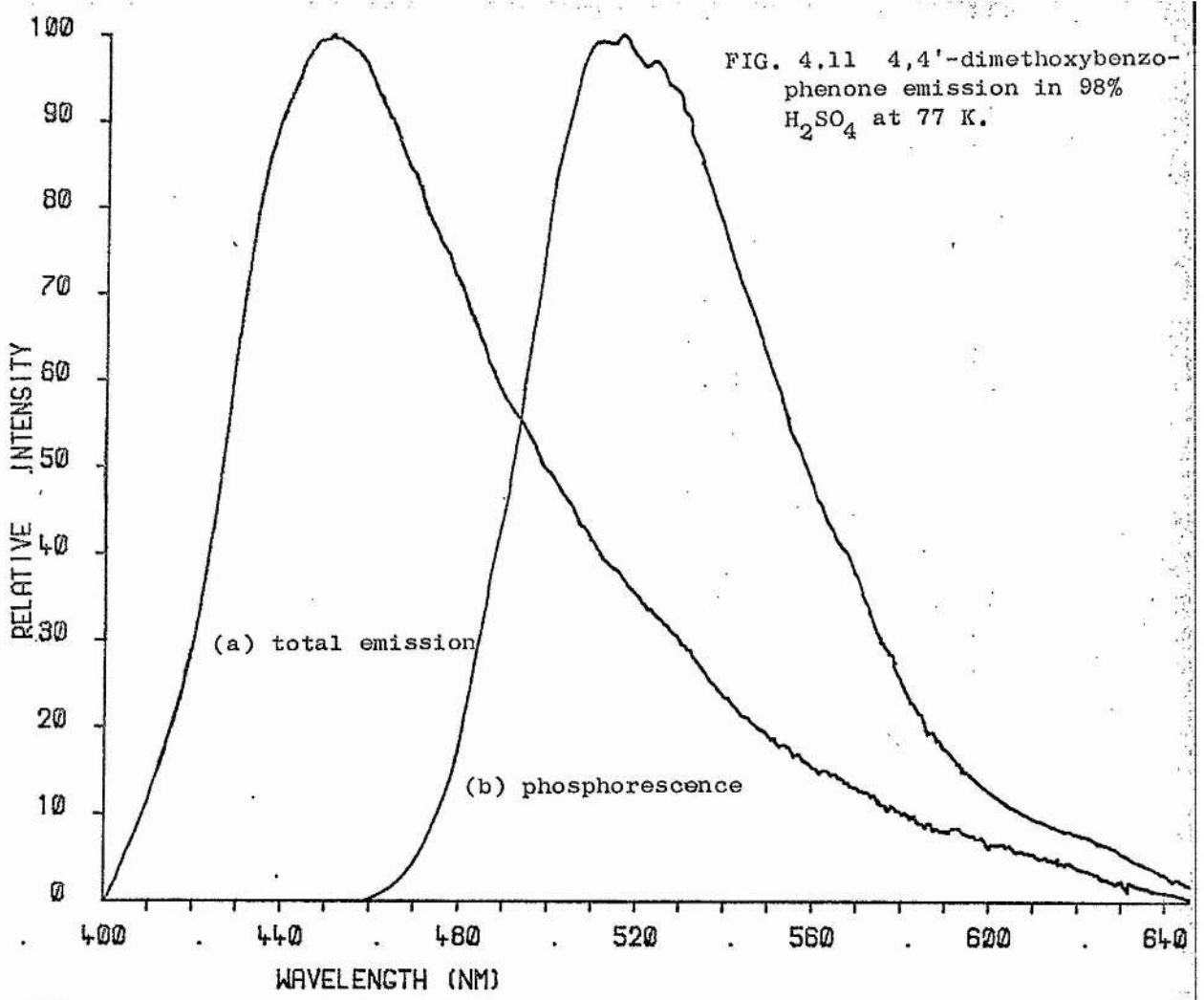

FIG. 4.11 4,4'-dimethoxybenzophenone emission in 98% H_2SO_4 at 77 K.

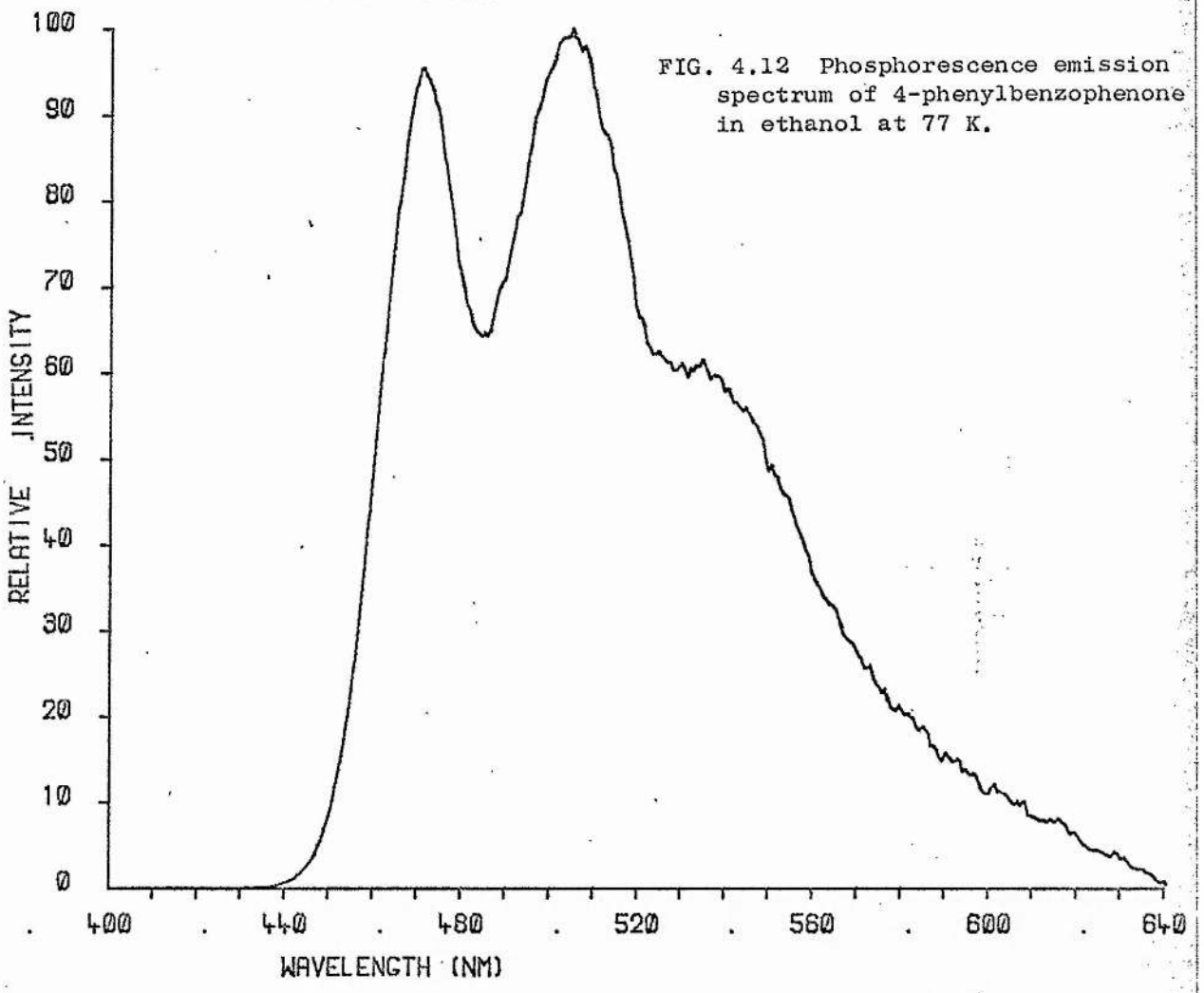

FIG. 4.12 Phosphorescence emission spectrum of 4-phenylbenzophenone in ethanol at 77 K.

lowest in both the singlet and triplet manifolds. In the case of the BH^+ form the relative quantum yield of fluorescence at 77 K is larger than that of phosphorescence which shows as a shoulder in the total emission spectrum. The calculated pK's for carbonyl protonation show the expected increase in basicity in the S_1 and T_1 states, a pK order of $T_1 > S_1 > S_o$, and a $\Delta pK(S_1-T_1)$ of 1.5 units.

In alkaline solutions the phenolate form of this molecule is obtained, which shows a new intense long wavelength band shown by Porter and Suppan to be of charge-transfer type. The spectral details given in Table 4.10 for this molecular form were obtained in 20% 1M NaOH/EtOH. The phosphorescence was characteristic of a charge transfer triplet with its lack of $n-\pi^*$ type structure and its longer lifetime. Fluorescence was also observed from this form at 77 K which is further evidence of the charge transfer character of the S_1 state. The lack of structure in the phosphorescence excitation spectrum is therefore compensated by the fact that an estimate of the 0-0 energy can be obtained by averaging the absorption and fluorescence maxima.

TABLE 4.10 Spectral Data for 4-O^--ϕ_2CO (BO^- and BOH forms: phenolate protonation)

Absorption Maxima λ/nm				Long Wavelength Excitation Maximum λ/nm		Fluorescence Maximum λ/nm		Phosphorescence Maxima λ/nm	
BO^-	ε	BOH	ε	BO^-	BOH	BO^-	BOH	BO^-	BOH
350	2.2×10^4	340	8.6×10^2	330	366	425		469	422
246	1.2×10^4	295	5.9×10^3					492	450
									483
									521
									570

lowest in both the singlet and triplet manifolds. In the case of the BH^+ form the relative quantum yield of fluorescence at 77 K is larger than that of phosphorescence which shows as a shoulder in the total emission spectrum. The calculated pK's for carbonyl protonation show the expected increase in basicity in the S_1 and T_1 states, a pK order of $T_1 > S_1 > S_o$, and a $\Delta pK(S_1-T_1)$ of 1.5 units.

In alkaline solutions the phenolate form of this molecule is obtained, which shows a new intense long wavelength band shown by Porter and Suppan to be of charge-transfer type. The spectral details given in Table 4.10 for this molecular form were obtained in 20% 1M NaOH/EtOH. The phosphorescence was characteristic of a charge transfer triplet with its lack of $n-\pi^*$ type structure and its longer lifetime. Fluorescence was also observed from this form at 77 K which is further evidence of the charge transfer character of the S_1 state. The lack of structure in the phosphorescence excitation spectrum is therefore compensated by the fact that an estimate of the O-O energy can be obtained by averaging the absorption and fluorescence maxima.

TABLE 4.10 Spectral Data for 4-O^--ϕ_2CO (BO^- and BOH forms: phenolate protonation)

Absorption Maxima λ/nm				Long Wavelength Excitation Maximum λ/nm		Fluorescence Maximum λ/nm		Phosphorescence Maxima λ/nm	
BO^-	ε	BOH	ε	BO^-	BOH	BO^-	BOH	BO^-	BOH
350	2.2×10^4	340	8.6×10^2	330	366	425		469	422
246	1.2×10^4	295	5.9×10^3					492	450
									483
									521
									570

The pK for the phenolic ionisation in the ground state is 6.5[30] and the excited state calculated pK values are; $pK(S_1)$ = 3.4, and $pK(T_1)$ = 1.5 (see Tables 4.4 and 4.6).

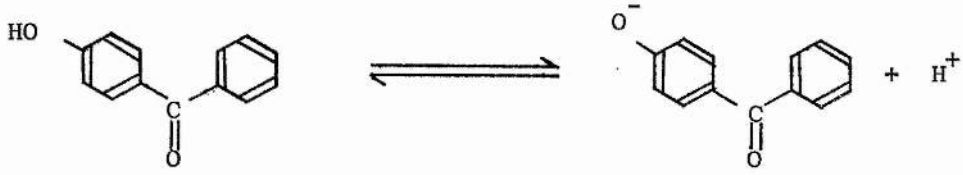

$pK(S_o) = 6.5$
$pK(S_1) = 3.4$
$pK(T_1) = 1.5$

These values differ from those obtained by Porter and Suppan[30] (i.e. $pK(S_1) = -4$ and $pK(T_1) = 3$) mainly in the $pK(S_1)$ values. A value of $pK(S_1) = -4$ can be obtained from calculations using our data if the maximum of the π-π^* band is used as the O-O energy of the phenol form. The O-O energy obtained from the phosphorescence excitation spectrum is much lower (see FIG. 4.13) and this gives a much smaller calculated $\Delta pK(S_1-S_o)$. The n-π^* absorption band is obscured in the absorption spectrum by the more intense π-π^* band and the first absorption maximum is that of the π-π^* band, but the n-π^* band is easily detected in the phosphorescence excitation spectrum and the O-O energy so obtained should certainly give a better estimate of the pK shift.

In a comparative study of the photoreduction of 4-hydroxy and 4-methoxybenzophenone Godfrey, Porter and Suppan[178] found anomalous behaviour in the 4-hydroxy case. While the spectra of both molecules were nearly identical and both had lowest triplet states of n-π^* type,

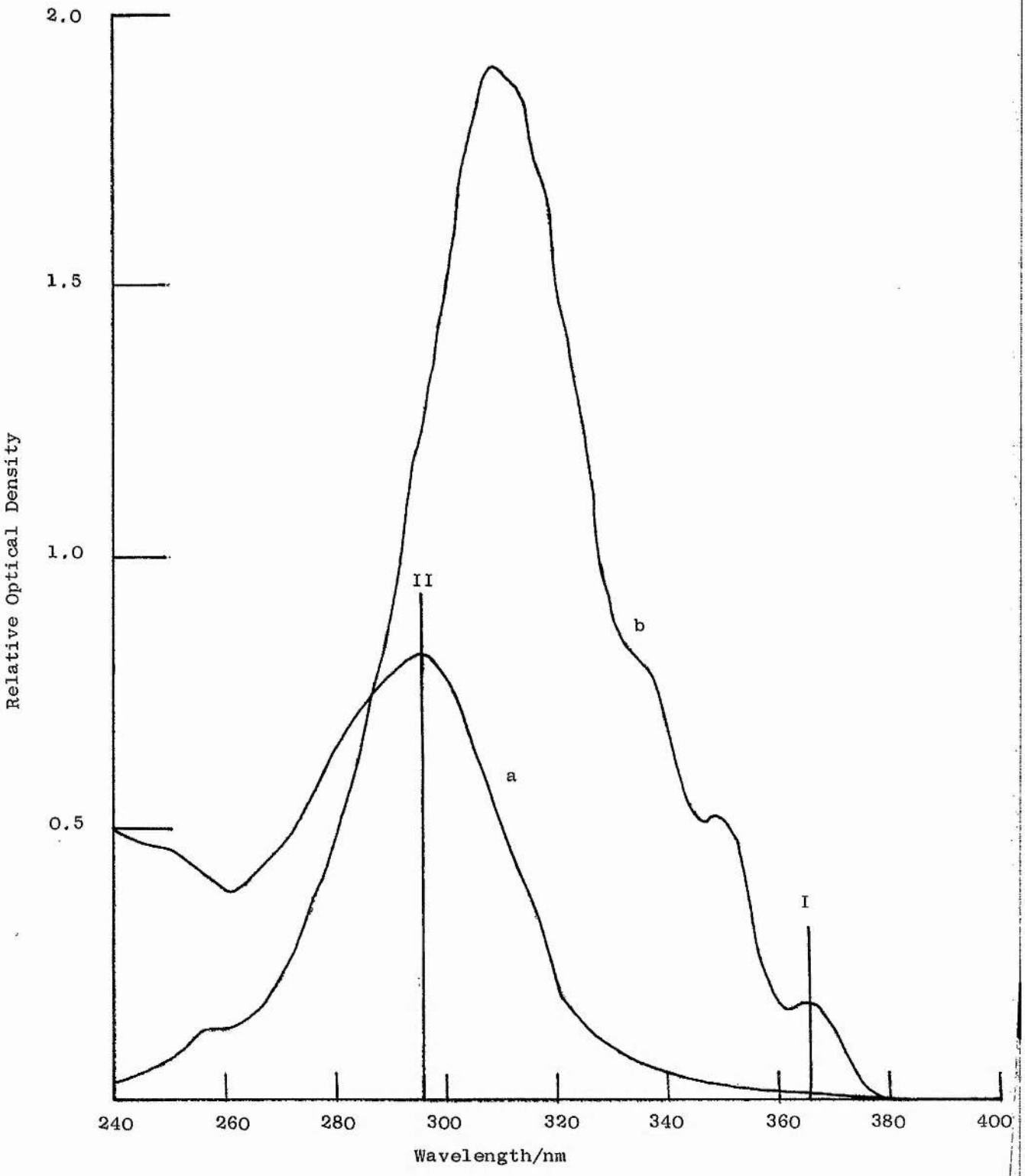

FIG. 4.13 Absorption (a) and phosphorescence excitation spectrum (b) of 4-hydroxybenzophenone (5.6×10^{-5} mol dm^{-3}) in ethanol.

I and II give the energy values used in different Förster Cycle calculations (see text).

the 4-methoxy reacts with propan-2-ol with a quantum yield of unity (as expected for an n-π^* triplet) whereas the 4-hydroxy is almost unreactive. The only difference between the molecules lies in the ability of the 4-hydroxy to ionise by losing the hydroxyl proton while the 4-methoxy cannot.

As CT triplet states are unreactive the lack of reactivity in alkaline solutions can be explained by the $pK(T_1)$ values obtained for loss of a proton by the hydroxyl group. At pH values greater than two the hydroxyl group would be ionised in the triplet state and as this ionised form has a lowest triplet of charge transfer character the lack of reactivity is expected. In fact 4-hydroxybenzophenone was found to be unreactive in acid solutions down to a pH less than one. Godfrey et al[178] postulated, because of their calculated $pK(S_1) = -4$, that in solutions of pH≈1 4-hydroxybenzophenone would on excitation ionise before radiationless conversion to the triplet was possible. All the triplets would therefore be formed in the unprotonated form, the lowest state of which is a charge transfer state. Protonation of this charge transfer triplet and then radiationless deactivation to the n-π^* triplet state was assumed to be the only route to $T_{n\pi^*}$ 4-hydroxybenzophenone at this acidity, since the calculated pK of

$$O^- — \phi_2CO(CT) + H^+ \longrightarrow HO — \phi_2CO(CT)$$

is -4[178] this reaction would be slow at pH = 1: hence the lack of reactivity.

FIG. 4.14 Diagrammatic representation of the possible routes from T_{CT} $O^- — \phi_2CO$ to $T_{n\pi^*}$ $HO-\phi_2CO$.

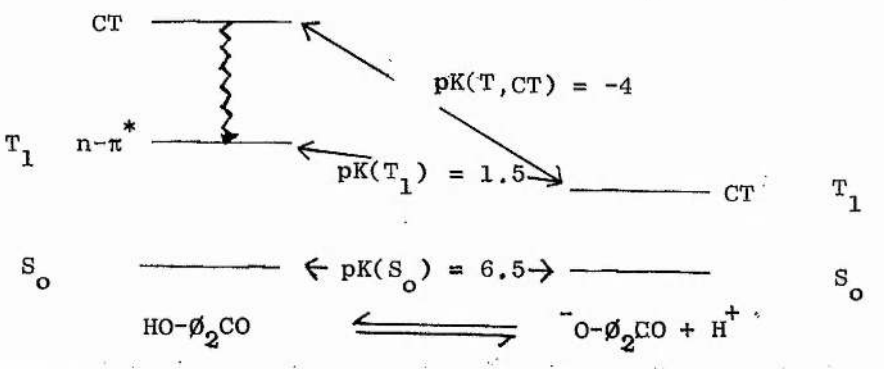

If on the other hand we consider the pK values calculated here the molecule on excitation to the S_1 state would not ionise in a solution of pH = 1 and the triplet state formed by intersystem crossing would be that of the unionised form ($T_{n\pi^*}$) which would be expected to be reactive. The low quantum yield of photoreduction can now be explained by considering the increased basicity of the carbonyl group in the excited state.

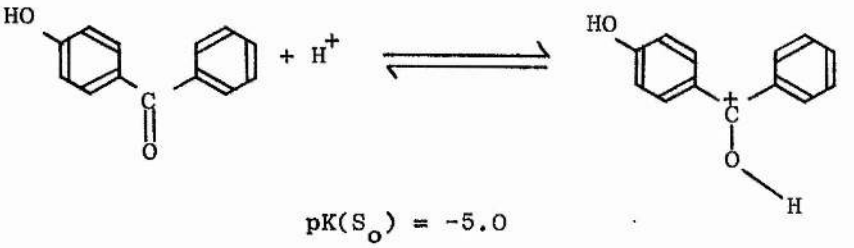

$pK(S_o) = -5.0$
$pK(S_1) = 0.0$
$pK(T_1) = 1.5$

At acidities greater than pH 1 the carbonyl group would be expected to protonate in the triplet state and this reaction would effectively compete with hydrogen abstraction. The pH values calculated above will not be the same in a solvent such as propan-2-ol, but they will give an indication of the type of changes in basicity to be expected and point to a possible explanation of the photostability of the compound.

4-phenylbenzophenone

The substitution of a phenyl group has little effect on the $n-\pi^*$ transition but, as would be expected from the extended π orbitals, has a marked effect on the $\pi-\pi^*$ transition. The absorption spectrum and the phosphorescence excitation spectrum indicate that the $n-\pi^*$ is still the lowest state in the singlet manifold. The B form shows no fluorescence at 77 K and its phosphorescence is long-lived

and not of the $n-\pi^*$ shape (see FIG. 4.12), showing that in this case the triplet is of $\pi-\pi^*$ type because of the large singlet-triplet splitting of the $\pi-\pi^*$ level. The BH^+ form has similar spectral properties to the other protonated forms, although the long wavelength absorption band tails off more slowly to longer wavelengths making the maximum more difficult to ascertain. The calculated pK values show that in this case the increase in basicity of the excited singlet is larger than that of triplet giving the pK order $pK(S_1) > pK(T_1) > pK(S_o)$ (See Tables 4.3 and 4.5)

TABLE 4.11 Spectral Data for 4-phenylbenzophenone (B and BH^+ forms: carbonyl protonation).

Absorption Maxima λ/nm				Long Wavelength Excitation Maximum λ/nm		Fluorescence Maximum λ/nm		Phosphorescence Maxima λ/nm	
B	ε_2	BH^+	ε_4	B	BH^+	B	BH^+	B	BH^+
350	5×10^2	386	3.1×10^4	374	397		480	471	535
291	1.2×10^4	309	9.5×10^3					505	

4-aminobenzophenone

The first protonation of this molecule occurs at the amino group at pH $\approx$ 0.5. This protonated amino form was studied in 20% 98% H_2SO_4/ EtOH. In ethanol the unprotonated amino form shows an intense absorption at long-wavelengths (see FIG. 4.15), similar to that observed for the phenolate form of 4-hydroxybenzophenone, which has been assigned to a charge transfer transition. The phosphorescence excitation spectrum shows no fine structure and the fluorescence and phosphorescence observed at 77 K are indicative of lowest singlet and triplet states of charge transfer character. These states explain the lack of reactivity of this compound in photoreduction reactions.

In dilute acid solutions the amino group protonates and the absorption spectrum changes to one similar in shape (see FIG. 4.15)

FIG. 4.15 Absorption spectra of 4-aminobenzophenone:
(a) 5.6×10^{-5} mol dm^{-3} in ethanol (NH_2-$Ø_2CO$);
(b) 2.1×10^{-4} mol dm^{-3} in 20% 98% H_2SO_4/ethanol ($\overset{+}{N}H_3$-$Ø_2CO$);
(c) 5.0×10^{-5} mol dm^{-3} in 98% H_2SO_4 ($\overset{+}{N}H_3$-$Ø_2\overset{+}{C}OH$).

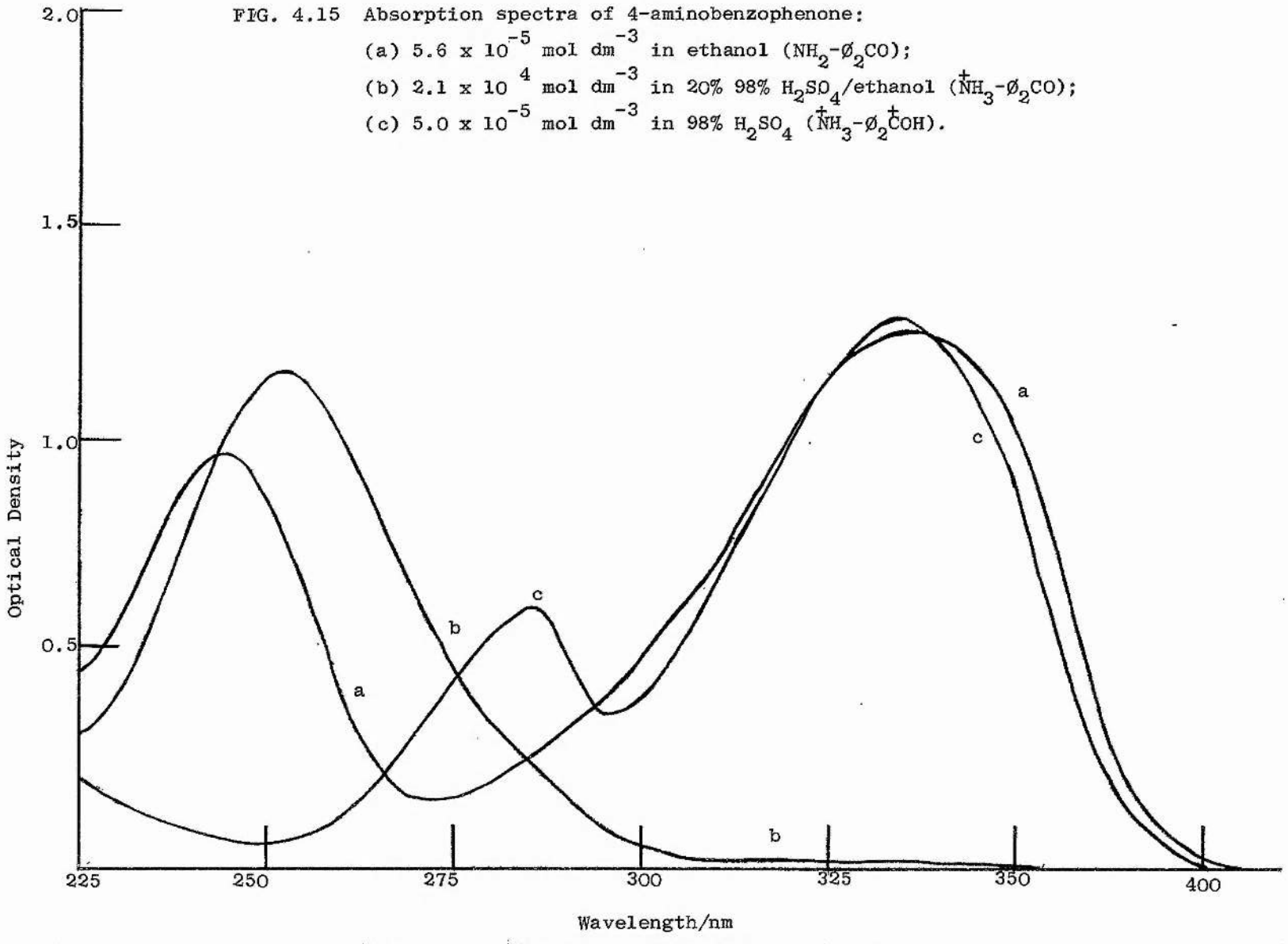

to that of the parent compound in ethanol i.e. a weak $n-\pi^*$ band at long wavelengths and a more intense $\pi-\pi^*$ band at shorter wavelengths. The phosphorescnece excitation spectrum shows the fine structure of the $n-\pi^*$ band and from this the O-O energy is obtained but unlike the cases of carbonyl protonation this method now gives the energy of the BH^+ form, while the O-O energy of the B form is obtained by averaging the absorption and fluorescence maxima of the CT singlet level. The treatment here is similar to that used to obtain data for pK calculations on the protonation of the phenolate ion of 4-hydroxybenzophenone. At 77 K the phosphorescence from the monoprotonated 4-aminobenzophenone is typical of $n-\pi^*$ phosphorescence. Confirmation that under these conditions the $n-\pi^*$ state is lowest has been obtained by Cohen[179] who showed that the monoprotonated molecule readily undergoes photoreduction with propan-2-ol. Protonation changes the substituent group from a strong electron donor to an electron acceptor and thus changes the character of the lowest excited levels from CT to $n-\pi^*$. The calculated excited state pKs for this amino protonation show the order $pK(S_o) > pK(S_1) > pK(T_1)$ as was found for the protonation of the $-O^-$ group in 4-hydroxybenzophenone. This is the reverse order from that normally found for carbonyl protonation but again the $pK(T_1)$ lies outside the $pK(S_o)$-$pK(S_1)$ range.

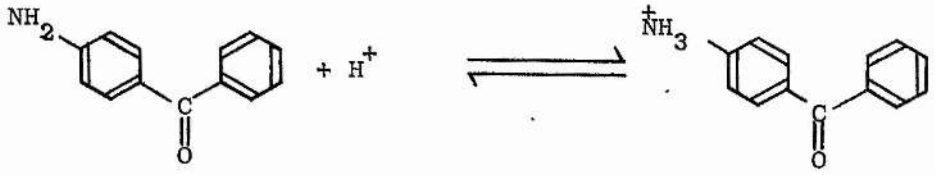

$pK(S_o) = 0.5$

$pK(S_1) = -2.2$

$pK(T_1) = -6.5$

TABLE 4.12 Spectral Data for 4-aminobenzophenone (BNH_2 and BNH_3^+ forms: amino protonation).

Absorption Maxima λ/nm				Long Wavelength Excitation Maximum λ/nm		Fluorescence Maximum λ/nm		Phosphorescence Maxima λ/nm	
BNH_2	ε	BNH_3^+	ε	BNH_2	BNH_3^+	BNH_2	BNH_3^+	BNH_2	BNH_3^+
335	2.2×10^4	330	2.1×10^2	346	369	439		481	415
244	1.7×10^4	252	2.1×10^4					510	446
									479
									517

The diprotonated form of 4-aminobenzophenone is observed in 98% H_2SO_4: the second protonation is assumed to be that of the carbonyl group.

TABLE 4.13 Spectral Data for 4-NH_3^+ - ϕ_2CO (B and BH^+ forms: carbonyl protonation).

Absorption Maxima λ/nm				Long Wavelength Excitation Maximum λ/nm		Fluorescence Maximum λ/nm		Phosphorescence Maxima λ/nm	
B	ε	BH^+	ε	B	BH^+	B	BH^+	B	BH^+
330	2.1×10^2	334	2.4×10^4	369	330		427	415	470
252	2.1×10^4	285	1.9×10^4					446	
								479	
								517	

This form of the molecule has very similar spectral properties (see FIG. 4.15 for the absorption spectrum) to those of the protonated dichloro derivative, which might be expected as the substituent, NH_3^+, is electron withdrawing. At 77 K fluorescence and phosphorescence, similar in relative quantum yield and relative position to these bands of protonated benzophenone, are detected. The calculated excited state pK's for the reaction:-

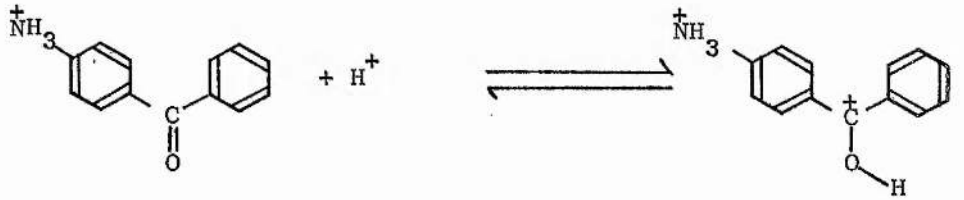

are found to have the xanthone order with an increased pK(S_1-T_1) separation (see Tables 4.3 and 4.5).

4-nitrobenzophenone

The absorption spectra of the B and BH^+ forms were similar to those of the parent compound and those other derivatives with electron-withdrawing substituents. Emission from the B form was very weak but some structure could be detected which was similar to that shown by n-π^* phosphorescence bands. The BH^+ form showed a weak emission and for neither form could meaningful excitation spectra be obtained. Little weight can be put on the calculations made with these results because the emissions were very weak and presence of impurities was not ruled out. The Förster Cycle calculations are also open to larger errors due to the absence of a phosphorescence excitation spectrum of the B form and fluorescence from BH^+ which help to locate the 0-0 energies. The calculated pK's show a large increase in triplet state basicity on excitation while the first excited singlet becomes a slightly weaker base.

TABLE 4.14 Spectral Data for 4-nitrobenzophenone (B and BH^+ forms: carbonyl protonation).

Absorption Maxima λ/nm				Long Wavelength Excitation Maximum λ/nm		Fluorescence Maximum λ/nm		Phosphorescence Maxima λ/nm	
B	ε	BH^+	ε	B	BH^+	B	BH^+	B	BH^+
345	4.4×10^2	338	2.4×10^4					410	515
266	2.0×10^4	291	1.4×10^4					459	

2-hydroxybenzophenone

2-hydroxybenzophenone and its derivatives are used as photostabilisers, protecting polymers against the undesirable effects of ultraviolet radiation, because of their strong absorption in the ultraviolet region and high photochemical stability[180]. This stability would appear to be due in part to their ability to undergo intramolecular hydrogen transfer rather than transfer from the solvent[181].

The long wavelength absorption band of the B form (see FIG. 4.16) is more intense than a $n-\pi^*$ band but less intense than the charge-transfer band of 4-aminobenzophenone. The phosphorescence spectrum was structured and short-lived like the emission from an $n-\pi^*$ type triplet level. The phosphorescence excitation spectrum did not clearly show any fine structure (although the presence of shoulders on the $\pi-\pi^*$ absorption band might have been an indication of an underlying $n-\pi^*$ band), making the location of the 0-0 energy more arbitrary and making assignment of the type of S_1 level difficult. Although the first absorption band was similar in shape and position to the charge transfer bands already discussed, no fluorescence was detected from B and the triplet level appeared to be of $n-\pi^*$ type.

TABLE 4.15 Spectral Data for 2-hydroxybenzophenone (B and BH^+ forms; carbonyl protonation).

Absorption Maxima λ/nm				Long Wavelength Excitation Maximum λ/nm		Fluorescence Maximum λ/nm		Phosphorescence Maxima λ/nm	
B	ε	BH^+	ε	B	BH^+	B	BH^+	B	BH^+
337	4.1×10^3	390	6.6×10^3	325	390			417	481*
262	1.3×10^4	336	1.4×10^4					445	503
		284	8.6×10^3					480	
								517	

* Shoulder

The long wavelength band of the BH^+ form was of a different shape to that of the protonated 4-substituted derivatives (see FIG. 4.16). Phosphorescence from BH^+ was shorter lived than that of the 4-substituted BH^+ and appeared as a broad band the maximum of which was difficult to determine. The presence of fluorescence from BH^+ at 77 K could not definitely be established although the maximum of the total emission spectrum was blue-shifted compared to that of the phosphorescence band, which might indicate that a weak fluorescence band lies very close to the phosphorescence.

Kysel[182] has reported values of 1.43 and -2.57 for $pK(S_1)$ and $pK(T_1)$ respectively of 2-hydroxybenzophenone but it is difficult to compare these values with the values obtained here, 2.1 and 0.4, as Kysel does not report any details of the energy values used in his calculation. The pK order obtained in both cases is the same, but difficulties in determination of the O-O energies make the calculations less reliable for this derivative.

2-methoxybenzophenone

This had very similar spectral features to the 2-hydroxy compound, the major difference bring in the long wavelength absorption band of the B form which was less intense and also showed its $n-\pi^*$ band structure more clearly in its phosphorescence excitation spectrum.

TABLE 4.16 Spectral Data for 2-methoxybenzophenone (B and BH^+ forms: carbonyl protonation).

Absorption Maxima λ/nm				Long Wavelength Excitation Maximum λ/nm		Fluorescence Maximum λ/nm		Phosphorescence Maxima λ/nm	
B	ε	BH^+	ε	B	BH^+	B	BH^+	B	BH^+
325	1.16×10^3	398	8×10^3	372	380			417	482
250	1.28×10^4	331	1.3×10^4					447	504
		285	9.1×10^3					481	526
								520	

FIG. 4.16 Absorption spectra of 2-hydroxybenxophenone: (a) 6.3×10^{-5} mol dm^{-3} in ethanol; (b) 1.3×10^{-4} mol dm^{-3} in 98% H_2SO_4 and (c) 2-hydroxy-5-nitrobenzophenone 5.8×10^{-5} mol dm^{-3} in ethanol.

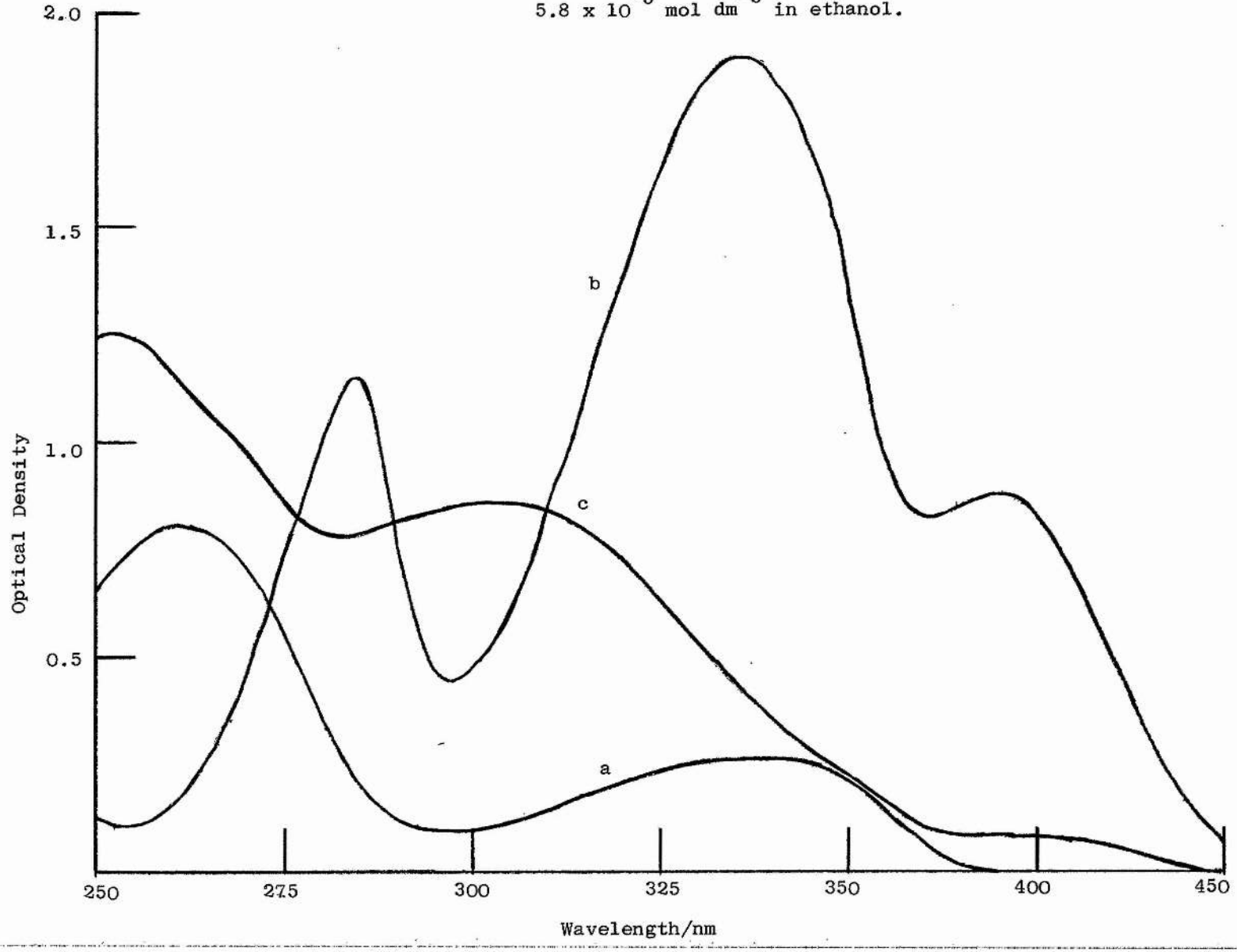

Fluorescence from the BH^+ form was weak and its maximam difficult to ascertain as the fluorescence and phosphorescence bands lay close together. As in the 2-hydroxy case, the Förster Cycle calculations are less reliable than in those cases where the 0-0 energies are readily determined; but in both cases the calculations indicate that the singlet and triplet states become stronger bases upon excitation and that the pK shifts for the two states are similar.

2-hydroxy-5-nitrobenzophenone

The B form has a weak absorption at longer wavelengths than any of the other derivatives studied (see FIG. 4.16). The BH^+ absorption is characteristic of the ortho hydroxy derivatives with an intense band with three maxima at long wavelengths. The phosphorescence and phosphorescence excitation spectra of B showed no fine structure and, while phosphorescence and fluorescence were observed at 77 K from BH^+, the bands were broad so that maxima were difficult to determine.

Kysel[182] calculates values of 4.22 and -9.50 for $pK(S_1)$ and $pK(T_1)$ respectively. Calculations here give values of -4.1 and -9.7, the large difference in $pK(S_1)$ values being explained if we assume that Kysel used the first π-π^* maximum (i.e. 303 nm in FIG. 4.16) as the 0-0 energy of the B form instead of the 400 nm maximum of the weak first absorption band used in this calculations. The ground state pK for this compound is -7.4[180] and both calculations show that while there is an increase in basic strength in the singlet state the triplet molecule becomes a weaker base.

TABLE 4.17 Spectral Data for 2-hydroxy-5-nitrobenzophenone (B and BH^+ forms: carbonyl protonation).

Absorption Maxima λ/nm				Long Wavelength Excitation Maximum λ/nm		Fluorescence Maximum λ/nm		Phosphorescence Maxima λ/nm	
B	ε	BH^+	ε	B	BH^+	B	BH^+	B	BH^+
400	2.7×10^2	382	1.3×10^4	390	385		470	531	505
303	9.7×10^3	325	1.7×10^4						
253	1.4×10^4	276	1.7×10^4						

2,2',4,4'-tetrahydroxybenzophenone

The absorption spectrum of the B form shows an intense band at long wavelengths similar to the C-T band of 4-aminobenzophenone.

TABLE 4.18 Spectral Data for 2,2',4,4'-tetrahydroxybenzophenone (B and BH^+ forms: carbonyl protonation).

Absorption Maxima λ/nm				Long Wavelength Excitation Maximum λ/nm		Fluorescence Maximum λ/nm		Phosphorescence Maxima λ/nm	
B	ε	BH^+	ε	B	BH^+	B	BH^+	B	BH^+
350	1.6×10^4	403	2.4×10^4	335	408		440	410	480
287	1.1×10^4	303	6.9×10^3					433	

The phosphorescence also showed similarities to that from the 4-amino derivative, indicating the possibility that in this compound also both the lowest singlet and triplet states are of C-T character. The BH^+ absorption spectrum showed a band, with two widely separated maxima, at long wavelengths. As in the case of the other o-hydroxy derivatives the fluorescence from BH^+ observed at 77 K lay close to the phosphorescence band although in this case it was slightly easier to detect as it appeared as a shoulder in the total emission

band. The calculated pK values indicate a large increase in basicity in both states and a pK order of $pK(S_1) > pK(T_1) > pK(S_o)$.

2-carboxybenzophenone

The unprotonated form showed spectral properties consistent with a $n-\pi^*$ lowest singlet and triplet levels. The BH^+ absorption was similar to that of other derivatives but at 77 K the two bands observed in the phosphorescence spectrum had different excitation spectra, indicating emission from different species. This compound is known to undergo a cyclohydration reaction in concentrated H_2SO_4 to form anthraquinone[183].

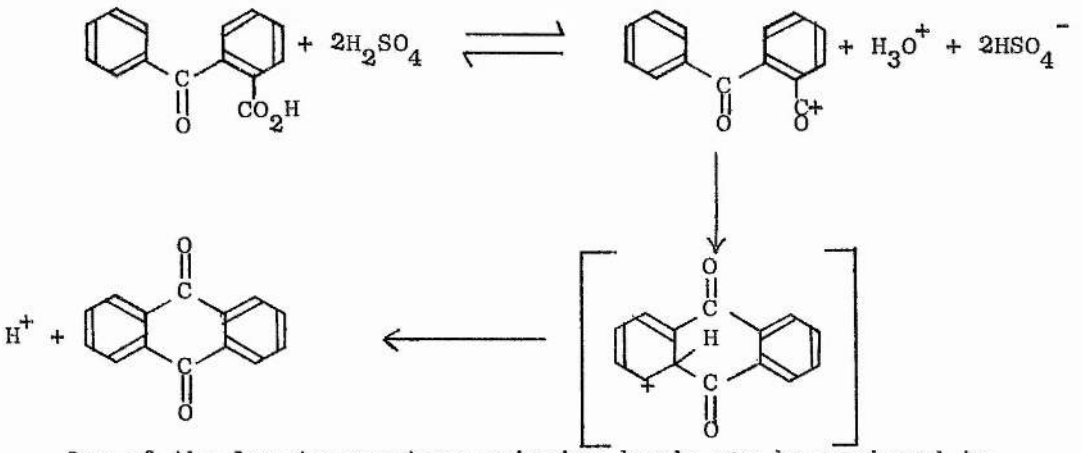

One of the low temperature emission bands can be assigned to the protonated anthraquinone molecule but the uncertainty in the origin of the other emission makes this compound unsuitable for application of the Förster Cycle.

TABLE 4.19 Spectral Data for 2-carboxybenzophenone, $BH^+ \equiv$ Spectral details of freshly prepared solution in 98% H_2SO_4.

Absorption Maxima λ/nm				Long Wavelength Excitation Maxima λ/nm		Fluorescence Maximum λ/nm		Phosphorescence Maxima λ/nm	
B	ε	BH^+	ε	B	BH^+	B	BH^+	B	BH^+
325	1.2×10^2	406	1.9×10^4	360	420			398	490
245	1.5×10^4	331	0.89×10^4		350			421	550
								451	

(c) Emission from Benzophenones in fluid solution

As these benzophenones had not been specially purified little weight can be put on any weak emissions observed. With this in mind the following is a description of the weak emission observed from solutions of the benzophenones in 98% H_2SO_4 at room temperature. In all cases except the 4-nitro derivative an emission was observed which, although always broad with no structure, covered approximately the same spectral region as the total emission spectrum at 77 K. Thus in the case of benzophenone itself the emission appears to be mainly phosphorescence whereas 4,4'-dimethoxybenzophenone, which has a much higher yield of fluorescence, shows emission appearing to be mainly fluorescence. In no cases could the emission be resolved into fluorescence and phosphorescence by our equipment. Solutions of dimethoxy, dichloro and 2-hydroxy in 98% H_2SO_4 were degassed but this did not affect the emission intensity. For the 2-hydroxy derivative, as for benzophenone, the emission is similar to phosphorescence which would have been expected to be oxygen quenched.

The dichloro compound was very insoluble in water and no emission of the B form could be detected from the very dilute aqueous solutions. The dimethoxy derivative was slightly more soluble and a weak emission was detected from aqueous solutions which was quenched by H^+. 2-hydroxybenzophenone which was reasonably soluble in water showed no emission in degassed or non-degassed aqueous solutions.

3. Acetophenones

(a) Introduction

To determine whether the pK behaviour observed for benzophenone derivatives might be more general and be true of other aromatic

carbonyl compounds the spectral data necessary to perform Förster Cycle calculations on several acetophenones were obtained. The experimental procedure was identical to that reported for the benzophenones, the base forms (B) being observed in ethanol solutions while for the BH^+ forms 98% H_2SO_4 was used, the exception to this being the protonated amino form of 4-aminoacetophenone which was measured in 20% 98% H_2SO_4/EtOH.

Acetophenone exhibits similar photochemical properties to those of benzophenone. In both the singlet and triplet manifolds the first excited level is of $n-\pi^*$ character. Lamola[184] showed in a phosphorescence study that acetophenone in a non-polar medium exhibits a $\pi-\pi^*$ triplet state only slightly above the $n-\pi^*$ triplet state. Acetophenone has a high energy $n-\pi^*$ state compared with other unsubstituted aldehydes and ketones[34] and, due to the smaller energy gap between the $n-\pi^*$ and $\pi-\pi^*$ triplets than in the case of benzophenone[185], acetophenone shows a much greater sensitivity of the ordering of $n-\pi^*$ and $\pi-\pi^*$ triplet levels to substitution[34]. It is generally observed that substituents such as bromo, methoxy, and hydroxy red shift $\pi-\pi^*$ transitions much more than they shift $n-\pi^*$ transitions[186] and therefore it is not unexpected that 4-bromo, 4 hydroxy and 4-methoxyacetophenone should exhibit spectroscopic properties indicative of a $\pi-\pi^*$ lowest triplet level. Yang[28] has investigated the photochemical and spectral properties of methyl substituted acetophenones and noted the same sensitivity of the ordering of the $n-\pi^*$ and $\pi-\pi^*$ triplet levels to substitution. In a recent study of solvent effects on acetophenone photoreduction, Lindqvist[188] concluded that a subtancial part of the low efficiency of photoreduction in polar solvents could be attributed to a decreased reactivity of the acetophenone triplet state and that this reduced reactivity was probably due to the greater $\pi-\pi^*$ character of the acetophenone triplet in polar solvents.

(b) Spectral Properties of and Förster Cycle Calculations for Acetophenones

The acetophenones investigated here showed the properties that would be expected from the introduction. All the derivatives, except 4-aminoacetophenone which showed a charge transfer band as its long wavelength absorption band, showed spectral properties consistent with the first excited singlet state being of $n-\pi^*$ type. Acetophenone and 4-fluoroacetophenone showed phosphorescence characteristic of an $n-\pi^*$ triplet state: while the data on 4-methyl, 4-chloro and 4-NH_3^+ are less definite, the indications are that the lowest lying triplet states are still essentially $n-\pi^*$ in nature. In the case of 4-hydroxy, 4-methoxy and 4-bromoacetophenone the emissions were consistent with $\pi-\pi^*$ triplet levels. The spectral data for these derivatives are reported in Table 4.20. The BH^+ forms of all the derivatives showed an intense $\pi-\pi^*$ type absorption at long wavelengths although the structure was considerably altered by substitution. The protonated carbonyl forms, except the halogen and nitro derivatives, showed fluorescence and phosphorescence at 77 K in 98% H_2SO_4. The phosphorescence was very long-lived in all cases, with a half-life probably > 1 sec. This long lifetime made effective measurement of the phosphorescence excitation spectra impossible on our apparatus. The 4-fluoro compound fluoresced and phosphoresced but the 4-chloro and 4-bromo showed only phosphorescence in 98% H_2SO_4 at 77 K and the lifetime of the phosphorescence was considerably shortened as the atomic weight of the halogen substituent was increased. Emission from both forms of the 4-nitro compound was too weak to study.

Details of the values used in the Förster Cycle calculations are given in Table 4.21 and the calculated pK shifts are shown in Table 4.22. The calculations are in general less reliable than those performed on

TABLE 4.20 Spectral Data for acetophenones.

SUBSTITUENT Pos.4	Absorption Maxima λ/nm				FIRST EXCITATION MAXIMUM λ/nm	FLUORESCENCE MAXIMUM λ/nm		PHOSPHORESCENCE MAXIMA λ/nm	
	B	ε	BH^+	ε	B	B	BH^+	B	BH^+
H	315	59	335	2.4×10^3	354		418	389	445*
	274	1×10^3	296	2.2×10^4				415	476
	241	1.2×10^4						446	
								477	
CH_3	320	79	313	2.2×10^4	352		419	401	465
	252	1.4×10^4						422	486
								452	
CH_3O	325	138	349	3.5×10^4	348		378	406	482
	278	1.4×10^4						430	
	272	1.5×10^4						464	
OH	330	2.0×10^2	337	2.6×10^4	346		387	411	475
	280	1.5×10^4						439	
NH_2 (a)	319	1.9×10^4	325	50	350 (BH^+) 370			452	390
	234	6.7×10^3	275	9.2×10^2				464	413
			238	1.2×10^4					429
NH_3^+	325	50	320	2.1×10^3	320		397	390	451
	275	9.2×10^2	279	2.0×10^4				413	
	238	1.2×10^4						429	
NO_2	345	3.0×10^2	335	2.5×10^3					
	263	1.3×10^4	288	2.0×10^4					
F	310	70	300	1.7×10^4	352		394	383	436
	243	1.2×10^4						409	453
								438	
								468	
Cl	325	150	337	2.1×10^4	357			398	477
	257	2.5×10^3						424	
								454	
Br	315	9.2×10^2	330	2.4×10^4	355			401	480
	255	9.0×10^3						426	
								460	

(a) Protonation of the amino group

* Shoulder

TABLE 4.21 Spectral Data used in Förster Cycle calculations on acetophenones.

SUBSTITUENT Pos. 4	$\lambda_{max/nm}$ for B	$\lambda_{max/nm}$ for BH^+			$\Delta\bar{\nu}/cm^{-1}$ for S_1-S_o	Phosphorescence $\lambda_{max/nm}$		$\Delta\bar{\nu}/cm^{-1}$ for T_1-S_o
		Absorption	Fluorescence	Mean		B	BH^+	
H	354	335	418	372	1700	389	445	3300
CH_3	352	313	419	360	600	401	465	3400
CH_3O	348	349	378	363	1200	406	482	3900
OH	346	337	387	362	1300	411	475	3200
NH_2 (a)	344 (b)	350 (c)			500	452	390	-3500
NH_3^+	350	320	397	359	700	390	451	3400
F	352	300	394	347	-400	383	436	3200
Cl	325 (d)	337			1100	398	477	4000
Br	315 (d)	330			1400	401	480	4100

(a) Protonation of the amino group.

(b) Value obtained from averaging absorption and fluorescence maxima. Other values, except (d), in this column are from phosphorescence excitation spectra..

(c) Value obtained from phosphorescence excitation spectrum.

(d) Long wavelength absorption maximum.

TABLE 4.22 pK^* values for acetophenones based on Förster Cycle calculations.

SUBSTITUENT Pos.4	$\Delta pK(S_1-S_o)$	$\Delta pK(T_1-S_o)$	$pK(S_o)$	$pK(S_1)$	$pK(T_1)$
H	3.6	7.0	-6.1	-2.5	0.9
CH_3	1.3	7.1	-5.5	-4.2	2.6
CH_3O	2.5	8.2	-4.8	-1.3	3.4
OH	2.8	6.7	-4.7	-1.9	2.0
NH_2 (a)	1.0	-7.3	≈0.5	1.5	-6.8
NH_3^+	1.5	7.4			
F	-0.8	6.7	-6.1	-6.9	0.6
Cl	2.3	8.4	-6.5	-4.2	1.9
Br	2.9	8.6	-6.5	-3.6	2.1

(a) Protonation of the amino group.

benzophenones because of increased difficulties in determining the 0-0 transition energies. FIG. 4.17 shows the absorption spectra of the B and BH^+ forms of acetophenone and FIG. 4.18 shows that of the BH^+ forms of 4-methylacetophenone and 4-methoxyacetophenone. Although the π-π^* band of the B forms is affected by substitution, the weak n-π^* band is the long wavelength band in all cases and the 0-0 energy can be obtained from the phosphorescence excitation spectrum. The BH^+ form of acetophenone (see FIG. 4.17) has a strong π-π^* band, λ_{max} = 296 nm, overlapping with a less intense π-π^* band at longer wavelengths. The maximum of the first band can be estimated and by averaging with the fluorescence maximum a reasonable estimation of the 0-0 band can be obtained. In the case of protonated 4-methylacetophenone the more intense of these bands is red shifted and the bands overlap to a greater extent (FIG. 4.18). It is now impossible to obtain a value of the maximum of the first absorption band from the absorption spectrum and the use of the fluorescence excitation spectrum also failed to resolve the overlapping bands. The maximum of the combined bands was used provisionally in the Förster Cycle calculations and as the maximum of the first band is expected to lie at a somewhat longer wavelength the Δ pK calculated and reported in Table 4.22 will be small. This effect is particularly marked in the case of the 4-fluoro compound and results in a small negative value of $\Delta pK(S_1-S_o)$ which is almost certainly due to this inability to obtain the 0-0 energy of the BH^+ form. For the protonated form of 4-methoxyacetophenone the more intense band is further red shifted than in the 4-methyl case (FIG. 4.18) and now appears to be the long wavelength band. The maximum of this band was used in the Förster Cycle calculations. In the cases of the 4-chloro and 4-bromo derivatives no fluorescence was observed from the BH^+ form at 77 K and to calculate $\Delta pK(S_1-S_o)$ the first absorption maxima of the B and BH^+ forms were used alone.

FIG. 4.17 Absorption spectra of acetophenone:

(a) $4,3 \times 10^{-4}$ mol dm^{-3} in ethanol;

(b) 8.0×10^{-5} mol dm^{-3} in 98% H_2SO_4.

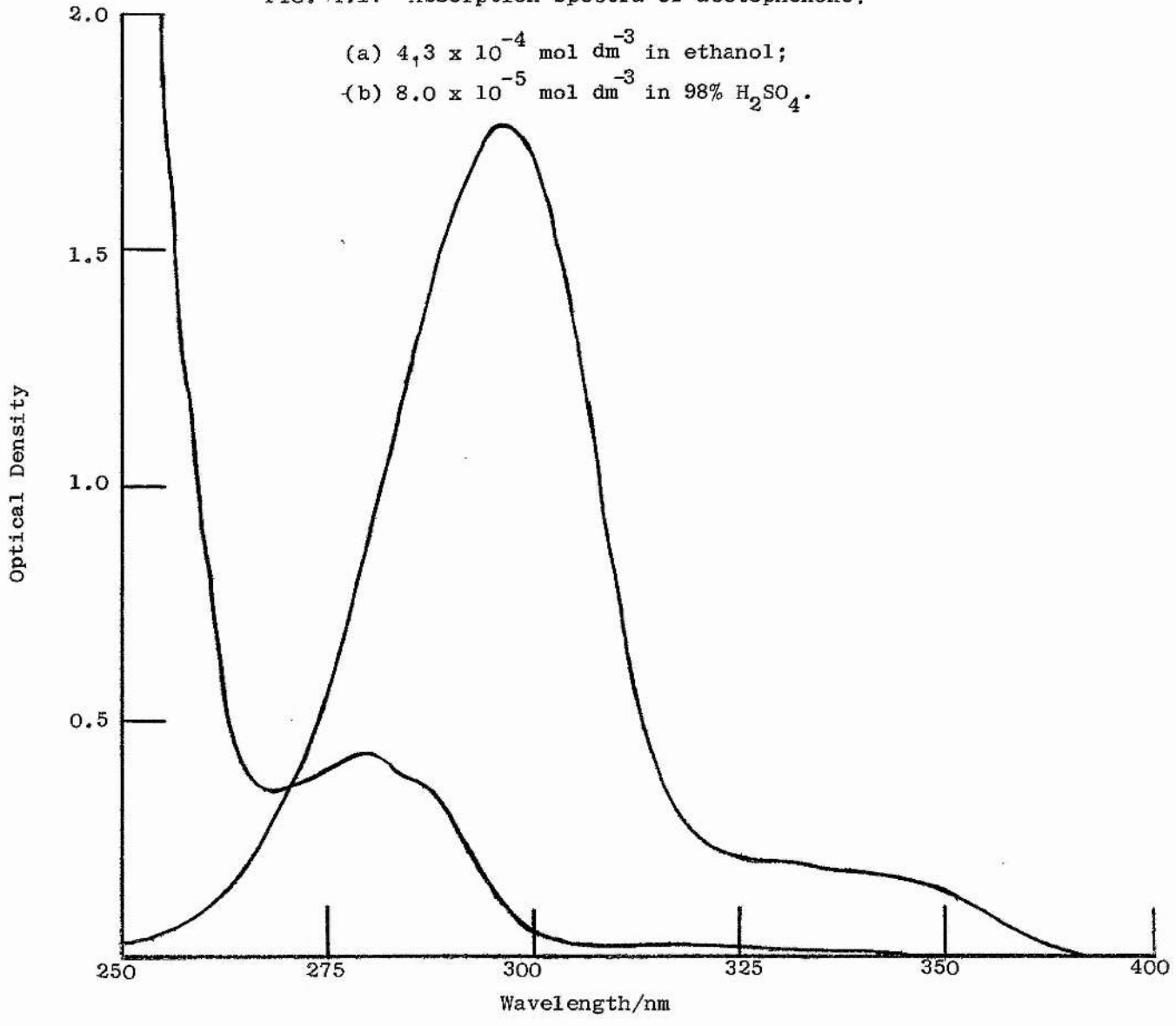

FIG. 4.18 Absorption spectra in 98% H_2SO_4:

(a) 4-methylacetophenone (5.4×10^{-5} mol dm^{-3});

(b) 4-methoxyacetophenone (3.7×10^{-5} mol dm^{-3}).

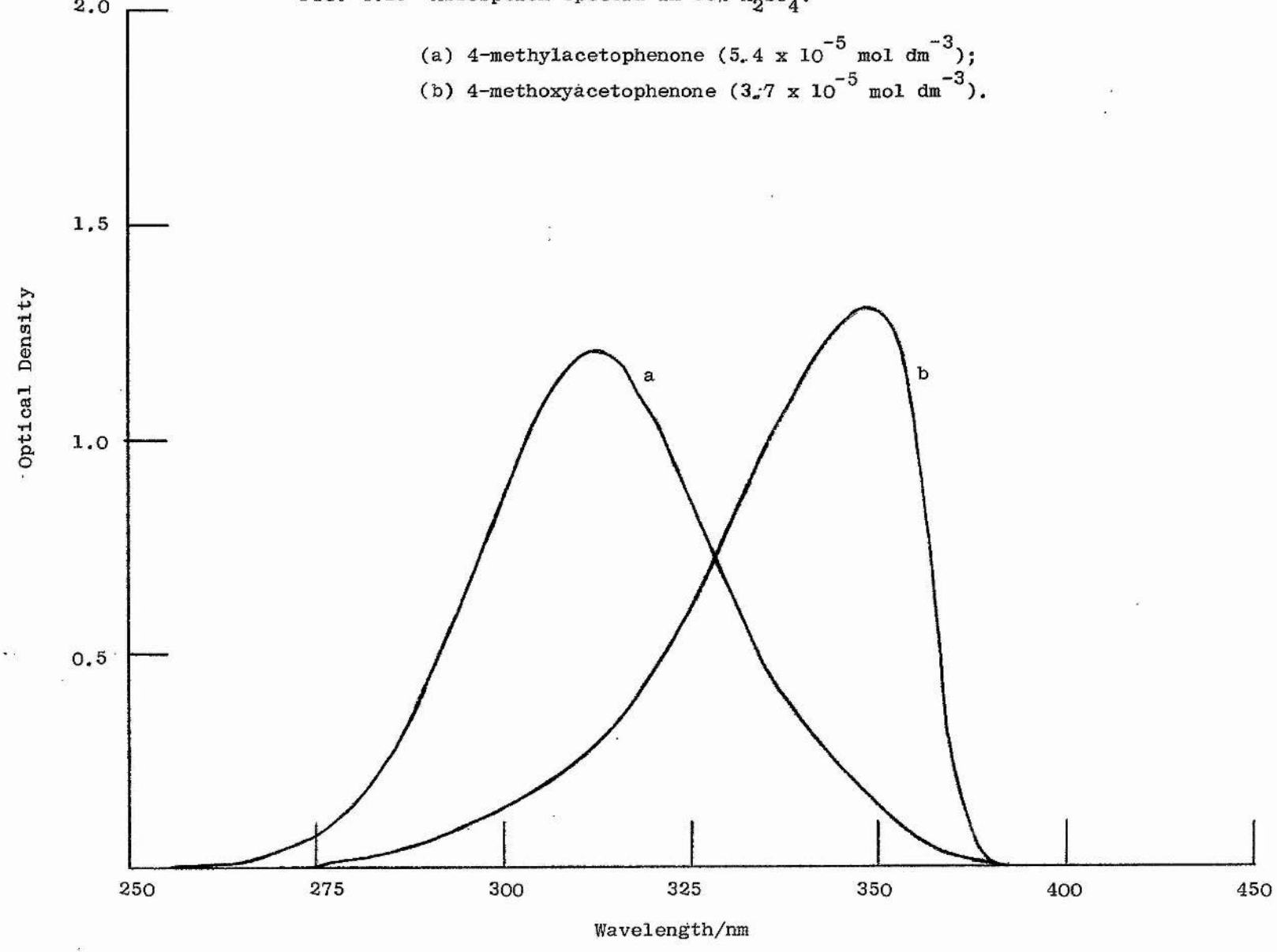

FIG. 4.19 shows the phosphorescence spectrum of acetophenone in ethanol which is typical of phosphorescence from an $n-\pi^*$ triplet having a short lifetime and showing the vibrational progression of the carbonyl group in its fine structure. The phosphorescence from the $\pi-\pi^*$ triplet state of 4-methoxyacetophenone in ethanol is shown in FIG. 4.20 and the fluorescence and phosphorescence spectra of this compound in 98% H_2SO_4 are shown in FIG. 4.21. In general the relative fluorescence quantum yields appeared greater than that for phosphorescence and the separation between the bands was larger than in the benzophenone derivatives. Thus in no case was the phosphorescence band entirely masked by the fluorescence in the total emission spectrum.

For protonation of the carbonyl group all the acetophenones studied show a similar pK order to xanthone and benzophenone i.e. $pK(T_1) > pK(S_1) > pK(S_o)$ (see Table 4.22). In the case of 4-aminoacetophenone protonation of the amino group shows a different pK order from the analogous reaction in the benzophenone series. In the S_1 state the amino group would appear in this case to become a slightly stronger base although the bascicity of this site in the T_1 state is much decreased as in 4-aminobenzophenone. This anomalous basicity of the first singlet state could perhaps be an artefact introduced by the difficulties in determination of the 0-0 energy. The unprotonated form of 4-aminoacetophenone has a broad charge-transfer band as its first absorption band the maximum of which is difficult to determine. Unlike the other B forms fluorescence is observed as well as phosphorescence at 77 K (see FIG. 4.22). The second protonation of this molecule, i.e. that of the carbonyl group, shows the expected pK changes upon excitation.

Weller and Urban[68] have reported a value of -1 for $pK(S_1)$ of acetophenone obtained by the fluorescence titration method and Weller et al[188] have separately reported a $\Delta pK(S_1-S_o)$ value of 9.0, obtained

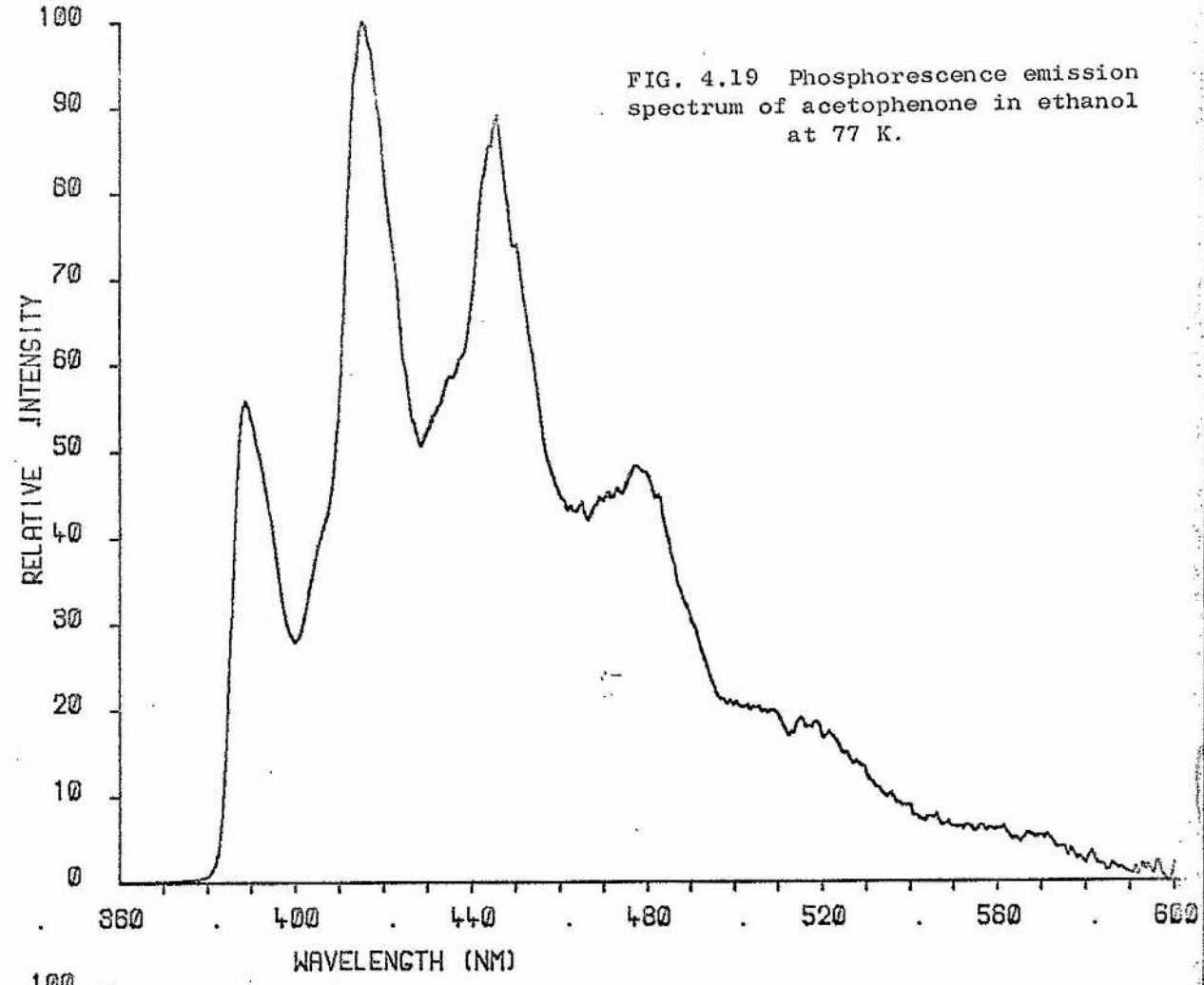

FIG. 4.19 Phosphorescence emission spectrum of acetophenone in ethanol at 77 K.

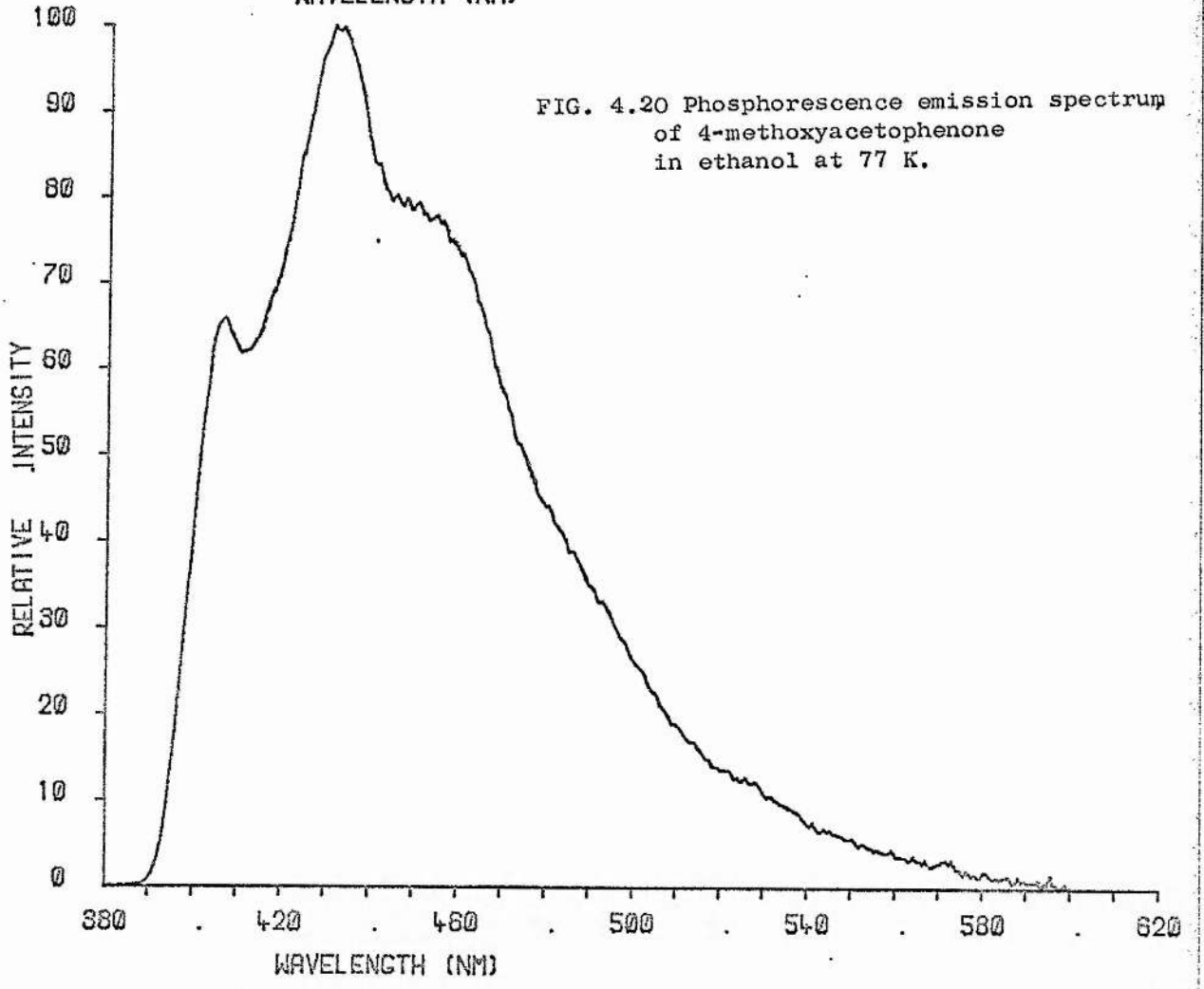

FIG. 4.20 Phosphorescence emission spectrum of 4-methoxyacetophenone in ethanol at 77 K.

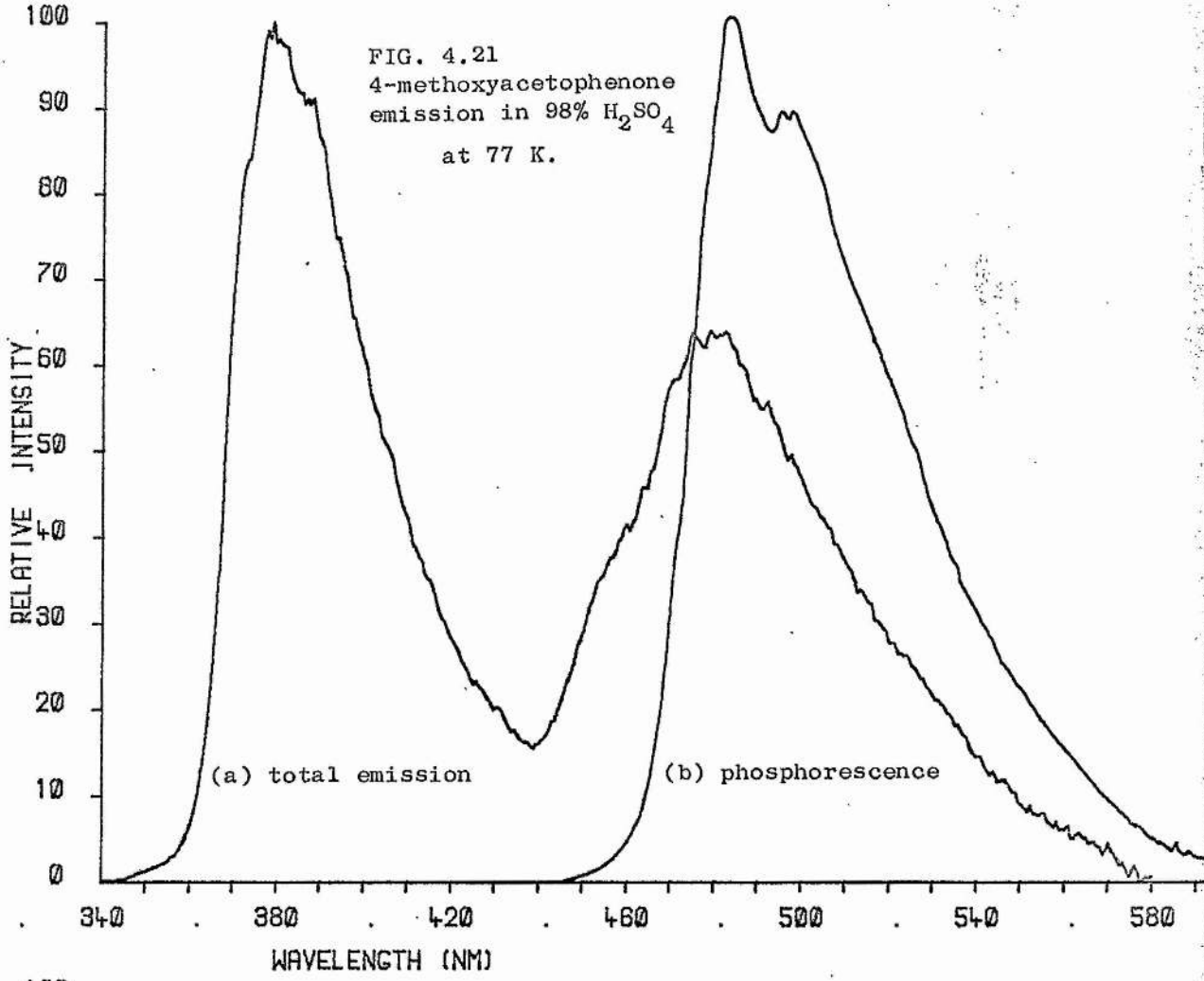

FIG. 4.21
4-methoxyacetophenone
emission in 98% H_2SO_4
at 77 K.

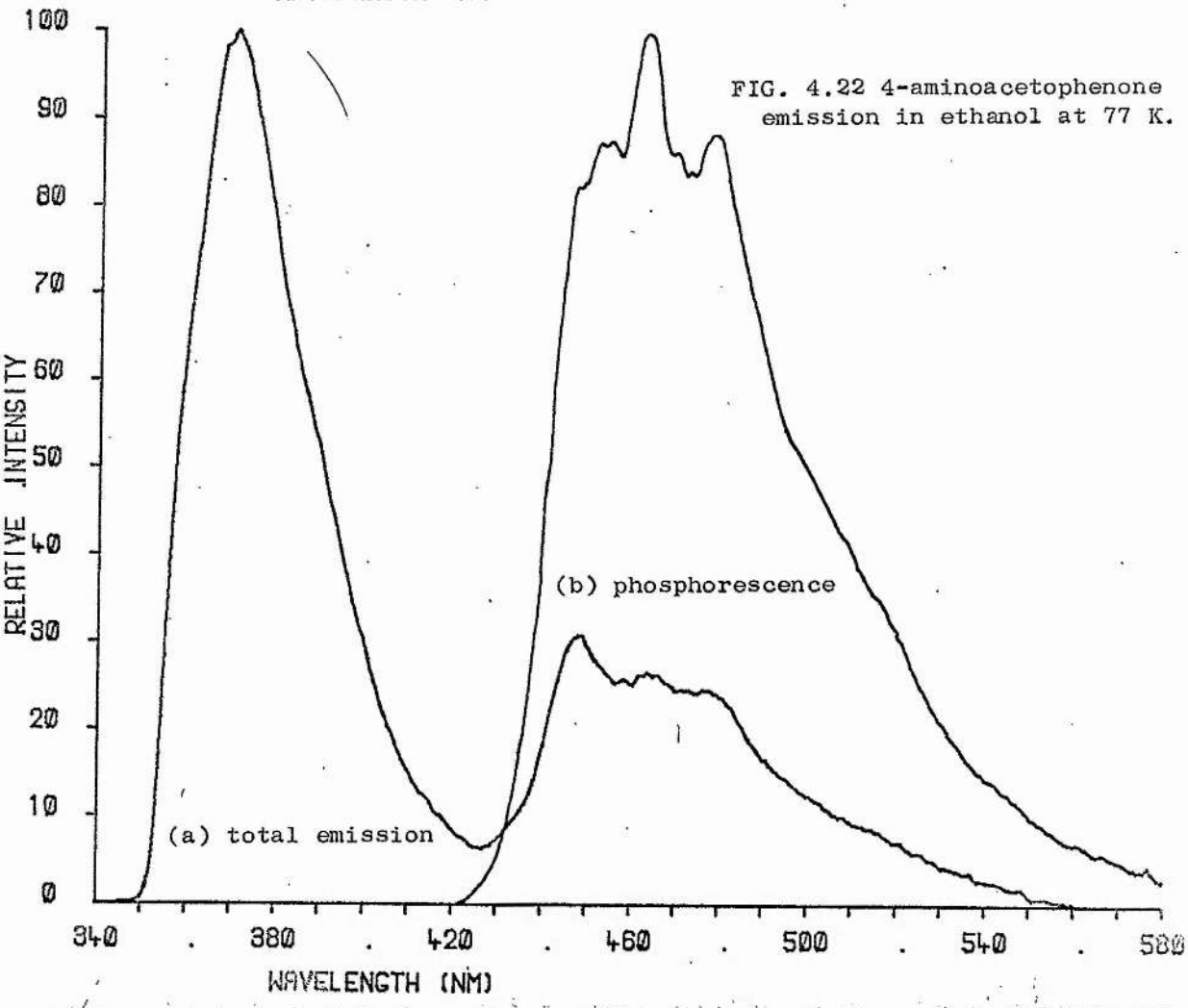

FIG. 4.22 4-aminoacetophenone
emission in ethanol at 77 K.

using the Förster Cycle, which leads to a $pK(S_1)$ value of +3. The value reported in this work is -2,5. The main difference in the calculated values probably comes from the fact that in Weller's case all the spectral data used in the calculations were obtained at room temperature while the value of -2,5 was obtained from spectral energies at 77 K. Temperature effects alone do not account for the difference in calculated values but the phosphorescence excitation spectrum at 77 K gives a direct determination of the 0-0 energy of the $n-\pi^*$ band of the B form, which will be to the long-wavelength side of any maximum obtained purely from the room temperature absorption spectrum and hence a smaller calculated $\Delta\ pK(S_1-S_o)$ will be obtained. It is arguable that the spectral energies obtained at low temperature for the singlet states are those which should be compared with the triplet state energies which must be obtained at low temperature.

(c) Emissions from Acetophenones in 98% H_2SO_4 at Room Temperature

The emissions observed from the acetophenones in 98% H_2SO_4 at room temperature were more intense than the corresponding emissions observed for the benzophenones but, as in the case of the benzophenones, because the derivatives had not been specially purified the possibility of interference from impurities must be noted. No emission was observed from the 4-nitro compound. In general the emission from the fluid solutions appeared, from a comparison with the low temperature spectra, to be mainly fluorescence. Although no phosphorescence bands were clearly visible in the total emission spectra at room temperature but were in the total emission spectra at 77 K, it is possible that the extension of the tail and overall red shift of the room temperature total emission spectra was due to underlying weak phosphorescence bands. FIG. 4.23 shows the phosphorescence and total emission at 77 K and the total emission at room temperature of

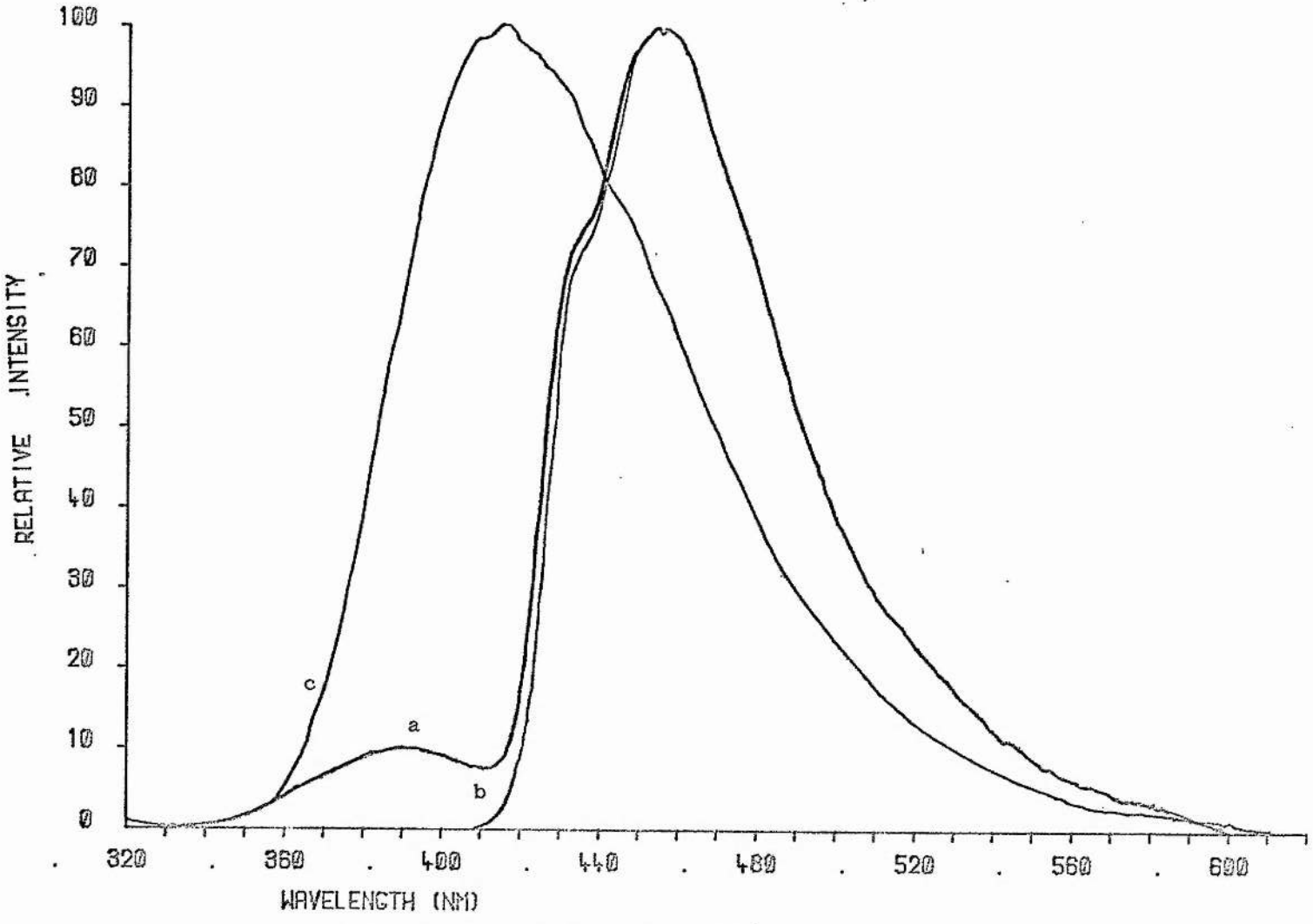

FIG. 4.23 4-fluoroacetophenone emission in 98% H_2SO_4:
(a) total emission 77 K; (b) phosphorescence at 77 K; (c) total emission at room temperature.

4-fluoroacetophenone in 98% H_2SO_4. Attempts to separate these emission bands into fluorescent and phosphorescent components failed and, as in the case of benzophenone, further experiments are necessary to clarify the nature of the solution emissions.

4. Anthraquinones

Anthraquinone, like acetophenone and benzophenones undergoes photoreduction in deoxygenated alcohols to give the corresponding hydroquinone[189]. The photoreactive state has been postulated to be the lowest triplet state which is $n-\pi^*$ in character[190] and the intersystem crossing quantum efficiency has been shown to be high[191].

Spectral data on the B and BH^+ forms of anthraquinone and anthraquinone-2-sulphonic acid were obtained as described before for the acetophenones and benzophenones (see Table 4.23). Both base forms had lowest singlet and triplet states of $n-\pi^*$ type and the BH^+ forms had intense $\pi-\pi^*$ bands as the long wavelength absorption bands. At 77 K anthraquinone in 98% H_2SO_4 showed a short-lived orange phosphorescence but no fluorescence and in fluid solution at room temperature an orange emission was also detected. Both these emissions were difficult to measure as they occur at a wavelength range where the R106 photomultiplier is insensitive (see Chapter 2.3(d)). The $\Delta\ pK(S_1-S_o)$ values were calculated from absorption maxima alone while for $\Delta\ pK(T_1-S_o)$ phosphorescence maxima were used. Using the $pK(S_o)$ value of -8.3[87] for anthraquinone the calculations give $pK(S_1) = -5.4$ and $pK(T_1) = 2.7$. For the sulphonic acid derivative the calculations indicate that the substitution (whether SO_3^- or HSO_3) has little effect on the pK changes observed in the excited states. A complication in the case of anthraquinone-2-sulphonic acid was its instability in 98% H_2SO_4 particularly under irradiation. (Anthraquinone itself was not stable compared with benzophenone).

TABLE 4.23 Spectral Data and Calculated Δ pK values for Anthraquinones.

SUBSTITUENTS POS.2	Absorption Maxima λ_{max}/nm		$\Delta\bar{\nu}$/cm^{-1} for S_1-S_o	Δ pK (S_1-S_o)	Phosphorescence Maxima λ_{max}/nm		$\Delta\bar{\nu}$/cm^{-1} for T_1-S_o	Δ pK (T_1-S_o)
	B	BH^+			B	BH^+		
H	390	414	1400	2.9	458	595	5000	10.0
SO_3H	400	420	1200	2.4	460	580	4500	9.0

A freshly prepared solution of the sulphonic acid in 98% H_2SO_4 showed no emission at room temperarure but a green emission gradually appeared in the area exposed to the radiation. The solution also changed colour from yellow to a brown-orange in the area exposed. A solution left standing on the bench appeared to show the same colour change but exhibited no emission. This would indicate different reactions and different products formed in the presence and absence of light. These properties were not further investigated.

The pK calculations indicate that the carbonyl protonation of anthraquinone has the xanthone pK order.

CHAPTER 5

DISCUSSION

(a) Förster Cycle Calculations

The primary assumption of the Förster Cycle (see Chapter 1 p. 24) is that the changes in entropy for the protonation reaction in the ground state and in the excited state are the same i.e. $\Delta S = \Delta S^*$. Other points raised in the discussion of the general applicability of and inherent errors in the Förster Cycle are based on practical difficulties of obtaining the energy values to be used in the calculation. A review of the general usefulness of the Förster Cycle was given by Jaffé[64] and several discussions have been reported since[50,59,75,76,192].

The assumption that ΔS is the same in the two electronic states has been shown to be a reasonable one since many $pK(S_1)$ values obtained from fluorescence intensities and from $\Delta\bar{\nu}$ measurements have differed by no more than the expected experimental errors of the fluorescence intensity measurements (see Table 1.1). On the other hand the $pK(S_1)$ values shown in Table 5.1 for carbonyl protonation show considerable differences between the two values, but it is not clear that this is due to a failure of the equal entropy assumption.

TABLE 5.1 $pK(S_1)$ values obtained from (a) fluorescence intensity measurements and (b) from Förster Cycle calculation for some aromatic carbonyl compounds.

Compound	$pK(S_o)$	$pK(S_1)$		b-a	REFERENCE
		a	b		
Acridone	-0.6	0.9	2.0	1.1	66,67
Acetophenone	-6.0	-1.0	3.0	4.0	68,188
1-Naphthaldehyde	-6.6	1.0	3.8	2.8	63
2-Naphthaldehyde	-7.1	1.0	3.6	2.6	63
Methyl 1-naphthyl ketone	-6.2	1.5	5.8	4.3	63
Methyl 2-naphthyl ketone	-6.2	1.5	5.3	3.8	63
Xanthone	-4.1	1.0	3.5	2.5	

The energy differences used in the Förster Cycle are the differences between the lowest vibrational level of the ground state and the lowest vibrational level of the excited state being considered. For many compounds it is difficult to pin-point the position of this, the 0-0 energy of the transition, since no vibrational structure is observed in their absorption or emission bands. This fact would therefore limit the use of the Förster Cycle to a very few compounds but is overcome by methods which give approximations to the 0-0 frequency. The more difficult it is to obtain a good value of the 0-0 frequency the more uncertain the pK^* value will be.

The $\Delta\bar{\nu}$ values used in Förster Cycle calculations are usually obtained in the following ways: taking the difference between (a) the absorption maxima (b) the fluorescence maxima and (c) the average of the absorption and fluorescence maxima for the two species involved in the reaction. Method (a) supposes that the probability distribution of transitions from S_o to vibronically excited states is similar for both species. Also the absorption spectra give the energy of the excited state before the equilibrium orientation of the solvent cage has been established and if these solvent effects are not identical for B and BH^+ they will not cancel out in a calculation of $\Delta\bar{\nu}$ and will lead to an error in Δ pK. Since the B and BH^+ forms are electronically quite different there is no reason to believe that the solvent effects will be identical. Method (b) is also subject to these errors but in this case it is the vibrational distribution and solvent reorientation of the ground state molecules that must be considered. Schulman et al[75] have suggested that, since the ground state thermodynamic reaction parameters are defined with respect to the ground state molecules in the ground state equilibrium solvent cage configuration, it would be most meaningful to define excited state thermodynamic parameters with respect to the excited species in their excited-state equilibrium

solvent cage configuration. In this scheme it was proposed that the best Förster Cycle calculated pK^* value would be obtained using fluorescence spectra alone. In fact, in some cases this was found to give a pK^* value similar to that obtained by fluorescence titration but in others much better calculated pK^* values were obtained using methods (a) and (c). It has been argued that only the average of the absorption and fluorescence provides a "best value" of the energy gap between the ground and excited state. In any case, there would appear to be no one valid approach to the Förster Cycle and the validity of employing absorption spectra alone, fluorescence spectra alone, or an average of the absorption and fluorescence maxima depends upon the relative importance of vibronic and solvent effects in the electronic spectra of the base and its conjugate acid. The pK^* values derived using (a), (b), or (c) in a particular case can differ significantly and the "best" method must be chosen on the experimental evidence for that case. With benzophenones the 0-0 frequency of the B form could be determined directly from the structured phosphorescence excitation spectrum while for BH^+ the method of averaging the fluorescence and phosphorescence maxima was used.

Another consideration mentioned by Jaffé was the effect of the nature of the electronic transition of the two species which according to Jaffé, must be of the same type for the Förster Cycle to be applicable. He suggested that if the absorption bands of the acid and base pair correspond to excitation to states of different electronic configuration, the proton transfer is necessarily accompanied by an electronic transition. The low probability of this phenomenon and the modification of the solvent shell likely to accompany the change of electronic state may, according to Jaffé, be expressed in terms of a large entropy effect. Since the electronic transitions of most substituted aromatic molecules do not correspond to a well-defined classification, but are

a combination of many transitions mixed through configuration interaction, the strict application of the above rule leads to the conclusion that the Förster Cycle can only be strictly applied in very few cases.

This factor may be important in the consideration of the calculations on carbonyl protonation since the base form generally has a $n-\pi^*$ transition while that of BH^+ is of $\pi-\pi^*$ character. Table 5.1 shows that there is always a difference of more than one pK unit between the Förster Cycle calculated and the directly measured $pK(S_1)$ for carbonyl protonation. Before considering the possible breakdown of the equal entropy assumption, another effect important to a consideration of carbonyl compounds must be discussed. There is always the possibility that for weak bases the $pK(S_o)$ value used is not based on the correct acidity function and, even if the acidity function is applicable to the ground state molecule, it may still be incorrect for the excited species. Contradictory evidence has been reported as to the acidity function followed by carbonyl protonation. Thus Greig and Johnson[193] reported that aromatic carbonyl group protonations do not follow the amide acidity function H_A; conversely Zalewski and Dunn[194] have concluded that the protonation behaviour of aromatic carbonyl compounds does follow H_A. The $pK(S_o)$ values given in Table 5.1 are based on the H_o' scale and conversion to the H_B or H_A scale would give more positive $pK(S_o)$ values thus increasing the $pK(S_1)$ discrepancy, while the $pK(S_o)$ values derived by Grieg and Johnson are generally more negative thus decreasing the $pK(S_1)$ differences.

In the xanthone case, for example, the difference between the Förster Cycle calculated $pK(S_1)(F)$ and the directly derermined value $pK(S_1)(D)$ of 2.5 units has three possible sources; it may be due to (a) unreliable estimates of the O-O energies, (b) basing the pK values on the wrong acidity function or (c) the invalidity of the equal entropy asumption of the Förster Cycle in this case. Without experimentally determining an acidity function for xanthone it is not

possible to estimate accurately the effect of (b). Since both H_B and H_A acidity scales (see FIG. 1.7) would give more positive $pK(S_o)$ ($pK(S_o)$ = -4.1 of xanthone is based on the H_o' scale) and thus increase the pK discrepancy, it seems unlikely at first sight that acidity function effects will explain the differences.

Assuming that $pK(S_o)$ = -4.1 holds for xanthone then we have calculated $pK(S_1)$ values using two independent sets of results. Through a normal Förster Cycle calculation using the spectroscopically determined energy levels $pK(S_1)(F)$ has been found to have a value of 3.6. The fact that a slightly better estimate is obtained in the xanthone case using the fluorescence maxima alone (see Table 3.6) may be due to the fact that the fluorescence spectra of both B and BH^+ forms were obtained in aqueous solutions of low acidity where the medium effects will not be large. In a similar Förster Cycle type calculation, but this time using the experimentally determined ΔH^o and ΔH^{o*} values, a $pK(S_1)(H)$ of -0.2 $\pm$ 0.5 is obtained (see Chapter 3.1(c)). This is a better estimate of the actual $pK(S_1)$ than that obtained from the spectral data and the negative deviation is more easily explicable in terms of an acidity function effect. Both $pK(S_1)(F)$ and $pK(S_1)(H)$ are calculated assuming equal entropy changes for the reaction in the ground and the excited state, but now using $pK(S_o)$ = -4.2, $pK(S_1)$ = 1.0, ΔH^o = 0 $\pm$ 2 kJ mol^{-1} and ΔH^{o*} = 21 $\pm$ 2 kJ mol^{-1} we can test for consitency by calculating values of ΔS and ΔS^* since

$$\Delta G^o = 2.303RT\ pK$$

$$\text{and}\ \Delta S^o = \frac{\Delta H^o - \Delta G^o}{T}$$

The calculations give ΔS^o = 78 J mol^{-1} K^{-1} and ΔS^{o*} = 55 J mol^{-1} K^{-1}. This calculated inequality of the reaction entropies will correspond to a pK error of 1.2 units in a Förster Cycle calculation. This deviation from equal entropies would tend to increase

the $pK(S_1)(F) - pK(S_1)(D)$ difference. In any case it would appear that neither acidity function effects nor the breakdown of the equal entropy assumption can explain the deviation of the $pK(S_1)(F)$, i.e. that calculated from spectral data, from the directly determined value. It seems likely that incorrect approximation of the 0-0 bands will be responsible for a substantial part of the deviation since an error of 1 nm at 350 nm corresponds to an error of 0.2 units in pK. From the above consideration it appears that even in cases where the electronic transition of B and BH^+ are of different type the Förster Cycle can be applied and the error in assuming $\Delta S = \Delta S^*$ will be no larger than that due to difficulties in the estimation of the 0-0 bands in these cases. In the case of xanthone it has been shown that the combined error from the equal entropy assumption and acidity function effects is of the order of 1.2 pK units.

(b) pK^* values of aromatic carbonyl compounds

The excited state pK values in Table 5.2 are a selection of those for which the Förster Cycle should give "good" values (i.e. the 0-0 transition energy could be determined reasonably accurately for the S_o-S_1 and S_o-T_1 transitions of the B and BH^+ forms). These results show that for the carbonyl compounds studied the usual order of pK values is $pK(T_1) > pK(S_1) > pK(S_o)$. This contradicts the commonly held view that all triplet state pK's are not very different from those of the ground state[146,195].

In the case of xanthone, since both the B and BH^+ forms fluoresce and give well-defined triplet-triplet absorption spectra, it was possible to verify the pK order by direct determination of the $[B]/[BH^+]$ ratios involved. Although the numbers obtained for $pK(T_1)$ and $pK(S_1)$ by this method are 2 to 3 units less than those obtained by the Förster Cycle, both methods give the same pK order and since the calculated $\Delta pK(T_1-S_1)$ of 3 was directly determined to have a value of 2, we can be

reasonably sure that the other systems, in which similar basic assumptions are made, will have an actual pK order which closely resembles the calculated pK order.

TABLE 5.2 pK^* values, based on Förster Cycle Calculation, for some aromatic carbonyl compounds.

Compound	$pK(S_o)$	$pK(S_1)$	$pK(T_1)$	$\Delta pK\ (T_1-S_1)$
Xanthone	-4.1	3.6	6.6	3.0
Benzophenone	-5.7	-3.6	-0.4	3.2
4,4'-Dichlorobenzophenone	-6.5	-2.9	2.1	5.0
4,4'-Dimethoxybenzophenone	-4.4	4.2	5.5	1.3
4-hydroxybenzophenone	-5.0	0	1.5	1.5
4-phenylbenzophenone	-5.0*	2.6	0.3	-2.3
4-NH_3^+-benzophenone	-6.0*	-4.3	-0.3	4.6
Acetophenone	-6.1	-2.5	0.9	3.4
4-methoxyacetophenone	-4.8	-1.3	3.4	4.7
4-hydroxyacetophenone	-4.7	-1.9	2.0	3.9

* These values are assumed for $pK(S_o)$ for the purpose of inclusion in this table.

The experimental evidence for xanthone indicates that the position of protonation in the S_o, S_1, and T_1 states is the carbonyl group. The calculated charge densities for xanthone showed the carbonyl to be electron deficient in the excited state as expected for an $n-\pi^*$ transition but it is also well known that the carbonyl group is a stronger base in the excited state. This must be due to the increased stability of the BH^+ form. The $n-\pi^*$ transition if present in the BH^+ form would be at much higher energy than it is in the B form and calculations using these energies would indicate that the molecule would become a weaker base in the excited state thus following the changes in charge density. Because of the high rate of internal conversion to S_1 and T_1 we need only consider the protonation of these

states and they have been experimentally shown to be stronger bases.

The pK^* behaviour of these compounds can now be interpreted in terms of the characteristics of the types of transition involved in the neutral and protonated molecules. In the unprotonated form benzophenone, for example, has a weak first absorption band of $n-\pi^*$ type, the first singlet of $\pi-\pi^*$ type being of higher energy. Since the S_1-T_1 splitting is small for $n-\pi^*$ states[11], T_1 for the unprotonated base does not lie far below S_1. The protonated molecule, however, has a first absorption band at longer wavelengths than that of B and of the intense $\pi-\pi^*$ type, with the important consequence that the S_1-T_1 splitting is greater than that for the $n-\pi^*$ transition of the base. The lower energy of the S_o-S_1 transition for BH^+ than B means that B becomes a stronger base upon excitation to S_1[59], and the greater S_1-T_1 splitting means that B becomes an even stronger base in the T_1 state: hence the observed order $pK(T_1)>pK(S_1)>pK(S_o)$. FIG. 5.1 shows a schematic representation of the relative energies of B and BH^+ for benzophenone in the S_o, S_1 and T_1 states.

It is in accord with the above interpretation that ring substitution in benzophenone can alter the pK order (see Table 4.5) since substituents affect the $n-\pi^*$ and $\pi-\pi^*$ transition energies and hence can alter the position and type of the excited states involved and the relative splittings in the B and BH^+ forms.

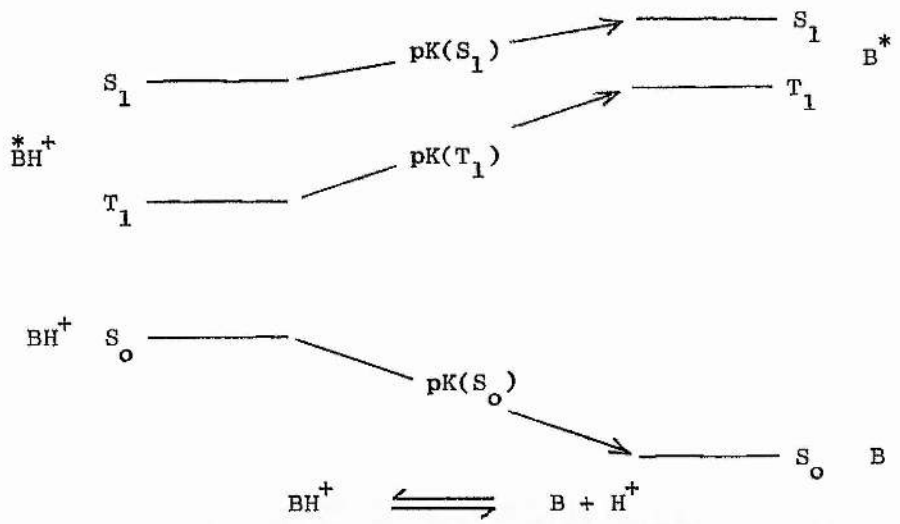

FIG. 5.1 Schematic representation of the relative energies of B and BH^+ for benzophenone in the S_o, S_1 and T_1 states.

Substitution of a phenyl group in the para position of the benzophenone molecule has, as shown in Chapter 4, little effect on the $n-\pi^*$ transition but has a marked effect on the $\pi-\pi^*$ transition. Thus, although phenyl substitution results in insufficient shift to invert the singlet $n-\pi^*$ and $\pi-\pi^*$ levels, the greater S_1-T_1 splitting of the $\pi-\pi^*$ system results in the lowest triplet of the base form being of $\pi-\pi^*$ character. The S_1-T_1 splitting of the $\pi-\pi^*$ level of the B form of 4-phenylbenzophenone is in fact found to be larger than the S_1-T_1 splitting of the BH^+ form (see TABLE 5.3) and therefore the Förster Cycle pK's have the order $pK(S_1) > pK(T_1) > pK(S_o)$.

Xanthone, like 4-phenylbenzophenone, also has the $n-\pi^*$ and $\pi-\pi^*$ first excited singlet states very close together and at first sight might therefore be expected to show the pK order of 4-phenylbenzophenone rather than that of benzophenone itself. But, although the first excited triplet state of xanthone is of $\pi-\pi^*$ character in polar solvents, in non-polar solvents it is of $n-\pi^*$ character unlike 4-phenylbenzophenone, showing that in the xanthone case the $n-\pi^*$ and $\pi-\pi^*$ triplet levels lie closer together because of the smaller $\pi-\pi^*$ S_1-T_1 splitting. Xanthone is, in fact, more related to the methoxy and hydroxybenzophenones which also have close lying singlet $n-\pi^*$ and $\pi-\pi^*$ levels, but in their case the triplet $n-\pi^*$ and $\pi-\pi^*$ levels do not lie close enough for inversion by polar solvents, the $n-\pi^*$ always being the lowest triplet state. Two possible reasons for the difference in magnitude of the $\pi-\pi^*$ splitting in 4-phenylbenzophenone and xanthone can be given. Either the extension of the π orbital system by the phenyl group in this case increases the splitting of the $\pi-\pi^*$ states, or in the case of xanthone and the hydroxy and methoxybenzophenones the first $\pi-\pi^*$ band has more charge transfer character and therefore a singlet-triplet splitting smaller than that expected from a $\pi-\pi^*$ transition. In Chapter 3.1(b) it was noted that

the relatively large solvent shift of the first π-π^* band of xanthone on changing from non-polar to polar solvents was an indication of charge transfer character.

Apart from the 4-phenyl case which has a different pK order, the benzophenone results indicate that an electron-withdrawing group, e.g. Cl or NH_3^+, increases the basicity of the triplet to a greater extent than that of the singlet, thus increasing the $pK(S_1)$-$pK(T_1)$ separation. With electron-donating groups there is a decrease in $\Delta\, pK(S_1\text{-}T_1)$ although the bascity of both states is increased. This may be an indication that the substituent groups have more effect on the singlet than on the triplet state: the electron-donating groups stabilise the singlet BH^+ form more than the triplet while electron-withdrawing groups have a similar but opposite effect.

All the above cases of carbonyl protonation, except for 4-phenylbenzophenone, show the pK order $pK(T_1) > pK(S_1) > pK(S_o)$, but as shown in Chapter 4 the precise order depends very much on the particular case involved. For example, in the case of 5-nitro-2-hydroxybenzophenone, we find the calculations indicate an increase in basic strength in the first singlet state but that the first triplet state, nevertheless, becomes a weaker base giving the order $pK(S_1) > pK(S_o) > pK(T_1)$. No general system of inequalities can be given for the three pK values: the case of each compound must be separately considered.

Table 5.3 shows the singlet-triplet splitting energies of the B and BH^+ forms of some of the compounds whose pK values have been calculated. The B forms all show the relatively small splitting expected for an n-π^* transition (i.e. ≈ 3000 cm^{-1}), except for the 4-phenylbenzophenone case which has a large S_1-T_1 splitting as explained. The splitting calculated for the xanthone (B) case is another indication of the charge transfer character of its first π-π^* band.

TABLE 5.3 Singlet-Triplet Splitting energies of the B and BH^+ forms of some aromatic carbonyls.

Compound	S_1-T_1 Splitting Energy/cm^{-1} B	BH^+
Xanthone	3100	4500
Benzophenone	2800	4300
4,4'-Dichlorobenzophenone	2900	5300
4,4'-Dimethoxybenzophenone	3100	3800
4-hydroxybenzophenone	3600	4700
4-phenylbenzophenone	5500	4900
4-NH_3^+ benzophenone	3000	5000
Acetophenone	2500	4300

The BH^+ forms all show very similar S_1-T_1 splitting which is much smaller than that expected from a $\pi-\pi^*$ system of this size (i.e. $\approx$ 10,000 cm^{-1}). This may be a similar effect to that observed in dye molecules where extensive delocalisation of the π system results in a relatively small S_1-T_1 split. For example the fluorescein cation has an S_1-T_1 split of 4000 cm^{-1}.[10] The singlet triplet splitting found for these BH^+ forms is also very similar to that observed for charge transfer states. The S_1-T_1 splittings found here for the CT states of $NH_2-\emptyset_2$ CO and $^-O-\emptyset_2CO$ were 5000 cm^{-1} and 4500 cm^{-1} respectively (see Table 4.10 and Table 4.12). It is not possible in the case of the BH^+ forms to use solvent shifts to indicate charge transfer characteristics as the species are only formed in strong acid media. A further indication of some charge transfer on excitation to the triplet is the increase in the calculated (see Chapter 3.1(g)) dipole moments of the BH^+ form of xanthone in the ground and triplet state which were 4.18 D and 8.23 D respectively.

Another similarity the BH^+ forms have to molecules with lowest CT states is their emission. O'Connell[196] has reported the

fluorescence of alcoholic solutions of 4-aminobenzophenone at 77 K and details of that emission and a similar fluorescence from the phenolate form of 4-hydroxybenzophenone are given in Chapter (4.2(b). Both these molecules have singlet and triplet states of charge-transfer character and show fluorescence and phosphorescence at 77 K while benzophenones with lowest $n-\pi^*$ singlet states show only phosphorescence. The BH^+ forms show very similar fluorescence and phosphorescence characteristics at 77 K to those of the benzophenones with lowest CT states. Some charge transfer character is to be expected since the positive charge of the BH^+ forms will be delocalised through the benzene rings, as illustrated by some simple resonance forms:

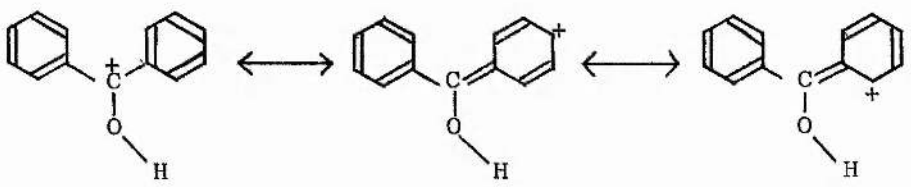

Although the S_1-T_1 splitting of the BH^+ forms is relatively small it is in most cases larger than the S_1-T_1 splitting of the $n-\pi^*$ level of the B form and hence in most cases the pK order $pK(T_1) > pK(S_1) > pK(S_o)$ is obtained. The cases reported in which the opposite pK order is found can be explained in a similar fashion to that given above. FIG. 5.2 shows a diagrammatic representation of the energy levels of the singlet and triplet forms involved in the successive protonations of $4-^{-}O-\emptyset_2CO$. (A similar diagram can be drawn for $NH_2-\emptyset_2CO$; the experimental data for the energy levels and the calculated pK's in both cases can be found in Tables 4.4 and 4.6).

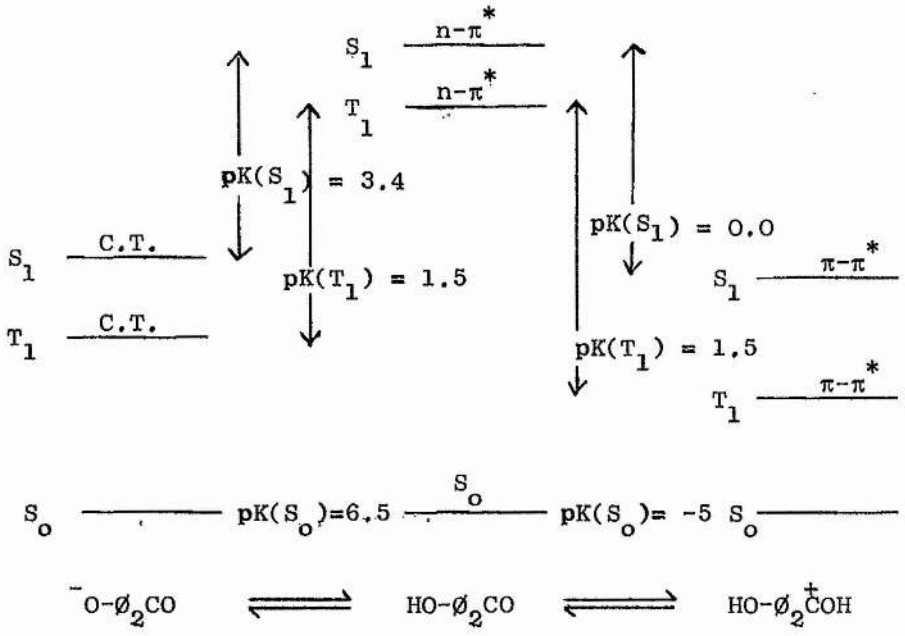

FIG. 5.2 Schematic representation of the relative energies of 4-hydroxybenzophenone and its prototropic forms in the S_1 and T_1 states.

In these cases the B forms have S_o-S_1 transitions at lower energy than the BH^+ forms (e.g. the protonated amino form) and therefore B becomes a weaker base in the excited state and, since the B forms have singlet states of CT type while those of BH^+ are n-π^*, the S_1-T_1 splitting of B will be greater than that for BH^+, thus making B an even weaker base in the triplet state. The second protonation in these cases is that of the carbonyl group and has similar behaviour to the carbonyl protonation already discussed. Thus in the case of 4-aminobenzophenone the CT singlet state is replaced on protonation of the amino group by an n-π^* state of higher energy and a smaller S_1-T_1 split thus giving the pK order $pK(S_o) > pK(S_1) > pK(T_1)$. The second protonation gives a π-π^* state of lower energy than the n-π^* state and larger S_1-T_1 splitting and therefore for this reaction the pK order is $pK(T_1) > pK(S_1) > pK(S_o)$.

If we consider some of the pK values in Table 1.2 we can use

the Förster Cycle to obtain information about the S_1-T_1 splitting of the lowest states of the species involved. In the case of 2-naphthylamine, protonation of the amino group results in an S_1 transition of higher energy, indicating that the molecule is a weaker base in the S_1 state. In the T_1 state the basic strength has been found to be very similar to that of the ground state. Therefore by Förster Cycle considerations the S_o-T_1 energy difference must be similar for the two forms and the S_1-T_1 splittings must have the relative magnitudes shown in FIG. 5.3.

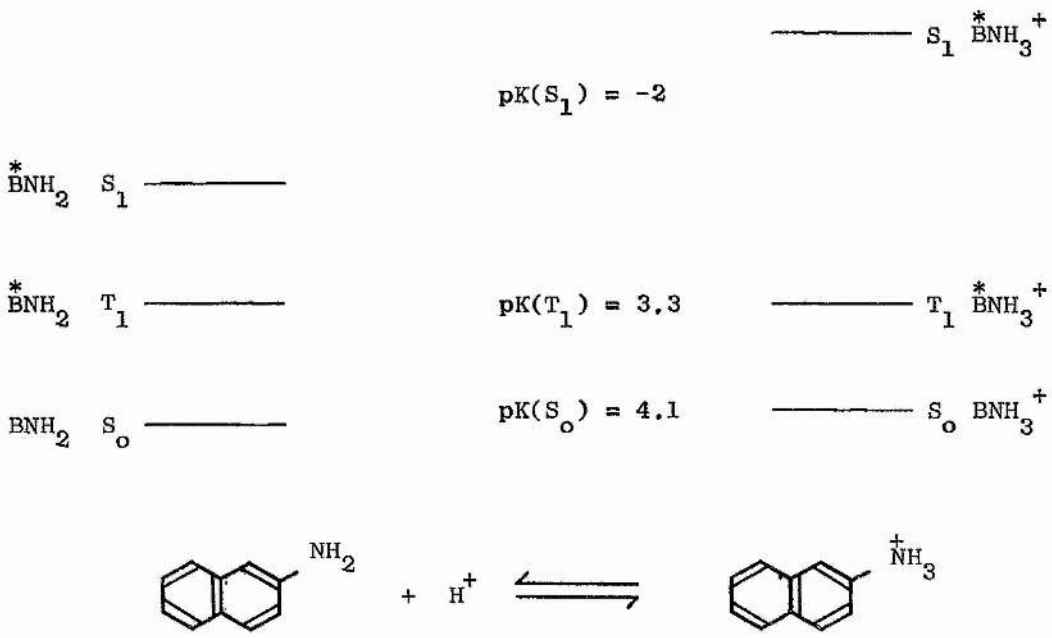

FIG. 5.3 Schematic representation of the energy levels of 2-napthylamine B and BH^+ forms in the singlet and triplet states.

Although it has been suggested that the long wavelength band of 2-naphthylamine is an n-π^* transition[197] other evidence[50] has tended to suggest that the long wavelength band of the neutral species is a π-π^* band. The S_1-T_1 splitting of the base form must be less than that of the BH^+ form, which would be the case if the respective

transitions were of $n-\pi^*$ and $\pi-\pi^*$ type. On the other hand the protonated amino group may be considered as a weak substituent through inductive effects whereas the unprotonated form has strong electron donating power and has been shown to increase the charge transfer character of a transition. These effects were noted in the benzophenones with NH_2 and NH_3^+ substituted. The order of pK's could therefore be accounted for by the small S_1-T_1 split of the charge transfer transition of the B form whereas the BH^+ has the large S_1-T_1 split of the parent naphthalene system. An identical argument can be put forward for the pK's of the 2-naphthol dissociation i.e. $pK(S_o) = 9.5$, $pK(S_1) = 3.0$ and $pK(T_1) = 7.7$.

APPENDIX I

Sources of compounds studied

The following compounds were obtained commercially and where indicated (*) recrystallised from the recommended solvents[112].

Xanthone* Benzophenone* Acetophenone 4-bromoacetophenone Anthraquinone* Anthraquinone-2-sulphonic acid sodium salt Quinine sulphate* Solochrome dark blue (PBBR)	British Drug Houses Ltd., Poole, England.
4,4'-dimethoxybenzophenone 4-hydroxybenzophenone 4-phenylbenzophenone 4-aminobenzophenone 4-nitrobenzophenone 2-hydroxybenzophenone 4-methylacetophenone 4-methoxyacetophenone	R.N. Emanuel Ltd., Wembley, England.
4-hydroxyacetophenone 4-aminoacetophenone 4-nitroacetophenone 4-fluoroacetophenone 2-aminopyridine*	Koch-Light Laboratories Ltd., Colnbrook, England.
3-aminophthalimide* N,N-dimethyl-m-nitroaniline* 4-dimethylamino-4'-nitrostilbene*	Eastman Kodak Co., Rochester, N.Y., U.S.A.
2,2',4,4-tetrahydroxybenzophenone 4-chloroacetophenone	Aldrich Chemical Co. Inc., Milwaukee, Wis., U.S.A.
4,4'-dichlorobenzophenone	NIPA Fine Chemicals and Organic Intermediates, Treforest Industrial Estate, South Wales.

4-hydroxyxanthone was obtained from Dr. J.R. Lewis, Department of Chemistry, University of Aberdeen.

3,6-dihydroxyxanthone was prepared from 2,2',4,4'-tetrahydroxybenzophenone by the method of Habacher and Doemberg[198].

2-hydroxy-5-nitrobenzophenone was prepared by nitrating 2-hydroxybenzophenone following the method of Hardlovic et al[180].

APPENDIX II

Program CALIB

```
                PROGRAM CALIB

C       PROGRAM TO EVALUATE THE CORRECTION CURVE FOR THE
C     SPECTROFLUORIMETER - OVER THE RANGE 300 - 750 NM.
C
C
C     THE STANDARDS ARE
C       (A)       2-AMINOPYRIDINE                 300-450 NM.
C       (B)       QUININE SULPHATE                400-540 NM.
C       (C)       3-AMINOPHTHALIMIDE              450-610 NM.
C       (D)       4-NITRODIMETHYLANILINE          470-650 NM.
C       (E)       ALUMINIUM PBBR CHELATE          580-700 NM.
C       (F)       4-DIMETHYLAMINO-4'-NITROSTILBENE   600-750 NM.
C         DATA   CARDS
C     CARDS 1-3   ABSOLUTE  SPECTRUM  OF  (A)
C     CARDS 4-6   ABSOLUTE  SPECTRUM  OF  (B)
C     CARDS 7-9   ABSOLUTE  SPECTRUM  OF  (C)
C     CARDS 10-12 ABSOLUTE  SPECTRUM  OF  (D)
C     CARDS 13-15 ABSOLUTE  SPECTRUM  OF  (E)
C     CARDS 16-18 ABSOLUTE  SPECTRUM  OF  (F)
C     CARD  19    NUMBER  OF  CORRECTION  CURVES
C     CARDS  20-21   TITLE  CARDS
C     CARD   22   EXCITATION  AND  EMISSION  SLIT  WIDTHS   (2F5.0)
C     CARDS  23-25   EXPTAL  SPECTRUM  OF  (A)
C     CARDS  26-28   EXPTAL  SPECTRUM  OF  (B)
C     CARDS  29-31   EXPTAL  SPECTRUM  OF  (C)
C     CARDS  32-34   EXPTAL  SPECTRUM  OF  (D)
C     CARDS  35-37   EXPTAL  SPECTRUM  OF  (E)
C     CARDS  38-40   EXPTAL  SPECTRUM  OF  (F)
C     CARDS  20-40   REPEATED  FOR  ANY  SUBSEQUENT  RUNS
C
C
C
      DIMENSION  AB1(100),AB2(100),AB3(100),AB4(100),AB5(100),AB6(100),
     1EX1(100),EX2(100),EX3(100),EX4(100),EX5(100),EX6(100),COR1(100),
     2COR2(100),COR3(100),COR4(100),COR5(100),COR6(100),IAVEL(100),
     3TITT(40),  RM1(100),  RM2(100),  RM3(100),  RM4(100),  RM5(100),
     4  RM6(100),  RM(100),FACTOR(100) ,RECIP(100)
C
C
      READ(5,10)(AB1(J),J=1,46)
      READ(5,10)(AB2(J),J=1,46)
      READ(5,10)(AB3(J),J=1,46)
      READ(5,10)(AB4(J),J=1,46)
      READ(5,10)(AB5(J),J=1,46)
      READ(5,10)(AB6(J),J=1,46)
   10 FORMAT(16F5.0)
C
C             ABSOLUTE SPECTRA READ.
C
      READ(5,20)NRUN
   20 FORMAT(I2)
C
C             NUMBER OF RUNS READ.
C
      DO 440 IL=1,NRUN
      READ(5,30)TITT
   30 FORMAT(20A4)
C
C             TITLE READ.
C
      READ(5,40)X,M
   40 FORMAT(2F5.0)
C
C             EXCITATION AND EMISSION SLITWIDTHS READ.
C
      READ(5,50)(EX1(J),J=1,46)
      READ(5,50)(EX2(J),J=1,46)
      READ(5,50)(EX3(J),J=1,46)
      READ(5,50)(EX4(J),J=1,46)
      READ(5,50)(EX5(J),J=1,46)
      READ(5,50)(EX6(J),J=1,46)
   50 FORMAT(16F5.0)
C
C             EXPTAL. SPECTRA READ.
C
      DO  60  J=1,16
   60 COR1(J)=EX1(J)/AB1(J)
      DO  70  J=17,46
   70 COR1(J)=0.0
      DO 80 J=1,10
   80 COR2(J)=0.0
      DO  90  J=11,26
   90 COR2(J)=EX2(J)/AB2(J)
      DO  100  J=27,46
  100 COR2(J)=0.0
C
      DO 110 J=1,15
  110 COR3(J)=0.0
      DO120  J=16,34
  120 COR3(J)=EX3(J)/AB3(J)
      DO  130  J=35,46
  130 COR3(J)=0.0
C
      DO 140 J=1,17
  140 COR4(J)=0.0
      DO 150 J=18,36
  150 COR4(J)=EX4(J)/AB4(J)
      DO 160 J=37,46
  160 COR4(J)=0.0
C
      DO 170 J=1,28
  170 COR5(J)=0.0
      DO 180 J=29,40
  180 COR5(J)=EX5(J)/AB5(J)
      DO 190 J=41,46
  190 COR5(J)=0.0
      DO 200 J=1,30
  200 COR6(J)=0.0
      DO 205 J=31,46
  205 COR6(J)=EX6(J)/AB6(J)
C
C             CORRECTION FACTORS HAVE BEEN CALCULATED.
C
      DO 210 J=1,46
  210   RM1(J)=COR1(J)
C
      F1=COR1(12)/COR2(12)
      DO 220 J=1,46
  220   RM2(J)=F1*COR2(J)
C
C             NORMALISATION BETWEEN A AND B AT 410 NM.
C
      F2=  RM2(19)/COR3(19)
      DO 230 J=1,46
  230   RM3(J)=F2*COR3(J)
C
C             B AND C AT 480 NM.
C
      F3=  RM3(24)/COR4(24)
      DO 240 J=1,46
  240   RM4(J)=F3*COR4(J)
C
C             C AND D AT 530 NM.
C
      F4=  RM4(29)/COR5(29)
      DO 250 J=1,46
  250   RM5(J)=F4*COR5(J)
C
C             D AND E AT 580NM.
C
      F5=  RM5(33)/COR6(33)
      DO 260 J=1,46
  260   RM6(J)=F5*COR6(J)
C
C             E AND F AT 620NM.
C
      DO 270 J=1,10
  270   RM(J)=  RM1(J)
      DO 271 J=11,13
  271   RM(J)=(  RM1(J)+  RM2(J))/2.0
      DO 272 J=14,15
  272 RM(J)=RM2(J)
      DO 273 J=16,17
  273 RM(J)=(RM2(J)+RM3(J))/2.0
      DO 274 J=18,24
  274 RM(J)=(RM2(J)+RM3(J)+RM4(J))/3.0
      DO 275 J=25,28
  275 RM(J)=(RM3(J)+RM4(J))/2.0
      DO 276 J=29,30
  276 RM(J)=(RM4(J)+RM5(J))/2.0
      DO 277 J=31,35
  277 RM(J)=(RM5(J)+RM6(J))/2.0
      DO 278 J=36,46
  278 RM(J)=RM6(J)
C
C             NORMALISED CORRECTION FACTORS AVERAGED.
C
      F=100.0/  RM(11)
      DO 285 J=1,46
       FACTOR(J)=RM(J)*F
  285 RECIP(J)=(1.0/FACTOR(J))*100.0
C
C             CORRECTION FACTOR NORMALISED TO 100.0 AT 400NM.
C
      DO 290 J=1,46
  290 IAVEL(J)=290+J*10
C
      DO 430 IC=1,4
      WRITE(6,300)IC
  300 FORMAT(1H1,10X,'COPY NUMBER ',I1,10X,'PAGE 1')
      WRITE(6,310)TITT
  310 FORMAT(1H0,2(10X,20A4/))
      WRITE(6,320)X,M
  320 FORMAT(1H0,15X,'EXCITATION SLIT WIDTH = ',F4.1,' NM.',5X,'EMISSION
     1 SLIT WIDTH = ',F4.1,' NM.')
      WRITE(6,330)
  330 FORMAT(1H0,2X,'WAVELENGTH',10X,'ABSOLUTE SPECTRA',23X,'EXPTAL. SPE
     1CTRA',20X,'CORRECTION FACTORS')
      WRITE(6,340)
  340 FORMAT(1H ,5X,'(NM)',3X,3(8X,'A',5X,'B',5X,'C',5X,'D',5X,'E',5X,'F
     1'))
      DO 360 J=1,46
      WRITE(6,350)IAVEL(J),AB1(J),AB2(J),AB3(J),AB4(J),AB5(J),AB6(J),
     1EX1(J),EX2(J),EX3(J),EX4(J),EX5(J),EX6(J),COR1(J),COR2(J),COR3(J),
     2COR4(J),COR5(J),COR6(J)
  350 FORMAT(1H ,5X,I4,6X,6(F5.1,1X),3X,6(F5.1,1X),3X,6(F5.3,1X))
  360 CONTINUE
C
      WRITE(6,370)IC
  370 FORMAT(1H1,10X,'COPY NUMBER ',I1,10X,'PAGE 2')
      WRITE(6,310)TITT
      WRITE(6,320)X,M
      WRITE(6,380)
  380 FORMAT(1H0,2X,'WAVELENGTH',10X,'NORMALISED CORRECTION FACTORS',35X
     1,'OVERALL CORRECTION FACTORS')
      WRITE(6,390)
  390 FORMAT(1H ,5X,'(NM)',11X,'A',8X,'B',8X,'C',8X,'D',8X,'E',8X,'F'
     1,19X,'MEAN',8X,'FINAL',12X,'RECIP')
      DO 410 J=1,46
      WRITE(6,400)IAVEL(J),  RM1(J),  RM2(J),  RM3(J),  RM4(J),  RM5(J),
     1  RM6(J),  RM(J),FACTOR(J),RECIP(J)
  400 FORMAT(1H ,5X,I4,9X,6(F7.5,2X),10X,F9.6,5X,F9.5,5X,F9.2)
  410 CONTINUE
      WRITE(6,420)
  420 FORMAT(1H0,25X,'*****************************************')
  430 CONTINUE
  440 CONTINUE
      STOP
      END
```

Program CALIB (continued)

Specimen computer printout.

EXCITATION SLIT WIDTH = 4.0 NM. EMISSION SLIT WIDTH = 4.0 NM.

WAVELENGTH (NM)	ABSOLUTE SPECTRA A	B	C	D	E	F	EXPTAL. SPECTRA A	B	C	D	E	F	CORRECTION FACTORS A	B	C	D	E	F
300	0.2	0.0	0.0	0.0	0.0	0.0	0.1	0.0	0.0	0.0	0.0	0.0	0.500	0.0	0.0	0.0	0.0	0.0
310	0.9	0.0	0.0	0.0	0.0	0.0	0.1	0.0	0.0	0.0	0.0	0.0	0.111	0.0	0.0	0.0	0.0	0.0
320	2.5	0.0	0.0	0.0	0.0	0.0	1.1	0.0	0.0	0.0	0.0	0.0	0.440	0.0	0.0	0.0	0.0	0.0
330	4.5	0.0	0.0	0.0	0.0	0.0	15.3	0.0	0.0	0.0	0.0	0.0	1.611	0.0	0.0	0.0	0.0	0.0
340	33.0	0.0	0.0	0.0	0.0	0.0	44.8	0.0	0.0	0.0	0.0	0.0	1.358	0.0	0.0	0.0	0.0	0.0
350	66.5	0.0	0.0	0.0	0.0	0.0	69.5	0.0	0.0	0.0	0.0	0.0	1.045	0.0	0.0	0.0	0.0	0.0
360	94.0	0.0	0.0	0.0	0.0	0.0	79.8	0.0	0.0	0.0	0.0	0.0	0.849	0.0	0.0	0.0	0.0	0.0
370	100.0	0.0	0.0	0.0	0.0	0.0	74.8	0.0	0.0	0.0	0.0	0.0	0.748	0.0	0.0	0.0	0.0	0.0
380	99.5	0.0	0.0	0.0	0.0	0.0	61.4	0.0	0.0	0.0	0.0	0.0	0.617	0.0	0.0	0.0	0.0	0.0
390	91.8	0.0	0.0	0.0	0.0	0.0	45.8	0.0	0.0	0.0	0.0	0.0	0.499	0.0	0.0	0.0	0.0	0.0
400	76.0	11.8	0.0	0.0	0.0	0.0	32.0	20.1	0.0	0.0	0.0	0.0	0.421	1.703	0.0	0.0	0.0	0.0
410	53.5	26.7	0.0	0.0	0.0	0.0	20.9	39.0	0.0	0.0	0.0	0.0	0.391	1.461	0.0	0.0	0.0	0.0
420	37.0	47.8	0.0	0.0	0.0	0.0	13.6	59.1	0.0	0.0	0.0	0.0	0.368	1.236	0.0	0.0	0.0	0.0
430	26.5	68.3	0.0	0.0	0.0	0.0	8.7	76.2	0.0	0.0	0.0	0.0	0.328	1.116	0.0	0.0	0.0	0.0
440	17.5	85.5	0.0	0.0	0.0	0.0	5.4	87.7	0.0	0.0	0.0	0.0	0.309	1.026	0.0	0.0	0.0	0.0
450	10.8	95.4	12.5	0.0	0.0	0.0	3.4	89.9	13.1	0.0	0.0	0.0	0.315	0.942	0.0	0.0	0.0	0.0
460	7.5	100.0	32.7	0.0	0.0	0.0	2.0	83.8	31.9	0.0	0.0	0.0	0.0	0.838	0.0	0.0	0.0	0.0
470	0.0	98.3	54.2	24.8	0.0	0.0	0.0	72.4	56.1	29.7	0.0	0.0	0.0	0.737	1.035	1.198	0.0	0.0
480	0.0	90.0	75.0	39.5	0.0	0.0	0.0	59.1	77.9	48.9	0.0	0.0	0.0	0.657	1.039	1.238	0.0	0.0
490	0.0	78.8	92.0	58.2	0.0	0.0	0.0	46.0	88.4	65.0	0.0	0.0	0.0	0.584	0.961	0.773	0.0	0.0
500	0.0	70.0	99.5	74.0	0.0	0.0	0.0	34.3	87.4	75.7	0.0	0.0	0.0	0.490	0.878	1.023	0.0	0.0
510	0.0	58.5	100.0	87.7	0.0	0.0	0.0	24.9	77.9	79.1	0.0	0.0	0.0	0.426	0.779	0.902	0.0	0.0
520	0.0	49.0	97.0	95.6	0.0	0.0	0.0	18.0	65.6	78.5	0.0	0.0	0.0	0.367	0.676	0.821	0.0	0.0
530	0.0	42.0	94.0	100.0	0.0	0.0	0.0	12.5	52.0	71.7	0.0	0.0	0.0	0.298	0.553	0.717	0.0	0.0
540	0.0	33.2	86.5	98.2	0.0	0.0	0.0	8.1	37.1	58.7	0.0	0.0	0.0	0.244	0.429	0.598	0.0	0.0
550	0.0	29.1	71.6	94.1	0.0	0.0	0.0	5.2	25.1	45.8	0.0	0.0	0.0	0.179	0.351	0.487	0.0	0.0
560	0.0	0.0	60.8	85.6	0.0	0.0	0.0	0.0	16.1	33.0	0.0	0.0	0.0	0.0	0.265	0.395	0.0	0.0
570	0.0	0.0	56.5	79.0	0.0	0.0	0.0	0.0	10.4	24.5	0.0	0.0	0.0	0.0	0.184	0.310	0.0	0.0
580	0.0	0.0	40.0	71.9	28.4	0.0	0.0	0.0	6.7	17.7	44.2	0.0	0.0	0.0	0.167	0.246	1.556	0.0
590	0.0	0.0	34.0	63.3	56.0	0.0	0.0	0.0	3.9	11.4	77.5	0.0	0.0	0.0	0.115	0.180	1.384	0.0
600	0.0	0.0	27.0	55.3	76.7	22.5	0.0	0.0	1.9	5.9	70.2	77.7	0.0	0.0	0.070	0.107	0.915	3.453
610	0.0	0.0	16.6	49.4	90.0	33.2	0.0	0.0	0.9	2.8	39.9	59.3	0.0	0.0	0.054	0.057	0.443	1.786
620	0.0	0.0	13.5	43.1	94.5	44.0	0.0	0.0	0.3	1.2	20.0	43.0	0.0	0.0	0.022	0.028	0.212	0.977
630	0.0	0.0	10.4	35.7	97.2	55.6	0.0	0.0	0.2	0.7	11.3	32.0	0.0	0.0	0.019	0.020	0.116	0.576
640	0.0	0.0	0.0	29.7	98.8	67.3	0.0	0.0	0.0	0.4	6.8	24.2	0.0	0.0	0.0	0.013	0.069	0.360
650	0.0	0.0	0.0	26.3	95.9	77.2	0.0	0.0	0.0	0.2	3.9	17.2	0.0	0.0	0.0	0.008	0.041	0.223
660	0.0	0.0	0.0	0.0	88.5	85.1	0.0	0.0	0.0	0.0	2.1	13.1	0.0	0.0	0.0	0.0	0.024	0.154
670	0.0	0.0	0.0	0.0	79.4	91.0	0.0	0.0	0.0	0.0	1.0	9.0	0.0	0.0	0.0	0.0	0.013	0.099
680	0.0	0.0	0.0	0.0	65.5	95.8	0.0	0.0	0.0	0.0	0.6	5.6	0.0	0.0	0.0	0.0	0.009	0.058
690	0.0	0.0	0.0	0.0	56.5	98.0	0.0	0.0	0.0	0.0	0.3	3.3	0.0	0.0	0.0	0.0	0.005	0.034
700	0.0	0.0	0.0	0.0	48.5	100.0	0.0	0.0	0.0	0.0	0.2	2.0	0.0	0.0	0.0	0.0	0.0	0.020
710	0.0	0.0	0.0	0.0	0.0	98.5	0.0	0.0	0.0	0.0	0.0	1.0	0.0	0.0	0.0	0.0	0.0	0.010
720	0.0	0.0	0.0	0.0	0.0	96.2	0.0	0.0	0.0	0.0	0.0	0.5	0.0	0.0	0.0	0.0	0.0	0.005
730	0.0	0.0	0.0	0.0	0.0	94.6	0.0	0.0	0.0	0.0	0.0	0.3	0.0	0.0	0.0	0.0	0.0	0.003
740	0.0	0.0	0.0	0.0	0.0	83.2	0.0	0.0	0.0	0.0	0.0	0.2	0.0	0.0	0.0	0.0	0.0	0.002
750	0.0	0.0	0.0	0.0	0.0	73.5	0.0	0.0	0.0	0.0	0.0	0.2	0.0	0.0	0.0	0.0	0.0	0.003

EXCITATION SLIT WIDTH = 4.0 NM. EMISSION SLIT WIDTH = 4.0 NM.

WAVELENGTH (NM)	NORMALISED CORRECTION FACTORS A	B	C	D	E	F	OVERALL CORRECTION FACTORS MEAN	FINAL	RECIP
300	0.50000	0.0	0.0	0.0	0.0	0.0	0.500000	114.07446	0.88
310	0.11111	0.0	0.0	0.0	0.0	0.0	0.111111	25.34987	3.94
320	0.44000	0.0	0.0	0.0	0.0	0.0	0.440000	100.38551	1.00
330	1.61053	0.0	0.0	0.0	0.0	0.0	1.610526	367.43994	0.27
340	1.35757	0.0	0.0	0.0	0.0	0.0	1.357574	309.72925	0.32
350	1.04511	0.0	0.0	0.0	0.0	0.0	1.045113	238.44142	0.42
360	0.84894	0.0	0.0	0.0	0.0	0.0	0.848936	193.68393	0.52
370	0.74800	0.0	0.0	0.0	0.0	0.0	0.748000	170.65544	0.59
380	0.61709	0.0	0.0	0.0	0.0	0.0	0.617085	140.78741	0.71
390	0.49891	0.0	0.0	0.0	0.0	0.0	0.498911	113.82596	0.88
400	0.42105	0.45557	0.0	0.0	0.0	0.0	0.438310	99.99998	1.00
410	0.39065	0.39065	0.0	0.0	0.0	0.0	0.390654	89.12733	1.12
420	0.36757	0.33067	0.0	0.0	0.0	0.0	0.349120	79.65141	1.26
430	0.32830	0.29838	0.0	0.0	0.0	0.0	0.298382	68.07561	1.47
440	0.30857	0.27433	0.0	0.0	0.0	0.0	0.274329	62.58794	1.60
450	0.31481	0.25203	0.0	0.0	0.0	0.0	0.126014	28.75006	3.48
460	0.0	0.22412	0.0	0.0	0.0	0.0	0.112061	25.56650	3.91
470	0.0	0.19698	0.17501	0.15623	0.0	0.0	0.176075	40.17139	2.49
480	0.0	0.17562	0.16150	0.0	0.0	0.0	0.170916	38.99418	2.56
490	0.0	0.15612	0.16247	0.10087	0.0	0.0	0.139821	31.89993	3.13
500	0.0	0.13105	0.14852	0.13345	0.0	0.0	0.137675	31.41048	3.18
510	0.0	0.11384	0.13172	0.11766	0.0	0.0	0.121073	27.62260	3.62
520	0.0	0.09825	0.11435	0.10712	0.0	0.0	0.106573	24.31447	4.11
530	0.0	0.07960	0.09354	0.09354	0.0	0.0	0.088890	20.28026	4.93
540	0.0	0.06525	0.07252	0.07798	0.0	0.0	0.075251	17.16850	5.82
550	0.0	0.04779	0.05927	0.06350	0.0	0.0	0.061385	14.00488	7.14
560	0.0	0.0	0.04477	0.05151	0.0	0.0	0.048143	10.98381	9.10
570	0.0	0.0	0.03112	0.04046	0.0	0.0	0.035791	8.16564	12.25
580	0.0	0.0	0.02832	0.03212	0.03212	0.0	0.032115	7.32701	13.65
590	0.0	0.0	0.01940	0.02349	0.02856	0.0	0.026026	5.93779	16.84
600	0.0	0.0	0.01190	0.01392	0.01809	0.01543	0.017159	3.91485	25.54
610	0.0	0.0	0.00917	0.00739	0.00915	0.00798	0.008565	1.95410	51.17
620	0.0	0.0	0.00376	0.00363	0.00437	0.00437	0.004367	0.99637	100.36
630	0.0	0.0	0.00325	0.00256	0.00240	0.00257	0.002485	0.56705	176.35
640	0.0	0.0	0.0	0.00176	0.00142	0.00161	0.001514	0.34532	289.59
650	0.0	0.0	0.0	0.00099	0.00084	0.00100	0.000996	0.22715	440.23
660	0.0	0.0	0.0	0.0	0.00049	0.00069	0.000688	0.15694	637.17
670	0.0	0.0	0.0	0.0	0.00027	0.00044	0.000442	0.10083	991.73
680	0.0	0.0	0.0	0.0	0.00019	0.00026	0.000261	0.05960	1677.92
690	0.0	0.0	0.0	0.0	0.00011	0.00015	0.000150	0.03433	2912.77
700	0.0	0.0	0.0	0.0	0.0	0.00009	0.000089	0.02039	4904.16
710	0.0	0.0	0.0	0.0	0.0	0.00005	0.000045	0.01035	9661.20
720	0.0	0.0	0.0	0.0	0.0	0.00002	0.000023	0.00530	18871.22
730	0.0	0.0	0.0	0.0	0.0	0.00001	0.000014	0.00323	30928.88
740	0.0	0.0	0.0	0.0	0.0	0.00001	0.000011	0.00245	40802.59
750	0.0	0.0	0.0	0.0	0.0	0.00001	0.000012	0.00277	36045.55

****

APPENDIX III

Program SPEKA

```
C
C                    PROGRAM SPEKA.
C       EXCITATION AND EMISSION SPECTRA - HITACHI MPF 2A - R106 PM.
C
C            THE EXPERIMENTAL AND CORRECTED SPECTRA AND THE CORRESPOND-
C       ING NORMALISED SPECTRA ARE PRINTED IN ALL CASES.
C
C          THE INTEGRATED VALUES OF THE CORRECTED SPECTRUM (EXPTAL) ARE
C       ALSO PRINTED, THE INTEGRATION BEING PERFORMED WITH RESPECT TO
C       WAVENUMBER.
C
C            THE PROGRAM PRODUCES PUNCHED CARD OUTPUT TO USE IN
C       PLOTTING PROGRAMS.
C
C                         INPUT.
C
C               CARD 1.   NUMBER OF SPECTRA TO BE PROCESSED.    I3.
C               CARD 2.   TITLE OF SPECTRUM.
C               CARD 3.   TITLE OF SPECTRUM.
C               CARD 4.   TITLE OF SPECTRUM.
C               CARDS 2-4 AS NECESSARY.
C
C                    TAPE.
C               START,STOP, (NP)    (2F5.0)
C               CODE NUMBER,EXCITATION OPTION.   (I3,I1)
C               (PUNCH 1 IF EXCITATION SPECTRUM)
C               VOLTAGES
C               99 +OCOCO OCR LF
C               AND FINALLY CR CR CR CR CR CR
C
C
C
      SUBROUTINE GETPT
      INTEGER ENDF
      INTEGER CHAR/Z40404040/,CR/Z0D404040/,CARD(80)
      NREC=0
      I=0
    1 CALL READPT(3,1,CHAR)
      CALL FASCII(CHAR)
      IF(CHAR.EQ.CR) GO TO 2
      ENDF=0
      I=I+1
      CARD(I)=CHAR
      GO TO 1
    2 IF(ENDF.EQ.1) GO TO 4
      ENDF=1
      NREC=NREC+1
      WRITE(4,3)(CARD(K),K=1,I)
    3 FORMAT(80A1)
      I=0
      CALL READPT(3,1,CHAR)
      GO TO 1
    4 CONTINUE
      DIMENSION X(1000),VAL(1000),Y(1000),Y1(1000),Y2(1000),A1(1000),
     1A2(1000),CORR(1000),AREA(1000),CCR(1000),ITIT(60),W(1000),WN(1000)
     2,NN(1000),V(1000),NC(1000),WMAX(50),AMAX(50)
C
C
      CALL GETPT
      READ(5,10)NRUN
   10 FORMAT(I3)
      DO 277 M=1,NRUN
      READ(5,20)ITIT
   20 FORMAT(20A4)
      READ(4,30)START,STOP
   30 FORMAT(2F5.0)
      READ(4,40)KODE,NEXCIT
   40 FORMAT(I3,I1)
      N=0
   50 N=N+1
      READ(4,51)NC(N),V(N),NR(N)
   51 FORMAT(I2,1X,F6.0,1X,I1)
      IF(NC(N)-90)50,50,52
   52 N=N-1
      G=N
      WINC=(STOP-START)/(G-1)
      DO 53 J=1,N
      R=NR(J)
      IF(R.EQ.0.0)E=0.000001
      IF(R.EQ.1.0)E=0.00001
      IF(R.EQ.2.0)E=0.0001
      IF(R.EQ.3.0)E=0.001
      IF(R.EQ.4.0)E=0.01
   53 VAL(J)=ABS(V(J)*E)*1000.0
C
C                  VALUES IN MILLIVOLTS.
C
      WEEVAL=100.0
      DO 54 J=1,N
   54 IF(VAL(J).LT.WEEVAL)WEEVAL=VAL(J)
      DO 55 J=1,N
   55 VAL(J)=VAL(J)-WEEVAL
C
C                  LOWEST VOLTAGE IS MADE EQUAL TO ZERO.
C
      DO 60 J=1,N
      X(J)=START+(J-1)*WINC
      W(J)=(1.0/X(J))*(10**7)
   60 CONTINUE
      BIGVAL=0.0
      DO 80 J=1,N
      IF(VAL(J).GT.BIGVAL)BIGVAL=VAL(J)
   80 CONTINUE
      DO 90 J=1,N
      F1=100.0/BIGVAL
   90 Y1(J)=VAL(J)*F1
C
      IF(NEXCIT-1)100,111,111
  100 COR(1)=0.71
      COR(2)=2.48
      COR(3)=0.98
      COR(4)=0.26
      COR(5)=0.32
      COR(6)=0.41
      COR(7)=0.52
      COR(8)=0.59
      COR(9)=0.71
      COR(10)=0.88
      COR(11)=1.00
      COR(12)=1.11
      COR(13)=1.24
      COR(14)=1.44
      COR(15)=1.57
      COR(16)=1.78
      COR(17)=2.00
      COR(18)=2.24
      COR(19)=2.44
      COR(20)=2.80
      COR(21)=3.15
      COR(22)=3.89
      COR(23)=4.08
      COR(24)=4.92
      COR(25)=5.76
      COR(26)=7.10
      COR(27)=8.99
      COR(28)=12.11
      COR(29)=13.56
      COR(30)=16.59
      COR(31)=24.12
      COR(32)=46.68
      COR(33)=93.59
      COR(34)=164.10
      COR(35)=272.04
      COR(36)=409.68
      COR(37)=593.70
      COR(38)=906.04
      COR(39)=1512.20
      COR(40)=2283.85
      COR(41)=4518.67
      COR(42)=8342.22
      COR(43)=13409.01
      COR(44)=24609.44
      COR(45)=42805.15
      COR(46)=45112.66
      DO 110 J=1,N
      K=(X(J)-300.0)/10.0+1.0
      A=X(J)-290.0-K*10.0
      CORR(J)=CCR(K)+A*(CCR(K+1)-CCR(K))/10.0
  110 Y1(J)=CORR(J)*VAL(J)
      GO TO 114
  111 COR(1)=0.07
      COR(2)=0.13
      COR(3)=0.17
      COR(4)=0.34
      COR(5)=0.52
      COR(6)=0.78
      COR(7)=0.99
      COR(8)=1.31
      COR(9)=1.67
      COR(10)=1.89
      COR(11)=2.34
      COR(12)=2.75
      COR(13)=3.32
      COR(14)=3.77
      COR(15)=4.42
      COR(16)=5.00
      COR(17)=5.39
      COR(18)=5.72
      COR(19)=6.04
      COR(20)=6.58
      COR(21)=7.36
      COR(22)=8.59
      COR(23)=10.00
      COR(24)=11.43
      COR(25)=12.63
      COR(26)=13.61
      COR(27)=14.53
      COR(28)=15.06
      COR(29)=15.81
      COR(30)=16.26
      COR(31)=17.06
      COR(32)=16.67
      COR(33)=17.37
      COR(34)=17.12
      COR(35)=16.60
      COR(36)=16.30
      COR(37)=16.51
      COR(38)=16.56
      COR(39)=15.28
      COR(40)=15.63
      COR(41)=16.00
      COR(42)=17.17
      COR(43)=17.45
      COR(44)=16.97
      COR(45)=19.94
      COR(46)=20.95
      COR(47)=24.39
      COR(48)=25.31
      COR(49)=21.58
      COR(50)=19.85
      COR(51)=20.00
      COR(52)=18.80
      COR(53)=18.68
      COR(54)=17.59
      COR(55)=16.99
      COR(56)=16.82
      COR(57)=16.92
      COR(58)=16.97
      COR(59)=16.49
      COR(60)=15.99
      COR(61)=15.38
      COR(62)=15.09
      COR(63)=14.56
      COR(64)=14.89
      COR(65)=14.77
      COR(66)=14.87
      COR(67)=14.63
      COR(68)=14.30
      COR(69)=13.74
      COR(70)=13.06
      COR(71)=12.42
      COR(72)=11.79
      COR(73)=12.02
      COR(74)=12.43
      DO 112 J=1,N
      K=(X(J)-235.0)/5.0+1.0
      A=X(J)-230.0-K*5.0
      CORR(J)=COR(K)+A*(COR(K+1)-COR(K))/5.0
  112 Y1(J)=VAL(J)/CORR(J)
C
C     Y1(J) IS CORRECTED SPECTRUM.
C
  114 BIGVAL=0.0
      DO 115 J=1,N
      IF(Y1(J).GT.BIGVAL)BIGVAL=Y1(J)
  115 CONTINUE
      DO 120 J=1,N
      F2=100.0/BIGVAL
  120 Y2(J)=Y1(J)*F2
C
C     Y2(J) IS NORMALISED CORRECTED SPECTRUM.
C
      DO 122 J=1,N
      IF(Y2(J).GT.99.9999)WMAX(M)=X(J)
  122 CONTINUE
C
C                  MAXIMUM INTENSITY WAVELENGTH NOTED.
C
      M1=N-1
      DO 130 J=1,M1
      WN(J)=W(J+1)-W(J)
      A1(J)=ABS(Y1(J+1)-Y1(J))
  130 A2(J)=((A1(J)*WN(J))/2.0)+WN(J)*Y1(J))/100.0
      AREA(1)=0.0
```

Program SPEKA (continued)

```
      AREA(2)=A2(1)
      DO 140 J=3,N
      AREA(J)=A2(J-1)+AREA(J-1)
  140 CONTINUE
      DO 150 J=1,N
      AREA(J)=ABS(AREA(J)/10.0)
      AMAX(M)=AREA(N)
  150 CONTINUE
C
C         LINE PRINTER OUTPUT
C
      IF(NEXCIT-1)180,160,160
  160 WRITE(6,170)
  170 FORMAT(1H1,30X,'EXCITATION SPECTRUM.       HITACHI MPF-2A.  CORRECT
     1ED FOR R106 PHOTOMULTIPLIER.')
      GO TO 195
  180 WRITE(6,190)
  190 FORMAT(1H1,30X,'EMISSION SPECTRUM.         HITACHI MPF-2A.  CORRECT
     1ED FOR R106 PHOTOMULTIPLIER.')
  195 WRITE(6,200)KODE
  200 FORMAT(1HO,45X,'SPECTRUM NUMBER  ',I3)
      WRITE(6,210)ITIT
  210 FORMAT(1HO,10X,3(20A4/))
      WRITE(6,220)
  220 FORMAT(1HO,14X,'EXPERIMENTAL SPECTRUM.',9X,'CORRECTED SPECTRUM.',
     15X,'INTEGRATION OF',10X,'WAVENUMBER')
      WRITE(6,230)
  230 FORMAT(1HO,   'WAVELENGTH',5X,'ACTUAL',4X,'NORMALISED',10X,'ACTUAL
     1',4X,'NORMALISED',4X,'ACTUAL CORR. SPEC.', 9X,'CM-1')
      DO 250 J=1,N
      WRITE(6,240)X(J),VAL(J),Y(J),Y1(J),Y2(J),AREA(J),W(J)
  240 FORMAT(1H ,3X,F6.2,6X,F6.3,6X,F6.2,10X,F8.3,6X,F6.2,10X,F8.3,16X,
     1F8.0)
      IF(X(J)-WMAX(M))250,245,250
  245 WRITE(6,246)
  246 FORMAT(1H+,'***',102X,'***')
  250 CONTINUE
      WRITE(6,260)WMAX(M)
  260 FORMAT(1HO,10X,'MAXIMUM EMISSION AT ',F5.1,' NM.')
      WRITE(6,270)AMAX(M)
  270 FORMAT(1HO,10X,'TOTAL INTEGRATED AREA = ',F6.2)
      WRITE(7,271)ITIT
  271 FORMAT(20A4)
      WRITE(7,272)START,WINC,STOP
  272 FORMAT(3F10.6)
      WRITE(7,273)KODE
  273 FORMAT(I3)
      WRITE(7,274)N
  274 FORMAT(I3)
      WRITE(7,275)(Y1(J),J=1,N)
  275 FORMAT(16F5.2)
  277 CONTINUE
      WRITE(6,280)
  280 FORMAT(1H1,30X,'SUMMARY OF RESULTS.')
      WRITE(6,290)
  290 FORMAT(1H ,30X,'--------------------')
      DO 310 M=1,NRUN
      WRITE(6,300)M,WMAX(M),AMAX(M)
  300 FORMAT(1HO,10X,'SPECTRUM NUMBER ',I2,'.',5X,'MAXIMUM EMISSION AT '
     1,F5.1,' NM.',5X,'INTEGRATED AREA = ',F9.4)
  310 CONTINUE
      STOP
      END
```

APPENDIX IV

Program SPEKBA

```
C
C                    PROGRAM SPEKBA.
C
C          THIS IS A PLOTTING PROGRAM DESIGNED TO USE THE PUNCHED
C     CARD OUTPUT FROM SPEKA.THE FIRST DATA CARD CHOOSES THE PLOTTING
C     ROUTINE(S) TO BE USED. THIS IS FORMATTED AS 4I1 WHERE 0 NEGLECTS
C     THE RELEVANT OPTION AND ANY OTHER NUMBER CALLS IT. THE OPTIONS ARE
C     (1) ALL THE SPECTRA ARE PLOTTED V. WAVELENGTH ON SEPARATE PLOTS,
C     EACH NORMALISED TO FULL SCALE. (2) ALL THE SPECTRA ARE PLOTTED ON
C     ONE PLOT WITH THE CORRECT RELATIVE SCALES AND THE MOST INTENSE
C     NORMALISED TO FULL SCALE. (3) AS FOR OPTION (1) BUT PLOTTED V.
C     WAVENUMBER. (4) AS FOR OPTION 2 BUT PLOTTED V. WAVENUMBER.
C        ANY OR ALL OF THESE OPTIONS MAY BE USED DURING A RUN.
C     THE SECOND DATA CARD GIVES THE NUMBER OF SPECTRA TO BE PLOTTED.
C             (THIS IS LIMITED TO A MAXIMUM OF 4 WITH THE PRESENT DIM-
C     ENSIONS EACH SPECTRUM HAVING LESS THAN 500 POINTS.)
C     THE FOLLOWING DATA CARDS ARE THE OUTPUT FROM SPEKA,NAMELY THREE
C     TITLE CARDS,START,INCREMENT AND STOP WAVELENGTHS,CODE NUMBER OF
C     SPECTRUM,THE NUMBER OF VALUES IN THE SPECTRUM,AND FINALLY THE
C     VALUES.
C
      DIMENSION ITIT(60),START(2),WINC(2),END(2),KODE(2),VAL(2,1000),
     1VAL1(2,1000),VAL2(2,1000),WAVEL(2,1000),WAVEN(2,1000),XMINL(2),
     2XMAXL(2),XMINN(2),XMAXN(2),NN(2)
      READ(5,1)NOPT1,NOPT2,NOPT3,NOPT4
    1 FORMAT(4I1)
      WRITE(6,5)
    5 FORMAT(1H1,30X,'THE FOLLOWING SPECTRA ARE BEING PLOTTED.*')
      READ(5,10)NDATA
   10 FORMAT(I2)
      DO 110 M=1,NDATA
      READ(5,20)ITIT
   20 FORMAT(20A4)
      READ(5,30)START(M),WINC(M),END(M)
   30 FORMAT(3F10.0)
      READ(5,40)KODE(M)
   40 FORMAT(I3)
      READ(5,50)NN(M)
   50 FORMAT(I3)
      N1=NN(M)
      READ(5,60)(VAL(M,N),N=1,N1)
   60 FORMAT(16F5.0)
      WRITE(6,70)KODE(M)
   70 FORMAT(1HO,15X,'SPECTRUM NUMBER *',I3)
      WRITE(6,80)ITIT
   80 FORMAT(1HO,20X,3(20A4/))
      WRITE(6,90)START(M),END(M),WINC(M)
   90 FORMAT(1HO,25X,F6.2,'TO *,F6.2,' NM. IN INCREMENTS OF *,F5.2,' NM.
     1*)
      WRITE(6,100)
  100 FORMAT(1HO,30X,'******',/)
  110 CONTINUE
C
C          DATA READ AND DETAILS OF SPECTRA TO BE PLOTTED ARE PRINTED
C             ON THE LINE PRINTER
C
      DO 140 M=1,NDATA
      BIGVAL=0.0
      N1=NN(M)
      DO 120 N=1,N1
  120 IF(VAL(M,N).GT.BIGVAL)BIGVAL=VAL(M,N)
      F=100.0/BIGVAL
      DO 130 N=1,N1
  130 VAL1(M,N)=F*VAL(M,N)
  140 CONTINUE
C
C             ALL SPECTRA NORMALISED TO 100
C
      IF(M.EQ.1) GO TO 180
      TOPVAL=0.0
      DO 160 M=1,NDATA
      N1=NN(M)
      DO 150 N=1,N1
  150 IF(VAL(M,N).GT.TOPVAL)TOPVAL=VAL(M,N)
  160 CONTINUE
      F1=100.0/TOPVAL
      DO 180 M=1,NDATA
      N1=NN(M)
      DO 170 N=1,N1
  170 VAL2(M,N)=VAL(M,N)*F1
  180 CONTINUE
C
C             ALL SPECTRA RESCALED.
C
      DO 200 M=1,NDATA
      N1=NN(M)
      DO 190 N=1,N1
      G=N
      WAVEL(M,N)=START(M)-WINC(M)+WINC(M)*G
  190 WAVEN(M,N)=10000.0/WAVEL(M,N)
  200 CONTINUE
C
C             CORRESPONDING WAVELENGTHS AND WAVENUMBERS CALCULATED.
C
      DO 210 M=1,NDATA
      X1=START(M)/20.0
      I=X1
      I=I*20
      XMINL(M)=I
      X2=END(M)/20.0
      I=X2
      I=(20*I)+20
      XMAXL(M)=I
  210 CONTINUE
C
C             HIGH AND LOW WAVELENGTHS FOR PLOTTER
C
      DO 220 M=1,NDATA
      X1=5000.0/START(M)
      I=X1
      I=(I*2)+2
      XMINN(M)=I
      X2=5000.0/END(M)
      I=X2
      I=I*2
      XMAXN(M)=I
  220 CONTINUE
C             HIGH AND LOW WAVENUMBER LIMITS FOR PLOTTER.
C
      IF(M.EQ.1) GO TO 240
      A=0.0
      B=10000.0
      DO 230 M=1,NDATA
      IF(START(M).LT.A)A=START(M)
      IF(END(M).GT.B)B=END(M)
  230 CONTINUE
      X1=A/20.0
      I=X1
      I=I*20
      XMINA=I
      X1=B/20.0
      I=X1
      I=I*20
      XMAXA=I
      X1=5000.0/A
      I=X1
      I=I*2
      XMAXB=I
C
C             HIGH AND LOW LIMITS FOR COMPOSITE PLOTS
C
C
C             PLOTTING COMMENCES
C
C                  PLOTTING OPTION 1.
C
  240 CONTINUE
      IF(NOPT1-1)340,250,250
  250 DO 330 M=1,NDATA
      XD=10.0
      YMIN=0.0
      YMAX=100.0
      YL=5.0
      YD=10.0
      XMAX=XMAXL(M)
      XMIN=XMINL(M)
      XL=(XMAX-XMIN)*0.025
      ZA=XMIN+40.0
      ZB=XMIN-80.0
      ZC=XMIN+50.0
      ZD=XMIN-52.0
C
      CALL PLOT(1,XMIN,XMAX,XL,XD,YMIN,YMAX,YL,YD)
      CALL PLOT(99)
C
      IMIN=XMIN
      IMAX=XMAX
      DO 270 I=IMIN,IMAX,40
      XX=I-18
      CALL PLOT(90,XX,-5.0)
      WRITE(3,260)I
  260 FORMAT(4X,I3,100X)
  270 CALL CHAR(0.1,10)
      CALL PLOT(99)
C
      CALL PLOT(90,ZA,-10.0)
      WRITE(3,280)
  280 FORMAT(15HWAVELENGTH (NM),100X)
      CALL CHAR(0.1,10)
      CALL PLOT(99)
C
      DO 300 K=10,110,10
      IY=K-10
      YY=IY
      CALL PLOT(90,ZD,YY)
      WRITE(3,290)IY
  290 FORMAT(18X,I3,100X)
  300 CALL CHAR(0.1,10)
      CALL PLOT(99)
C
      CALL PLOT(90,ZD,66.5)
      WRITE(3,305)
  305 FORMAT(8HRELATIVE,100X)
      CALL CHAR(0.1,10)
      CALL PLOT(99)
C
      CALL PLOT(90,ZD,63.5)
      WRITE(3,306)
  306 FORMAT(9HINTENSITY,100X)
      CALL CHAR(0.1,10)
      CALL PLOT(99)
C
      CALL PLOT(90,ZC,105.0)
      WRITE(3,310)KODE(M)
  310 FORMAT(14HSPECTRUM NUMBER ,I3,100X)
      CALL CHAR(0.1,10)
      CALL PLOT(99)
C
      N1=NN(M)
      DO 320 N=1,N1
  320 CALL PLOT(90,WAVEL(M,N),VAL1(M,N))
      CALL PLOT(99)
C
      CALL PLOT(7)
C
  330 CONTINUE
C
C                  PLOTTING OPTION 2.
C
  340 IF(NOPT2-1)420,350,350
  350 XD=10.0
      YMIN=0.0
      YMAX=100.0
      YL=5.0
      YD=10.0
      XMAX=XMAXA
      XMIN=XMINA
      XL=(XMAX-XMIN)*0.025
      ZA=XMIN+40.0
      ZB=XMIN-80.0
      ZC=XMIN+50.0
      ZD=XMIN-52.0
C
      CALL PLOT(1,XMIN,XMAX,XL,XD,YMIN,YMAX,YL,YD)
      CALL PLOT(99)
C
      IMIN=XMIN
      IMAX=XMAX
      DO 360 I=IMIN,IMAX,40
      XX=I-18
      CALL PLOT(90,XX,-5.0)
      WRITE(3,355)I
  355 FORMAT(4X,I3,100X)
  360 CALL CHAR(0.1,10)
      CALL PLOT(99)
C
      CALL PLOT(90,ZA,-10.0)
      WRITE(3,370)
  370 FORMAT(15HWAVELENGTH (NM),100X)
      CALL CHAR(0.1,10)
      CALL PLOT(99)
C
      CALL PLOT(90,ZC,105.0)
      WRITE(3,375)
  375 FORMAT(14HCOMPOSITE PLOT)
      CALL CHAR(0.1,10)
      CALL PLOT(99)
C
      DO 390 K=10,110,10
```

Program SPEKBA (continued)

```
      IY=K-10
      YY=IY
      CALL PLOT(90,ZB,YY)
      WRITE(4,380)IY
  380 FORMAT(1HX,I3,100X)
  390 CALL CHAR(0,1,10)
      CALL PLOT(99)
C
      CALL PLOT(90,ZD,66.5)
      WRITE(3,405)
  405 FORMAT(8HRELATIVE,100X)
      CALL CHAR(0,1,10)
      CALL PLOT(99)
C
      CALL PLOT(90,ZD,63.5)
      WRITE(3,406)
  406 FORMAT(9HINTENSITY,100X)
      CALL CHAR(0,1,10)
      CALL PLOT(99)
C
      DO 410 M=1,NDATA
      N1=NN(M)
      DO 400 N=1,N1
  400 CALL PLOT(90,WAVEL(M,N),VAL2(M,N))
      CALL PLOT(99)
C
  410 CONTINUE
      CALL PLOT(7)
  420 CONTINUE
C
C                  PLOTTING OPTION 3.
C
      IF(NOPT3-1)540,450,450
  450 CONTINUE
      DO 530 M=1,NDATA
      XD=-1.0
      YMIN=0.0
      YMAX=100.0
      YL=5.0
      YD=10.0
      XMIN=XMINN(M)
      XMAX=XMAXN(M)
      XL=(XMIN-XMAX)*0.5
      ZA=XMIN-2.0
      ZB=XMIN+4.0
      ZC=XMIN-2.5
      ZD=XMIN+2.6
C
      CALL PLOT(1,XMIN,XMAX,XL,XD,YMIN,YMAX,YL,YD)
      CALL PLOT(99)
C
      IMAX=XMAX
      IMIN=XMIN
      DO 470 L=IMAX,IMIN
      XX=L+1
      CALL PLOT(90,XX,-5.0)
      WRITE(3,460)L
  460 FORMAT(5X,I2,100X)
  470 CALL CHAR(0.1,10)
      CALL PLOT(99)
C
      CALL PLOT(90,ZA,-10.0)
      WRITE(3,480)
  480 FORMAT(24HWAVENUMBER (CM-1 X 10-3),100X)
      CALL CHAR(0.1,10)
      CALL PLOT(99)
C
      DO 500 K=10,110,10
      IY=K-10
      YY=IY
      CALL PLOT(90,ZB,YY)
      WRITE(3,490)IY
  490 FORMAT(1HX,I3,100X)
  500 CALL CHAR(0.1,10)
      CALL PLOT(99)
C
      CALL PLOT(90,ZD,66.5)
      WRITE(3,505)
  505 FORMAT(8HRELATIVE,100X)
      CALL CHAR(0.1,10)
      CALL PLOT(99)
C
      CALL PLOT(90,ZD,63.5)
      WRITE(3,506)
  506 FORMAT(9HINTENSITY,100X)
      CALL CHAR(0.1,10)
      CALL PLOT(99)
C
      CALL PLOT(90,ZC,105.0)
      WRITE(3,510)KODE(M)
  510 FORMAT(16HSPECTRUM NUMBER ,I3,100X)
      CALL CHAR(0.1,10)
      CALL PLOT(99)
C
      N1=NN(M)
      DO 520 N=1,N1
  520 CALL PLOT(90,WAVEN(M,N),VAL1(M,N))
      CALL PLOT(99)
C
       CALL PLOT(7)
C
  530 CONTINUE
C
C                  PLOTTING OPTION 4.
C
  540 IF(NOPT4-1)630,550,550
  550 CONTINUE
      XD=-1.0
      YMIN=0.0
      YMAX=100.0
      YL=5.0
      YD=10.0
      XMIN=XMINB
      XMAX=XMAXB
      XL=(XMIN-XMAX)*0.5
      ZA=XMIN-2.0
      ZB=XMIN+4.0
      ZC=XMIN-2.5
      ZD=XMIN+2.6
C
      CALL PLOT(1,XMIN,XMAX,XL,XD,YMIN,YMAX,YL,YD)
      CALL PLOT(99)
C
      IMAX=XMAX
      IMIN=XMIN
      DO 570 L=IMAX,IMIN
      XX=L+1
      CALL PLOT(90,XX,-5.0)
      WRITE(6,560)L
  560 FORMAT(5X,I2,100X)
  570 CALL CHAR(0.1,10)
      CALL PLOT(99)
C
      CALL PLOT(90,ZA,-10.0)
      WRITE(3,580)
  580 FORMAT(24HWAVENUMBER (CM-1 X 10-3),100X)
      CALL CHAR(0.1,10)
      CALL PLOT(99)
C
      CALL PLOT(90,ZC,105.0)
      WRITE(3,585)
  585 FORMAT(14HCOMPOSITE PLOT)
      CALL CHAR(0.1,10)
      CALL PLOT(99)
C
      DO 600 K=10,110,10
      IY=K-10
      YY=IY
      CALL PLOT(90,ZB,YY)
      WRITE(3,590)IY
  590 FORMAT(1HX,I3,100X)
  600 CALL CHAR(0.1,10)
      CALL PLOT(99)
C
      CALL PLOT(90,ZD,66.5)
      WRITE(3,605)
  605 FORMAT(8HRELATIVE,100X)
      CALL CHAR(0.1,10)
      CALL PLOT(99)
      CALL PLOT(90,ZD,63.5)
      WRITE(3,606)
  606 FORMAT(9HINTENSITY,100X)
      CALL CHAR(0.1,10)
      CALL PLOT(99)
C
      DO 620 M=1,NDATA
      N1=NN(M)
      DO 610 N=1,N1
  610 CALL PLOT(90,WAVEN(M,N),VAL2(M,N))
      CALL PLOT(99)
C
  620 CONTINUE
      CALL PLOT(7)
  630 CONTINUE
      STOP
      END
```

REFERENCES

1. W.A. Noyes, Jr., G.B. Porter and J.E. Jolley, Chem.Rev., 1956, 56, 49.
2. A. Jablonski, A.Physik, 1935, 94, 38.
3. D.M. Hercules, Fluorescence and Phosphorescence Analysis (Wiley., 1966).
4. J.G. Calvert and J.N, Pitts, Jr., Photochemistry (Wiley, 1966).
5. G. Porter and M.R. Topp, Proc.Roy.Soc., 1970, A315, 163.
6. M. Kasha, Discussions Faraday Soc., 1950, 9, 14.
7. G. Porter and P. Suppan, Trans.Faraday Soc., 1965, 61, 1664.
8. G. Porter in Reactivity of the Photoexcited Organic Molecule, Proc. 13th Conf. on Chemistry, Brussels, 1965 (Interscience, 1967).
9. S.P. McGlynn, F.J. Smith and G. Cilento, Photochem.Photobiol, 1964, 3, 269.
10. S.P. McGlynn, T. Azumi and M. Kinoshita, Molecular Spectroscopy of the Triplet State (Prentice-Hall, 1969).
11. J.N. Murrell, The Theory of the Electronic Spectra of Organic Molecules (Methuen, 1963).
12. J.C.D. Brand, J.Chem.Soc., 1956, 858.
13. Y. Kanda, H. Kaseda and T. Matumura, Spectrochim. Acta., 1964, 20, 1387.
14. S.A. Carlson and D.M. Hercules, J.Amer.Chem.Soc., 1971, 93, 5611.
15. L. Goodman, J.Mol.Spectroscopy, 1961, 6, 109.
16. C.A. Parker and C.G. Hatchard, Trans.Faraday Soc., 1961, 57, 1894.
17. R.N. Nurmukhametov, V.G. Plotnikov and D.N. Shigorin, Zh.F.Kh., 1966, 5, 40.
18. F. Wilkinson and A.R. Horrocks in Luminescence in Chemistry, Ed. E.J. Bowen (Van Nostrand, 1968).
19. E. Clementi and M. Kasha, J.Mol.Spectry., 1958, 2, 297.
20. M.A. El-Slayed, J.Chem.Phys., 1963, 38, 2834.
21. V.G. Plotvikov, Opt.Spectry., 1967, 22, 401.

22. C.A. Parker, Photoluminescence of Solutions (Elsevier, 1968).

23. R.T. Williams and J.W. Bridges, J.Clim.Pathol., 1964, 17, 371.

24. R.T. Williams, J.Roy.Inst.Chem., 1959, 83, 611.

25. A. Rosen and R.T. Williams, Photoelec. Spectrometry Group Bull., 1961, 13, 339.

26. M. Kasha, Light and Life, Eds. W.B. McElroy and B. Glass (John Hopkins Press, 1961).

27. J.N. Pitts, Jr. and J.K.S. Wan, in the Chemistry of the Carbonyl Group, Ed. S. Patai (Interscience, 1966).

28. N.C. Yang in Reactivity of the Photoexcited Organic Molecule, Proc. 13th Conf. on Chemistry, Brussels, 1965 (Interscience, 1967).

29. P. Suppan, J.Mol.Spetr., 1969, 571.

30. G. Porter and P. Suppan, Pure Appl.Chem. 1964, 9, 499.

31. R.S. Becker, Theory and Interpretation of Fluorescence and Phosphorescence (Wiley Interscience, 1969).

32. S. Lower and M. El-Slayedı, Chem.Rev., 1966, 66, 199.

33. L. Vanquickenbome and S. McGlynn, J.Chem.Phys., 1966, 45, 4755.

34. D. Kearns and W. Case, J.Amer.Chem.Soc., 1966, 88, 5087.

35. G. Porter and P. Suppan, Trans.Faraday Soc., 1966, 62, 3375.

36. Specialist Periodical Reports. Photochemistry, 1, 2, and 3, The Chemical Society, London.

37. R.B. Cundall and A. Gilbert, Photochemistry (Nelson, 1970).

38. O.L. Chapman, Organic Photochemistry Vol. 1 (Arnold, 1967).

39. D.C. Neckers, Mechanistic Organic Photochemistry (Reinhold, 1967).

40. P.J. Wagner and G.S. Hammond, Advances in Photochemistry, 5 ed. W.A. Noyes, G.S. Hammond and J.N. Pitts (Interscience, 1968).

41. R. Hoffman and R.B. Woodward, Acc.Chem.Research, 1968, 1, 17.

42. J.N. Brönsted, Rec.Trav.chim., 1923, 42, 718.

43. J.N. Brönsted, Phys.Chem., 1934, A169, 52.

44. V.A. Palm, Ü.L. Haldna and A.J. Talvik, in The Chemistry of the Carbonyl Group, ed. S. Patai (Interscience, 1966).

45. K. Weber, Z. Phys.Chem., 1931, B15, 18.

46. Th. Förster, Naturwiss., 1949, 36, 186.

47. Th. Förster, Z. Elektrochem., 1950, 54, 42.

48. Th. Förster, Z. Elektrochem., 1950, 54, 531.

49. Th. Förster, in Photochemistry in the Liquid and Solid States, ed. F. Daniels (Wiley, 1960).

50. S.G. Schulman and A.C. Capomacchia, Spectrochim.Acta., 1972, 28A, 1.

51. A. Weller, Z. Physik.Chem., 1958, 17, 224.

52. A. Weller, Z.Physik.Chem., 1955, 3, 238.

53. A. Weller, Z. Elektrochem., 1952, 56, 662.

54. A. Weller, Z. Elektrochem., 1954, 58, 849.

55. A. Weller, Z.Physik.Chem., 1957, 13, 335.

56. A. Weller, Progr.Reaction Kinetics, ed. G. Porter (Pergamon, 1961), 1, 189.

57. G. Jackson and G. Porter, Proc.Roy.Soc., 1961, A200, 13.

58. L. Lindqvist, Ark.Kemi., 1960, 16, 79.

59. E. Vander Donckt, Progr.Reaction Kinetics, ed. G. Porter (Pergamon, 1970), 5, 273.

60. H.H. Jaffé and M. Orchin, Theory and Applications of Ultraviolet Spectroscopy (Wiley, 1962).

61. E. Vander Donckt and G. Porter, Trans.Faraday Soc., 1968, 64, 3218.

62. E.L. Wehry and L.B. Rogers, Spectrochim.Acta., 1965, 21A, 1976.

63. A.C. Hopkinson and P.A.H. Wyatt, J.Chem.Soc.(B), 1967, 1333.

64. H.H. Jaffé and H.L. Jones, J.Org.Chem., 1965, 30, 964.

65. A. Weller, Z. Elektrochem., 1957, 61, 956.

66. H. Kokubun, Naturwiss., 1957, 44, 233.

67. H. Kokubun, Z. Elektrochem., 1958, 62, 599.

68. A. Weller and W. Urban, Angew.Chem., 1954, 66, 336.

69. A.R. Watkins, J.Chem.Soc., Faraday Trans 1. 1972, 68, 28.

70. E. Vander Donckt and G. Porter, Trans.Faraday Soc., 1968, 64, 3215.

71. A.R. Watkins, Z Physik.Chem., 1972, 78, 103.

72. S.G. Schulman, A.C. Capomacchia and M.S. Rietta, Anal.Chim.Acta., 1971, 56, 91.

73. S.G. Schulman and L.B. Sanders, Anal.Chim.Acta., 1971, 56, 83.

74. S.G. Schulman, J.Pharm.Sci., 1971, 60, 371.

75. S.G. Schulman, P.T. Tidwell, J.J. Cetorelli, and J.D. Winefordner, J.Amer.Chem.Soc., 1971, 93, 3179.

76. S.G. Schulman, A.C. Capomacchia and B. Tussey, Photochem.Photobiol., 1971, 14, 733.

77. A. Grabowska and B. Pakula, Photochem.Photobiol., 1969, 9, 339.

78. S.C. Lahiri and S. Aditya, Indian J.Chem., 1971, 9, 492.

79. H. Leonhardt, L. Gordon and R. Livingston, J.Phys.Chem., 1971, 75, 245.

80. J. Brinen, D. Rosebrook, and R. Hirt, J.Phys.Chem., 1963, 67, 2651.

81. S.G. Schulman, L.B. Sanders and J.D. Winefordner, Photochem.Photobiol., 1971, 13, 381.

82. A. Grabowska and B. Pakula, Proc.Int.Conf.Lumin., 1966, 368.

83. J. Faure and J. Joussot-Dubien, J.Chim.Phys., 1966, 63, 621.

84. J. Faure, R. Bonneau and J. Joussot-Dubien, Photochem.Photobiol., 1967, 6, 331.

85. A.K. Chibisov, Russ.Chem.Rev., 1970, 39, 891.

86. L.P. Hammett and A.J. Deyrup, J.Amer.Chem.Soc., 1932, 54, 2721.

87. M.A. Paul and F.A. Long, Chem.Rev., 1957, 57, 1.

88. M.J. Jorgenson and D.R. Hartter, J.Amer.Chem.Soc., 1963, 85, 878.

89. E.M. Arnett and G.W. Mach, J.Amer.Chem.Soc., 1964, 86, 2671.

90. K. Yates, J.B. Stevens and A.R. Katritzky, Can.J.Chem., 1964, 42, 1957.

91. R.L. Hinman and J. Lang, J.Amer.Chem.Soc., 1964, 86, 3796.

92. T.G. Bonner and J. Philips, J.Chem.Soc., 1966, 650.

93. N.C. Deno, J.J. Jaruzelski and A. Schriesheim, J.Amer.Chem.Soc., 1955, 77, 3044.

94. F.A. Long and J. Schulze, J.Amer.Chem.Soc., 1961, 83, 3340.

95. M.T. Reagan, J.Amer.Chem.Soc., 1969, 91, 5506.

96. C.H. Rochester, Acidity Functions (Academic Press, 1970).

97. A.C. Hopkinson, Ph.D. Thesis, Sheffield, 1966.

98. S. Udenfriend, Fluorescence Assay in Biology and Medicine (Academic Press, 1962).

99. Perkin Elmer Instruction Manuel, Model MPF-2A, 1970.

100. C.A. Parker and W.J. Barnes, Analyst, 1957, 82, 606.

101. J.D. Winefordner and P.A. St. John, Anal.Chem., 1963, 35, 2211.

102. C.G. Hatchard and C.A. Parker, Proc.Roy.Soc., 1956, A235, 518.

103. C.E. White et al., Anal.Chem., 1960, 32, 438.

104. R. Argauer and C.E. White, Anal.Chem., 1964, 36, 368.

105. R.F. Chen, Anal.Biochem., 1967, 20, 339.

106. R. Argauer and C.E. White, Fluorescence Analysis (Dekker, 1970).

107. R. Lippert, W. Nägele, I. Seibold-Blankenstein, W. Staiger and W. Voss, Z.Anal.Chem., 1959, 170, 1.

108. W.H. Meluish, J.Phys.Chem., 1960, 64, 762.

109. C.A. Parker and W.T. Rees, Analyst, 1960, 85, 587.

110. J. Eisenbrand and H.E. Hauprich, Pharmazie, 1967, 22, 652.

111. R. Rusakowicz and A.C. Testa, J.Phys.Chem., 1968, 72, 2680.

112. Dictionary of Organic Compounds, Eyre and Spottiswoode, London.

113. R.C.A., Information Sheet, 1P28/1-66.

114. F.R. Lipsett, J.Opt.Soc.Amer., 1959, 49, 673.

115. C.A. Parker, Anal.Chem., 1962, 34, 502.

116. G.K. Turner, Science, 1964, 146, 183.

117. G.M. Edelman, Rev.Sci.Instr., 1965, 36, 809.

118. H.V. Drushel, A.L. Sommers and R.C. Cox, Anal.Chem., 1963, 35, 2166.

119. P. Byron and J.B. Hudson, Talanta, 1968, 15, 714.

120. J.N. Demas and G.A. Crosby, J.Phys.Chem., 1971, 75, 991.

121. G. Porter, Proc.Roy.Soc., 1950, A200, 284.

122. G. Porter, Techniques of Organic Chemistry, Vol. VIII, Part 2, Ed. Weissberger, (Interscience, 1963).

123. G. Porter and M.A. West, Flash Photolysis, to be published in Investigation of Rates and Mechanisms of Reactions, Second Edition, Part II, ed. G.G. Hammes (Wiley, Interscience).

124. R.N. Dixon, J.Roy.Inst.Chem., 1963, 87, 75.

125. J.W. Boag, Photochem.Photobiol., 1968, 8, 565.

126. G. Porter and M. Windsor, Disc.Faraday Soc., 1954, 17, 178.

127. W.G. Herkstoeter, A.A. Lamola and G.S. Hammond, J.Amer.Chem.Soc., 1964, 86, 4537.

128. R.N. Nurmukhametov, L.A. Mileshina, and D.A. Shigorin, Opt.Spekr., 1967, 22, 404.

129. D.N. Shigorin, V.M. Voznyak, G.A. Ozerova, R.N. Nurmukhametov and A.K. Piskunov, Proc.Int.Conf.Lumin., 1966, 540.

130. H.J. Pownall and J.R. Huber, J.Amer.Chem.Soc., 1971, 93, 6429.

131. Y.H. Li and E.C. Lim, Chem.Phys.Lett., 1970, 7, 15.

132. W.A. Case and D.R. Kearns, J.Chem.Phys., 1970, 52, 2175.

133. P.J. Wagner, M.J. May, A. Hang and D.R. Graber, J.Amer.Chem.Soc., 1970, 92, 5269.

134. Y. Kanda, J.Stanislaus and E.C. Lim, J.Amer.Chem.Soc., 1969, 91, 5085.

135. N.Y.C. Chu and D.R. Kearns, J.Amer.Chem.Soc., 1972, 94, 2619.

136. S.Y. Wang, Photochem.Photobiol., 1964, 3, 395.

137. A.I. Tolmachev, L.N. Schulezhko and A.A. Kisilenko, Z. Obsch.Khim., 1965, 35, 1708.

138. I. Degani, R. Fochi and G. Spunta, Boll.sci.Fac.Chim.ind.Bologna, 1968, 26, 3.

139. E.M. Arnett and R.D. Bushick, J.Amer.Chem.Soc., 1964, 86, 1564.

140. A. Albert and E.P. Serjeant, Ionisation Constants of Acids and Bases (Methuen, 1962).

141. V. Zander and E. Ehrhardt, Bull.Chem.Soc.Jap., 1966, 39, 1694.

142. A. Beckett and G. Porter, Trans.Faraday.Soc., 1963, 59, 2038.

143. Quantum Chemistry Program Exchange, No. 141, Chemistry Department Indiana University, Bloomington, Indiana 47401.

144. Tables of Interatomic Distances and Configuration in Molecules and Ions, ed. L.E. Sutton, Special Publications Nos. 11 and 18, The Chemical Society, London.

145. R. Hoffmann and J.R. Swenson, J.Phys.Chem., 1970, 74, 415.

146. M.J.S. Dewar and N. Trinajstic, J.Chem.Soc.(A), 1971, 1220.

147. B. Tinland and C. Decoret, Spectroscopy Letters, 1970, 3, 345.

148. H.H. Jaffé, D.L. Beveridge and H.L. Jones, J.Amer.Chem.Soc., 1964, 86, 2934.

149. R. Daudel, Advan.Quantum.Chem., 1970, 5, 1.

150. J.B. Birks, Photophysics of Aromatic Compounds, (Wiley Interscience, 1970).

151. A. Weller, in Fast Reactions and Primary Processes in Chemical Kinetics, ed. S. Claesson (Wiley Interscience, 1967).

152. A. Weller and D. Rehm, Israel J.Chem., 1970, 8, 259.

153. M. Kasha, J.Chem.Phys., 1952, 20, 71.

154. Th. Förster, Disc.Faraday Soc., 1959, 27, 7.

155. K.H. Grellmann, A.R. Watkins and A. Weller, J. Luminescence, 1970, 1, 2, 678.

156. K.H. Grellmann, A.R. Watkins and A. Weller, J.Phys.Chem., 1972, 76, 469.

157. L.H. Stephenson and G.S. Hammond, Pure Appl.Chem., 1968, 16, 125.

158. M.T. McAll, G.S. Hammond, O. Yonemitsu and B. Witkop, J.Amer.Chem. Soc., 1970, 92, 6991.

159. P. Pringsheim, Fluorescence and Phosphorescence, (Interscience, 1949).

160. Th. Förster, Fluoreszenz Org. Verb., (Vandenhoeck and Rupreckt, 1951).

161. R.W. Stoughton and G.K. Rollefson, J.Amer.Chem.Soc., 1939, 61, 2634.

162. J. Weiss, Trans.Faraday Soc., 1946, 42, 133.

163. M. Kasha, Disc.Faraday Soc., 1950, 9, 309.

164. H. Leonhardt and A. Weller, Luminescence of Organic and Inorganic Materials, ed. Kallmann and Spruch (Wiley, 1962).

165. A.R. Watkins, personal communication.

166. A.V. Karyakin and G.G. Babicheva, Opt. Spekr., 1968, 24, 1006.

167. R.W. Stoughton and G.K. Rollefson, J.Amer.Chem.Soc., 1940, 62, 2264.

168. E.J. Bowen, N.J. Holder, and G.B. Woodger, J.Phys.Chem., 1962, 66, 2491.

169. A.V. Buettner and J. Dedinas, J.Phys.Chem., 1971, 75, 187.

170. J. Dedinas, J.Phys.Chem., 1971, 75, 182.

171. M.B. Ledger and G. Porter, J.Chem.Soc., Faraday Trans. I, 1972, 68, 539.

172. R. Steward, M.K. Ganqer, R.B. Moodie and L.J. Meunster, Can.J.Chem., 1963, 41, 1065.

173. J.A. Leisten and P.R. Walton, J.Chem.Soc., 1964, 3180.

174. C.A. Parker and T.A. Joyce, Trans.Faraday Soc., 1969, 65, 2823.

175. T.D. Brown and M.S. Shepherd, J.Chem.Soc., Dalton Trans., 1972, 1616.

176. S. Karamat Hussain and P.A.H. Wyatt, J.Chem.Soc., Faraday Trans. I, 1972, 68, 130.

177. Th. Förster, personal communication.

178. T.S. Godfrey, G. Porter and P. Suppan, Disc.Faraday Soc. 1965, 39, 194.

179. S.G. Copen and M.N. Siddiqui, J.Amer.Chem.Soc., 1964, 86, 5047.

180. P. Hrdlovic, D. Bellus and M. Lazar, Coll.Czeck.Chem,Commun., 1968, 33, 59.

181. A. Beckett and G. Porter, Trans.Faraday Soc., 1963, 59, 2051.

182. O. Kysel, International Symposium on Macromolecular Chemistry, 1969, 5, 263.

183. M. Liler, Reaction Mechanisms in Sulphuric Acid (Academic Press, 1970).

184. A.A. Lamola, J.Chem.Phys., 1967, 47, 4810.

185. M. Batley and D.R. Kearns, Chem.Phys.Lett., 1968, 2, 423.

186. J. Petruska, J.Chem.Phys., 1961, 34, 1120.

187. H. Lutz, M. Duval, E. Bréhéret and L. Lindqvist, J.Phys.Chem., 1972, 76, 821.

188. H. Beens, K.H. Grellmann, M. Gurr and A.H. Weller, Disc.Faraday Soc., 1965, 39, 183.

189. F. Wilkinson, J.Phys.Chem., 1962, 66, 2569.

190. K. Tickle and F. Wilkinson, Trans.Faraday Soc., 1965, 61, 1981.

191. A.A. Lamola and G.S. Hammond, J.Chem.Phys., 1965, 43, 2129.

192. S.G. Schulman, L.B. Sanders and J.D. Winefordner, Photochem. Photobiol., 1971, 13, 381.

193. C.C. Greig and C.D. Johnson, J.Amer.Chem.Soc., 1969, 90, 6453.

194. R.I. Zalewski and G.E. Dunn, Can.J.Chem., 1968, 46, 2469.

195. S.G. Schulman, Fluorescence News, 1972, 6, 1.

196. E.J. O'Connell, Chem.Comm., 1969, 571.

197. C. Reid, Excited States in Chemistry and Biology (Butterworths, 1957).

198. M.H. Habacher and S. Doemberg, J.Pharm.Sci., 1964, 53, 1067.